

HYBRID ENERGY SYSTEMS WITH SMALL MODULAR  
REACTOR BASED NUCLEAR POWER PLANTS AND  
RENEWABLE ENERGY SOURCES: MODELING, OPERATION  
AND PLANNING STUDIES

A dissertation submitted to the  
College of Graduate and Postdoctoral Studies  
in partial fulfillment of the requirements  
for the degree of Doctor of Philosophy  
in the Department of Electrical and Computer Engineering  
University of Saskatchewan  
Saskatoon

By  
Bikash Poudel

©Bikash Poudel, November, 2020. All rights reserved.

Unless otherwise noted, copyright of the material in this thesis belongs to the author

# Permission to Use

In presenting this dissertation in partial fulfillment of the requirements for a Postgraduate degree from the University of Saskatchewan, I agree that the Libraries of this University may make it freely available for inspection. I further agree that permission for copying of this dissertation in any manner, in whole or in part, for scholarly purposes may be granted by the professor or professors who supervised my dissertation work or, in their absence, by the Head of the Department or the Dean of the College in which my dissertation work was done. It is understood that any copying or publication or use of this dissertation or parts thereof for financial gain shall not be allowed without my written permission. It is also understood that due recognition shall be given to me and to the University of Saskatchewan in any scholarly use which may be made of any material in my dissertation.

## Disclaimer

Reference in this dissertation to any specific commercial products, process, or service by trade name, trademark, manufacturer, or otherwise, does not constitute or imply its endorsement, recommendation, or favoring by the University of Saskatchewan. The views and opinions of the author expressed herein do not state or reflect those of the University of Saskatchewan, and shall not be used for advertising or product endorsement purposes.

Requests for permission to copy or to make other uses of materials in this dissertation in whole or part should be addressed to:

Head of the Department of Electrical and Computer Engineering  
57 Campus Drive  
University of Saskatchewan  
Saskatoon, Saskatchewan S7N 5A9 Canada

OR

Dean  
College of Graduate and Postdoctoral Studies  
University of Saskatchewan  
116 Thorvaldson Building, 110 Science Place  
Saskatoon, Saskatchewan S7N 5C9 Canada

# Abstract

With increasing environmental concerns over greenhouse gas emissions, more emphasis is being given to the generation technologies with a low carbon footprint. Renewable energy sources (RESs) such as wind and photovoltaics (PVs) are the most popular among clean energy alternatives, but the intermittency, uncertainty and lack of inertia associated with them are major concerns. Another major hurdle in this global transition to clean energy is providing economic and reliable energy to the remote and offgrid communities with limited access to the electric grid and natural gas pipelines. Small modular reactors (SMRs), an emerging nuclear power plant (NPP) technology with flexibility in size and improved power maneuvering capability, offer clean energy solutions for electrical grids and isolated communities. This research work investigates the planning and dynamic aspect of SMR and RES, focusing on exploring the issues and realizing the benefits offered by SMR due to its smaller size, flexible operation and cogeneration.

The combination of SMR and distributed RES in remote communities is governed by SMR's capability to respond to the demand fluctuations. The flexibility requirements of remote communities increase almost proportionally with the increment in the RES penetration level. Therefore, it is essential to analyze SMR's flexible operation in the context of the flexibility requirements it has to provide in remote communities in the presence of RES penetration. In this research work, SMR's flexible operation is investigated with its operating limits for ramp rate and the net power variation in load following and frequency regulation modes. Electrical energy storage (EES) is used as an energy buffer to absorb the fluctuations and facilitate SMR-RES synergy in remote communities. The benefit of EES in the synergy is quantified in terms of the improvement in SMR's plant load factor.

The proposed application of SMRs with RESs in an isolated system requires them to continually operate in flexible mode and respond to large demand variations. The approximated turbine-governor models currently used in power system software cannot correctly represent SMR, resulting in erroneous simulated dynamics. This thesis proposes a detailed dynamic model of SMR and integrates it with the standard turbine-governor model in PSS®E software. The proposed model mimics the source dynamics by including the component models

for the reactor core, primary coolant circuit, steam generator and the secondary coolant circuit of the SMR plant. The proposed model improves the accuracy of power system dynamics and facilitates the analysis of internal reactor responses.

SMR's cogeneration scheme for district heating will be advantageous for remote communities with limited access to electric grid and gas pipelines. The proper coordination of steam distribution for heat and electricity, on the other hand, could significantly improve the load following capability allowing the system to host distributed RES to form standalone SMR-RES hybrid energy systems in isolated communities. SMR, being the primary source of energy, will be responsible for maintaining the system's performance while adhering to its operational limits for flexible operation. The battery energy storage system (BESS) and thermal energy storage (TES) could play a significant role in alleviating the fluctuations in power and heat sides. In this context, this thesis proposes a simulation model of the SMR-RES hybrid energy system with a detailed dynamic model of a cogenerating SMR and a quasi-static model of the DH system. Furthermore, a multi-time scale operational scheme is proposed to operate the hybrid energy in load following and frequency regulation modes. An optimization problem is also proposed to optimally operate the hybrid energy system and evaluate RES hosting capability based on steady-state and dynamic constraints related to the reactor, power system, and district heating system.

Another excellent opportunity with SMR is in electrical grids as a new generation plant or as a clean energy replacement to the ageing fossil fuel-based thermal plants. Various electrical and non-electrical factors impact the deployment of SMR in electrical grids. In this thesis, the electrical grid considerations of SMR's siting and sizing are investigated, focusing on steady-state, dynamic and safety aspects. The steady-state aspect includes the accessibility to the electrical grid, transmission line and voltage limits, generation congestion, load demand and the hosting capacity. The dynamic aspect focuses on analyzing the impact of SMR's siting and sizing on system frequency and voltage dynamics. The safety aspect, on the other hand, assesses the suitability of a site based on the offsite power reliability. The proposed framework of SMR's siting and sizing is implemented in the Saskatchewan provincial electrical grid with no previous nuclear experience.

The combination of SMR and RES offers an excellent clean energy solution to the remote

communities and electrical grids. In this context, the proposed models, simulations and research findings in this thesis would help deploy the proposed energy solutions to realize sustainable clean energy systems.

# Acknowledgements

First of all, I would like to express my sincere gratitude to my supervisor Dr. Ramakrishna Gokaraju for his invaluable guidance, support and motivation throughout my Ph.D. study. His immense knowledge, vision, experience and enthusiasm inspired me to accomplish this research work. I am privileged to have had an opportunity to study under his supervision.

I would also like to extend my thanks to Dr. Kalpesh Joshi (Postdoctoral fellow in the research group) for the collaboration and feedback he provided on the joint research work.

I gratefully acknowledge the financial assistance provided by the Sylvia Fedoruk Canadian Centre for Nuclear Innovation, Natural Sciences and Engineering Research Council of Canada (NSERC) and Electranix Corporation, Winnipeg, Canada. I sincerely thank the Department of Electrical and Computer Engineering at the University of Saskatchewan for providing the Department scholarship.

I am very grateful to Dr. Esam Hussein, University of Regina, for the leadership he provided for the overall Fedoruk Center project. I would like to thank Mr. Dennis Woodford, Electranix Corporation, for his valuable feedback on the research work. I would also like to thank the International Atomic Energy Agency (IAEA), Vienna, Austria, for providing the nuclear power plant simulators.

Special thanks go to my advisory committee members: Dr. Nurul A. Chowdhury, Dr. Akindele Odeshi and Dr. Li Chen for their insightful comments and suggestions throughout my Ph.D. program.

My sincere thanks go to my graduate study professors, Dr. Nurul A. Chowdhury, Dr. Rajesh Karki and Dr. Sherif O. Faried, for broadening my knowledge in the field of power systems. I am also thankful to my friends: Dr. Shane Jin, Mr. Jason Pannell, Mr. Asim Chaulagain, Mr. Nripesh Ayer, Mr. Kiran Raj Timalsena, Mr. Prajjwal Gautam, Mr. Tej Krishna Shrestha and Mr. Safal Bhattarai for sharing their knowledge and providing valuable suggestions.

Last but not least, I owe my deepest gratitude to my parents, brother and sister for their love, encouragement and constant support throughout my years of graduate studies.

# Dedication

*To my father, **Khem**  
and  
my mother, **Radha***

# Table of Contents

<b>Permission to Use</b>	<b>i</b>
<b>Abstract</b>	<b>iii</b>
<b>Acknowledgements</b>	<b>vi</b>
<b>Dedication</b>	<b>vii</b>
<b>Table of Contents</b>	<b>viii</b>
<b>List of Tables</b>	<b>xv</b>
<b>List of Figures</b>	<b>xvi</b>
<b>List of Abbreviations</b>	<b>xxi</b>
<b>List of Publications</b>	<b>xxiii</b>
<b>1 Introduction</b>	<b>1</b>
1.1 Background . . . . .	1
1.2 Literature Review of Small Modular Reactors . . . . .	3
1.2.1 SMR State of the Art . . . . .	3
1.2.2 Flexible Operation . . . . .	6
1.2.2.1 General Concept . . . . .	6
1.2.2.2 Experience and Challenges with NPPs . . . . .	7
1.2.3 Synergy with Renewables . . . . .	11
1.2.4 Dynamic Model for Power System Studies . . . . .	14
1.2.5 Energy Solution for Isolated Communities . . . . .	16
1.2.6 Siting and Sizing in Electrical Grids . . . . .	17
1.2.6.1 Non-Electrical Considerations . . . . .	17
1.2.6.2 Electrical Grid Considerations . . . . .	19
1.3 Research Objectives . . . . .	22
1.4 Research Contribution . . . . .	24
1.5 Thesis Organization . . . . .	25

<b>2</b>	<b>Exploring Synergy Among New Generation Technologies– Small Modular Reactor, Energy Storage and Distributed Generation: A Strong Case for Remote Communities</b>	<b>29</b>
2.1	Abstract . . . . .	30
2.2	Introduction . . . . .	30
2.3	Overview of Potential Benefits . . . . .	33
2.4	Small Modular Reactors . . . . .	34
2.5	The Remote Feeder – Modelling with SMR, EES and Distributed Generators	36
2.5.1	Modelling a Remote Feeder . . . . .	37
2.5.2	Hosting Capacity Analysis . . . . .	38
2.6	The Case Study . . . . .	41
2.6.1	Case Study 1: Potential for SMR – without EES . . . . .	42
2.6.2	Case Study 2: Potential for SMR with EES . . . . .	42
2.7	Conclusion . . . . .	45
<b>3</b>	<b>Investigating Small Modular Reactor’s Design Limits for its Flexible Operation with Photovoltaic Generation in Microcommunities</b>	<b>47</b>
3.1	Abstract . . . . .	48
3.2	Nomenclature . . . . .	49
3.3	Introduction . . . . .	49
3.4	Small Modular Reactor Based Nuclear Power Plants . . . . .	52
3.4.1	SMR – State of the Art . . . . .	52
3.4.2	SMR Suitability for Remote Locations . . . . .	53
3.4.3	Challenges of Flexible Operations . . . . .	54
3.5	Flexibility Requirements and Design Limits . . . . .	55
3.5.1	Variability Introduced by PV distributed generation (PVDG) . . . . .	56
3.5.2	Aspects of Flexible Operations . . . . .	56
3.5.3	Operating Limits of SMR . . . . .	57
3.5.4	SMR Model for Power System Studies . . . . .	62
3.6	Analysis for Design Requirements . . . . .	64
3.6.1	Multi-Timescale Simulation Approach . . . . .	64

3.6.2	The Remote Feeder . . . . .	66
3.7	Results and Discussion . . . . .	67
3.8	Conclusion . . . . .	71
<b>4</b>	<b>A Dynamic Model of Small Modular Reactor-Based Nuclear Plants for Power System Studies</b>	<b>73</b>
4.1	Abstract . . . . .	74
4.2	Nomenclature . . . . .	74
4.3	Introduction . . . . .	76
4.4	Reactor Modeling & Integration to Turbine . . . . .	78
4.4.1	Reactor Core Model . . . . .	79
4.4.1.1	Reactor Neutronic Model . . . . .	80
4.4.1.2	Reactor Thermal Hydraulic Model . . . . .	80
4.4.1.3	Hot Leg and Cold Leg . . . . .	81
4.4.2	Steam Generator Model . . . . .	81
4.4.3	Integration to the Turbine-governor Model . . . . .	82
4.5	Reactor Model Performance and Validation . . . . .	84
4.5.1	Steady-State Performance and Validation . . . . .	86
4.5.2	Dynamic Performance of the Isolated SMR model . . . . .	87
4.5.2.1	Response to Step Change in Reactivity . . . . .	87
4.5.2.2	Response to Step Change in Valve Opening . . . . .	89
4.6	Power System Dynamic Studies with SMR . . . . .	89
4.6.1	Case I: Without Reactor . . . . .	91
4.6.2	Case II: With Uncontrolled Reactor . . . . .	92
4.6.3	Case III: With Controlled Reactor . . . . .	94
4.6.4	Comparison . . . . .	94
4.7	Conclusion . . . . .	95
<b>5</b>	<b>Small Modular Reactor Based Hybrid Energy System for Electricity &amp; District Heating</b>	<b>96</b>
5.1	Abstract . . . . .	96
5.2	Nomenclature . . . . .	97

5.3	Introduction . . . . .	98
5.4	Proposed SMR Plant Coupled to DH System . . . . .	101
5.5	Dynamic Modeling . . . . .	102
5.5.1	Secondary Coolant . . . . .	102
5.5.1.1	Turbine Bypass System . . . . .	102
5.5.1.2	Steam Extraction System . . . . .	103
5.5.2	Turbine-Governor Model . . . . .	103
5.5.3	District Heating System Model . . . . .	104
5.5.3.1	Heat Exchange Stations . . . . .	105
5.5.3.2	Thermal Energy Storage . . . . .	106
5.5.3.3	DH Pipeline . . . . .	106
5.5.4	Power Output Models of Wind and PV Plants . . . . .	107
5.5.5	Battery Energy Storage System (BESS) Dynamic Model . . . . .	107
5.6	Case Study . . . . .	108
5.6.1	Test System Description . . . . .	108
5.6.2	LTF Simulation Results . . . . .	111
5.6.3	STF Dynamic Results . . . . .	114
5.7	Conclusion . . . . .	118
<b>6</b>	<b>Optimal Operation and RES hosting in SMR Based Hybrid Energy System for Electricity &amp; District Heating</b>	<b>120</b>
6.1	Abstract . . . . .	121
6.2	Nomenclature . . . . .	121
6.2.1	System Variables . . . . .	121
6.2.2	Sets and Subscripts . . . . .	123
6.3	Introduction . . . . .	124
6.4	System Modeling . . . . .	125
6.4.1	SMR Dynamic Model . . . . .	125
6.4.2	District Heating System Model . . . . .	127
6.4.3	BESS Dynamic Model . . . . .	129
6.5	Multi-Timescale Operational Scheme . . . . .	129

6.6	Problem Formulation . . . . .	130
6.6.1	Objective Function . . . . .	130
6.6.2	Constraints . . . . .	131
6.6.2.1	Power Flow and Network Limits . . . . .	131
6.6.2.2	Power Balance and Generator Limits . . . . .	131
6.6.2.3	SMR Ramping Constraints . . . . .	132
6.6.2.4	DH System Design Constraints . . . . .	133
6.6.2.5	STF Dynamic Response Constraints . . . . .	134
6.6.3	RES Hosting and Optimal Operation Problem . . . . .	134
6.7	Case Study . . . . .	135
6.7.1	Test System Description . . . . .	135
6.7.2	Sample Simulation Results . . . . .	137
6.7.2.1	LF Simulation Results . . . . .	137
6.7.2.2	Dynamic Simulation Results . . . . .	140
6.7.3	Optimization Results . . . . .	141
6.8	Conclusion . . . . .	144
<b>7</b>	<b>Analysis for Siting and Sizing of a Small Modular Reactor – A Case Study in Canada</b>	<b>146</b>
7.1	Abstract . . . . .	147
7.2	Introduction . . . . .	147
7.3	The Case System . . . . .	148
7.4	Methodology . . . . .	150
7.4.1	Overall Approach . . . . .	150
7.4.2	OPF Formulation . . . . .	151
7.4.3	Modified OPF Including Contingency Assessment . . . . .	152
7.4.4	SMR with PHES . . . . .	155
7.5	Case Study and Results . . . . .	156
7.5.1	Case 1: Without SMR . . . . .	156
7.5.2	Case 2: With 100 MW SMR at Each Site . . . . .	157
7.5.3	Case 3: Optimum SMR Size with Loss Minimization . . . . .	157

7.5.4	Case 4: N-1 Contingency Constrained OPF . . . . .	159
7.5.5	Case 5: With PHES . . . . .	160
7.5.6	Comparison of Various Cases . . . . .	161
7.6	Conclusion . . . . .	162
<b>8</b>	<b>An Approach to Assess Reliability of Offsite Power as Site Selection</b>	
	<b>Criteria for a Nuclear Power Plant</b>	<b>163</b>
8.1	Abstract . . . . .	164
8.2	Introduction . . . . .	164
8.3	System Model . . . . .	165
8.3.1	The Electrical Grid . . . . .	165
8.3.2	Emergency Power Supply System . . . . .	167
8.4	The Overall Approach . . . . .	167
8.4.1	Reliability Evaluation of Offsite Power . . . . .	167
8.4.2	Reliability Assessment of Onsite EPSS . . . . .	169
8.4.3	Result and Discussion . . . . .	171
8.5	Conclusion . . . . .	172
<b>9</b>	<b>Conclusions and Future Works</b>	<b>173</b>
9.1	Conclusions . . . . .	173
9.2	Future Works . . . . .	177
	<b>References</b>	<b>178</b>
	<b>Appendix A Project Specific Studies: SMR Siting and Sizing in Saskatchewan</b>	
	<b>Electrical Grid</b>	<b>195</b>
A.1	The Case Systems . . . . .	195
A.2	Steady-State Aspects . . . . .	197
A.2.1	Southern Saskatchewan Electrical Grid . . . . .	198
A.2.2	Northern Saskatchewan Electrical Grid . . . . .	200
A.3	Dynamic Aspects in Southern SEG . . . . .	200
A.4	Safety Aspects . . . . .	206
A.5	Results and Discussion . . . . .	206
A.6	Conclusion . . . . .	208

<b>Appendix B Program Codes for Modeling and Simulation</b>	<b>210</b>
B.1 FORTRAN Code for SMR Model in PSS®E . . . . .	210
B.2 Matlab Code for Quasi-Static DH System Model . . . . .	217
B.3 Python Code for the Dynamic Simulation in PSS®E . . . . .	224

# List of Tables

2.1	Main features of the remote feeder . . . . .	37
2.2	Hosting capacity of the remote feeder . . . . .	39
2.3	Load factor of SMR . . . . .	44
3.1	Operating limits of SMR . . . . .	58
3.2	Validating the SMR operating limits. Legend: ✓ Power cycle executed successfully ✗ Low-pressure alarms triggered ☒ Turbine and generator breaker tripped. . . . .	60
4.1	Reactor core and SG parameters [56] [57] . . . . .	84
4.2	SMR steady-state results for various power levels . . . . .	87
5.1	DH system design parameters . . . . .	110
5.2	Wind and PV parameters . . . . .	111
6.1	System parameters . . . . .	138
7.1	Demand-generation scenario . . . . .	149
7.2	Transmission loss with 100 MW SMR at each site . . . . .	157
7.3	SMR for highest daily peak load day of the year . . . . .	158
7.4	SMR dispatch for lowest daily peak load day of the year . . . . .	158
7.5	Sizing of SMR for maximum loss reduction . . . . .	159
7.6	SMR for highest peak load day of the year . . . . .	159
7.7	SMR dispatch for lowest daily peak load day of the year . . . . .	160
7.8	Contingency constrained final sizing of SMR . . . . .	160
7.9	Sizing of SMR with PHES . . . . .	161
7.10	With SMR and PHES . . . . .	161
8.1	Component failure data . . . . .	170
A.1	Load and generation for present and future cases . . . . .	197
A.2	Final results for siting and sizing in Southern SEG . . . . .	207
A.3	Final results for siting and sizing in Northern SEG . . . . .	208

# List of Figures

1.1	SMR designs for non-electrical applications [15] . . . . .	4
1.2	Integral pressurized water reactor–schematic of NuScale SMR (reproduced from [18] with permission from NuScale Power, LLC) . . . . .	5
1.3	A typical example of daily flexible operation (reproduced from [18] with permission from IAEA) . . . . .	7
1.4	Planned load following by Bruce Nuclear Generating Station . . . . .	8
1.5	Flexibility requirements and design limits of German PWRs [18] . . . . .	10
1.6	Typical variation of wind speed and solar irradiation in a day . . . . .	12
1.7	Research areas of SMR site selection [70] . . . . .	18
1.8	A generic event tree for SBO in NPP [81] . . . . .	21
2.1	System level schematic overview of iPWR [88] . . . . .	35
2.2	Schematic diagram and geographical map of remote feeder in north Saskatchewan, Canada . . . . .	38
2.3	Hourly load profile at the substation . . . . .	40
2.4	Voltage profiles of four end nodes . . . . .	41
2.5	Demand profile at substation with power from PVDGs . . . . .	43
2.6	SMR with PVDG and BES . . . . .	44
2.7	End node voltages before and after using BESS . . . . .	45
2.8	End node voltages (for node 4 and 1102) before and after using BESS . . . . .	46
3.1	An underground sitting configuration of a NuScale iPWR module (reproduced from [28] with permission from NuScale Power, LLC) . . . . .	53
3.2	Normalized global horizontal irradiance (GHI) profile at Varennes, ON, Canada - [103] . . . . .	56
3.3	Operating limits chosen for SMR: (a) power ramp rates and net allowable change in power, (b) ramp rates for load following, and (c) ramp rates for frequency regulation . . . . .	59

3.4 Response to the REO transition from 100% to 20% @ 80% REO/min (a) Generator and turbine trip, (b) Valve operations and the corresponding changes in pressure header . . . . . 61

3.5 Valve positions and pressure variations - with IAEA SMR simulator – for the power cycle of 100-60-100@ 80% REO – Low-pressure alarm . . . . . 62

3.6 GGOV1 turbine-governor model tuned to match the reactor dynamics . . . . . 63

3.7 The multi-timescale simulation platform . . . . . 64

3.8 The modified remote feeder including an SMR and five PVDG plants with a collective capacity of 12 MW . . . . . 67

3.9 TSPF quarter-hourly simulations - (a) overall demand profiles with different PV profiles (b) voltage profile of end nodes with CS PV profile . . . . . 68

3.10 TSPF per-minute simulation from 6 AM to 6 PM with different PV profiles . . . . . 69

3.11 Dynamic simulation with per second perturbation: (a) 75% PV penetration (b) 55% PV penetration . . . . . 70

3.12 Low pressure alarm triggered at time  $t = 20$  min when ramping up from 40% to 80% REO@80% REO/min . . . . . 71

4.1 Schematic diagram of NuScale iPWR module . . . . . 79

4.2 Three lump representation of HCSG. . . . . 81

4.3 GGOV1 modified and integrated with the SMR model; shaded region shows the modifications with new modules. . . . . 83

4.4 Valve mapping process with  $p_{ref}$  corresponding to: Map1-100%, Map2-90%, and Map3-50% REO of SMR . . . . . 83

4.5 Constant average coolant temperature control mode . . . . . 85

4.6 Dynamic responses for a step change in input variables. Solid lines represent the responses for 5% step increase in reactivity; dotted lines represent the responses for 10% step increase in valve opening. . . . . 88

4.7 SMR connected to a power system . . . . . 89

4.8 Responses: (a) Thermal power with rod control, (b) Steam pressure with different valve rate limits. . . . . 90

4.9 Power system dynamic responses for step changes in electrical demand. Legend: Case I(.....), Case II(- - -), Case III(—). . . . . 92

4.10 Reactor dynamic responses for step changes in electrical demand. Legend: Case II(- - -), Case III(—). . . . . 93

5.1 NuScale iPWR module cogenerating heat and electricity . . . . . 101

5.2 Control block for the turbine bypass system . . . . . 103

5.3 A section of modified GGOV1. Encircled portion shows the inclusion of turbine bypass and steam extraction systems. . . . . 103

5.4 Block diagram of the DH system . . . . . 104

5.5 IEEE 30-bus network used for the case study. Encircled 33 kV portion is isolated by keeping four 230/33 kV transformers out of service. . . . . 109

5.6 (a) Electrical and heating load demand profiles, (b) PV irradiance and wind speed profiles. . . . . 110

5.7 LTF system response considering the daily load and RES profiles. (Part-1) . . . 112

5.8 LTF system response considering the daily load and RES profiles. (Part-2) . . . 113

5.9 3-bus equivalent network for STF assessment. . . . . 114

5.10 Power system responses during the worst 15 min of the day. Legend: WBYWOBA-with turbine bypass without BESS, BESS 5 MW-with turbine bypass and BESS of size 5 MW, BESS 10MW-with turbine bypass and BESS of 10 MW. (Part-1) 115

5.11 Power system responses during the worst 15 min of the day. Legend: WOBYBA-without turbine bypass and BESS, WBYWOBA-with turbine bypass without BESS, BESS 5 MW-with turbine bypass and BESS of size 5 MW, BESS 10MW-with turbine bypass and BESS of size 10 MW. (Part-2) . . . . . 116

5.12 Reactor side responses during the worst 15 min of the day. Legend: WOBYBA-without turbine bypass and BESS, WBYWOBA-with turbine bypass without BESS, BESS 5 MW-with turbine bypass and BESS of size 5 MW, BESS 10MW-with turbine bypass and BESS of size 10 MW. . . . . 117

6.1 Block diagram of the SMR model interfaced between the governor output and turbine input of the turbine-governor model. . . . . 126

6.2 Control block for the turbine bypass system . . . . . 127

- 6.3 Block diagram of the DH system . . . . . 128
- 6.4 Proposed multi-timescale operational scheme . . . . . 130
- 6.5 Feasible operation region of a cogenerating SMR unit. . . . . 132
- 6.6 33 kV portion of IEEE 30-bus network used for the case study. The respective node numbers are same as the original test system. . . . . 136
- 6.7 (a) Electricity and heat load demand profiles, (b) PV irradiance and wind speed profiles. . . . . 137
- 6.8 Results for optimal operation in LF mode for 1 month period with 50 MW RES penetration. (Part-1) . . . . . 139
- 6.9 Results for optimal operation in LF mode for 1 month period with 50 MW RES penetration. (Part-2) . . . . . 140
- 6.10 3-bus equivalent network for dynamic simulation. . . . . 141
- 6.11 Power system responses during the worst 2.5 hour period of the month. . . . . 142
- 6.12 Reactor side responses during the worst 2.5 hour period of the month. . . . . 143
- 6.13 Optimization results for different RES penetration for  $V_{str} = 20000 \text{ m}^3$  and BESS size of 10 MW. . . . . 144
- 7.1 The case system . . . . . 149
- 7.2 Overall approach for the siting and sizing problem of SMR . . . . . 150
- 7.3 (a) Daily peak load variation curve (b) Load duration curve . . . . . 151
- 7.4 Island formation under contingency . . . . . 153
- 7.5 Future scenario without new generation . . . . . 156
- 7.6 Comparison of various cases(a) Tr. loss (b) EENS . . . . . 162
- 8.1 (a) Saskatchewan electrical grid (b) Two-Train configuration of EPSS in NPP substation [143] . . . . . 166
- 8.2 Offsite power failure rates . . . . . 169
- 8.3 Offsite power restoration times . . . . . 169
- 8.4 RBD for power supply to bus 3AS . . . . . 170
- 8.5 SBO probability at different nodes in SEG . . . . . 171
- A.1 Topographical map and medium term cases of Southern and Northern SEG developed in PSS®E . . . . . 196

A.2 Generation-load scenario of Southern SEG regions for medium-term . . . . . 198

A.3 Hosting capacity analysis: flowchart and the results obtained . . . . . 199

A.4 A frequency response showing the measurements of interest . . . . . 200

A.5 Southern SEG with SMR hosting locations and contingency location for dynamic  
simulation . . . . . 201

A.6 Frequency nadir boxplots for major contingencies with SMR at different nodes . 202

A.7 Voltage nadir boxplots for major contingencies with SMR at different nodes . . 202

A.8 ROCOF boxplots for major contingencies with SMR at different nodes . . . . . 203

A.9 Nadir based FRM boxplots with SMR at different nodes . . . . . 204

A.10 Frequency nadir for different cases . . . . . 205

A.11 FRM boxplots for different cases . . . . . 206

# List of Abbreviations

AGC	Automatic generation control
ALFC	Advanced load follow control
BA	Balancing Authority
BESS	Battery energy storage system
CDF	Core damage frequency
CNSC	Canadian Nuclear Safety Commission
CRIEPI	Central Research Institute of Electric Power Industry
DH	District heating
ECCS	Emergency core cooling system
EENS	Expected energy not supplied
EES	Electric energy storage
EMT	Electromagnetic transient
EPRI	Electric Power Research Institute
EPSS	Emergency power supply system
FC	Frequency control
FRM	Frequency response measure
FRO	Frequency response obligation
HCSG	Helical coil steam generator
HTGR	High-temperature gas-cooled reactor
HX	Heat exchange station
IAEA	International Atomic Energy Agency
IFRO	Interconnection frequency response obligation
iPWR	Integral pressurized water reactor
LF	Load following
LOCA	Loss of coolant accident
LOOP	Loss of offsite power
LTF	Long time frame

MTTF	Mean time to failure
NERC	North Americal Electric Reliability Corporation
NPP	Nuclear power plant
NRHES	Nuclear-renewable hybrid energy system
OPF	Optimal power flow
PHES	Pumped hydroelectric energy storage
PSS®E	Power system simulator for engineering
PV	Photovoltaics
PVDG	Photovoltaic distributed generation
PWR	Pressurized water reactor
RBD	Reliability block diagram
REO	Rated electrical output
RES	Renewable energy source
ROCOF	Rate of change of frequency
RPV	Reactor pressure vessel
RTDS	Real Time Digital Simulator
SBO	Station blackout
SEG	Saskatchewan Electrical Grid
SG	Steam generator
SMR	Small modular reactor
SOC	State of charge
STF	Short time frame
TES	Thermal energy storage
TSPF	Time series power flow

# List of Publications

## Published

### Peer-reviewed Journal Papers

1. **B. Poudel** (PhD student), K. A. Joshi (PDF), and R. Gokaraju (Supervisor), “A dynamic model of small modular reactor based nuclear plant for power system studies,” *IEEE Transactions on Energy Conversion*, vol.35, no.2, pp 977-985, June 2020.
2. K. A. Joshi (PDF), **B. Poudel** (PhD student) and R. Gokaraju (Supervisor), “Exploring synergy among new generation technologies– small modular reactor, energy storage and distributed generation: A strong case for remote communities”, *Journal of Nuclear Engineering and Radiation Science*, vol. 6, no. 2, April 2020.
3. K. A. Joshi (PDF), **B. Poudel** (PhD student) and R. Gokaraju (Supervisor), “Investigating small modular reactor’s performance characteristics for hosting photovoltaic generation in microcommunities,” *Journal of Nuclear Engineering and Radiation Science*, October 2020, doi.org/10.1115/1.4048896

### Peer-reviewed Conference Papers

1. **B. Poudel** (PhD student), K. Joshi (PDF), and R. Gokaraju (Supervisor), “An approach to assess reliability of offsite power as site selection criteria for a nuclear power plant,” in *42nd Annual CNS/CNA Student Conference*, Saskatoon, Canada, June 2018, pp. 1–6.
2. **B. Poudel** (PhD student), K. A. Joshi (PDF), and R. Gokaraju (Supervisor), “Analysis for siting and sizing of a small modular reactor– a case study in Canada,” in *20th National Power System Conference*, Tiruchirappalli, India, Dec 2018, pp. 1–6.

## Submitted Journal Papers

1. **B. Poudel** (PhD student) and R. Gokaraju (Supervisor), “Small modular reactor (SMR) NPP based hybrid energy system for electricity & district heating,” submitted to *IEEE Transactions on Energy Conversion*, June 08, 2020. (Revised: October 2, 2020)
2. **B. Poudel** (PhD student) and R. Gokaraju (Supervisor), “Optimal operation of SMR-RES hybrid energy system for electricity & district heating,” submitted to *IEEE Transactions on Energy Conversion*, September 21, 2020.

# 1 Introduction

## 1.1 Background

Incremental as well as transformational adaptation in the energy sector is necessary to contain the global mean surface temperature within the  $1.5\text{ }^{\circ}\text{C}$  by the year 2040 [1]. By 2030, Canada has committed to reducing GHG emissions by 30% below 2005 levels while SaskPower has set that goal to 40% by doubling the renewables mostly with wind energy.

The renewable energy sources (RES) such as wind and photovoltaics (PV), although very promising, are marred with challenges due to their inherent variability, uncertainty, and site-specific characteristics [2, 3]. The wind and PV plants, on the other hand, don't inherently offer inertial and governor response, and the system frequency response will get poorer with the increase in their penetration level. A reliable generation alternative in terms of base power and the flexible peaking source is thus an obligation before we consider lessening the fossil fuel-based power from the grid. Hydropower is a reliable and clean RES with excellent baseload and peaking generation capabilities. However, the large water resource necessary for electricity production with hydropower may not be available at all locations in need of a new generation.

The clean energy supplement to the offgrid communities and weakly connected parts of an electrical grid has been a difficult challenge, and one of the major hindrance for the movement towards the emission-free electrical system. There are currently 292 remote communities with a total population of approximately 194,281 people in Canada, which mostly rely on diesel generators for their energy needs as they are far away from the network of gas pipelines and have no local source of fuel for electricity production [5]. The government of Canada is committed to reduce and possibly eliminate the reliance on diesel-based energy in rural and remote communities. The clean energy for rural and remote communities (CERRC) program

was introduced with the aim to deploy renewable energy technologies and search for other innovative clean energy technology [6].

Remote communities have the potential to develop RES to fulfill their energy demand while removing the diesel-generators [7]. However, in the absence of flexible local generation, the hosting capacity for RES is limited by the weak grid infrastructure, and a large-scale energy storage is needed to accommodate more RES [8]. Several challenges arise as the penetration level of RES increases, including but not limited to (a) need for quick-acting diesel-generators to absorb RES intermittency, (b) requirement of synchronous condensers for voltage stability and dump loads to handle excess generation from RES, and (c) low efficiency of diesel-generators at partial or low-load operation with high power generation from RES [4, 9]. The grid centered reinforcements such as transmission line upgrades and reactive compensation by means of capacitor banks, synchronous condensers and flexible alternating current transmission system (FACTS) devices can solve most of the network and voltage issues. However, a mix of baseload and peaking generation is necessary for the active power balance in a system with intermittent and non-dispatchable RES.

Nuclear power, an excellent clean energy alternative, has been often overlooked due to public apprehension for nuclear catastrophe mainly arising from the nuclear accidents at Three Mile Island, Chernobyl and Fukushima in past decades. The regulations have been stricter with nuclear plants following the Fukushima Daiichi nuclear disaster [10]. However, the technological improvements in modern NPPs have been incredible with the flexibility in size, safety and security. The improvements were commended as the "Nuclear Renaissance, a new hope" by an Issue of 2006 IEEE PES Magazine [11–14].

Small modular reactor (SMR), a novel nuclear fission reactor, is a clean energy technology that offers various advantages over conventional nuclear power plant technologies, such as reduced size, improved safety features, modularity, scalability, reduced capital and operational costs, diverse energy application and improved maneuverability [15]. The reactor modules can be manufactured in the factory and transported to the plant location by feasible means of transportation, such as heavy trucks and rails. They're available in sizes typically up to 300 MW [15]. The small size and modularity of SMR provide an opportunity to develop a standalone micro-grid for remote and off-grid loads centers. The SMR size of 50 to 300 MW

could replace the conventional fossil fuel-based thermal plants that are approaching the end of their lifespan.

Besides, an SMR driven synchronous generator would provide inertia to the power system, which is critical to maintaining the power system stability. The SMR, unlike the conventional nuclear power plants, has improved governor response, and load following capabilities [16–18]. The ability of SMR to offer base and variable power complements the intermittency and non-dispatchability of the RES, such as wind and solar PVs [19,20]. With their capacity of load following and rapid response rates, SMRs are expected to be more readily adaptable to integrate with intermittent and uncertain RES [15,21,22]. The mix of SMR and renewable has the prospect of being one of the future generation mixes in many parts of the world, including Canada.

## 1.2 Literature Review of Small Modular Reactors

### 1.2.1 SMR State of the Art

SMRs are being developed in all major technological lines of reactors, including water-cooled reactors, high-temperature gas-cooled reactors, fast neutron spectrum reactors, and molten salt reactors [20]. SMR designs are primarily envisioned for the provision of the energy for a wide range of applications, a replacement to the ageing fossil fuel-based thermal plants, enhanced safety consideration and better economic performance [15,23].

Out of more than 50 SMR designs under development, three are in advanced stage of the development [15]. Among the three SMRs, CAREM is an integral pressurized water reactor (iPWR) plant based on an indirect steam cycle with highly enhanced safety features. The prototype module CAREM-25 has a thermal rating of 100 MW and can produce electrical power of 30 MW. The module is designed to supply electricity for regions with small electrical demand and support seawater desalination. HTR-PM is a pebble-bed high-temperature gas-cooled reactor (HTGR) located in Rongcheng Shandong province, China. The third SMR design, KLT-40s in Russia has recently started operation in 2019. It is a pressurized water reactor (PWR) developed for floating nuclear power unit (FNPP) with each module

producing electrical power of 35 MW. It can provide the cogeneration capabilities for electricity and heat supply to the isolated and remote communities. Pinawa, Manitoba, is one of the remote demonstration sites in Canada targeting to establish an operating SMR plant by 2023 [24]. The 10 MW/35 MWth StarCore HTGR plant proposed for Pinawa aims to promote agricultural development and provide cheaper heat and electricity. Similarly, under Carbon Free Power Project (CFPP), the Utah Municipal Power Systems (UAMPS) is planning to construct a 12 module NuScale SMR at the Idaho site [25]. It is planned to start operating by 2030 and targets to provide clean electricity to the member states.

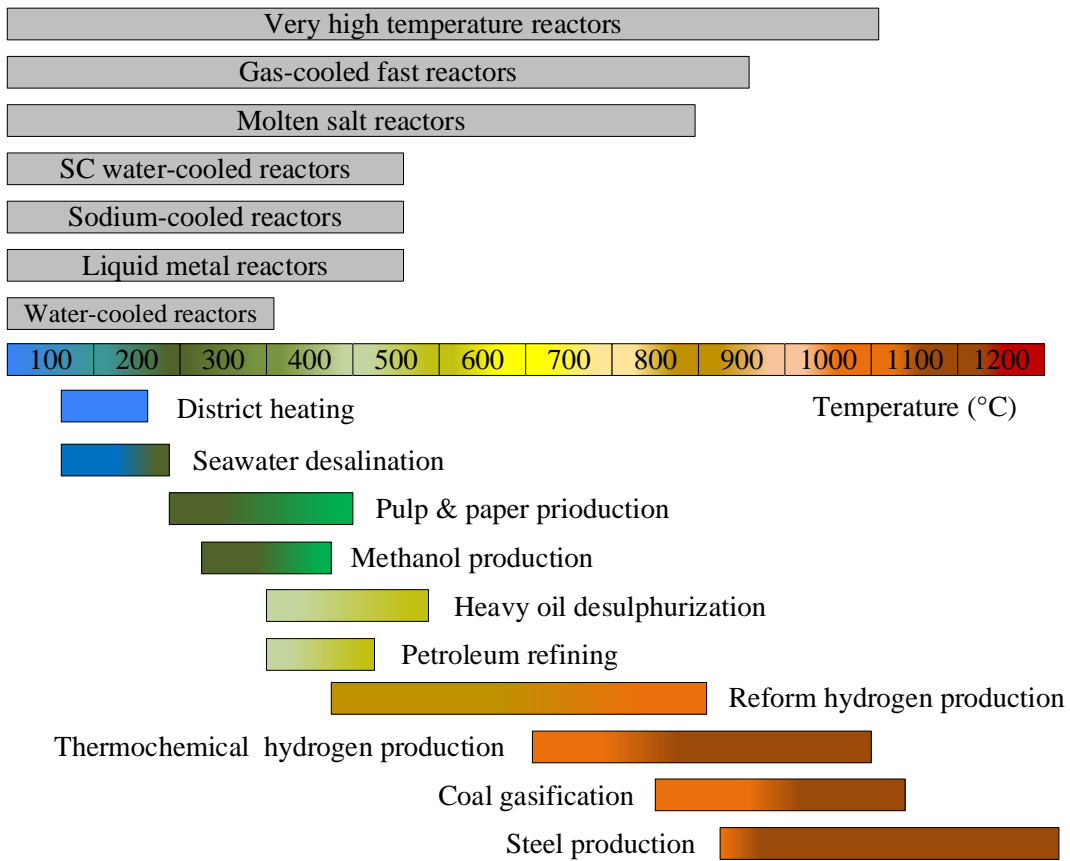


**Figure 1.1:** SMR designs for non-electrical applications [15]

Employing the nuclear plants for cogeneration application along with power generation significantly boosts the financial performance. The study cases of various model cities throughout the world have pointed the suitability of SMR scale reactors for district heating, hydrogen production, water desalination, and various other application in addition to electricity production [26, 27]. The studies showed that the application of SMR in a remote

location for electricity and district heating is beneficial not only for economic payback but also for flexibility of operation. Fig. 1.1 shows the non-electrical application with various lines of reactor technology. The type of cogeneration feasible with the reactor is primarily based on the steam temperature. The reactors with high temperature steam can support all variety of industrial applications, including hydrogen production, coal gasification and steel production. For the reactors with low temperature steam, the industrial application such as water desalination, pulp and paper production and district heating are some of the feasible options. The temperature boosting techniques such as vapor compression, electrical heating, heat recuperation or chemical heating could, however, be used to provide the topping heat to the process steam to make them suitable for any process applications.

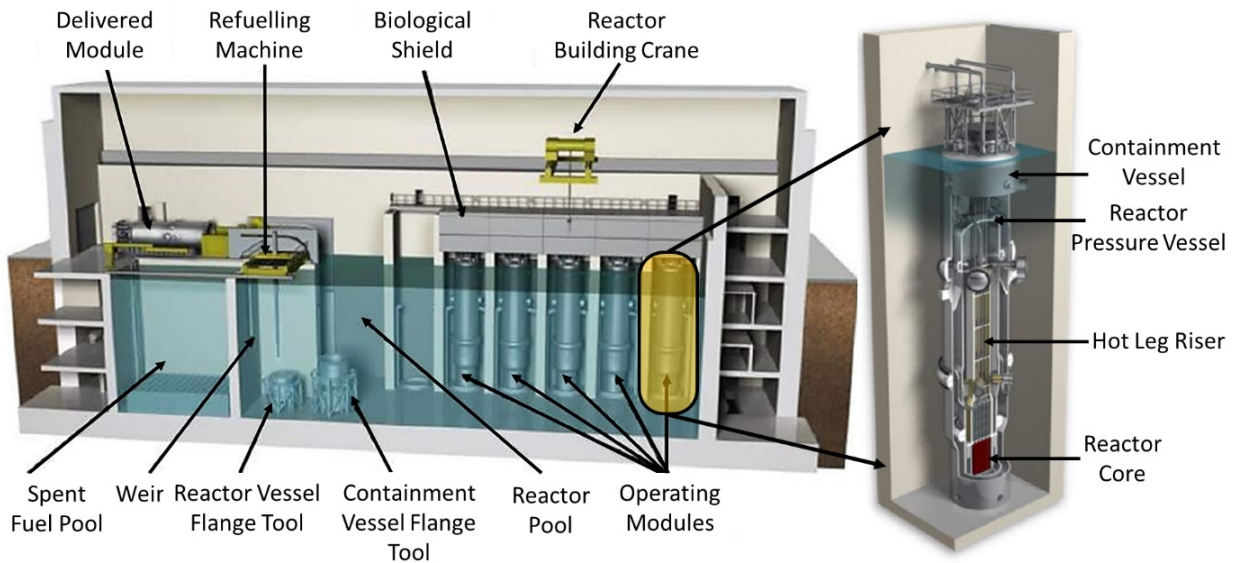


**Figure 1.2:** Integral pressurized water reactor—schematic of NuScale SMR (reproduced from [18] with permission from NuScale Power, LLC)

SMR plant could be constructed as a single or multi-module plant and have incorporated the enhanced or inherent safety designs. The integral reactor designs, such as with integral pressurized water reactors (iPWRs), largely reduce the loop piping and external components leading to the compact containment and enhancing the safety of the reactor structure. SMR designs with passive safety features include natural circulation of coolant flow under all operating conditions, eliminating the risk associated with the failure of circulating coolant pumps [28]. Superior thermal efficiency is achieved with the use of helical coil steam gener-

ators (HCSG) submerged in water and once-through counter-flow design without using the reactor coolant pumps [15]. One of the design concepts is that of the reactor pool with multiple independent modules submerged in the pool, as shown in Fig. 1.2. The NuScale power modules shown in Fig. 1.2 are each rated at 50 MWe scalable to 12 modules in a single facility.

## 1.2.2 Flexible Operation

### 1.2.2.1 General Concept

The steady balance between generation and consumption is a necessity of an electrical grid. For the electrical grid to sustain, some generation units should be able to vary their electrical power output. For some generation schemes, it is not technically or economically feasible to frequently vary their output and thus are operated at constant output close to full rated power, referred to as baseload plants. Traditionally, the generation units only had to respond to the continual electrical load variation, grid disturbances, and generation contingencies. With the power system shifting towards highly variable and uncertain RESs such as wind and PVs, the burden of flexible power has been increased for the generation units participating in the flexible operation.

Flexible operation includes voluntary or involuntary power change of different duration and periodicity executed by a generation plant in response to the grid requirements. Generation units may need to adjust their outputs in different timeframes in hours, minutes or seconds. Fig. 1.3 shows the typical form of daily flexible operations the generating units have to offer, which can be placed in two categories: frequency control and load following. The frequency control invokes the change in generation output in response to the frequency disturbances. The frequency deviation is indicative of the necessity of the change in generation output. Hence, the power output is varied using the closed-loop governor system with frequency as the feedback. The frequency disturbances are fast and occur frequently, but usually require a smaller change in generation. The power variation for frequency control is usually limited within  $\pm 10\%$  of generator rated output.

On the other hand, the load following requires a slower change in generation output com-

pared to the frequency control. The load following could happen in a planned or unplanned way. The changes could be large or small, but the generation units usually have sufficient information to decide the magnitude and rate of the variation in advance.

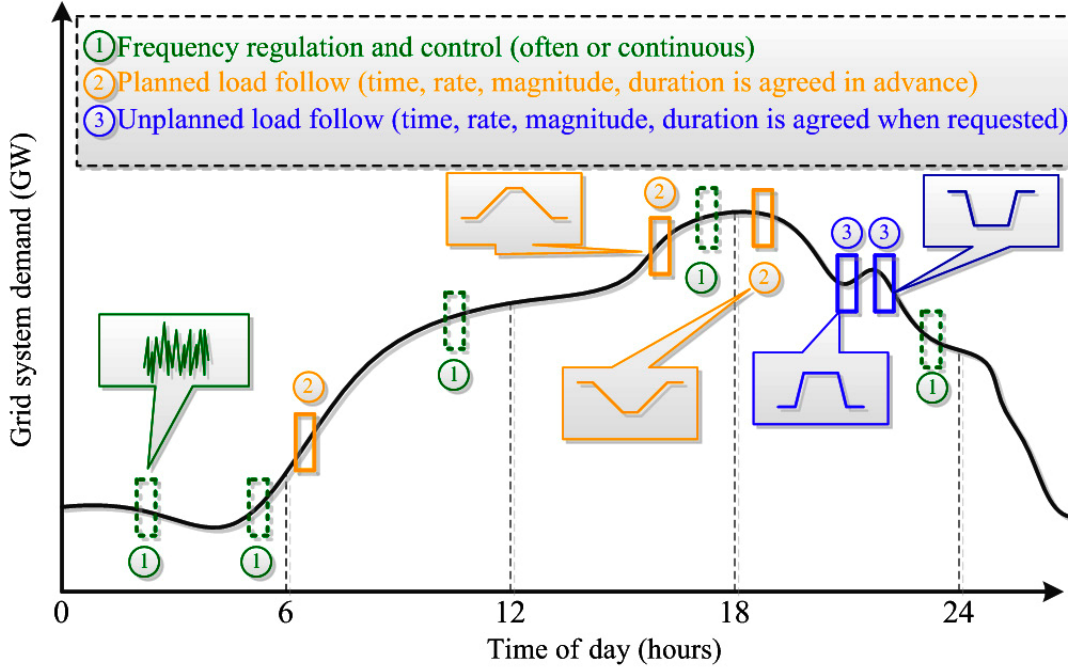


**Figure 1.3:** A typical example of daily flexible operation (reproduced from [18] with permission from IAEA)

### 1.2.2.2 Experience and Challenges with NPPs

Historically, NPPs in North America were operated as baseload plants. Although not designed to follow load frequently, the CANDU based NPPs in Canada have demonstrated the load following and load cycling potentials in the past [29–31]. Back in the 1980s, reactor units in Bruce B experienced nine months of load-cycling for up to 60% rated electrical output (REO) of reactor power reductions [29]. Chalk River Laboratories based assessment concluded that the reactor fuel could withstand such daily and weekly load cycling [31].

The power maneuvering capability of NPPs for electrical demand variation was discussed in several past IEEE PES publications, such as [32–35]. Reference [32] showed the suitability of conventional PWRs for various power maneuvering operations, including load rejection, small step load changes, day/night load follow cycle and rapid power changes. It concluded

that the conventional PWRs are more than capable of varying their outputs to meet the fluctuating demands, and the steam bypass is not needed for power change of up to 20% REO. Reference [33], on the other hand, modeled a CANDU reactor of Pickering Nuclear Generating Station and tested the model for grid disturbances along with the short term frequency response and load following capabilities. The reactor-follow-turbine mode was concluded to be a preferred operation mode of the reactor for the frequency regulation as it offered a faster response. Reference [34] focused on different control methods for co-ordinating the reactor control with the turbine valve operation to improve the reactor's response during the islanding event. Reference [35] used a multivariate control strategy for an advanced boiling water reactor (ABWR) for load following and frequency regulation. The step changes of 40% increase and 50% decrease were simulated at a ramp rate of 10% REO/min. It showed that the power control above 70% REO power level could be achieved without the control rod operation.

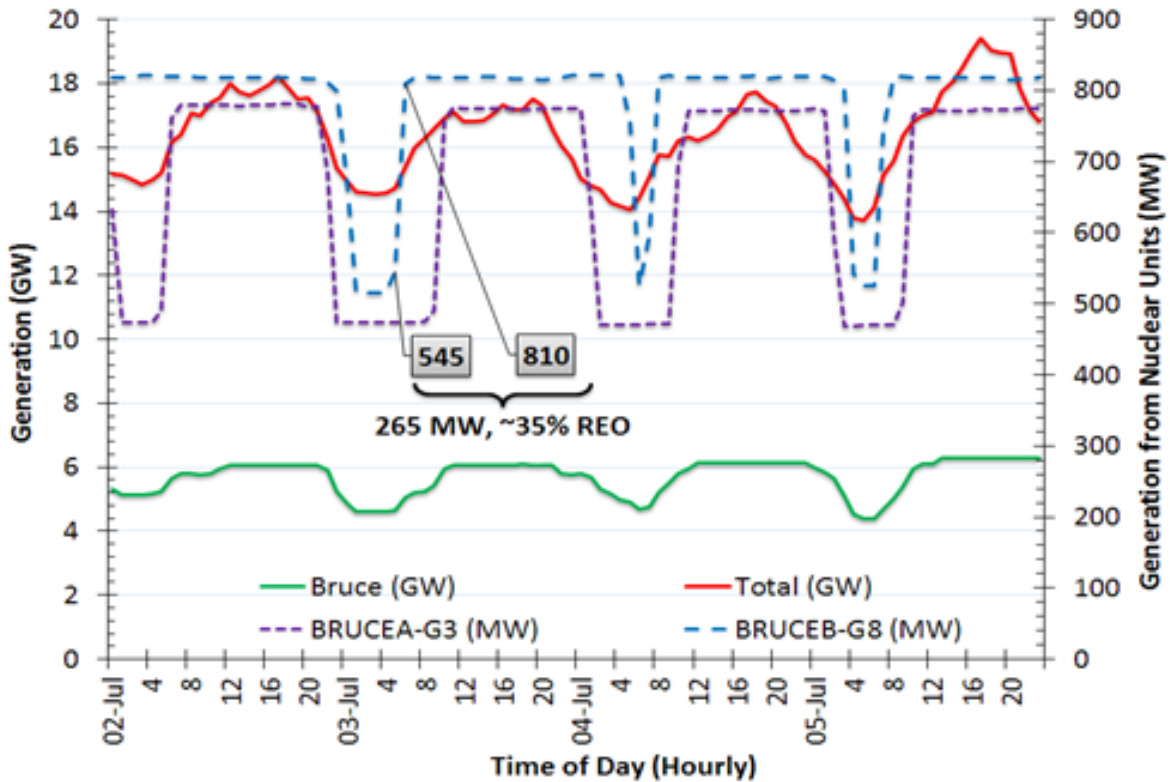


**Figure 1.4:** Planned load following by Bruce Nuclear Generating Station

More recently, the Bruce Nuclear Generating Station in Ontario, Canada, had contributed

to planned load following requirements in July 2015. Fig. 1.4 shows the total demand and the overall response of Bruce Nuclear Generating Stations in GW (axis on the left), whereas the large change in the output of two units of Bruce NPP – namely G3 and G8 – are in MW (axis on the right). The load following has caused a reduction of power close to 35%REO for each unit. However, it should be noted that the SMR’s flexible operation in isolated or weakly connected grids will be more stringent with the increasing RES.

It is essential to understand various underlying challenges of flexible operation with NPPs. Flexible operations in NPPs can be achieved with the following means: taking one or more modules offline, maneuvering reactor power for one or more modules with reactivity control, and bypassing the steam directly to the condenser to compensate rapid changes in electrical demand [25]. These options are the basis of flexible operations for all of the conventional reactor designs and the newer reactor designs coming up in the future.

The control rod operation comes with its own set of issues. Frequent use of control rod for large power variations leads to thermal fatigue and ageing of the reactor system, structures and components [17, 18]. The control rod operation induces the core power redistribution affecting the power densities along the core length, which could have a significant impact on fuel safety limits. Similarly, the reactor power variation influences the thermal expansion of fuel pallets imposing the pallet cladding hard contacts, which could result in cracks and mechanical failure of the cladding. This cladding stress is proportional to local power density, which is affected by the control rod operation. The frequent use of the control rod could also induce shadow corrosion, which could distort the channels and ultimately cause the hard contact between core components and the supports.

The counter reactivity of fuel and moderator temperatures pose a challenge in reactor control. Moreover, the temperature variation in the primary circuit results in a change in coolant density hence changing the boric acid concentration making the power control even more difficult. Fission product poisoning due to Xenon-135 ( $^{135}\text{Xe}$ ), a strong neutron absorber produced during the fission of heavy nuclei, adds another challenge to the reactor power control. Another fission product Iodine-135 also decays to  $^{135}\text{Xe}$  in 6-7 hours. The variation of negative reactivity due to  $^{135}\text{Xe}$ , thus, lasts for several hours of power variation, which poses a significant challenge for reactor power control. Further, the variation in the

axial distribution of  $^{135}\text{Xe}$  with control rod movement also aggravates the problem. Similarly, the frequent use of the turbine bypass system for the power control results in additional wear and tear of the condenser shell and tubes, steam bypass lines, and the associated valves [18]. Due to these various challenges, the reactor control is regulated with various limits in terms of the size of variation, ramp rates and the total number of maneuvers.

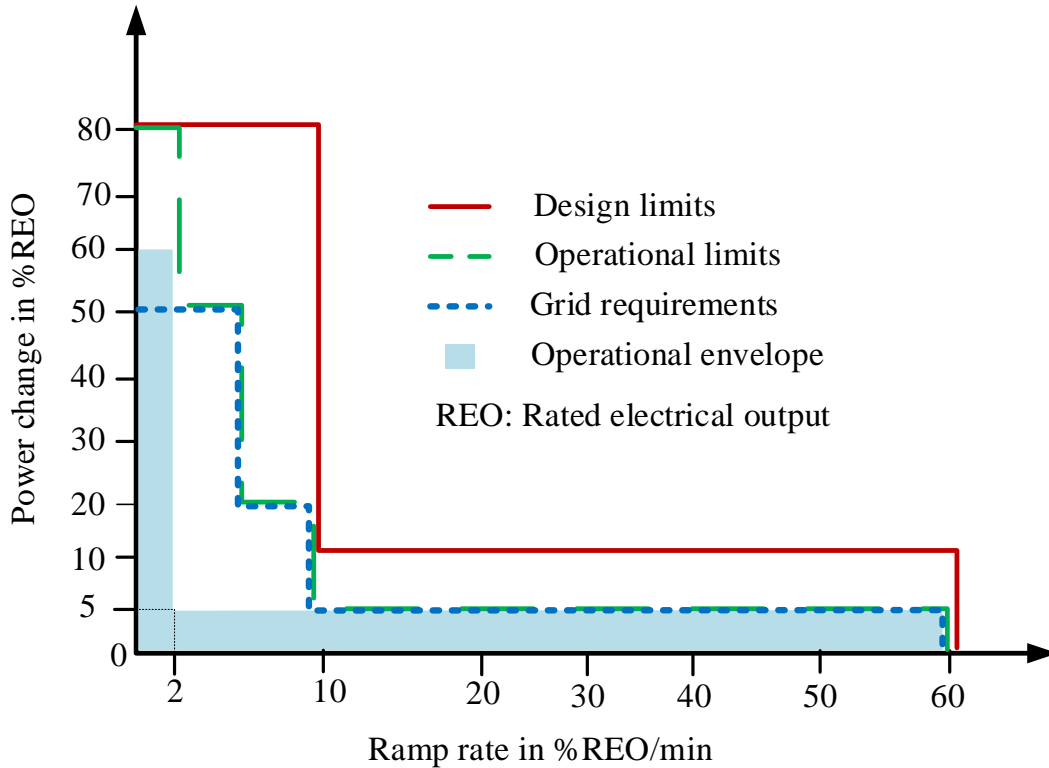


**Figure 1.5:** Flexibility requirements and design limits of German PWRs [18]

Some NPPs in Europe have been participating in flexible operations in both load following and frequency regulation modes for several years now [36]. Fig. 1.5 shows the flexibility scheme and the design limits of a German PWR in terms of ramp rate and total power changes. The graph shows the operational and design limits approved by the regulatory body with a comprehensive safety analysis test during commissioning. As seen from the graph, if the power change is small, large ramp rates could be used, which is the case of load following. However, if the power change is large, lower ramp rates should be used, which is the case of frequency regulation. The design limits are the power variation limits for the reactor based on the design safety criteria. The operational limits are set well below their design

limits while fulfilling the grid requirements. In actual operation, however, the NPPs usually operate within the planned range of frequency control and load following, as shown by the blue shaded region.

As per the recent IAEA report [18], the new generation NPPs equipped with advanced load follow control (ALFC) can offer demand variations of up to 20%REO with ramp rates of 60%REO/min. Similarly, a load follow control simulated in [37] shows the 100 MWe SMR offering power change as of 80%REO with ramp rates of up to 80%REO/min. With the improvements in control technology and new power maneuvering schemes, the design limits of SMR will continue to improve over a foreseeable future.

### 1.2.3 Synergy with Renewables

Nuclear and renewables are two technologies contrasting in various technical facets; however, they have a combined goal of providing low-cost electricity without emitting GHG. The electrical power from renewable energy resources, such as wind and Photovoltaic (PV), depends on the weather parameters like wind speed and solar irradiation, making them intermittent and non-dispatchable. Fig. 1.6 shows a typical variation of wind speed and solar irradiation for a 24-hour period. The electrical power output with these profiles could vary as high as 70% of the installed size of the wind and PV plants within a minute duration. Besides, the inverter-based generation from wind turbines and photovoltaic panels inherently lack the inertia necessary for the power system stability [38–40]. The NPPs have always been excellent baseload plants and provide inertia to the power system to maintain stability. However, they traditionally did not offer flexibility to complement the generation intermittency imposed by the renewable generation.

The hybrid energy system research by Joint Institute for Strategic Energy Analysis (JISEA), [41] explored the synergy with nuclear power and renewables discussing various possibilities of industrial applications such as hydrogen production and energy for transportation. It also explored the non-technical aspects of small modular reactors deployment in commercial and military usage. It indicated that the nuclear-renewable mix is economically advantageous with the reduced requirement of electrical power storage and peak power generation units if economically modeled using flexible industrial components.

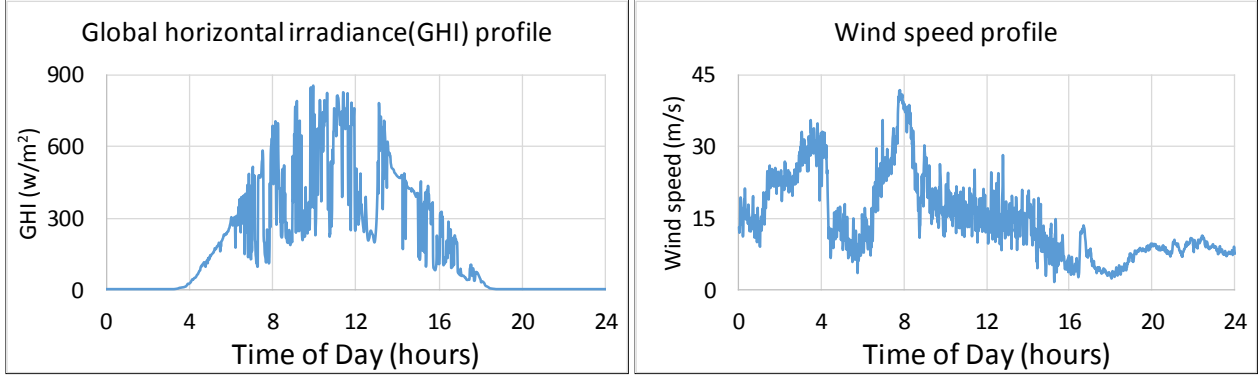


**Figure 1.6:** Typical variation of wind speed and solar irradiation in a day

Reference [42] explored opportunities with nuclear-renewable hybrid energy system (NRHES) with six different interaction modes, namely the interactions among various interconnection modes such as thermal, electrical, chemical, hydrogen fuels, mechanical and information for the opportunities and issues, cost-benefit scenario, and the possibility of flexible operations. The electrical storage such as pumped hydro energy storage, battery energy storage and compressed air energy storage on the electrical side, thermal storage on the steam side, scheduled hydrogen production plants to utilize the steam during off-peak periods were mentioned as means to support the flexible operation. The crucial role of information technology, generation-demand forecast, grid monitoring and management system, energy market information synthesis and the time-based intelligent industrial and electrical production schedules to realize the benefits of hybrid energy systems were also discussed.

Under the NRHES project, two hypothetical NRHESs, one based on Texas gasoline, and the other one based on Arizona desalination were analyzed and reported in two-part reports, [43] and [44]– [43] evaluating the dynamic performance, while [44] analyzing the financial aspects. For both scenarios, RESs variability was smoothed using the battery energy storage modelled as a low pass filter with different time constants. The requirement of battery storage was the tradeoff of the power smoothing requirement and the cost involved. The dynamic performance was tested based on the NRHES’s ability to provide electrical grid frequency stability, operating reserve capacity, and load following ramps while hosting renewable penetration. The hybrid system offered RES penetration more than 20% for Texas Gasoline while more than 14% for Arizona desalination. The NRHES Texas could

offer operating reserve capacity up to 25% to the ancillary market while NRHES Arizona could offer up to 16%.

For financial assessment, the two NRHES scenarios were compared against the case where the energy is offered by a decoupled natural gas based system. The NRHES were found to be financially profitable in most of the cases and were very attractive if the carbon cost is considered. The incentive offered under flexible electrical power generation plays a significant role in a system coupled with variable renewable energy to decide the full hybridization with industries. The opportunity cost of not producing industrial products to offer resource adequacy and flexibility to the electrical grid could be too high considering the additional cost necessary for the subsystems to facilitate the flexible operation. It however also depend upon the industrial product and could be beneficial for different market scenarios.

The third scenario reported in [45], proposed that the heat produced by NRHES on Texas is sold to the industrial customer instead of producing gasoline. For the fourth scenario, a hydrogen production plant is chosen as an industry to couple with NRHES. The report in [46] provided the dynamic modeling for the high temperature steam electrolysis (HTSE) plant for hydrogen production, which is one of the highest priority industrial processes. The dynamic operability and controllability of the proposed scheme was analyzed with the system and component models under the step load changes, RES variations, and load following operations. The gas turbine power plant (GTPP) was employed to support the frequency regulation for fast changes. The HTSE plant was found to be capable of dynamically apportioning thermal and electrical systems to offer flexibility to the electrical grid while also producing industrial products without generating GHGs. Similarly, the GTPP covered the rapid dynamics of grid demand, which the other systems could not follow.

Considering SMR's capability to offer excellent load following and frequency regulation responses, it can host large renewable penetration, even with the uncertainty and intermittency in RES. The frequency responsive control strategies such as wind inertia and control will also help the cause by participating, even though marginally, in stabilizing the system frequency during disturbances [47]. The prospect of SMR-renewable synergy is solid, with manufacturers like NuScale working on the design features of SMR to enhance the response rates [25, 48].

## 1.2.4 Dynamic Model for Power System Studies

The IEEE standard turbine-governor models used for thermal plants in power system simulations approximate the source dynamics prior to the turbine valve and represent the entire steam generation process with a first-order transfer function characterized by a time constant [49]. The mechanical power output of the turbine is considered a linear function of the valve position, and the steam pressure at the turbine inlet is assumed constant. The simplification only works for smaller disturbances in an interconnected system with a large number of flexible generators where each generating unit has a minimal responsibility to vary their power. When the generation plants have to respond to large demand variations, the dynamics represented by the approximated turbine-governor models would be inaccurate [49]. In response, TGOV5 turbine-governor model, as an example, was developed to accurately represent the steam turbine and boiler system by modeling the internal behavior of the fuel system.

There have been numerous models of conventional NPPs developed for thermodynamic studies. Since the NPPs were predominantly used as baseload plants and rarely used in flexible operation, very few attempts were made to integrate the reactor model with turbine-governor models for grid-integration studies. However, the need for dynamic model of NPPs and its essential role for power system dynamic studies were highlighted in a number of past key IEEE PES publications such as [50, 51]. References [50, 51] present the dynamic models of conventional NPPs for power system studies. Given the NPPs were mostly operated in baseload mode, these models were intended to simulate the reactor dynamics during the electrical disturbances rather than to incorporate the influence of reactor steam pressure transients in power system dynamics. Central Research Institute of Electric Power Industry (CRIEPI) based light water reactor model to represent pressurized water reactor (PWR) and boiling water reactor (BWR) in [50] was aimed for short-term stability of the system focusing on large disturbances such as faults isolating the NPP from the electrical grid. Such large disturbances lead to the rapid operation of the turbine valve introducing large temperature, pressure, and reactivity transients inside the reactor.

Electric Power Research Institute (EPRI) and CRIEPI based joint publication, [51], was

an extension of the NPP model in [50] for mid to long-term stability of the power system focusing on smaller disturbances. Two sources of disturbance were considered. The first one is an occasional governor action which disrupts the thermodynamic balance between primary and secondary of the reactor, introducing the transients inside the reactor. The second one is due to the grid frequency and voltage transients, which introduce the flow transients inside the reactor as the coolant re-circulation pumps are operated with the auxiliary systems powered from the electrical grid.

Recent publication [52] also attempted to integrate the NPP model in power system simulation. The pressurized water reactor (PWR) model proposed in [52] was simulated against small and slow changes with total NPP response within 5% of its rated electrical output (REO) and the ramp rate limited to 30% REO/minute. The NPP models such as in [53], [54] and [55] were also used for power system studies, but have similar limitations of small and slow variations. The SMR models proposed in [56, 57] represent the reactor dynamics in finer details. The 45 MWe NuScale SMR module proposed in [56, 57] models the important features of the reactor such as the natural circulation of the primary coolant and a moving-boundary steam generator with three distinct fluid state sections on the secondary side, namely sub-cooled region, two-phase mixture, and the superheated region. However, the models are intended for thermodynamic studies and not integrated with the turbine-governor for power system studies.

Similarly, the 100 MWe SMR model developed in [37] simplifies the thermodynamic relations for controller design. Model of NHR200-II in [58] is a cogeneration based 200 MWth reactor, with the valve bypass system in the secondary circuit supporting the district heating system and facilitating the faster response to the steam demand from the turbine.

While the SMR models available in current literature were proposed for the different kinds of applications, none of them have been integrated into the power system for power system dynamic studies. In a nutshell, there is a need for detailed SMR dynamic models that can be integrated into standard turbine-governor models for the accurate and reliable representation of SMRs in the power system studies.

### 1.2.5 Energy Solution for Isolated Communities

The flexibility in size and the modularity of SMR can help replace diesel generator based power in remote and isolated communities. SMRs are being proposed to be deployed in the northern territories of Canada for industrial mining and rural electrification, and they are expected to unlock the vast social and economic benefits [59]. With secure but flexible power from SMR, the system could be explored for hosting local distributed RES. The modular units of SMR could be added incrementally with time to increase the plant capacity to match the increasing energy demands of remote communities. The compact size of fuel and longer refuelling time adds an advantage for the deployment in remote communities where transportation is one of the major problem. A 4S (super-safe, small and simple) reactor, for example, has a refuelling time of 30 years of operation in full power [15].

The improvements in cogeneration technology make SMRs suitable for diverse energy applications, which boosts the financial payback and strengthens the load following capability of SMRs to host RESs [60–66]. For remote communities with limited access to the electrical grid and natural gas pipelines, the prospect of SMR for heat and electricity seems even more promising. The integrated pressurized water reactor (iPWR)- based SMRs such as NuScale can provide low temperature heat suitable for district heating (DH) [66]. In addition to various power maneuvering schemes of SMR [25], the coordination of steam usage for electricity and district heating, supported by electrical and thermal storage, can effectively fulfill the flexibility requirements while keeping the reactor dynamics within design limits. With flexible size, modularity, improved power maneuvering capability, cogeneration based district-heating scheme and capacity to operate for years with each fuel cycle, SMRs could play a vital role in developing sustainable energy systems in remote communities [67].

SMR usage for heat and electricity is investigated in some recent references, such as [22, 58, 68, 69]. Reference [68] analyzed the techno-economic aspects of different reactor technologies, while [22, 69] proposed the thermodynamic models of cogeneration system for heat and electricity with various SMR technologies. While the above references propose the SMR model for heat and electricity, there is a lack of research investigating the operation of co-generating SMR in practical energy systems.

Firstly, there is a need for proper simulation models of cogenerating SMRs. The models should accurately represent the electrical, thermal and reactor side characteristics and integrate with the electrical and district heating system models in standard software platforms. Secondly, the operation schemes have to be designed to optimally utilize and coordinate various system components under normal and abnormal operating circumstances. Finally, a comprehensive planning and dynamic study should be conducted using the proposed simulation models for validating the SMR-renewable combination for the supplement of heat and electricity requirements of isolated communities [23].

## **1.2.6 Siting and Sizing in Electrical Grids**

SMR offers a viable, clean energy solution for large as well as small electrical grids. Many Canadian utilities, such as SaskPower, are weighing on the possibility of having SMRs in their electrical system with most of the coal-based thermal plants set to be decommissioned in the near future. Introducing new technology into the system requires a comprehensive investigation of the probable issues. Fig. 1.7 shows various aspects that should be considered for SMR's site selection. These aspects are discussed below as non-electrical and electrical grid considerations.

### **1.2.6.1 Non-Electrical Considerations**

The siting of SMR requires assessments focusing on various non-electrical aspects such as geographical, geological, environmental, regulatory and legal considerations [59, 70–73]. The current evaluation criteria for SMRs differs from conventional NPPs mainly on required cooling flow [73].

The geographical aspect of SMR siting involves Geographical Information System (GIS) based multi-criteria decision making in terms of various criteria such as population density, access to transportation, access to the electrical grid and the presence of surface water. The potential sites are given scores in each criterion based on their favorability to the corresponding criteria. Finally, weights are assigned to each criterion, and the final siting grade for each site is obtained. The sites selected should be accessible to ground transportation. As SMR modules are factory-made, the selected site should have easy access to rails or heavy trucks to

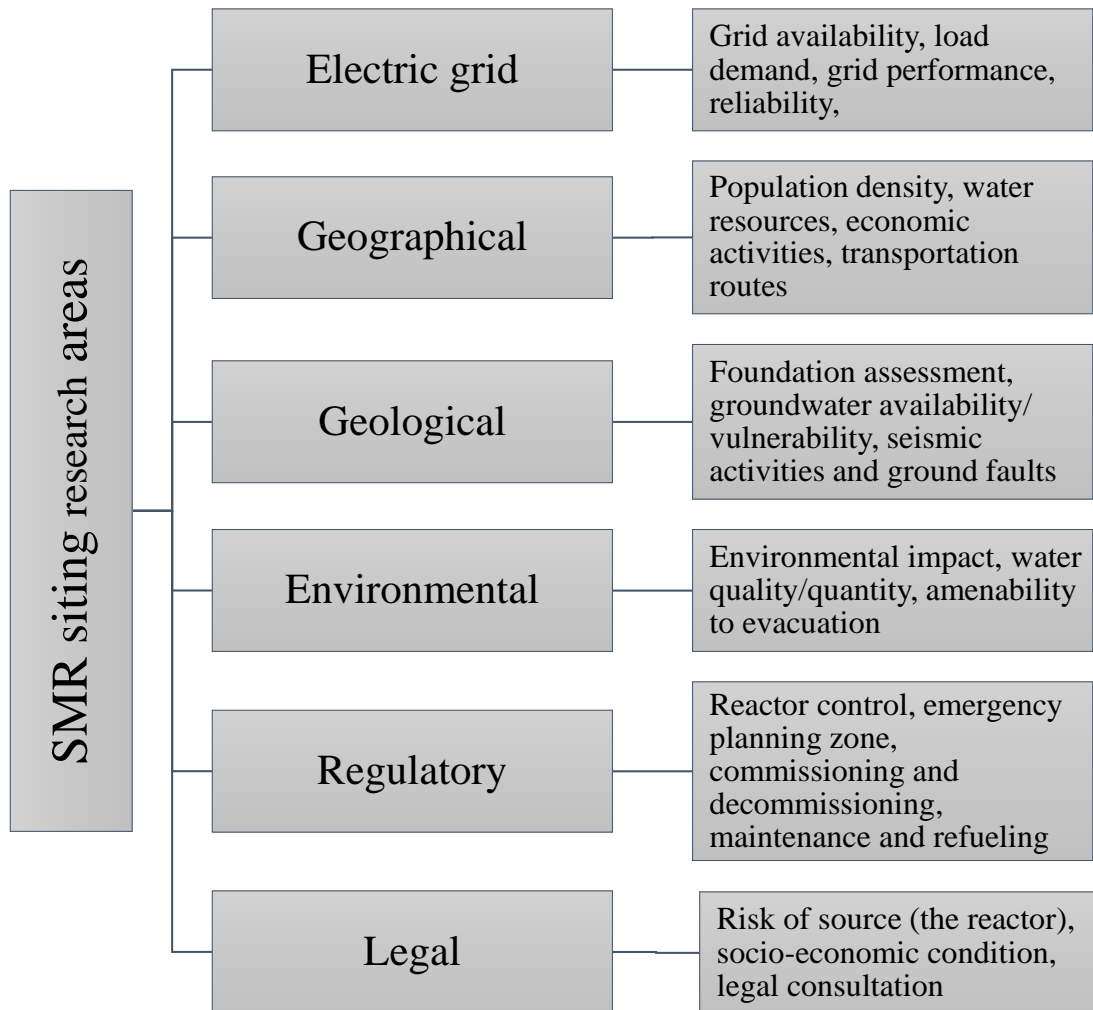


**Figure 1.7:** Research areas of SMR site selection [70]

transport the modules to the siting location. The preference should be given to the shortest route to ensure the minimum cost of transportation. Additionally, the transportation route should be selected to reduce the risk of nuclear materials exposure to the population and environment.

Under geological consideration, the surface and subsurface geological conditions of potential sites are analyzed. The characteristics of glacial deposits and mass wasting phenomena significantly impact the stability of a site. The natural geological phenomena such as earthquakes and faults and anthropogenic activities such as mining should be identified. Climate change should be adequately assessed before validating the sites. The accurate forecast is necessary to identify the temperature, precipitation and flooding at the

potential sites. The sites susceptible to landslides and flooding should be excluded.

SMR plants need water for cooling and heat transport. The site should have the sustainable water capacity available to support SMR plants' operation throughout its lifetime. The risk of decline in water resources due to anthropogenic activities or climate change has to be considered while selecting the site. Adequate water management and advanced reactor cooling facilities can reduce the water requirement and broaden the scope of sites for SMR. The risk of accidental radionuclide release to the water resources also needs to be assessed. An assessment is necessary to analyze the vulnerability of groundwater and the hydrogeological properties of the potential sites.

The exclusion zones are usually demarcated around a nuclear facility to minimize radioactive exposure to the public for any unforeseen nuclear accidents [74]. The conventional NPPs based on CANDU reactors consider the exclusion zone radius of at least one kilometre. Modern SMRs with inherent and passive safety features aim to minimize or even eliminate the emergency zones. The risk of radioactive exposure with SMR based NPPs is significantly reduced with the use of coated fuel particles, large negative reactivity coefficient of SMRs, passive decay heat cooling, passive emergency shutdown system, and the placement of reactor underwater, underground and with concrete double-wall containment.

The legal aspects of SMR siting include general regulatory and liability issues and the distinctive set of issues that might arise in the context of indigenous communities. The impact of provincial and federal stand on this novel nuclear technology has to be properly assessed.

#### **1.2.6.2 Electrical Grid Considerations**

In the context of electrical grid-based assessments, the SMR's siting problem is combined with the sizing problem. The siting and sizing of SMR are analyzed in three different aspects: steady-state, dynamic, and safety.

The steady-state aspect includes the demand-supply adequacy in the short-term and long-term, minimization of transmission loss, reduction in carbon-based fuel consumption, and improvement in the reliability of the power supply while meeting various operational constraints. The system adequacy evaluation considering single and multiple contingencies

with reasonable spinning reserve resources would also fall under steady-state assessments. The placement and size of SMR should be optimized such that the upper and lower voltage violation limits and the transmission line thermal limits are not exceeded under the reasonable contingency level (N-1, N-2, and N-3) considered for the system. The site-specific factors such as the hosting capacity of the transmission infrastructure, load demand of the regional pockets, and the generation congestion must be considered while introducing a new plant in the system. Additional resources such as transmission lines and reactive compensation could help the system host SMR while keeping an agreement with North American Electric Reliability Corporation (NERC) compliance. Issues with SMRs in weak grids under abrupt contingencies, such as power evacuation problems as discussed in [75] are also explored as a part of the steady-state aspect of siting and sizing problem.

The dynamic aspect includes the impact of SMRs on power system stability and dynamics. An SMR, with inertia, load following and frequency response capabilities, can improve the dynamic performance of the system. The size of an SMR at an electrical node is capped by the dynamic limits of voltage stability and transmission line loading capability. An oversized or improperly placed SMR may violate the power system limits with frequency and voltage fluctuations, and potentially leading to a system-wide blackout. The frequency and voltage response under contingencies with SMR have to be evaluated and verified against the interconnection obligations set by the NERC. The initial rate of change of frequency (ROCOF), frequency overshoot and nadirs, settling frequency, time-based frequency measures, and other frequency response metrics are defined under BAL-003 and PRC-024 standards as the dynamic responsibility metrics of an individual entity in an interconnection [76, 77].

The safety aspect of SMR siting analyzes various sites in terms of their capability to keep SMR safe under normal and abnormal circumstances. The probabilistic safety assessment (PSA) is used to analyze various nuclear events in terms of their potential to lead to nuclear accidents. The International Nuclear Safety Advisory Group (INSAG) has set the lower threshold of core damage frequency (CDF) of  $10^{-5}$  per reactor-year for all future reactors [78]. In response to 2011 Fukushima Daiichi nuclear accident, the nuclear regulatory bodies have set even stricter risk levels for NPPs [10, 79, 80]. NPPs are equipped with an emergency cooling system to safely shut down the reactors in case of nuclear accidents. Some modern SMRs

implement passive safety features to reduce the reliance on the power supply to cool down reactors during an emergency shutdown. However, the emergency cooling system is essential to increase the speed of decay heat removal for such systems. The emergency cooling system is supplied with multiple power sources to ensure its availability under any circumstances.

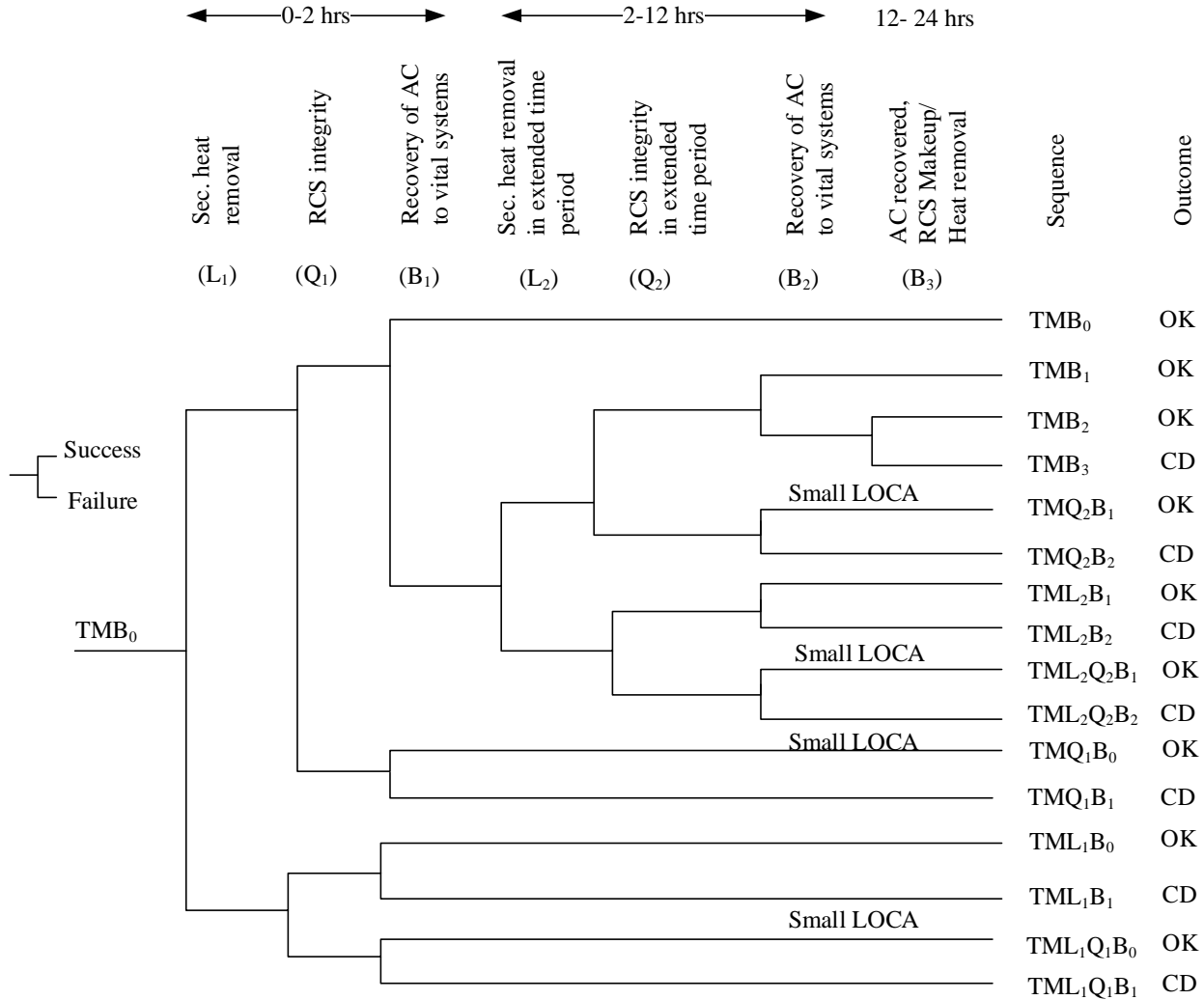


**Figure 1.8:** A generic event tree for SBO in NPP [81]

Offsite power is one of the major sources of power for the emergency cooling system, crucial in maintaining safety during emergencies. Risk analysis performed for conventional NPPs shows that the loss of all ac power, a station blackout(SBO) scenario, is a significant contributor to the risk of core damage (CD), contributing as much as 70% of cumulative risk in some of the plants [81]. Fig. 1.8 shows the generic event tree following the SBO event in an NPP station. It was found that the core damage probability in 2- 12 hours following the

SBO event is as significant as the early failures. In any case, the restoration of offsite power ensures safety, while the inability to recover the offsite power results in core damage. Thus, both the loss of offsite power (LOOP) probability and subsequent restoration time must be considered while selecting the plant site.

Although SMRs have improved safety schemes compared to the conventional NPPs, a reliable offsite power supply is still essential to ensure transience in the system does not lead to a nuclear disaster. This aspect, thus, focuses on an approach analyzing the reliability of the offsite power. The objective is to formulate a simple way to compare various sites in terms of their capability to keep SMR safe. The potential hosting sites for SMR could be compared in terms of their capability to avoid SBO scenario based on the offsite power failure rates and restoration times.

### 1.3 Research Objectives

This research aims to develop the simulation models and investigate energy mix scenarios with SMR and RES, including investigation for the siting and sizing of SMR. To accomplish the above overarching goal, the objectives of this Ph.D. research are:

1. Investigate the synergistic mix of SMR and distributed PV generation to develop sustainable clean energy systems in remote and isolated communities by taking advantage of smaller size and flexible operation of SMR.
2. Develop an integrated dynamic model of an SMR based NPP to investigate internal reactor dynamics for small and large electrical disturbances.
3. Investigate the optimal operation of SMR-RES hybrid energy systems, supported by the battery energy storage system (BESS) and thermal energy storage (TES), to supplement the heat and electricity needs of isolated communities. Evaluate the optimum size of RESs (wind and PVs) that could be hosted in such hybrid energy systems.
4. Investigate steady-state, dynamic and safety aspects of siting and sizing of SMR in electrical grids.

The **first objective** is discussed in Chapters 2 and 3. Chapter 2 provides an overview of SMR technology and its potential synergy scenarios with renewable energy sources along with a case study investigating the SMR-PV hybrid energy system in an existing remote feeder in northern Saskatchewan. The benefit of electrical energy storage (EES) as an enabler to bridge two different generation technologies—SMR, firm and dispatchable but flexible operation constrained by techno-economic boundaries and PV, intermittent and non-dispatchable—is quantified in terms of the improvement in the plant load factor. In Chapter 3, the aspects of the flexible operation is further explored by investigating the flexibility requirements of a remote community with PV generation in terms of load following and frequency regulation, and juxtaposing them against the flexible operation capability of SMRs.

The proposed application of SMR with intermittent RES in isolated communities results in large and frequent disturbances that SMR has to respond to. The adaptation of standard approximated turbine-governor models to represent SMR dynamics can result in inaccuracies in dynamic response. Hence, a dynamic model of SMR is proposed for power system studies in Chapter 4, as the **second objective**.

The **third objective** is discussed in Chapters 5 and 6. In Chapter 5, the dynamic model of SMR is further developed by including steam bypass and steam extraction system and integrated into a hybrid energy system model consisting of power system components (electrical grid, wind, PVs and BESS) and DH system components (heat exchange stations, TES and DH pipeline). In Chapter 6, a multi-timescale operational scheme is proposed, and a multilevel optimization problem is formulated for the optimal operation and RES hosting in the proposed hybrid energy system.

While the first three objectives focus on the opportunities with SMR in remote communities or isolated systems, the siting and sizing of SMRs in electrical grid are analyzed in Chapters 7 and 8, and Appendix A, as the **fourth objective**. The case system, Saskatchewan Electrical Grid (SEG), consists of two isolated networks, Southern SEG representing a strong electrical grid and Northern SEG representing a weak electrical grid. The steady-state aspect of SMR siting and sizing in a weak electrical grid is discussed in Chapter 7. Chapter 8 discusses the safety aspect of SMR siting and sizing in strong and weak electrical grids. The steady-state and dynamic aspect of SMR siting and sizing in a strong electrical grid is

discussed in Appendix A.

## 1.4 Research Contribution

To accomplish the objective discussed in the Section 1.3, several contributions are made in this thesis. The contribution of each manuscript is elaborated in the respective chapters. However, a summary of the contributions is discussed below.

Although the suitability of SMRs in remote and isolated communities and their synergy with intermittent RES is promising, there is a clear need for comprehensive planning and dynamic studies to evaluate the technical feasibility of the energy mix. The first contribution made in this thesis in Chapter 2 is the exploration of synergy scenarios of SMR-PV hybrid energy system and the role of EES as an enabler to facilitate the proposed synergy. A time-series power flow based steady-state case study quantified the potential benefits in terms of the SMR plant load factor. The second contribution in the context of SMR-PV synergy in Chapter 3 is to evaluate the flexibility requirements of remote micro-communities hosting PV generation, and SMR's potential to fulfill those flexibility requirements. The literature study is conducted to understand the challenges and experiences of flexible operation with conventional NPPs. The operating limits of SMR in both load following and frequency regulation modes are extrapolated from the operating limits of conventional NPPs and validated with the standard SMR simulator provided by the IAEA. Based on the steady-state and dynamic performance, the maximum RES hosting capability with SMR's flexible operation is identified.

While there is a clear need for a detailed dynamic model of SMR for power system studies, very few attempts were made to integrate the SMR dynamic models with turbine-governor models in power system simulations. The third contribution in this thesis in Chapter 4 is to develop a detailed thermodynamic model of SMR and integrate it with the standard turbine-governor model in PSS®E software. The model is validated using the standard SMR simulator provided by IAEA.

The fourth contribution made in this thesis in Chapter 5 is to develop a comprehensive SMR-RES hybrid energy system model for the integrated heat and power simulation. The

hybrid energy system included the dynamic model of cogenerating SMR, a quasi-static model of DH system, wind, PV, BESS and TES. A case study demonstrates the application of the proposed model in a modified IEEE 30-bus test system. A multi-timescale simulation approach is also proposed to decouple the simulation in load following and frequency regulation modes. The fifth contribution in the context of SMR-RES hybrid energy system in Chapter 6 is to formulate a multilevel optimization problem for the optimal operation and RES hosting in the hybrid energy system considering the steady-state and dynamic constraints based on reactor, power system and the district heating system. The proposed optimization scheme is implemented in a modified IEEE 30-bus test system with a month-long generation and demand profiles.

The sixth contribution made in this thesis in Chapters 7 and 8, and Appendix A is to develop a framework for siting and sizing of SMR in strong and weak electrical grids without previous nuclear facility. In this thesis, the electrical grid considerations of the siting and sizing problem are analyzed, focusing on steady-state, dynamic, and safety aspects. The framework consists of various scores ranging from the avoidance of a site to the degrees of suitability.

## 1.5 Thesis Organization

This thesis consists of four parts. Part-I consisting of Chapters 2 and 3 discusses the synergy between SMR and RES. Part-II (Chapters 4) discusses the dynamic model of SMR for power system studies. Part-III comprising Chapters 5 and 6 and investigates the SMR based hybrid energy system for electricity and DH. Part-IV consisting of Chapters 7 and 8, and Appendix A discusses the siting and sizing of SMR in electrical grids.

The individual chapters of this manuscript-style thesis are organized as follows:

Chapter 2 entitled “Exploring Synergy Among New Generation Technologies– Small Modular Reactor, Energy Storage and Distributed Generation: A Strong Case for Remote Communities” provides an overview of SMR technology and its synergy with distributed renewable energy sources with the case studies exploring SMR-PV-EES hybrid system scenario in an existing remote feeder in northern Saskatchewan. In this work, a combination of SMR and

PV is identified for the case system using the steady-state hosting capacity analysis. The results are shown to assess the EES's role as an enabler of the synergy in terms of SMR's plant load factor.

Chapter 3 is titled "Investigating Small Modular Reactor's Design Limits for its Flexible Operation with Photovoltaic Generation in Micro-Communities." This chapter further extends the work in Chapter 2 by investigating the flexible operation (load following and frequency regulation) in remote communities. In this chapter, the design limits of conventional NPPs are reviewed to extrapolate the operating limits for SMR. The flexibility requirement of an isolated community hosting SMR with PV generation is evaluated by considering the "Very Variable" and "Clear Sky" profiles of PV irradiance. A case study is conducted comparing the flexibility requirements of a remote community with the flexible operation capability of SMR to identify the maximum penetration level of PV.

Chapter 4 is titled "A Dynamic Model of Small Modular Reactor Based Nuclear Plants for Power System Studies". This chapter proposes a new dynamic model of SMR for power system simulations. The dynamic model is developed using FORTRAN programming and integrated with the IEEE standard GGOV1 turbine-governor model in Siemens PSS®E software. The proposed dynamic model will have a large impact for investigating future power systems consisting of SMR based NPPs. The dynamic equations of the proposed model were discussed, followed by the steady-state and dynamic validation of the model. A case study is conducted to demonstrate the power system dynamic simulation with the inclusion of the reactor model. The comparative results are shown to illustrate the improvement in system dynamic accuracy with the integration of the reactor model.

Chapter 5 is titled "Small Modular Reactor Based Hybrid Energy System for Electricity & District Heating". This chapter proposes a simulation model of SMR-RES hybrid energy systems for electricity and district heating. The dynamic model of SMR introduced in Chapter 4 is further developed to include the steam bypass system and steam extraction system to facilitate cogeneration. The proposed hybrid energy system model consisted of the steady-state and dynamic models of cogenerating SMR, DH system, wind, PV, BESS and TES. A multi-timescale simulation approach is proposed to decouple the flexible operation in two separate time frames for load following (discrete, quarter-hourly) and frequency regu-

lation (continuous). A case study is shown to demonstrate the load following and frequency regulation with 24-hr load and generation profiles.

Chapter 6 is titled “Optimal Operation and RES hosting in Small Modular Reactor Based Hybrid Energy System for Electricity & District Heating”. This chapter further develops the simulation models developed in Chapter 5 to optimize the operation of the hybrid energy system and increase renewable hosting capacity. A multi-timescale operational scheme is proposed for the flexible operation of the hybrid energy system. An optimization approach is shown for maximum RES hosting capability in the hybrid energy system considering the power system, reactor, and DH system constraints.

Chapter 7 is titled “Analysis for Siting and Sizing of a Small Modular Reactor– A Case Study in Canada”. This chapter investigates various power system issues of hosting SMR in a weak electrical grid. The Northern SEG is considered the test system. A security-constrained loss reduction based optimal power flow is conducted to evaluate the optimal size of SMR for different potential sites. The complementary role of pumped hydro energy storage is also discussed to improve the sizing of SMR at various nodes. Finally, the optimal place and size of SMR in the weak electrical system are evaluated.

Chapter 8 is titled “An approach to assess the reliability of offsite power as a site selection criteria for a nuclear power plant”. This chapter investigates the safety aspect of siting an NPP (including SMRs) in electrical grids. The offsite power, being a critical power source for the emergency power supply of NPPs, has to be reliable in terms of both failure frequency and the restoration times. The offsite power reliability, variable at different sites, is used to evaluate the SBO probability to identify the safest location for NPP in the Saskatchewan province.

Chapter 9 summarizes the research work and provides overall conclusions. It also provides suggestions for future works in this area.

Appendix A discusses the siting and sizing of SMRs in electrical grids as a final report for the funding organization (Sylvia Fedoruk Canadian Centre for Nuclear Innovation). The overall project was led by Prof. Esam Hussein, Dean of Engineering, University of Regina, with my supervisor Prof. Gokaraju as one of the co-principal investigators. The report provides the steady-state and dynamic results of the siting and sizing of SMR in the Southern

SEG, representing the strong electrical grid in the assessment. This work will be presented at a future conference.

# 2 Exploring Synergy Among New Generation Technologies— Small Modular Reactor, Energy Storage and Distributed Generation: A Strong Case for Remote Communities

## Preamble

This study aims to fulfill a part of the first objective of the thesis mentioned in Section 1.3. The contribution of this study to the overall research is to provide an overview of SMR technology and examine the preliminary feasibility of SMR-RES synergy in remote communities based on steady-state aspects.

In this study, the combination of SMR and PV generation for an existing remote feeder in northern Saskatchewan will be evaluated using the hosting capacity analysis. The benefit of including electrical energy storage in SMR-PV synergy will be quantified in terms of the SMR plant load factor. The network and load data of the case system are obtained from the publicly available facility map of the SaskPower system.

<sup>1</sup>A paper based on this work is published in *ASME Journal of Nuclear Engineering and Radiation Science* in February 2020. This work was also presented in *1st International Conference on Generation IV and Small Reactors (G4SR-1)* in November 2018. Dr. Kalpesh Joshi (Postdoctoral fellow (PDF) in the research group) and I developed the methodology under the guidance of Prof. Gokaraju to assess the SMR-PV-EES hybrid energy system's performance in terms of plant load factor. I assisted Dr. Joshi in performing the simulation

---

<sup>1</sup>K. A. Joshi, B. Poudel and R. Gokaraju, "Exploring synergy among new generation technologies— small modular reactor, energy storage and distributed generation: A strong case for remote communities", *Journal of Nuclear Engineering and Radiation Science*, vol. 6, no. 2, April 2020.

studies in PSS®Sincal. Dr. Joshi and I wrote the paper, which was subsequently edited by Prof. Gokaraju.

## 2.1 Abstract

With a steady rise in power demand in remote communities in Canada, utilities are looking for new options to provide a reliable supply of electricity. While distributed generation (DG) is a promising option, scaling and firming up the capacity of distributed generators is essential. Alternatively, small modular reactors (SMRs) can be used as a prime local source of electricity for remote feeders provided they are flexible enough to respond to the fluctuations in demand. Electrical energy storage (EES) can be used as a buffer to absorb fluctuations in demand and generation, and as a critical back-up for the SMR on-site power supply system by replacing the diesel generator sets. The synergy of SMR-EES-DG can be an all-inclusive alternative with a win-win situation for both the utility and remote communities. This paper discusses the technical feasibility of the proposed synergy using an example of an existing remote feeder in Saskatchewan, Canada. The integral pressurized water reactor is considered along with the photovoltaic (PV) generation in an existing remote feeder in Northwest Saskatchewan to estimate the plant load factor of the SMR with and without the PV generation and EES. The results quantify the benefit of having EES support the SMR in hosting more PV generation in remote communities. EES, when used in support of the SMR to host 60% PV penetration, the plant load factor improves by as much as 5%.

## 2.2 Introduction

Sustainable development, as defined in [82], ‘meets the needs of the present without compromising the ability of future generations to meet their own needs.’ The first step towards sustainable development is the decarbonization of the energy sector. Nuclear energy, despite its limitations – such as safety concerns, high capital cost and the need to operate it close to its capacity – remains the most promising and secure carbon-free source of energy [82]. At the same time, renewable energy sources such as wind and solar are on an upswing and are

emerging as an alternative carbon-free source of energy. The integration of non-dispatchable distributed generators in the existing power supply infrastructure poses several challenges due to their inherent variability, uncertainty, and site-specific characteristics [2]. Both distributed generation and nuclear power, have unique benefits as well as challenges. While energy storage is the obvious choice to resolve the issues brought forth by the increasing penetration of distributed generators, the prohibitive costs and a near absence of mature storage technology hampers the energy share of renewable sources. With existing wind power generation at multiple sites in the Saskatchewan grid and the prospect of photovoltaic generators installations in the future, it is worthwhile to explore the benefits of having renewables backed by an SMR in remote communities. The five wind farms in Saskatchewan with the combined capacity of 221 MW typically feed the main grid at medium to high voltage level [83]. On the other hand, the photovoltaic generation is more flexible in size and can be used to feed the local demand while supplying power at the low voltage levels, typically in the range of 230 V to 25 kV. For remote load centres, the option of a grid infrastructure upgrade is the conventional solution for improved reliability of the supply system. However, local photovoltaic generation in remote areas can be a viable and cost-effective alternative. A recent study of a remote feeder in Saskatchewan for photovoltaic distributed generation (PVDG) has shown that the combination of energy storage and PVDG can be a viable technical and economical alternative to infrastructure upgrades [8]. However, without a substantial local generation capacity to act as a supplier of base-demand, the remote communities continue to be largely dependent on the distant utility supply [5]. The long and sparse rural feeders face the problems of frequent outages and poor voltage profile. While the inherent intermittency and uncertainty associated with renewable energy sources pose many problems in distribution and sub-transmission grids, the load following capability and dispatchability of SMRs complemented by an EES can be exploited in mitigating these issues.

Research in nuclear and renewable energy is ongoing independently with few notable attempts to explore the possible synergy between the two [25, 41, 84]. While many aspects of this synergy need to be explored, priority areas for research and development of the hybrid energy systems are identified in [41, 84] as follows:

1. Modelling for the integration of new generation technology: While the models of most

distributed generation and emerging storage technologies have either been developed or are being refined, the models, for example, the modular reactors and smart inverters will still need to be developed for planning and operations studies.

2. Pilot projects and studies for a demonstration of disparate generation technologies: Pilot projects and demonstration site for the first of a kind SMR project is underway in Canada [85] and possibly in some other nations. Policy level studies in [86,87] show the viability of nuclear-renewable mix from an energy policy perspective for large-scale systems. However, the challenges in short-term planning and operations in small edge-of-the-grid or off-grid load centres remain largely unexplored.
3. Implementation enablers such as energy storage and innovative energy conversion components: The increasing deployments of grid-scale, as well as portable energy storage systems, have led to sporadic growth in research activity and publications. However, the role of battery energy storage with the modular reactors to help them host more renewable generation is not well researched to the best of authors' knowledge.

The work presented in this article is part of an on-going exercise of a detailed technical feasibility analysis exploring the requirements and necessary conditions for synergy between the two disparate generation technologies with EES as an enabler. The on-going project deals with all the three aspects stated above. The authors have developed a working model of a remote feeder in northern Saskatchewan in PSS®E. Details of the feeder model are included in Section 2.5. For the steady-state analysis, a simplified electrical equivalent model of SMR, as well as EES, are used, whereas photovoltaic generation plants are represented by a standard set of models developed and used by the authors in [8]. Two scenarios are discussed in this article to demonstrate the potential synergy between nuclear and renewable generation with the enabling technology of EES:

- Scenario 1: Potential for SMR with and without photovoltaic generation
- Scenario 2: Potential for SMR with photovoltaic generation and EES

The article is organized into six sections and a list of references. The overview of potential benefits – of having a synergy among the nuclear and renewable generation enabled by

battery storage – is presented in Section 2.3. A discussion on SMR technology and the role of EES in integrating renewables with SMR is included in Section 2.4. This is followed by the modelling details of the remote feeder in Section 2.5, which precedes the results in Section 2.6. Concluding remarks with a summary of the work are presented in Section 2.7.

## 2.3 Overview of Potential Benefits

Apart from many site-specific and non-technical advantages, the following critical technical benefits can be explored while attempting to achieve synergy between SMR and renewable energy sources:

- **Capacity Firming** – The intermittent generation from distributed generators needs to be supported by a supplementary source to provide a firm generation capacity in order to meet the needs of scheduled power to the grid or consumers. It requires either an energy buffer or a dispatchable generation. With the load following capability of SMR being capped by the economic viability, a combination of EES and SMR can act both as a flexible as well as a firm source of power that can help meet the scheduled power demand of the customers or grid.
- **Infrastructure Investment Deferral** – Load centres are situated far from generating stations, especially so in the case of remote communities. With their steady rise in demand for the reliable supply of electricity, the long and sparse distribution feeders need to be upgraded to carry bulk power to these remote load centres. A combination of SMR and distributed generators can provide an attractive alternative to infrastructure upgrades. As a local generation, SMR and distributed generators in remote communities can serve the increasing local demand while importing limited power from the far-off generating plants. The modularity of SMR can be used to incrementally increase the generation capacity as per the rising demand while the distributed generators feed peak loads.
- **Load Following and Voltage Support:** With a non-dispatchable generation from the distributed generators and the need for SMR to operate at or near its capacity, the use of energy storage can fill the gap between the firm but an inflexible generation from SMR

and the variable but a non-dispatchable generation from distributed generators. The right combination can potentially lead to an independently controllable and sustainable energy system. The firm generation from SMR ensures long-term energy security while distributed generators can help meet the peak demands with the EES acting as an energy buffer.

- **Transmission Congestion Relief:** If the remote communities have their local generation, the long and sparse remote feeder will have reduced demand from the main grid, which in turn will relieve the transmission congestion. This can also lead to investment deferral in upgrading the transmission line capacity.
- **SMR Applications Beyond Electricity:** Based on the outlet temperature, thermal and electrical power output, and target market, SMRs can potentially be used for district heating, industrial process heat, hydrogen production, desalination, and isotope production among other non-electrical applications.
- **EES as a Critical Backup Supply:** While new-generation nuclear reactors and SMRs may be inherently safe by design or have passive safety system – meaning that their emergency core cooling system can operate without any actuators or electrical power – EES can act as a reliable on-site source of electricity for SMR as well as for critical loads of the remote community.

## 2.4 Small Modular Reactors

In order to meet the growing demand for secure and carbon-free electrical energy, interest in SMRs is growing internationally, given its smaller size, modularity and scalability, safety features and capacity to feed the load at remote centres. SMRs are characterized by their small size, typically in the range generally below 300 MWe. They can be mostly manufactured in the factory and installed into the plant rather than stick-built on the site. The modular design makes it possible to scale the plant up by incrementally adding each module. Because of these features, SMRs are expected to be more readily adaptable to integrate with intermittent and uncertain generation sources such as wind and solar. The combination of

emissions-free renewables and nuclear power can reduce the overall greenhouse gas emissions in response to climate change concerns.

Different new and improved technologies for SMRs are being developed, such as integral pressurized water reactors (iPWR), high temperature gas cooled reactors, and molten salt reactors. In this work, the iPWR is considered as an SMR, and it should be noted that the restrictions in operating range and rates of change in reactor thermal power vary for different reactor technologies. The iPWR technology is primarily implemented in pressurized water reactors with enhanced safety features and modularity in construction. As shown in Fig. 2.1, the primary circuit components in an iPWR are placed within the reactor pressure vessel, eliminating the need for primary circuit pipework, with the intention of enhancing safety and reliability, and completely overcoming the loss of coolant accidents [88]. It also keeps the core and reactor assembly submerged in water, which ensures continued cooling without any hydro-pneumatic or electrical actuators, adding passive safety features. The forced cooling, however, supplements the convection cooling in some designs.

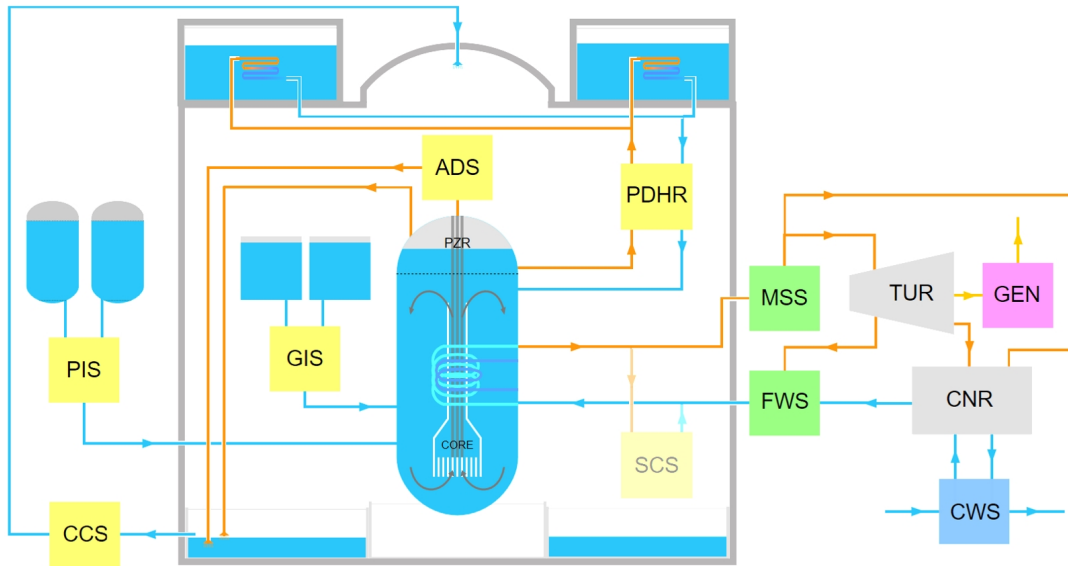


**Figure 2.1:** System level schematic overview of iPWR [88]

Among the recent developments in SMR technology, NuScale Power, USA claims the suitability of its multi-module reactors for integration with renewables, primarily based on its capability of load following [28]. The new modular design of small nuclear reactors can

offer flexibility to adjust to hourly changes in wind generation. As per the report [84], most of the new light water nuclear reactors designs are capable of operating in a load following mode and could change their power level once or twice per day in the range of 100%-50% (or lower) of the rated power, with a ramp rate of up to 5% (or even more) of rated power per minute. The range of change in rated electrical output (REO) is capped at 50% REO. However, the rapid fluctuations in demand and generation from distributed generators can only be overridden by relying on the combination of reactor power maneuvering and bypassing the steam turbine [25]. The smaller size and modular construction of new reactors can be very well suited for growing load demands in remote areas.

## **2.5 The Remote Feeder – Modelling with SMR, EES and Distributed Generators**

To undertake an exercise with realistic scenarios, an existing remote feeder in the northern part of Saskatchewan province is chosen. The remote feeder is modelled in PSS®E along with the simplified electrical equivalent model for the SMR. It can be placed close to the main substation or along the feeder with 72 kV lines. In this exercise, the SMR is placed at node 501, which is the farthest node with a voltage level of 72 kV. While a very high ramp rate of up to 60% REO/min can be assumed with SMRs for frequency control, a ramp rate of 10% REO/min is used in this research work for load following. The values of the range of REO and gradient are conservative for SMRs and are based on the recent report on non-base load operations of nuclear power plants by IAEA [18]. The modelling of PVDG is based on the measured weather data for solar irradiation and wind velocity for three sites, available in [89]. The PVDG model is derived and simplified from the comprehensive PV array modelling in [90] and matched with the land requirements from the PV Watts calculator [91]. The EES is modelled as a battery energy storage system (BESS) with relevant data chosen from the Electrical Storage Handbook [92].

### 2.5.1 Modelling a Remote Feeder

This research work is based on a remote feeder that serves to supply a couple of remote communities in northern Saskatchewan, Canada, with the aggregate demand of around 10 MW. The remote feeder, which is close to 300 km in length, has three main bays at the originating substation. The sparse and small load centres are far off, posing the challenge of maintaining a healthy voltage profile. The feeder is therefore equipped with three voltage regulators and a capacitor bank as well. Publically available datasets [93] are used along with the electrical grid-map to model the feeder in PSS®E accurately.

Table 2.1 lists the main parameters and features of this remote feeder, whereas Fig. 2.2 shows the map as well as the schematic arrangement of major electrical components including load centres and transformers. The feeder has three transformers feeding three different communities from the originating substation. One of the feeders has several voltage regulators (section from node 101), whereas the longest section (from node 2) has a capacitor bank connected at the far end (node 901). The load centres are populated by a combination of load profiles from [94] and [95] to formulate a sample hourly load profile for 24 hours. The sample load profile is then coordinated with the weather data for modelling the PVDG inputs at different sites.

**Table 2.1:** Main features of the remote feeder

Type	Sub-Transmission, Distribution
Nodes	31
Lines	18
Source to load (farthest load) distance	278 km (approx.)
Transformers	9
Voltage Regulators	3
Voltage Levels	Three - 72 kV, 25 kV, 14.4 kV

## 2.5.2 Hosting Capacity Analysis

Hosting capacity analysis is used to assess the capacity of the feeder to accommodate the local generation observing the operating constraints and physical limits of all the major electrical components. It includes the current capacity of conductors, power and energy capacity of the transformers, voltage regulators and capacitors, thermal overloading of all the components, min-max operating limits for node voltages and capacity utilization of significant components. It is typically used for non-dispatchable distributed generators based on renewable energy sources such as wind and solar, as it runs the time series power flow (TSPF) simulations with variable power generation values from PVDGs. However, it can also be used for relatively less flexible and dispatchable power generators such as SMR.

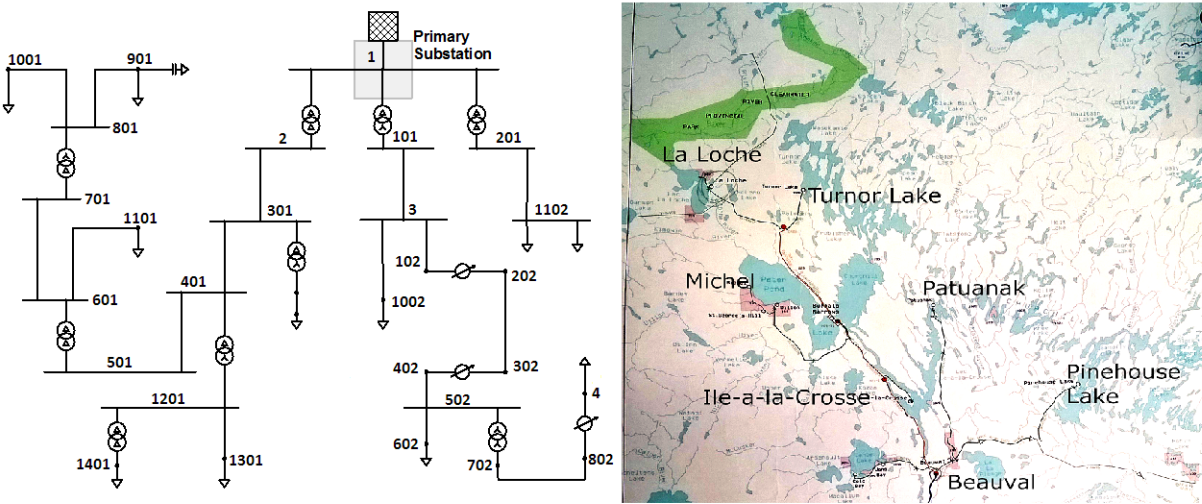


**Figure 2.2:** Schematic diagram and geographical map of remote feeder in north Saskatchewan, Canada

The results of the hosting capacity analysis decide the maximum capacity of a PVDG that can be safely connected at different nodes. With a sample daily load profile showing the variation in load demand from 6 MW to 11 MW in Fig. 2.3, the hosting capacity analysis is performed using this sample load profile and the MVA capacity at different nodes for PVDGs is obtained – refer to Table 2.2. Out of the 11 end nodes (refer to Fig. 2.2), four end nodes with moderately sized load centres and receptive to the benefits of small local generation are selected. The selected nodes for the PVDGs are 4, 602, 1102 and 1301, highlighted with

boldface letters in Table 2.2.

**Table 2.2:** Hosting capacity of the remote feeder

Node	S [MVA] ↓	Vmin [%]	Vmax [%]	Icap [%]
101	8.044	95.867	105.355	45.968
201	8.044	96.075	105.72	69.914
401	5.547	95.867	105.732	45.968
3	3.299	95.867	105.423	45.968
102	3.299	95.867	105.942	45.968
302	3.299	95.867	105.417	45.968
202	3.299	95.867	105.417	45.968
<b>4</b>	<b>3.299</b>	<b>95.867</b>	<b>105.375</b>	<b>47.492</b>
1002	3.299	95.867	105.902	45.968
<b>1102</b>	<b>1.675</b>	<b>96.738</b>	<b>105.72</b>	<b>54.055</b>
1002	1.675	95.867	105.891	45.968
<b>602</b>	<b>1.675</b>	<b>95.867</b>	<b>105.608</b>	<b>45.968</b>
402	1.675	95.867	105.853	54.028
1201	0.863	95.867	105.719	54.054
1401	0.863	95.867	105.726	54.054
601	0.863	95.867	105.864	54.054
1101	0.863	95.867	105.942	54.028
<b>1301</b>	<b>0.863</b>	<b>95.867</b>	<b>105.79</b>	<b>54.028</b>
702	0.507	95.867	105.102	49.088
802	0.507	95.867	105.102	49.088

The collective capacity of PVDGs that can be hosted at these nodes is close to 7 MW. Table 2.2 also shows the minimum and maximum operating voltage in the feeder with allowable MVA capacity of PVDG at each node. It should be noted that the operating voltage should stay within the limits of 94% to 106% of nominal voltage level as per the standard CAN3-C235-83 (R2015) – preferred voltage levels in AC systems [96]. The time series simulations are run using site-specific solar insolation data to verify the operating voltage limits with

PVDGs at the selected nodes. Fig. 2.4 shows the voltage variation at these nodes with their time-varying injection of real power as a function of time of day. The size of PVDG at the selected nodes are: (1) 3 MW at node 4, (2) 1.5 MW at nodes 602 and 1102, and (3) 500 kW at node 1301. The installed capacity of PVDGs is collectively 6.5 MW. A separate exercise to assess the hosting capacity of the feeder for SMR is carried out. The difference between the feeder hosting capacity for PVDG and that of SMR is that the former has a time-varying intermittent generation, whereas SMR can act as a dispatchable baseload supply. In this analysis, 5 MW and 10 MW of SMR sizes are considered at the nodes with voltage levels higher than 25 kV. It is observed that the 10 MW SMR can be hosted at either the primary substation or along the 72 kV feeder with nodes – 2, 301, 401, 501. All these nodes can also host the 5 MW SMR.

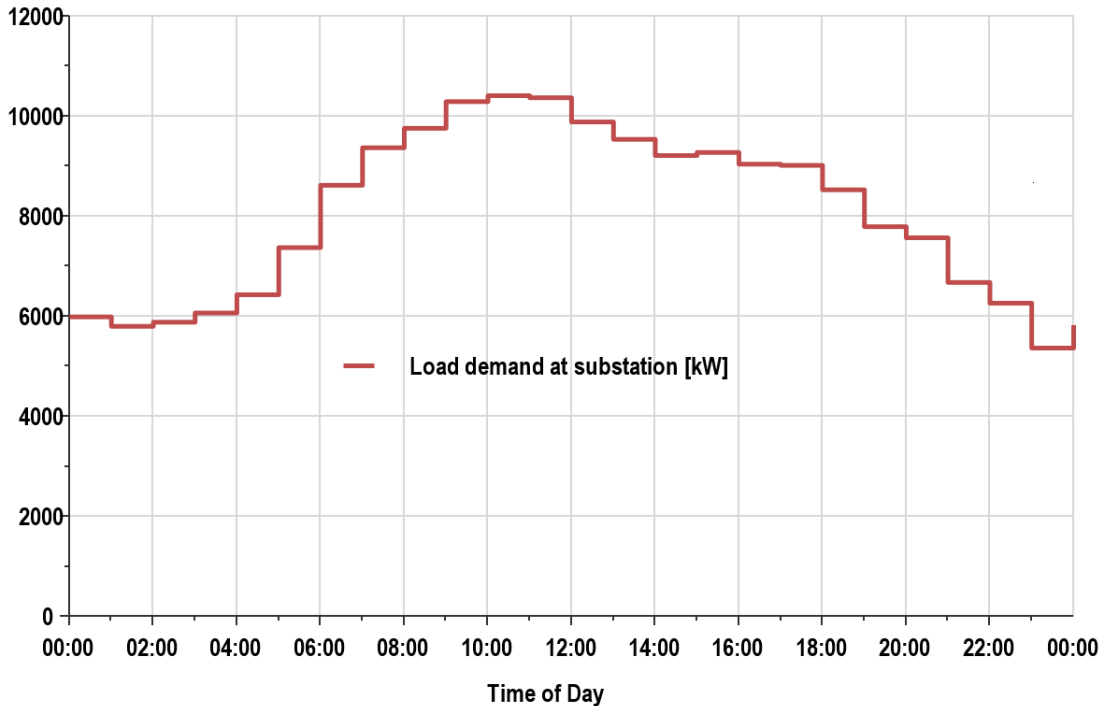


**Figure 2.3:** Hourly load profile at the substation

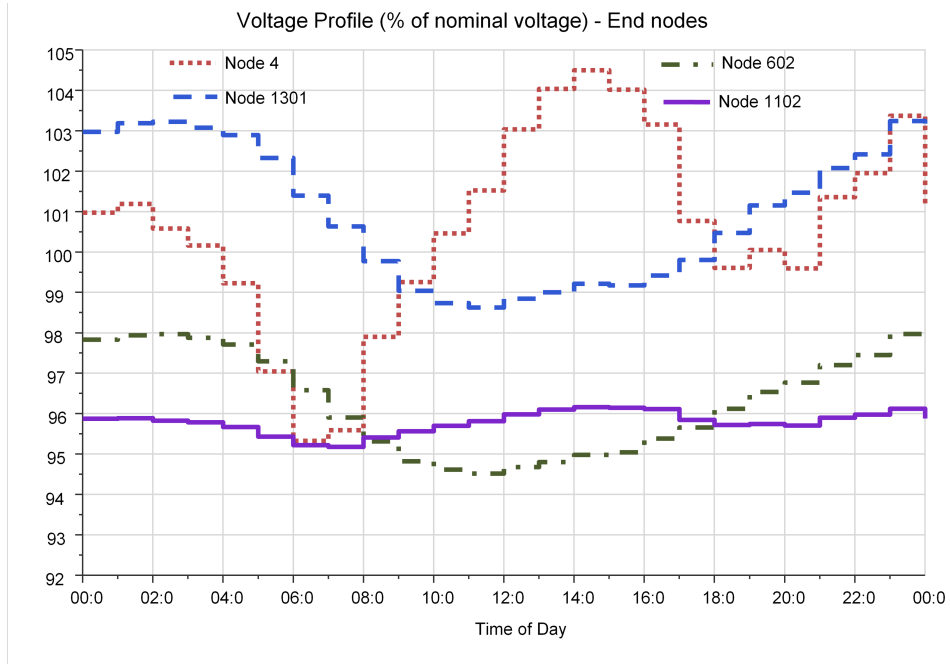


**Figure 2.4:** Voltage profiles of four end nodes

## 2.6 The Case Study

The economic consequences of load following are mainly related to the reduction of the load factor. In the case of nuclear energy, fuel costs represent a small fraction of the electricity generating cost if compared with fissile sources. Thus, operating at higher load factors is profitable for nuclear power plants, since they cannot make savings on the fuel cost while not producing electricity [17]. On the other hand, the availability of EES can help absorb the fluctuations in demand and generation from PVDGs and schedule the load following.

Therefore, two scenarios are considered for this feeder to host PVDGs while observing its effect on the SMR's load factor: first without EES, and the second with EES. The objective is to evaluate the suitable size of SMR and achieve its operation with the maximum load factor. EES can also be considered as a second back-up and independent source of power replacing one of the diesel generator sets of SMR. However, consideration of this possibility is not extended in this analysis. It may warrant an investigation as to what amount of stored energy can act as a reliable back-up along with a diesel generator set.

### 2.6.1 Case Study 1: Potential for SMR – without EES

Starting with the sample load profile shown in Fig. 2.3, the collective output power from the four PVDGs is obtained and used to determine the net demand at the substation in Fig. 2.5. The collective installed capacity of the four PVDGs is 6.5 MW, and on a typical sunny day in winter, it reaches up to 6 MW. As a result of coinciding demand and increasing PV generation, the net demand at substation witnesses a definite reduction. The reduced demand during peak hours stays around 5 MW, whereas the peak demand of the day at the substation is still close to 9.5 MW (in the morning hours) and 8.5 MW (in the evening hours). With the maximum output from PVDGs, the new net demand at substation varies from close to 5 MW to 9.5 MW. The local generation from PVDGs results in reduced reactive power as the amount of active power drawn along the long feeder sections has reduced.

Given the new net demand profile at the substation, a 5 MW SMR at node 501 or the primary substation can continue to operate without the need to regulate its output. However, a 10 MW SMR will have to respond to the changes in demand and will need to operate at considerably less plant load factor almost all throughout the day. During a typical summer day, PVDGs operate over a longer period, further reducing the electrical output of the SMR. It should also be noted that in the event of no PVDGs connected to the feeder, the 10 MW SMR cannot be used without curtailing its output for most time of day, as is evident from the demand profile given in Fig. 2.5.

### 2.6.2 Case Study 2: Potential for SMR with EES

In the second scenario, a 2.5 MW, 7.5 MWh BESS is considered alongside the SMR. The BESS setpoints are adjusted to coordinate with the substation demand of  $P_{min}$  and  $P_{max}$ . Alternatively, it can be adjusted to the values of measured power at the node BESS is placed. In the present case, the BESS is set to operate in charging mode when the net demand hits 8 MW ( $P_{min}$ ). The discharging mode gets activated when the net demand crosses  $P_{max}$  setpoint. Thus, the operation of BESS flattens the load profile absorbing the most severe fluctuations in demand. As a result, the net demand at substation node stays within the band of 8 MW to 10 MW, as shown in Fig. 2.6.

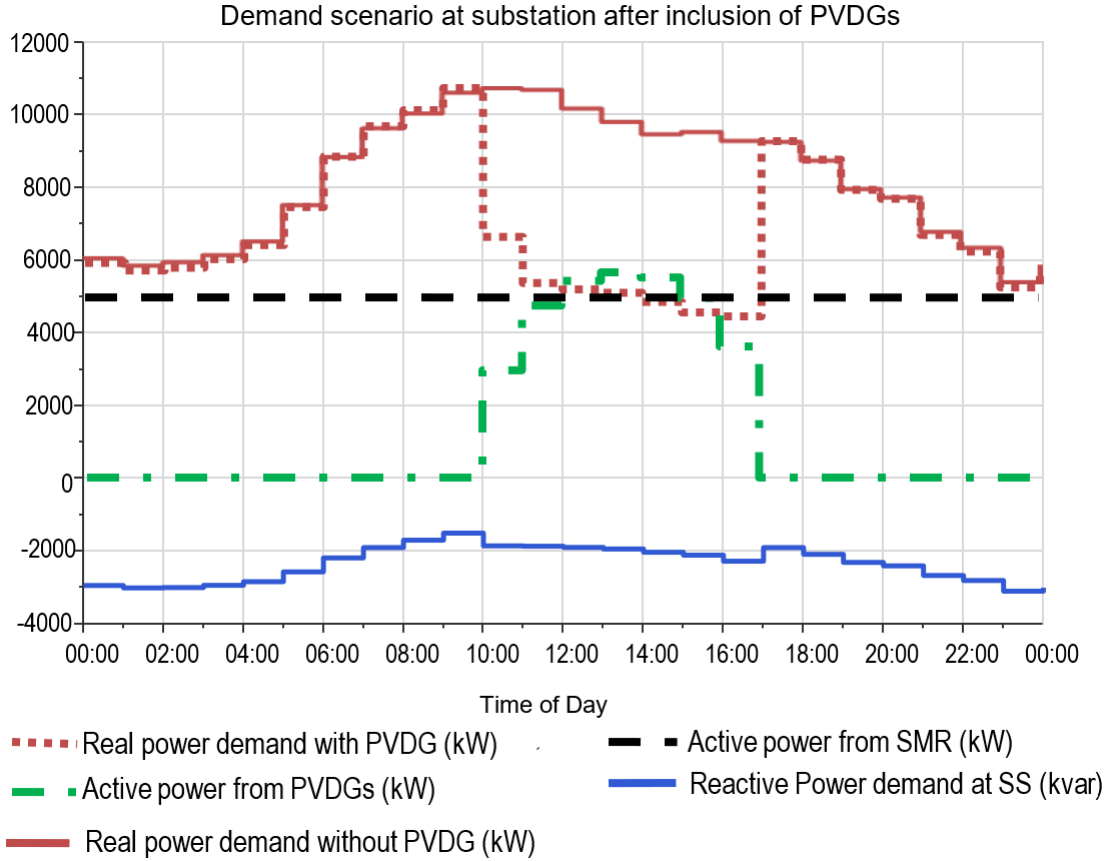


**Figure 2.5:** Demand profile at substation with power from PVDGs

With the function of load following outsourced to BES, the 10 MW SMR can now be used to deliver 8 MW continuously without maneuvering the reactor power or bypassing the turbine for regulating the SMR output. However, with the net load profile staying within the 8 MW to 10 MW band, SMR's load following capability can be used to match the load profile. In such a case, the load factor can be calculated and compared to quantify the benefit of BES. Load factor (LF), as defined in [17], is as follows:

$$LF(\%) = \frac{EG}{REG} \times 100 \quad (2.1)$$

where EG is the net electrical energy supplied during the reference period as measured at the unit outlet terminals, and REG is the reference energy generation, i.e. the net electrical energy, which would have been supplied if a unit was continuously operated at the reference unit power during the entire reference period (24 hours here). Using the load following

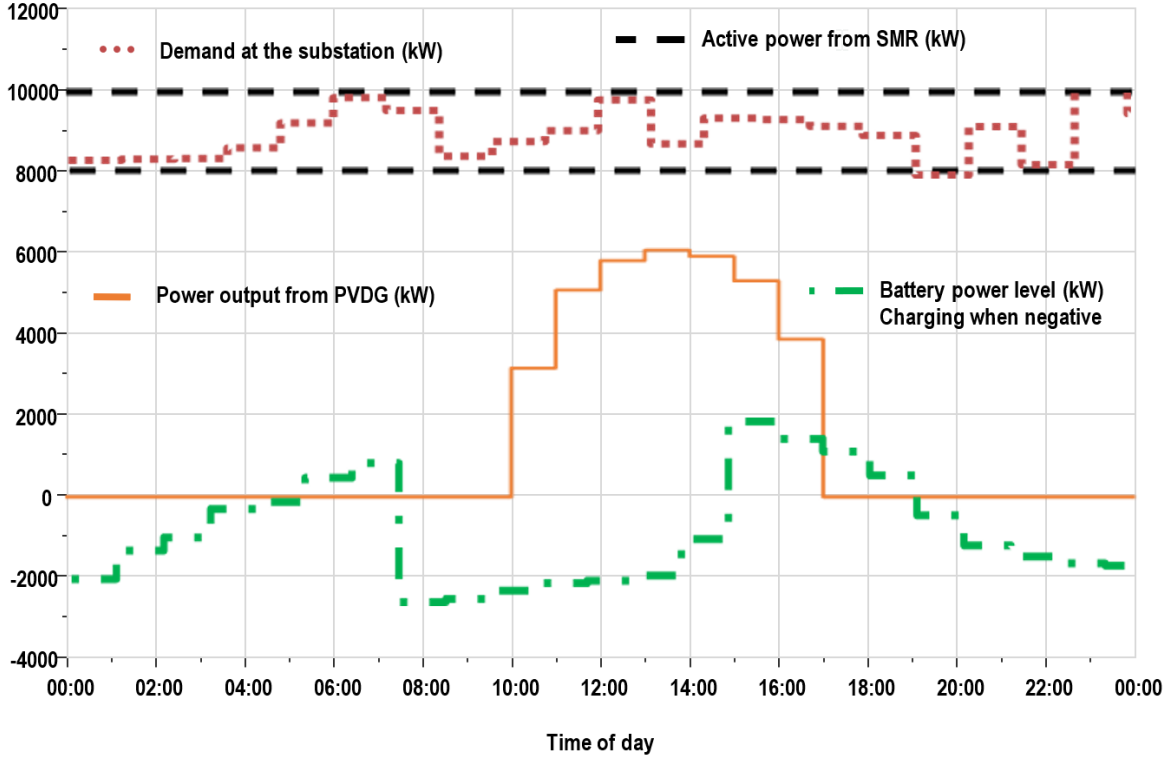


**Figure 2.6:** SMR with PVDG and BES

capability in the range of 100% to 50% REO and with 10% REO/min of a gradient, the LF as defined above is obtained for the 10 MW SMR and tabulated below:

**Table 2.3:** Load factor of SMR

Without PVDG – No EES	83.54 % (200.5/240)
With PVDG – No EES	69.48 % (166.75/240)
With PVDG and EES	88.125 % (211.5/240)

The load factor results in Table 2.3 show that the inclusion of renewables in off-grid communities with SMR can cause the load factor of SMR to reduce considerably. It also implies large and frequent changes in SMR output power to follow the load profile. BESS can be effective in absorbing the fluctuations in load profile and can help improve the SMR’s load factor significantly (from 70% with PVDG to 88%). BESS can also have a positive impact on the feeder voltage profile, as shown in the end-node voltage profiles in Fig. 2.7.

Similar results can be obtained with different seasonal load profiles and PVDG generation

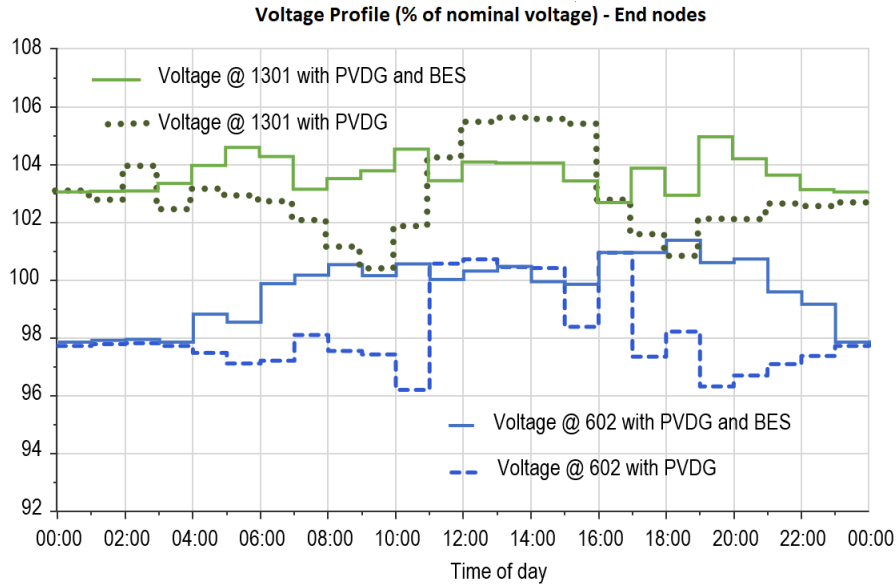


**Figure 2.7:** End node voltages before and after using BESS

profiles to ensure the adequacy of the BESS power and energy rating. It should be noted that the net demand of the substation is reduced to zero, as the SMR with 8 MW output power is operated along with the BESS and PVDG. In that case, the remote feeder has its own sustainable energy system, which fulfils all its electricity needs from within its local sources and has the capacity to provide power to the outer grid if needed. It should also be noted that the availability of BESS ensures that the critical loads of the remote communities can be supplied uninterrupted power for a few hours. It also helps increase the use of renewable energy from PVDGs or wind power. Over and above that, given the increased power and energy capacity, it can also replace the diesel generator set to act as an independent and reliable alternative power supply for SMR.

## 2.7 Conclusion

Remote communities face the challenge of fulfilling their energy demands from emission-free energy sources. While SMRs are a carbon-free and secure source of energy, the fluctuating demands at sparse load centres in remote communities can lead to reduced plant load factor for SMRs. On the other hand, photovoltaic and wind power generation provide good alternatives. However, non-dispatchable generation dominated by the uncertain and cyclical weather

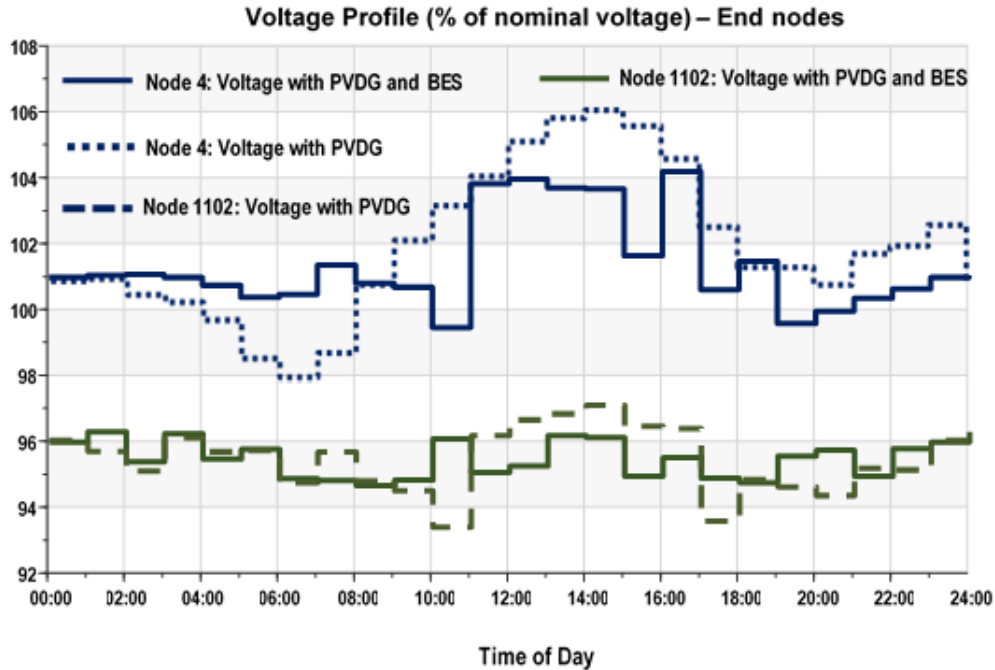


**Figure 2.8:** End node voltages (for node 4 and 1102) before and after using BESS

effects poses many techno-economic challenges. Electrical energy storage can help bridge the above gap and bring these disparate technologies together. The case study results for an existing feeder in northern Saskatchewan show that battery energy storage is an effective tool to strike a balance between non-dispatchable generation from renewable energy sources and dispatchable generation but with limited flexibility from SMRs. The case study shows that the plant load factor of the SMR can be substantially improved while also facilitating the absorption of all power from the photovoltaic generation in remote communities.

# 3 Investigating Small Modular Reactor's Design Limits for its Flexible Operation with Photovoltaic Generation in Microcommunities

## Preamble

This study ensues the research work in Chapter 2 to fulfill the first objective of the thesis mentioned in Section 1.3. The contribution of this study to the overall research is to investigate the flexible operation of SMR in the presence of highly variable RES in remote communities.

This study will explore the experience of non-baseload operation with conventional NPPs to propose plausible operating limits of SMR for load following and frequency control. An existing remote feeder in northern Saskatchewan will be used as a case system to host SMR and PV generation. The time series power flow (TSPF) simulation will be conducted to determine the flexibility requirements of the case system in the presence of large PV generation. The TSPF, dynamic and reactor simulations will be performed to evaluate the maximum PV generation that SMR can support in a remote community.

<sup>1</sup>This manuscript has been published in *ASME Journal of Nuclear Engineering and Radiation Science* in October 2020. Dr. Joshi led in exploring the synergy of renewables with nuclear energy. I contributed by assisting Dr. Joshi in developing the approach and research methodology under the guidance of Prof. Gokaraju. I carried out the dynamic studies in PSS®E and assisted Dr. Joshi to simulate the TSPF in PSS®Sincal. We jointly wrote the

---

<sup>1</sup>K. A. Joshi, B. Poudel and R. Gokaraju, "Investigating small modular reactor's performance characteristics for hosting photovoltaic generation in microcommunities," *Journal of Nuclear Engineering and Radiation Science*, October 2020, doi.org/10.1115/1.4048896.

paper, which was subsequently edited by Prof. Gokaraju. I also substantially contributed to revising the paper and addressing reviewers' questions after Dr. Joshi's PDF term ended in June 2019.

### 3.1 Abstract

The use of flexible and dispatchable generation from the small modular reactors (SMRs) combined with the non-dispatchable generation from renewable energy systems (RES) can be an effective alternative to pursue the mandate of replacing the fossil-fuel based electricity with the carbon-neutral energy systems in the remote microcommunities. This paper evaluates the feasibility of SMRs' flexible operations in microcommunities with the photovoltaic (PV) generation as a case study. Considering the design limits of SMRs for (a) the range of net change in electrical power output and (b) the ramp rates of net change in turbine power, a power system study is conducted to cover the three aspects of flexible operations, namely: (1) Planned load following, (2) Unplanned load following, and (3) Frequency regulation. A generic governor model in PSS®E is adapted to incorporate the reactor's operating limits for the dynamic simulation. The multi-timescale approach, combining (a) steady-state time series power flow (TSPF) analysis and (b) dynamic simulations with high-resolution solar irradiation datasets, is proposed to assess the implications of SMR's design limits. The results obtained on an existing remote feeder with three sets of operating limits— namely the conventional, advanced and extreme limits of ramp rates— juxtapose the SMRs' performance, given the challenging operating conditions with PV generation in remote locations. The results indicate that the SMR under study can accommodate the highest permissible PV penetration obtained by the hosting capacity analysis of the feeder under the clear sky conditions. However, dynamic simulations with the extreme PV variabilities show that the PV penetration level should be further limited so that the maximum deviations in SMR power levels stay within 40% of its rated capacity. SMR provides adequate frequency support for the PV penetration of up to 50% of the feeder maximum demand in this study.

## 3.2 Nomenclature

$\Delta f$	Frequency deviation at time $t$ , Hz
$f_0, f_t$	Frequency in Hz at time $t = 0$ , and at any time $t$ , Hz
$k_p$	Coefficient of primary frequency control, p.u./Hz
$k_{s,\tau}$	Coefficient of secondary frequency control at interval $\tau$
$P_{0,\tau}$	Power set point for the time interval $\tau$ , p.u.
$P_{d,t}$	Overall demand at time $t$ obtained from the TSPF simulation, MW
$P_{e,t}$	Net electrical power at time $t$ , p.u.
$P_{m,t}$	Turbine output power at time $t$ , p.u.
$P_{NPP}$	Rated Electrical output of NPP, MW
$P_{r,t}$	Reference electrical power set point at time $t$ , p.u.
$P_{sc,t}$	Scheduled power of SMR plant at time $t$ , MW
$r$	Generator droop constant
$R_{FC}, R_{LF}$	Ramp rates in FC and LF modes, p.u./min
$R_{open}, R_{close}$	Turbine valve opening and closing rates in p.u./s
$T_{act}$	Turbine valve actuation time constant, s
$V_{max}, V_{min}$	Maximum and minimum positions of the turbine valve in p.u.

## 3.3 Introduction

Interest in the small modular reactor (SMR) based nuclear power plants is growing internationally, given its smaller size, modularity and scalability, safety features and capacity to feed the load at remote load centers. SMRs are characterized by their small size, typically up to 300 MW [15]. With their capacity of load following and rapid response rates, SMRs are expected to be more readily adaptable to integrate with intermittent and uncertain generation sources such as wind and solar [15, 25].

Microcommunities (islands and remote villages) with less than 100,000 people or equivalent in households face a difficult challenge of a reliable and carbon-free source of energy [97]. As per the status report on remote and off-grid communities in Canada, there are cur-

rently 292 remote communities with a total population of approximately 194,281 people (2006 Statistics Canada Census) in Canada. Remote communities can develop renewable energy systems (RES) to support their energy demand [7–9]. SMRs could play a vital role in developing sustainable energy systems in remote load centers [67].

The technical and economic aspects of the nuclear-renewable systems are investigated in the Idaho National Laboratory (INL) based nuclear-renewable hybrid energy system (NRHES) projects reported in [42–44]. The opportunities, issues, and cost-benefit scenarios of NRHESs with six different interaction modes, namely thermal, electrical, chemical, hydrogen fuels, mechanical and information, were explored in [42]. Two hypothetical NRHESs based on Texas Gasoline and Arizona Desalination were analyzed and reported in two-part reports, [43] and [44]. Reference [43] investigated the dynamic performance, while [44] analyzed the financial aspects. Both the hybrid systems were found to be beneficial in hosting renewables and flexible operation.

Technical operating limits of a nuclear power plant (NPP) for its flexible operations were represented and applied to the problem of unit commitment and economic dispatch in the presence of RES in [98]. The case system consisted of several thermal generators in addition to an NPP, wind and PV plants with a total peak load of 9,308 MW. Using mixed integer linear programming formulation with hourly data, the study in [98] shows that the curtailment of renewable generation can be reduced improving the overall economics of the generation mix without any energy storage. The analysis in [98] and the hourly-profile based analysis for SMR's operation within microgrids in [19] inferred that the SMRs could be used to meet the baseload requirements of a microgrid; while the renewable energy supports the peak load. A 100 MW microgrid case system utilized in [19] consisted an SMR, wind and PV plants, while the main grid accounted for any imbalance between the generation and load in the microgrid.

The dynamic assessment is essential for SMRs considering the large demand variation it has to face due to RES intermittency. Even in the early 1990s, references such as [50, 51] from Ontario Hydro, Canada and CRIEPI, Japan reported the need for integrated dynamic models for conventional NPPs. The dynamic models of SMR based NPPs were proposed recently in [56]. The control strategies to improve the power maneuvering response of NPPs were analyzed in [35, 99]. The role of operating limits of an SMR for the application of load

following and frequency regulation remains unexplored in the existing literature.

Authors' previous works, [100–102], investigated various planning, operational and dynamic aspects of SMRs in electrical grids. The off-site power system's reliability was analyzed and quantified in [100] as a criterion of site selection of NPPs. In [101], an SMR model was developed and integrated into the GGOV1 turbine-governor model using PSS®E simulation software and was used for a power system dynamic study. The proposed model incorporated the reactor dynamics in power system simulation and facilitated the analysis of the internal reactor response during power system disturbances. In [102], a steady-state assessment was conducted to explore synergy among SMR, RES, and energy storage for remote communities while also quantifying the improved plant load factor for SMR.

Solar generation when compared with the wind generation has several advantages including the size, cost, scalability, and ease of transportation and installation, for the far-off remote microcommunities. Therefore, the objective of the research presented in this article is to investigate the implications of the design limits of an SMR in managing the high intermittency of local PV generation. The scope of the investigation is to analyze the three aspects of SMR's flexible operations in the presence of PV intermittency, i.e. (a) planned load following, (b) unplanned load following, and (c) frequency regulation. To this end, the contribution of the presented work is: (a) an adapted model of the turbine-governor system to account for the SMR's design limits, and (b) a multi-timescale simulation platform using steady-state time series power flow (TSPF) analysis and dynamic simulations to assess the feasibility of SMRs' flexible operations in the presence of highly intermittent RES.

The rest of the paper is organized as follows: Section 3.4 briefly discusses the SMRs' state-of-the-art and potential application in microcommunities; Section 3.5 relates the requirements of flexible operations with the SMR's design limits. Section 3.6 discusses the multi-timescale approach for steady-state and dynamic analysis; Section 3.7 presents the results with and without PV generation and discusses the implications of SMR's design limits on its flexible operations; Section 3.8 concludes with the inferences.

## 3.4 Small Modular Reactor Based Nuclear Power Plants

The four major driving forces behind the SMR design are the provision of the energy for a wide range of applications, replacement for the ageing fossil fuel-based thermal plants, enhanced safety considerations and better economic performance [15]. SMRs will help meet the sustainable development goals set up by the Intergovernmental Panel on Climate Change, while reducing the green-house gas emissions. SMRs could be constructed as a single or multi-module plant and have passive safety features [67]. Construction of the transportable modules in factories significantly lowers the construction time and cost, offering the promise for better economic performance as compared to the conventional NPPs.

### 3.4.1 SMR – State of the Art

SMRs are being developed in all principle lines of reactors, including water-cooled reactors, high-temperature gas-cooled reactors, fast neutron spectrum reactors, and molten salt reactors. There are currently more than 50 different designs of SMR under development, while three designs are in a demonstration phase [15]. Among the three SMRs, HTR-PM, a pebble bed high-temperature gas-cooled reactor located in Rongcheng Shandong province, China, and CAREM, an integral pressurized water reactor (iPWR) plant located in the northern part of Buenos Aires province, Argentina, are scheduled to complete construction by 2020. On the other hand, KLT-40s, a Russian floating nuclear power station, has entered the operation phase in December 2019.

One of the design concepts is that of the reactor pool with multiple independent modules submerged in the pool, as shown in Fig. 3.1. The NuScale integral pressurized water reactor (iPWR) module shown in Fig. 3.1 is rated at 60 MWe (recently updated REO rating) scalable to 12 modules in a single facility [28]. This design's passive safety feature includes the natural circulation of coolant flow under all operating conditions, eliminating the risk associated with the failure of circulating coolant pumps. Under the Carbon Free Power Project (CFPP), the Utah Municipal Power Systems (UAMPS) is planning to construct a 12 module NuScale SMR at the Idaho site [25]. The SMR plant is expected to start full operation by 2030 and targets to provide clean electricity to the member states under UAMPS.

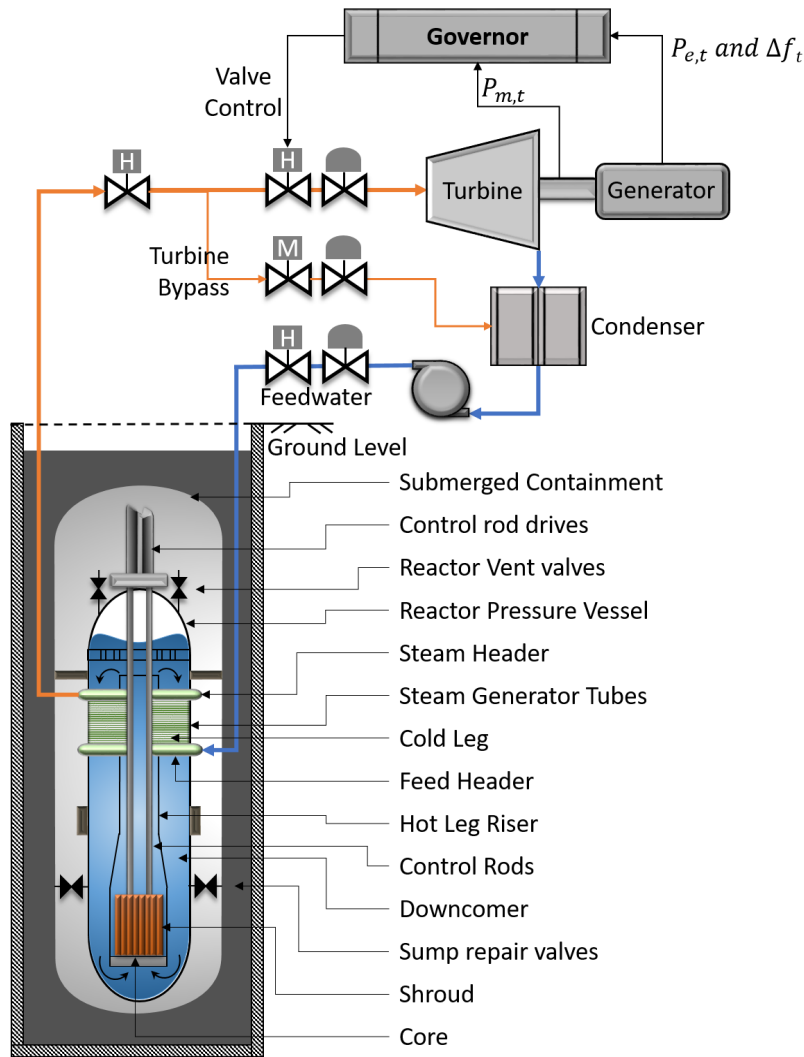


**Figure 3.1:** An underground sitting configuration of a NuScale iPWR module (reproduced from [28] with permission from NuScale Power, LLC)

### 3.4.2 SMR Suitability for Remote Locations

Due to their smaller size, SMRs are especially suitable for the regions with smaller electrical grids and could be deployed incrementally to match the growing energy demands. Another major advantage of SMR is the compact size of its fuel. A 4S (super-safe, small and simple) reactor, for example, has a refueling time of 30 years of operation in full power [15]. For the remote communities with limited access to fuel transportation, SMRs' capability to operate with the compact size of fuel with extended refueling time is going to be very useful.

### 3.4.3 Challenges of Flexible Operations

The power variations in NPPs could be achieved with three different options: taking one or more modules offline, maneuvering reactor power using the control rod, and bypassing the excess steam directly to the condenser [25]. These three options are the basis for flexible operations for most of the conventional reactor designs and new reactor designs coming up in the future. The first option qualifies only for a system where the multiple modules are implemented to support the electrical demand.

Flexible operation through control rod maneuvering comes with its own sets of problems [17,18]. Among various challenges, thermal fatigue gets aggravated for most of the reactor structures, systems and components under the large and frequent cyclic thermal loading due to variable power system conditions. The ageing of active components such as control rod drives, valves, pumps, nozzles and pipes also hastens due to the increased flexible operation. The operation of the control rod, on the other hand, causes the core power redistribution, thus affecting the power densities across the core, which could have a significant impact on fuel safety limits. Besides, the reactor control is also challenged by the counter-reactions from fuel and moderator temperatures. Fission product poisoning adds another challenge to the reactor power control. Xenon-135 ( $^{135}\text{Xe}$ ) is a strong neutron absorber produced during the fission of heavy nuclei. The variation of negative reactivity due to  $^{135}\text{Xe}$  lasts for several hours of power variation, which poses a significant challenge for reactor power control.

If the power variation is attained by bypassing the steam to the condenser, the condenser shell and tubes, steam bypass lines, and the associated valves will be subjected to additional wear and tear with increased heat load and flow rates of the bypassed steam [18]. Cogeneration can also boost the load following capability of NPPs by coordinating the generated steam for electricity production and heat applications. The steam, excess to the electricity production, could be utilized for a variety of heat applications such as hydrogen production, seawater desalination and district heating while keeping the reactor at a higher power level. Thermal energy storage could play a vital role in improving the flexibility in both electricity generation and heat applications.

Experience of load following and frequency control with NPPs in France shows that

the maximum allowed change in rated electrical output (REO) of the NPP– for primary and secondary frequency control– was capped at  $\pm 7\%$  REO [36]. German PWR designs allow up to  $\pm 10\%$  REO of total change for the frequency control. Typically, the response from governor and automatic generation control (AGC) of an NPP for frequency control is restricted to only  $\pm 2\text{-}10\%$  REO. AGC operates in autonomous mode with ramp rates as high as  $\pm 60\%$  REO/minute, whereas a much slower ramp of  $\pm 2\text{-}10\%$  REO/minute is used for planned load following [18]. The load following is typically conducted between 20-100% REO with the maximum change of full 80% in a single ramp. NPPs are also regulated to limit the number of large power cycles to reduce the impact on the reactor components. It should be noted that the said ramp rates and the range of permissible change in REO are adequate and have been in use for long in strong electric grid supported by several other rapid response plants such as gas turbines and hydro plants. However, the high ramp rates over a wider range of net change in power output - when considered for an SMR in an isolated or weakly connected grid - implies challenging conditions.

This paper mainly focuses on identifying the flexibility requirements of a remote community while the electrical grid is powered with SMR and PV plants. The reactor side design limits are defined and implicated in the case study to demonstrate the feasibility of the SMR's flexible operation with PV in a remote community.

### **3.5 Flexibility Requirements and Design Limits**

The NPPs have primarily been used in a baseload mode in North America and are seldom required to share the demand fluctuations. However, over the years, certain European NPPs have gained experience operating one or more units of the NPPs in load following mode [18]. Recently, an NPP with the advanced load follow control (ALFC) is reported in [18] to have successfully demonstrated to follow load by ramping down its output by 14% REO in 30 seconds and ramping it up at the same rate at the end of 15 minutes interval. Such an ALFC is critical in meeting the requirements of unplanned load following.

### 3.5.1 Variability Introduced by PV distributed generation (PVDG)

For communities of smaller size, PV generation is a more feasible option than other forms of RES. To consider the realistic scenario of variability introduced by PV generation, a high-resolution (sub-seconds) datasets of 17 sensors recording the global horizontal irradiance is used to represent a typical ‘Clear Sky’ (CS) and a ‘Very Variable’ (VV) PV generation profile. The datasets in [103] can reasonably represent a 5 to 10 MW of PV plant, eliminating the effect of spatial distribution. The ‘Very Variable’ PV profile has large and frequent variations in PV power output with ramps as high as 85% REO/min (up) and 140% REO/min (down), as depicted in Fig. 3.2.

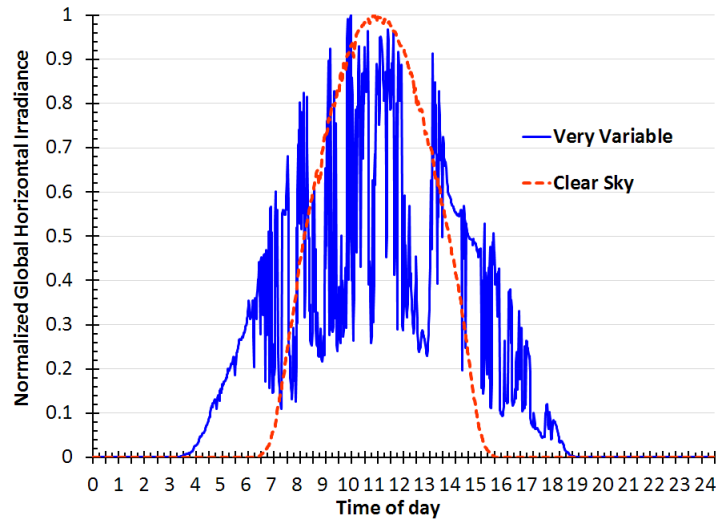


**Figure 3.2:** Normalized global horizontal irradiance (GHI) profile at Varennes, ON, Canada - [103]

### 3.5.2 Aspects of Flexible Operations

Major electrical aspects to consider for the flexible operations of an SMR are as follows: (1) Planned and unplanned load following, (2) Frequency regulation autonomously operated by the AGC, (3) Power cycles – ramping up and down over a range of power output, and (4) Low power operation. Given the promising features of SMRs for flexible operations [15], planned load following might not continue to be a major concern. However, unplanned load

following and SMRs' capacity to absorb uncertain intermittency caused by the increasing share of RES needs to be assessed for its adequacy.

The power plant's net electrical output can be represented by the three components shown in (3.1).

$$P_{e,t} = P_{0,\tau} + k_p \Delta f_t + k_{s,\tau} P_{r,t} \quad (3.1)$$

where  $k_p \Delta f_t$ — Automatic primary control

$k_{s,\tau} P_{r,t}$ — Automatic secondary control,  $k_{s,\tau} \in [-1, 1]$

$\Delta f_t = f_0 - f_t$ — Frequency deviation at time  $t$

$$-7\% P_{NPP} \leq k_p \Delta f_t + k_{s,\tau} P_{r,t} \leq 7\% P_{NPP} \quad (3.2)$$

While the set point  $P_{0,\tau}$  is updated at every time interval  $\tau$ , the momentary changes in power demand are met by the automatic primary and secondary control. The governor system is primarily responsible for the primary frequency control. The frequency deviation is sensed by the governor, which commands the turbine valve to operate in order to match the generation and demand. The secondary frequency control, on the other hand, is carried out mainly through AGC, which gathers information from the interconnection to determine the power variation necessary at each plant to bring the frequency back to the nominal value. In case of a grid-connected load following NPP in France [36], the allowable instantaneous change in  $P_{e,t}$  is  $\pm 7\%$  of  $P_{NPP}$  (REO of the NPP), as in (3.2).

$k_{s,\tau}$  in (3.1) and (3.2) is supplied by the transmission system operator for the large grid-connected NPP. However, in the case of SMR, which may or may not have a strong connection with the grid, the value of  $k_{s,\tau}$  is determined locally by the expected load profile and generation from RES.

### 3.5.3 Operating Limits of SMR

The design limits of SMRs will continue to evolve over a foreseeable future. However, as per the recent IAEA report [18], the new NPPs with ALFC can arguably be expected to absorb fluctuations in demand of up to 20% REO at a high ramp rate of 60% REO/min. At the same time, developments in controller designs claim that the ramp rates up to 80% REO/min are

achievable while restricting the overshoots within safe limits [37]. The said high ramp rates are typically used for frequency regulation. However, considering the SMRs’ design limits and the achievable ramp rates with the controllers prevalent in the industry, three operating limits, namely A (Conventional), B (Advanced) and C (Extreme), are defined in Table 3.1.

**Table 3.1:** Operating limits of SMR

Operating Limits	Mode	
	Load Following (LF)	Frequency Control (FC)
A (Conventional)	$\pm 80\%$ REO @ 10% REO/min	$\pm 10\%$ REO @ 60% REO/min
B (Advanced)	$\pm 80\%$ REO @ 20% REO/min	$\pm 20\%$ REO @ 80% REO/min
C (Extreme)	$\pm 80\%$ REO @ 40% REO/min	$\pm 40\%$ REO @ 80% REO/min

Fig. 3.3(a) depicts the above operating limits as a relationship between the power ramp rates and the allowable range of change in REO at a given ramp rate. The existing large NPPs’ operating limits are a subset of the operating limit A in Fig. 3.3(a). Fig. 3.3(b) and (c) show the slow and fast ramp rates for the LF and FC modes of SMR operation, respectively. The selection of the limits, defined in Table 3.1, are validated by the test-simulations performed to obtain the thermodynamic characteristics utilizing an IAEA based SMR simulator [88].

Note the difference in time-scales and range of change in REO in Fig. 3.3(b) and (c). Multi-timescale simulations with steady-state and dynamic models are necessary to accommodate different time-scales in the range of seconds to hours. The simulations over a longer time-frame assess the operating limits for the LF mode of operation. In contrast, the shorter time-frame simulations are necessary for the FC mode of operation.

The IAEA based SMR simulator simulates a comprehensive thermal and hydraulic model of 45MWe (recently updated to 60 MWe) NuScale iPWR to facilitate hands-on training for nuclear professionals for NPP design, safety, control and operation. The users can simulate the step changes in the turbine valve and control rod and alter the set points, limits and

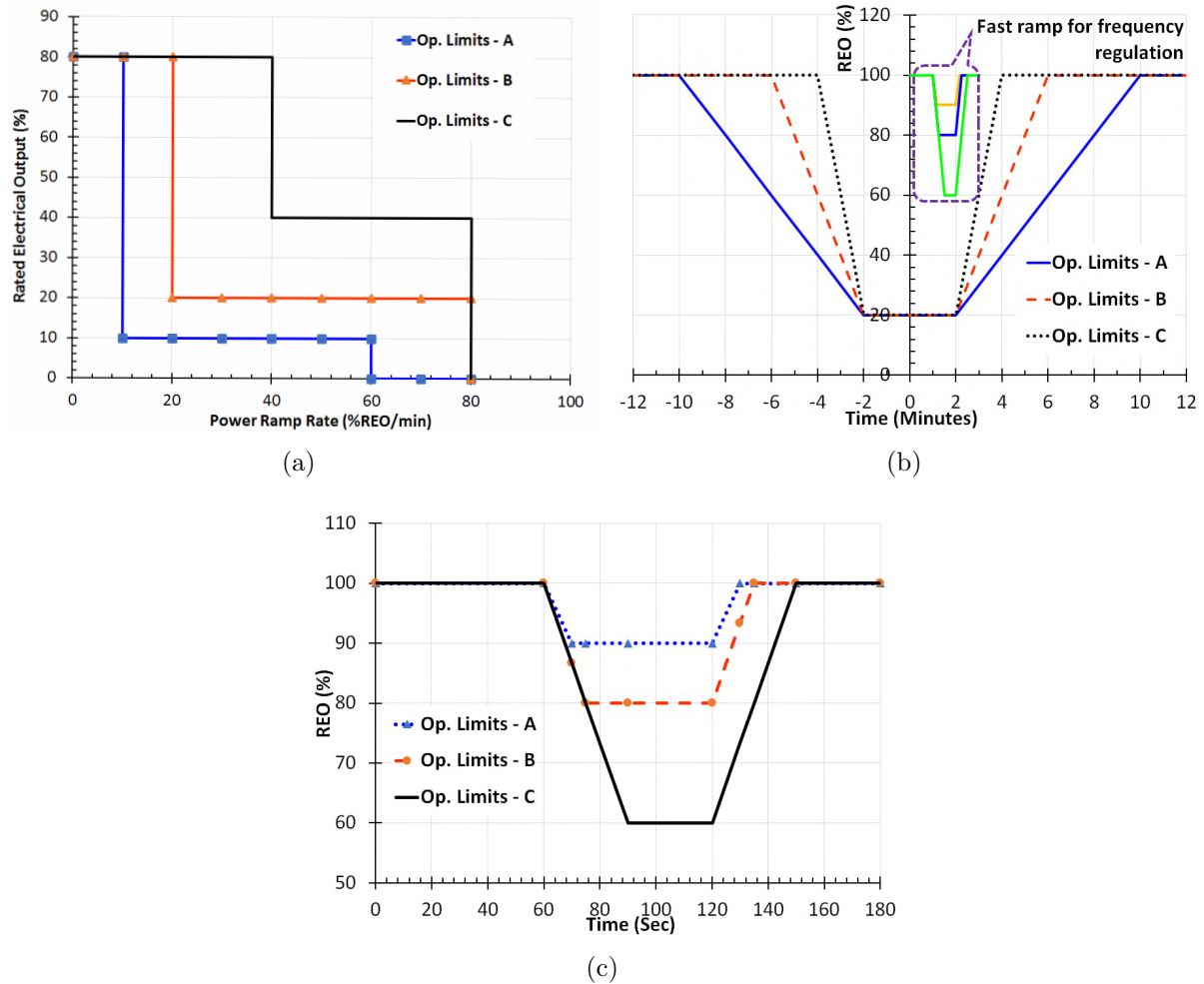


**Figure 3.3:** Operating limits chosen for SMR: (a) power ramp rates and net allowable change in power, (b) ramp rates for load following, and (c) ramp rates for frequency regulation

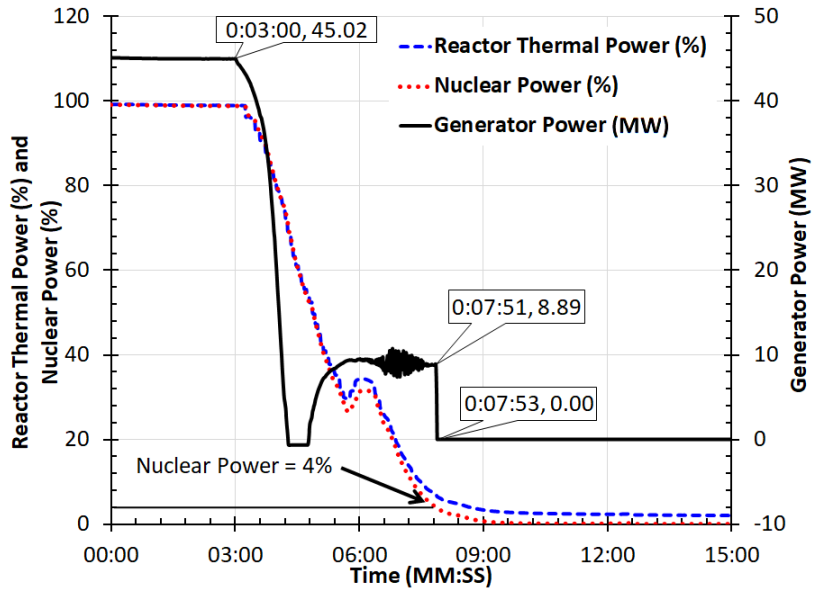
the rates of operations of various mechanical and hydraulic components in the primary and secondary coolant circuit. The reactor can operate in the turbine-leading or reactor-leading mode, and several transient and malfunction scenarios, including station blackout (SBO), loss of coolant accident (LOCA) and component tripping could be simulated. The real-time alarming systems with manual/automatic corrective actions provide users with the control room experience of NPP operation in a simulation environment. The simulator also allows the users to simulate the reactor model in different stages of life, respectively, beginning of life, middle of life and end of life. Moreover, the user can select primary coolant flow as natural circulation or forced circulation using primary coolant pumps.

**Table 3.2:** Validating the SMR operating limits. Legend: ✓ Power cycle executed successfully ✗ Low-pressure alarms triggered ☒ Turbine and generator breaker tripped.

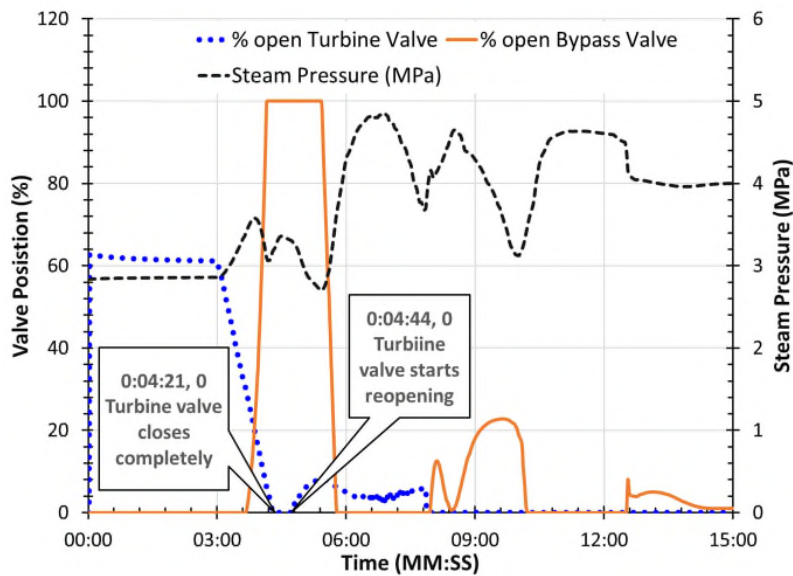
Power Cycles (% REO)	Ramp Rates (% REO/min)				
	10	20	40	60	80
100-80-100	✓	✓	✓	✓	✓
100-60-100	✓	✓	✓	✓	✗
100-40-100	✓	✓	✓	✓	✗
100-20-100	✓	✓	✗	✗	☒

The three operating limits are validated by performing simulations with different ramp rates over a wide range of operations, utilizing an SMR simulator platform provided by IAEA [88]. It should be noted here that the power variation is achieved only by means of reactivity control. Table 3.2 lists the set of simulations performed and shows the results qualitatively. The slow and fast ramps are tested over a small and large range of change in  $P_{e,t}$  of the SMR. Results in Table 3.2 show that the SMR cannot handle the variation of 80% REO in its output at a high ramp of 80% REO/min. The smaller range of change up to 60% REO can still be managed with a low-pressure alarm during quick ramping.

Fig. 3.4 shows the reactor response for REO variation from 100% to 20% at the rate of 80% REO/min simulated in the SMR simulator. In Fig. 3.4(a), the ‘Nuclear Power’ refers to the power produced by the neutron flux in the fuel rod, the ‘Reactor Thermal Power’ refers to the power transferred from reactor core to the primary coolant, and the ‘Generator Power’ refers to the electrical power output of the generator. The extreme ramp of 80% REO/minute cannot be extended to cause a change of 80% REO as it leads to a turbine trip with nuclear power going below the 4% limit, which triggers the turbine trip, as shown in Fig. 3.4(a). It is observed in Fig. 3.4(a) and (b) that the power available to the turbine follows the trajectory of the turbine valve position with a time lag. While the turbine valves are not supposed to close completely as the desired power level is 20%, they continue to move and overshoot. The valves overshoot to catch up with the higher ramp, close at the time 4:21, and start reopening at around 4:44, as depicted in Fig. 3.4(b). Another small overshoot is again observed after valve reopening. This trajectory is also followed by the reactor thermal



(a)



(b)

**Figure 3.4:** Response to the REO transition from 100% to 20% @ 80% REO/min (a) Generator and turbine trip, (b) Valve operations and the corresponding changes in pressure header

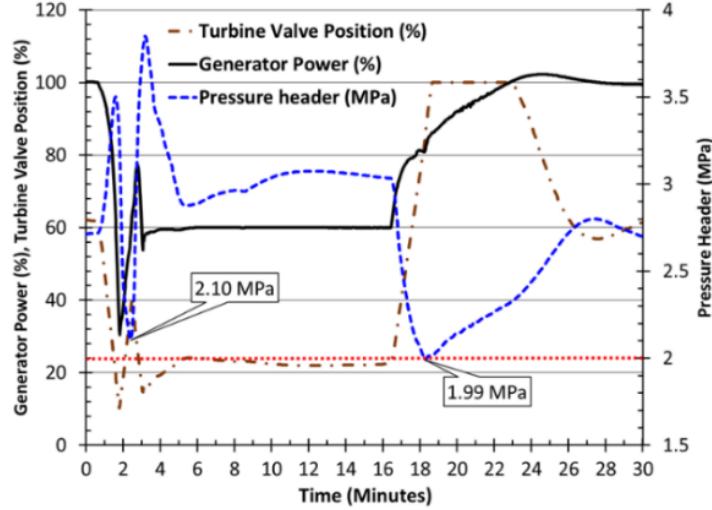


**Figure 3.5:** Valve positions and pressure variations - with IAEA SMR simulator – for the power cycle of 100-60-100@ 80% REO – Low-pressure alarm

power a bit later. On the other hand, meanwhile the reactor control system continues to steer the control rods down to reduce the reactor power level, which ultimately leads to the reactor rundown at 7:53. The operating limit C is therefore restricted to 40% REO in FC mode. It should also be noted that the power cycle 100-60-100 @ 80% REO/min also results in a low-pressure alarm, as shown in Table 3.2. However, the low-pressure alarm is caused by a momentary low pressure in pressure header, which exceeds 2 MPa limit for a very short while and is quickly increased and restored to 2.7 MPa, refer to Fig. 3.5. Therefore, the operating limit B is restricted with a conservative range of change up to 20% REO in output power, whereas operating limit C is set to exploit the maximum attainable range of REO at high ramp rates.

### 3.5.4 SMR Model for Power System Studies

The SMR’s electric generator model should reflect its capability to respond with the ramp rates defined earlier as three operating limits. While the dynamic model of an SMR was developed and integrated with a turbine-governor model in our earlier work in [101], this paper focuses on incorporating the SMR’s operating limits. From among the available turbine-governor models for power system studies, the GGOV1 is a generic model and have the configurable parameters to modify the turbine power ( $P_{m,t}$ ) characteristics [49]. Fig. 3.6



in the turbine mechanical power characteristics, which are then obtained and matched with the PSS®E dynamic simulations.

## 3.6 Analysis for Design Requirements

The three dimensions of the analysis are: (1) performing multi-timescale simulations for LF and FC mode of SMR operation, (2) verifying the reactor dynamics by the SMR simulator with different operating limits, and (3) estimating the adequacy of SMR operating limits with three variability levels – without PV and with the two PV profiles – CS and VV.

### 3.6.1 Multi-Timescale Simulation Approach

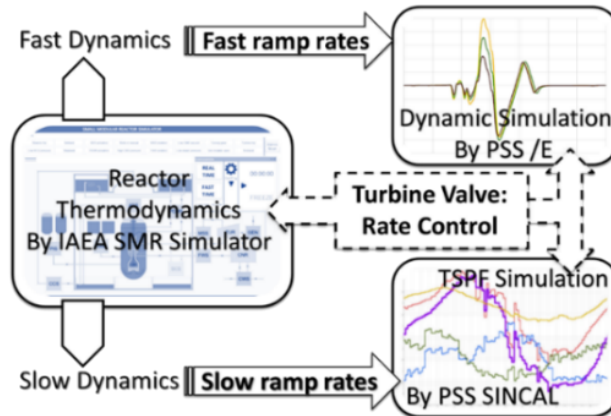


**Figure 3.7:** The multi-timescale simulation platform

The multi-timescale approach shown in Fig. 3.7 coordinates the two different timescales of LF and FC mode of SMR operation with the reactor simulator. The multi-timescale approach implies two aspects: (1) multiple periods of simulations, e.g. simulations period over a day, few hours, and 15 minutes; and (2) simulations with different time resolutions, i.e. quarter-hourly for a full day, per-minute for the few-hours duration and per-second for 15-minute simulations. The LF mode of operation is tested for a day period with TSPF simulations using steady-state models, whereas the FC mode of operation is tested for 900 seconds using dynamic models.

The power system studies are performed with PSS®E and PSS®SINCAL software,

whereas the reactor dynamics are obtained from the SMR simulator coordinating the valve rate control, as shown in Fig. 3.7. The per-second simulations use the dynamic models in PSS®E with demand data updated by per-second perturbation while utilizing high-resolution PV datasets for updating demand at this rate. Whereas, the longer time-frame simulations are performed using steady-state models in PSS®SINCAL using averaged aggregate demand for each time interval. The following major steps outline the overall procedure:

1. Populate the feeder nodes with a combination of residential, commercial and industrial (quarter-hourly) load profiles for a day,
2. Perform the PV hosting capacity analysis with TSPF simulations and select the first few nodes with the highest PV hosting capacity to collectively represent over 90% PV penetration that the feeder can host. In this study, selecting the first five nodes accommodates over 90% of the allowable PV penetration.
3. Process the high-resolution data of Global Horizontal Irradiance (GHI) to account for the effect of spatial distribution, connect the permissible PVDG at the selected nodes with normalized high-resolution GHI data for PV profiles, [103] - CS and VV,
4. Perform the TSPF simulations and verify the end node voltages with the two PV profiles – they should stay within limits specified by the standards [96].
5. Choose the operating limits (A, B or C) and set-points for SMR power generation for base-case (No PV) and clear sky PV power generation profiles for every two hours - the set-points should be chosen such that the AGC has the least range of power fluctuations during two hours for both the cases (base-case and clear sky)
6. Run TSPF simulations at a quarter-hourly resolution for a duration of 24 hours – spot the time of day when the LF mode is not adequate to meet the demand variations,
7. Run the TSPF simulations at the interval of one minute for the selected time slots – identify the intervals when the ramp rate in LF mode is not adequate to match with the rate of change in demand,

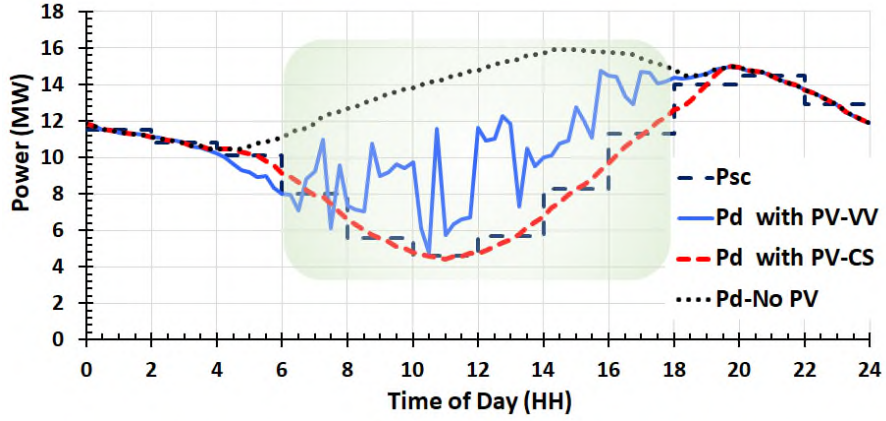
8. Perform dynamic simulations with high-resolution PV data and linearly interpolated demand data in PSS®E for the select intervals – observe the frequency deviation,
9. Obtain the reactor dynamics – valve operations, control rod movements, pressure header - for the most significant variation in demand. Observe the limit violations and triggering of alarms,
10. If frequency deviations or reactor dynamics exceed their respective allowable range, reduce the capacity of all PVDG by 5%, repeat the procedure from Step 5,
11. Repeat the procedure for each operating limit and obtain the maximum allowable capacity of PVDG.

### 3.6.2 The Remote Feeder

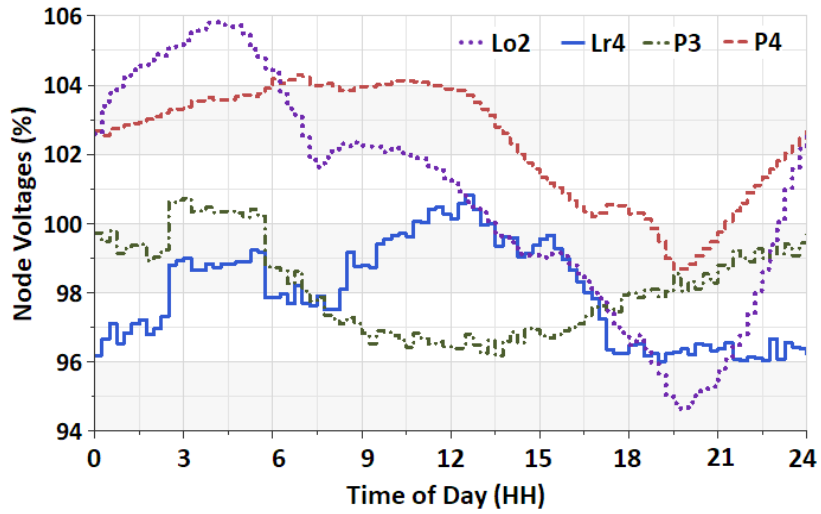
An existing remote feeder in the province of Saskatchewan, Canada, from [8] is utilized to represent the feeder supplying electricity to three microcommunities, refer to Fig. 3.8. The three microcommunities, Patuanak, Pinehouse and La Ronge, have sparsely distributed load consumers with a total population in the range of 1,500 to 3,000. The overall demand of the feeder at the substation stays within 16 MW. The feeder has several low-voltage distribution lines with voltage regulators. An iPWR with the REO capacity of 20 MWe is considered and shown at the top in Fig. 3.8.

The PV hosting capacity analysis, as a first step, determines the maximum size of the PV generation that can be accommodated on the feeder without voltage/current and power limit violations of the electrical components such as conductors, load and transformers (MVA limits). For the remote feeder shown in Fig. 3.8, the hosting capacity analysis allows up to 75% (of the maximum demand, i.e. 16 MW) of PV penetration. The collective installed capacity of the five PV plants is 12 MW, with the largest being 6 MW at the 138 kV voltage level and the smallest being 1 MW plant on 25 kV sections.





(a)



(b)

**Figure 3.9:** TSPF quarter-hourly simulations - (a) overall demand profiles with different PV profiles (b) voltage profile of end nodes with CS PV profile

and VV profiles. Three sample regions are shown highlighted in Fig. 3.10 with high rates of change in net power demand at SMR terminals.

All three operating limits are adequate to manage the steady rise and fall in demand with the CS profile of PVDG. Slow ramps can manage the steady rise or fall in demand over a relatively long duration in the LF mode of operation. However, the large and frequent variations caused by the VV profile of PVDG need the FC mode of operation with high ramp rates – as the net change in demand is large and sudden. An extreme instance of a large and sudden change in demand within 15 minutes interval is highlighted in Fig. 3.10

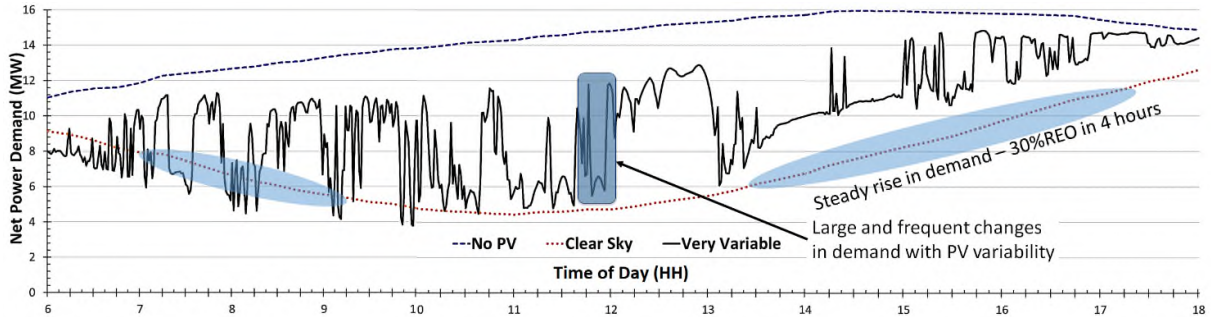
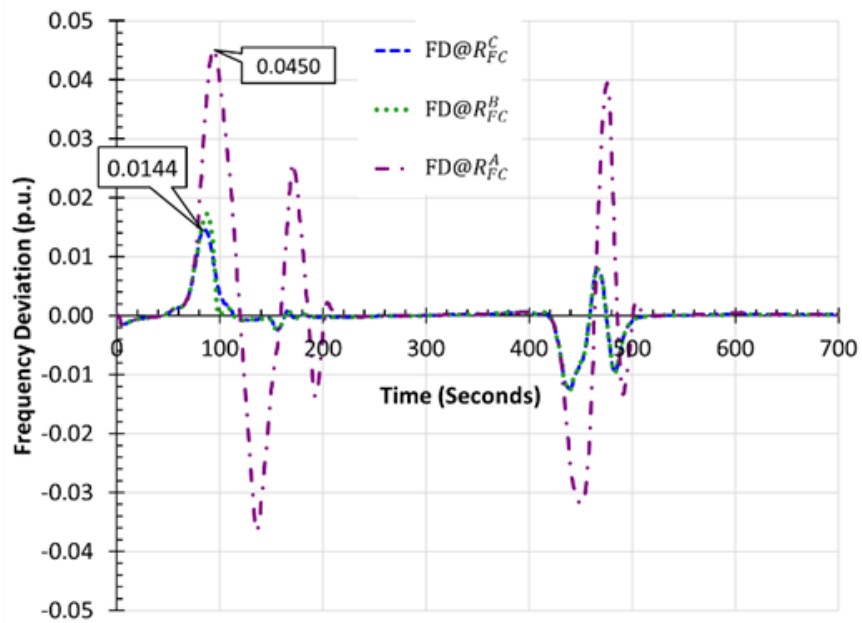


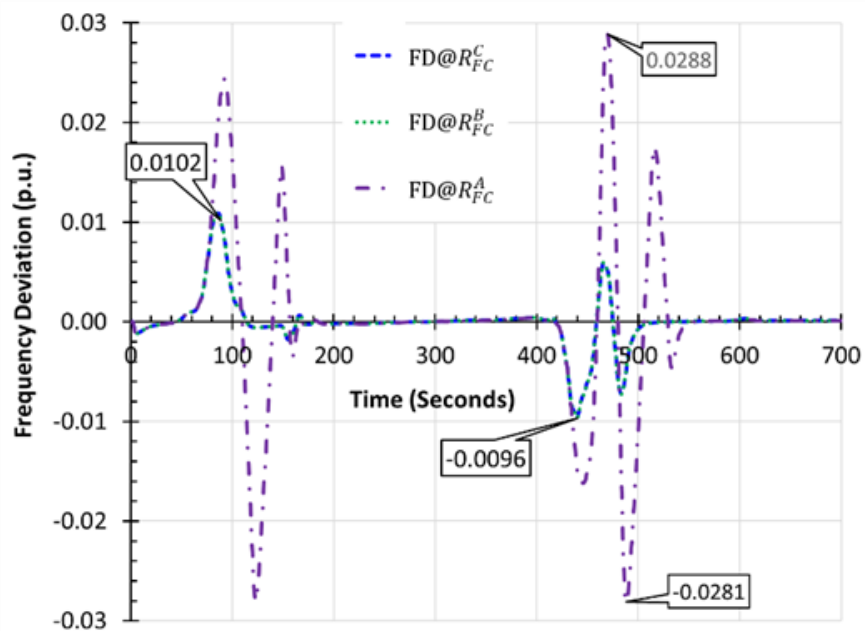
**Figure 3.10:** TSPF per-minute simulation from 6 AM to 6 PM with different PV profiles

at time 11:45 AM-to-12:00 PM. SMR's operation in FC mode is simulated in PSS®E with dynamic simulation perturbed at every second with updated values of net electrical power demand incorporating the high PVDG variability. The results of frequency deviation with different operating limits are shown in Fig. 3.11 (a). If the FC mode of operation is restricted for such large change (exceeding 25% REO) in demand – as in operating limits A and B – the frequency deviation can be as high as 4.5%, i.e. 62.7 Hz in a 60 Hz system. With the operating limit C, the p.u. deviation in frequency can still be as high as 1.44%. While operating limit C can reduce the frequency deviations, it cannot maintain it within the tight bounds of  $\pm 1\%$ . The maximum level of PV variability that can be handled is observed to be 55%, PV penetration as shown in Fig. 3.11 (b). It is interesting to note that the frequency deviation obtained by operating limits B and C in Fig. 3.11 (b) are almost the same at 55% PV penetration.

It should be noted here that the results of frequency deviation with the ramp rate of 60% REO/min marginally differ from the ones obtained with 80% REO/min – so much so that they cannot be distinguished visually in Fig. 3.11. It implies that the ramp rate of 60% REO/min is sufficient to limit the most severe intermittency with high penetration of PV. However, the same ramp rate (or higher rate) is not feasible for frequency regulation when the net change in power exceeds the 40% REO mark. Moreover, the 100-60-100% power cycle can be allowed, but the deeper power cycle of 80-40-80% REO@80% REO/min is not allowable. The said power cycle, when initiates a ramp of 40% to 80% REO, results in a low-pressure header (and triggers the low-pressure header alarm), as shown in Fig. 3.12. Therefore, the PV penetration should be so limited to cause maximum demand variations of



(a)



(b)

**Figure 3.11:** Dynamic simulation with per second perturbation: (a) 75% PV penetration (b) 55% PV penetration

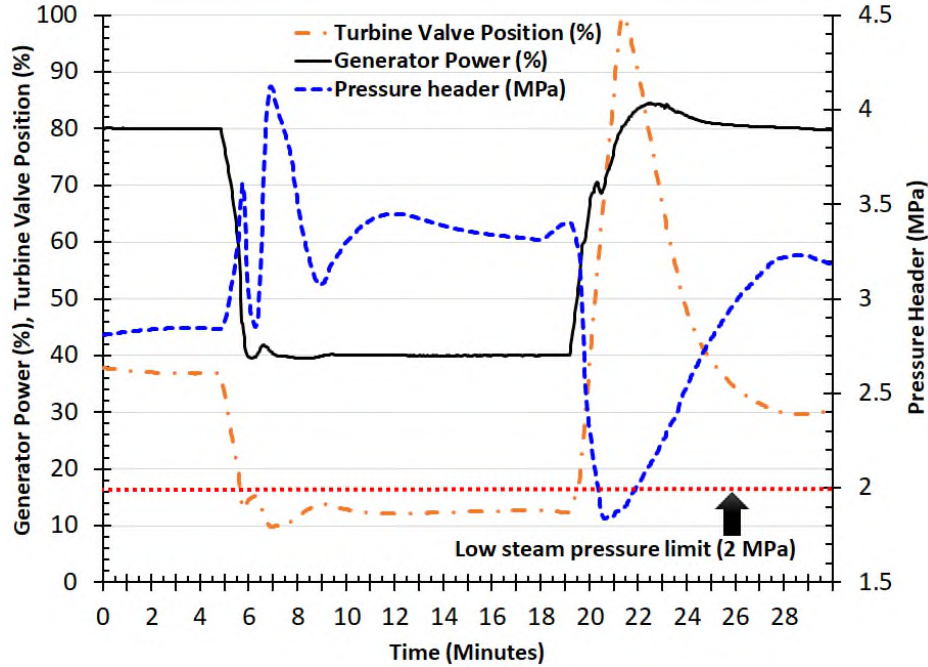


**Figure 3.12:** Low pressure alarm triggered at time  $t = 20$  min when ramping up from 40% to 80% REO@80% REO/min

40% REO or less.

### 3.8 Conclusion

Operating limits of SMR are investigated for SMR’s flexible operation in remote microcommunities with variability introduced by PVDGs. The two major operating limits – namely, the range of net change in turbine power and the rate at which the same can be obtained – are considered in assessing SMR’s performance with the ‘Very Variable’ profile of PV generation. A generic turbine-governor model in PSS®E is tuned to incorporate the SMRs’ operating limits. The multi-timescale simulations – from the quarter-hourly interval to per-second resolution – are performed to assess the load following and frequency control mode of operation of the SMR in an islanded remote feeder. The results show that the ramp rates of 60% REO/minute are sufficient to match the ramp rates of highly intermittent PV profile. The results show that the PV penetration of anything exceeding 50% of local demand can cause frequent and large frequency deviations – which can further trigger PV inverter tripping, potentially leading to widespread disconnection of other inverters. Another practical concern

that could arise is the increased number of power cycles that the SMR must perform due to the PV variability – it can be anything from at least one per day to dozens of large cycles in an overcast day. Furthermore, the results also imply that the SMR module operating close to its capacity is the preferred candidate to absorb the large and frequent change in demand.

SMR's capacity to manage the extreme PV variabilities is investigated and reported in this study, including the steam bypass and reactivity control. However, other arrangements such as cogeneration and energy storage, not considered in this work, can further augment this capacity.

# 4 A Dynamic Model of Small Modular Reactor-Based Nuclear Plants for Power System Studies

## Preamble

This study aims to fulfill the second objective of the thesis mentioned in Section 1.3. The contribution of this chapter to the overall research is to develop an integrated SMR dynamic model that would be used to simulate the SMR-RES hybrid energy system in Chapters 5 and 6.

In this study, a dynamic model of an SMR will be proposed and integrated with a standard turbine-governor model. The SMR model will be validated using a standard SMR simulator. A case study will demonstrate the inclusion of the SMR dynamic model in power system studies and its advantage in improving the accuracy of power system response.

The modeling data of NuScale SMR is obtained from the US Nuclear Regulatory Commission (NRC) website. The SMR simulator for the model validation is provided by the International Atomic Energy Agency (IAEA).

<sup>1</sup>A paper based on this work has been published in *IEEE Transactions on Energy Conversion* in November 2019. I developed the SMR dynamic model in PSS®E and simulated the results of the case study under the guidance of Prof. Gokaraju. Dr. Joshi, as a co-author, provided the feedback comments and assisted in the literature review. I wrote the paper and also addressed the reviewers' questions.

---

<sup>1</sup>B. Poudel, K. A. Joshi, and R. Gokaraju, "A dynamic model of small modular reactor based nuclear plant for power system studies," *IEEE Transactions on Energy Conversion*, vol.35, no.2, pp 977-985, June 2020.

## 4.1 Abstract

Small modular reactors (SMRs), an emerging nuclear power plant technology, are suitable for large grids as well as remote load centers and offer load following and frequency response capabilities. While the SMRs have expectedly higher response rates, detailed dynamic models, including reactor dynamics, are necessary for power system dynamic studies. This paper presents a dynamic model of an integral pressurized water reactor (iPWR)-type SMR, modeled in Siemens PTI PSS®E, to assess the contribution of the reactor to the power system dynamics. The proposed SMR model mimics the heat generation process and subsequent heat transfer process with the inclusion of the reactor core based on point kinetics, primary coolant based on natural circulation, and a simplified three lump representation of the steam generator. Controllers are designed to operate the turbine valve and reactor control rod in closed loops. The SMR model is integrated with the modified turbine-governor system, and a power system study is conducted. Results show the power system and internal reactor responses when subjected to electrical demand variations of 20% rated electrical output (REO) with a valve rate limit of  $\pm 80\%$  REO/min.

## 4.2 Nomenclature

$\alpha_f, \alpha_c$	Fuel and moderator temperature coefficients of reactivity, ( $-2.16 \times 10^{-5}$ , $-1.8 \times 10^{-4}$ /°C)
$\beta$	Delayed neutron fraction, (0.007)
$\dot{m}_{cp}, \dot{m}_{cs}$	Mass flow rate of primary coolant, secondary coolant, kg/s
$\dot{m}_{cp,0}$	Mass flow rate of primary coolant at rated SMR power, kg/s
$\eta_T$	Turbine efficiency
$\Lambda$	Prompt neutron lifetime, ( $2 \times 10^{-5}$ s)
$\lambda$	Decay constant, ( $0.1 \text{ s}^{-1}$ )
$\mu_{max}, \mu_{min}$	Maximum and minimum valve position
$\phi$	Average neutron flux, pu
$\rho, \rho_{ext}$	Net core reactivity, reactivity due to the control rod operation

$\tau$	Fraction of thermal power in the fuel, (0.97)
$A_{fc}$	Effective heat transfer area: fuel to primary coolant, m <sup>2</sup>
$A_{pm}, A_{ms}$	Effective heat transfer area: primary coolant to steam generator (SG) metal lump, SG metal lump to secondary coolant, m <sup>2</sup>
$c_m, c_{sw}, c_{sv}$	Specific heat capacity of SG metal lump, saturated liquid in secondary of SG, saturated vapor in secondary of SG, kJ/(kg °C)
$c_{pf}, c_{pc}, c_p$	Specific heat capacity of fuel lump, primary coolant lump in core region, primary coolant lump in SG, kJ/(kg °C)
$c_{pi}$	Specific heat capacity of feedwater to the secondary of SG, kJ/(kg °C)
$h_{fc}, h_{pm}, h_{ms}$	Heat transfer coefficient: fuel to coolant, primary coolant to SG metal lump, SG metal lump to secondary coolant, W/(m <sup>2</sup> °C)
$K_P, K_I$	Proportional, integral gain for rod control
$m_c, m_p$	Mass of primary coolant in the core region, primary coolant in SG region, kg
$m_f, m_m$	Mass of fuel lump, SG metal lump, kg
$m_{HL}, m_{CL}$	Mass of primary coolant in hot leg, in cold leg, kg
$m_{sw}, m_{sv}$	Mass of saturated liquid in secondary of SG, saturated vapor in secondary of SG, kg
$P_0, P_{th}$	SMR rated, instantaneous thermal power, MW(th)
$P_{elec}$	SMR electrical output, MW(e)
$p_{sat}, p_{ref}, p_{in}$	Saturated pressure at secondary of SG (steam pressure), reference pressure setpoint, pressure input of the flow model, MPa
$R_{open}, R_{close}$	Governor control for turbine valve opening, closing rate limits, % RE-O/min
$T_f, T_m, T_{sat}$	Average temperature of fuel, SG metal lump, secondary coolant lump in SG region, °C
$T_p, T_{HL}, T_{CL}$	Average temperature of primary coolant in SG region, hot leg, cold leg, °C
$T_{c1}, T_{c2}$	Average temperature of primary coolant at coolant node 1, coolant node 2, °C

$T_{fi}$	Feedwater inlet temperature, °C
$U_w, U_v$	Internal energy of saturated liquid and vapor in SG secondary, kJ/kg
$v_w, v_v$	Specific volume of saturated liquid and vapor in SG secondary, m <sup>3</sup> /kg
$\Delta T_f$	Deviation in fuel temperature from initial steady state, °C
$\Delta T_{c1}, \Delta T_{c2}$	Coolant node 1, coolant node 2 temperature deviations from initial steady state, °C

### 4.3 Introduction

A recent study [104] shows that low-cost nuclear power can substantially reduce the average generation cost when a carbon constraint of 50 g CO<sub>2</sub>/kWh or stricter is adopted. While nuclear power remains a strong contender as a provider of carbon-neutral electricity production for baseload generation [105], the smaller size and faster dynamics of small modular reactors (SMRs) make them potentially more suitable for flexible operations [25, 67, 98, 106]. Historically, nuclear power plants (NPPs) in North America have been operated as baseload plants. However, NPPs in Europe have experienced flexible operation for both load following and frequency control for several years [17, 18, 36]. In the changing scenario of the increasing share of intermittent generation from renewable energy sources, NPPs and SMRs are required to operate in the flexible mode under which they may be subjected to large, sudden, and frequent variations in their electrical output.

While many models have been developed for different reactor types of conventional NPPs and advanced models are being developed for SMRs [107], very few attempts have been made to develop a model that adequately represents the reactor dynamics in electric grid-integration studies with an appropriate turbine model. Given that existing NPPs have limited participation in absorbing demand fluctuations and grid disturbances, nuclear reactor dynamics are neither sufficiently represented nor integrated with the turbine-governor model in current power system simulation software packages.

The IEEE standard turbine-governor models approximate the internal source dynamics prior to the turbine valve and represent them with a first-order transfer function characterized by the charging time constant [49]. The steam pressure at the turbine inlet is assumed constant, and the mechanical power developed by the turbine is considered a linear function

of the control valve position. This simplification works well with large interconnected systems in which each plant has a limited contribution to frequency control and balancing demand-generation. The inaccuracies, however, become apparent when the demand variations are large and the machines to regulate the frequency are fewer in number.

The need for dynamic models of NPPs and their important role in power system dynamic studies were highlighted in a number of past key IEEE PES publications, e.g. [34, 35, 50, 51]. References [50, 51] present dynamic models of conventional NPPs for power system studies. Control strategies to improve the power maneuvering response were analyzed in [34, 35].

Recent publications such as [52] focus on small and slow changes, e.g., the NPP's response is limited to within 5% of its rated electrical output (REO) to the grid disturbance. The NPP model for a pressurized water reactor (PWR) plant in [52] uses a sliding average-temperature control program for the reactor with a simple turbine-governor model for grid integration. While the said NPP model represents the PWR in sufficient detail for power system studies, it was only tested for a small range of output variation with a limited ramp rate (30% REO/min). Other NPP models such as those in [53], [54], and [55] for grid-integrated studies have similar limitations of small and slow variations while including the nuclear reactor dynamics.

The 45 MWe NuScale SMR models developed in [56, 57] represent the reactor dynamics in finer detail, with consideration of primary coolant based on natural circulation and a moving boundary model of the steam generator (SG) with three distinct fluid state sections on the secondary side: the sub-cooled region, two-phase mixture, and the superheated region. The 100 MWe SMR model developed in [37] simplifies the thermodynamic relations of the reactor model for the purpose of controller design. All of the SMR models discussed have a sufficient level of accuracy based on their application, but none have attempted to integrate the dynamic model to the power system for power system dynamic studies.

Some NPPs in Europe operate in frequency control mode with ramp rates as high as 60% REO/min [17, 18]. The advanced controller design claims the possibility of ramp rates as high as 80% REO/min [37]. Further, the NERC guideline recommends the use of a GGOV1 turbine-governor model for grid-integrated generation plants [49, 108], and specifies different allowable frequency excursions for different regions [76]. Inaccuracies in frequency response

during power system planning studies could lead to inadequate protection designs, hampering power system security.

In a nutshell, for the accurate and reliable representation of SMRs in power system studies, the following developments are required to bridge the existing research gaps:

1. A reactor model that can be integrated with the generic turbine model in power system dynamic simulations; and
2. Representation of reactor dynamics that can characterize the variation in prime-mover output during large and sudden fluctuations in electrical demand.

The authors' previous research works, [75,100], investigate the power system aspect of having an SMR in an electrical grid, with [100] focusing on the power system's reliability to quantify the safety aspect of NPPs and [75] analyzing the steady-state power system issues of SMRs in a weak electrical grid. This paper aims to establish a dynamic model of an SMR to facilitate power system dynamic studies.

The paper is organized as follows. Section 4.4 describes the reactor model and integration with the turbine system. Section 4.5 discusses the reactor model performance and validation. Section 4.6 utilizes the reactor model for power system simulation and shows the results for primary frequency control. Section 4.7 gives conclusions of the research work.

## 4.4 Reactor Modeling & Integration to Turbine

This section covers mathematical modeling of the 45 MWe NuScale SMR and its integration to the IEEE standard GGOV1 turbine-governor system.

Fig. 4.1 is a schematic diagram of a NuScale iPWR module. The reactor core consists of 37 standard  $17 \times 17$  fuel assemblies, with the core height almost half the height of a nominal PWR [109]. The reactor core is equipped with two groups of control rod assemblies responsible for power regulation and shut down operations. The fuel is uranium dioxide ( $\text{UO}_2$ ), with U-235 enrichment less than 4.95%. The primary coolant circuit is equipped with a pressurizer to keep the pressure within the reactor pressure vessel (RPV) constant during the operation. The primary coolant flow is based on natural circulation. Each reactor module consists of

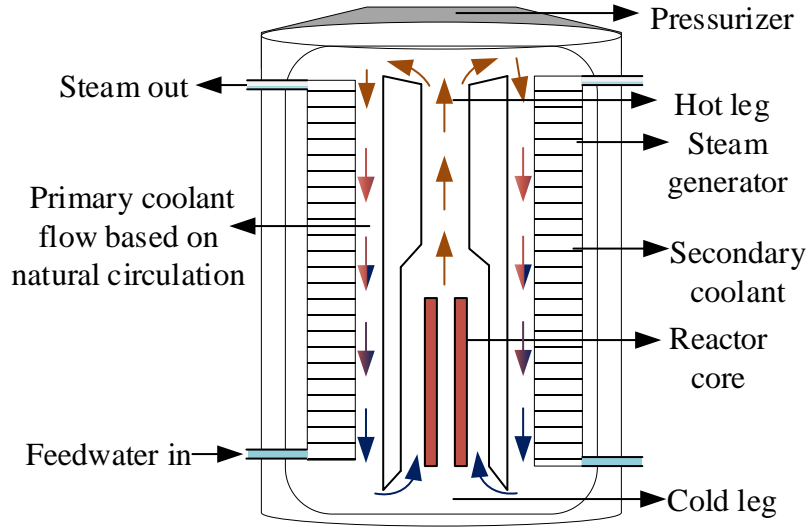


**Figure 4.1:** Schematic diagram of NuScale iPWR module

two vertical, once-through, helical coil steam generators (HCSG) located between the hot leg riser and the external diameter wall [110]. Each steam generator comprises a total of 506 tubes forged with Inconel 690 alloy. Preheated feedwater enters through the lower plenum of the steam generator, where it boils after receiving heat from the primary coolant. The upper plenum of the steam generator delivers steam to the turbine units.

#### 4.4.1 Reactor Core Model

The reactor core model incorporates the neutron dynamics inside the core, the thermal hydraulics responsible for the power transfer from the core to the primary coolant, and the natural convection inside the primary coolant circuit. The pressurizer maintains the RPV pressure very close to the rated value even during large transients [111, p. 89], [112]. Moreover, the physical properties of the pressurized primary coolant are mainly influenced by the coolant temperature rather than the pressure. Therefore, the dynamics of the pressurizer operation is neglected, and the RPV pressure is assumed to be constant. The coolant lumps are assumed well stirred with uniform temperature.

#### 4.4.1.1 Reactor Neutronic Model

The core neutronics is described with the average neutron flux formulated as a point kinetics model consisting of a single energy model and a neutron precursor group obtained by combining six groups of delayed neutrons.

$$\frac{d\phi}{dt} = \frac{\rho}{\Lambda} - \frac{\beta}{\Lambda}\phi + \lambda C \quad (4.1)$$

$$\frac{dC}{dt} = \frac{\beta}{\Lambda}\phi - \lambda C \quad (4.2)$$

The net core reactivity ( $\rho$ ) can be expressed as a summation of fuel and moderator temperature reactivity feedbacks and the reactivity due to the control rod operation.

$$\rho = \rho_{ext} + \alpha_f \Delta T_f + \alpha_c \frac{(\Delta T_{c1} + \Delta T_{c2})}{2} \quad (4.3)$$

#### 4.4.1.2 Reactor Thermal Hydraulic Model

Mann's model is adopted to describe the heat transfer process between a fuel lump and primary coolant [113]. The primary coolant in the core region is represented by two coolant nodes. The dynamic models of fuel and primary coolant temperatures in the reactor core region are expressed as:

$$\frac{dT_f}{dt} = [\tau P_0 \phi + h_{fc} A_{fc} (T_{c1} - T_f)] / m_f c_{pf} \quad (4.4)$$

$$\begin{aligned} \frac{dT_{c1}}{dt} = & [(1 - \tau) P_0 \phi + h_{fc} A_{fc} (T_f - T_{c1})] / m_c c_{pc} \\ & + 2\dot{m}_{cp} (T_{c1} - T_{c2}) / m_c \end{aligned} \quad (4.5)$$

$$\begin{aligned} \frac{dT_{c2}}{dt} = & [(1 - \tau) P_0 \phi + h_{fc} A_{fc} (T_f - T_{c1})] / m_c c_{pc} \\ & + 2\dot{m}_{cp} (T_{cL} - T_{c1}) / m_c \end{aligned} \quad (4.6)$$

The temperature variation across the primary coolant circuit results in variation in the

coolant density, thus creating the natural buoyancy force to vertically carry the coolant through the reactor core and hot leg riser. The primary coolant mass flow rate ( $\dot{m}_{cp}$ ) based on the natural circulation can be expressed as a function of thermal power [56], as shown in (4.7).

$$\dot{m}_{cp} = \dot{m}_{cp,0} * \sqrt[3]{P_{th}/P_{th,0}} \quad (4.7)$$

#### 4.4.1.3 Hot Leg and Cold Leg

The average temperature of hot leg and cold leg regions can be expressed with first-order transfer functions:

$$\frac{dT_{HL}}{dt} = \frac{T_{c2} - T_{HL}}{\tau_{HL}}, \quad \frac{dT_{CL}}{dt} = \frac{2T_P - T_{HL} - T_{CL}}{\tau_{CL}} \quad (4.8)$$

where  $\tau_{HL} = \frac{m_{HL}}{\dot{m}_{cp}}$  and  $\tau_{CL} = \frac{m_{CL}}{\dot{m}_{cp}}$ .

#### 4.4.2 Steam Generator Model

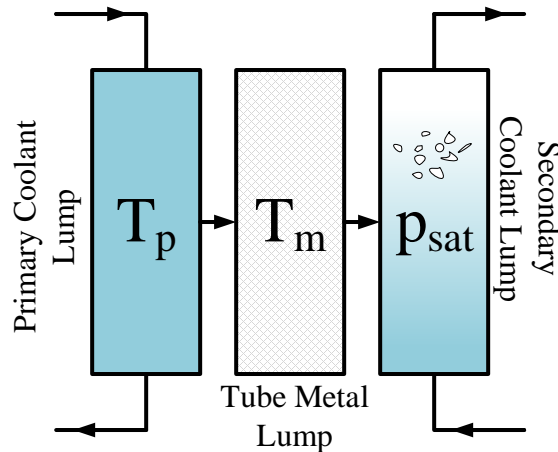


**Figure 4.2:** Three lump representation of HCSG.

The H.B Robinson-based simplified three-lump SG Model A is adopted to represent the HCSG of the NuScale SMR [114, p. 27-39]. The model consists of three segments, representing primary coolant, tube metal, and secondary coolant, respectively. The heat transfer process between the coolant and metal tube is based on the average temperature of each lump. The secondary coolant lump is assumed to be in saturated condition with preheated feedwater

entering the SG and saturated vapor coming out of it. The feedwater pumps and feedwater regulating valves continuously monitor and regulate the feedwater flow rate to keep up with the steam flow rate during normal and transient conditions [112, 115]. Perfect feedwater control is assumed, which means the feedwater flow rate to the SG is always equal to the steam flow rate to the turbine.

Fig. 4.2 is a schematic diagram of the SG model. The secondary coolant lump is represented by its saturated pressure  $p_{sat}$ , whereas the primary coolant lump and the tube metal lump are represented by their average temperatures  $T_p$  and  $T_m$ , respectively. The thermodynamics of the SG is described by the following differential equations, obtained by combining mass and energy balance equations [114, p. 35-42].

$$\frac{dT_p}{dt} = K_{HL}(T_{HL} - T_p) + K_m(T_m - T_p) \quad (4.9)$$

$$\frac{dT_m}{dt} = K_{mp}(T_p - T_m) + K_{ms}(T_{sat} - T_m) \quad (4.10)$$

$$\frac{dP_{sat}}{dt} = \frac{K_{sm}(T_m - T_{sat}) - \dot{m}_{cs}(U_v - c_{pi}T_{fi})}{K_s} \quad (4.11)$$

where  $K_{HL} = \frac{\dot{m}_{cp}}{m_p}$ ,  $K_m = \frac{h_{pm}A_{pm}}{m_p c_p}$ ,  $K_{mp} = \frac{h_{pm}A_{pm}}{m_m c_m}$ ,  $K_{ms} = \frac{h_{ms}A_{ms}}{m_m c_m}$ ,  $K_{sm} = h_{ms}A_{ms}$ ,  $K_s = m_{sw} \frac{dU_w}{dp} + m_{sv} \frac{dU_v}{dp} - m_{sv} \frac{U_{wv}}{v_{wv}} \frac{dv_g}{dp}$ ,  $U_{wv} = U_v - U_w$ , and  $v_{wv} = v_v - v_w$ .

### 4.4.3 Integration to the Turbine-governor Model

The proposed dynamic model is integrated with the turbine system of a synchronous generator. The GGOV1 turbine-governor model is chosen for the integration because of the following advantages: the adjustable valve opening/closing rate limits; the governor can be controlled in isochronous or droop control mode; and load limiter signal can be customized and activated with reactor dynamic safety protocols.

The necessary modifications to the GGOV1 model to make it compatible with the proposed SMR model are illustrated in Fig. 4.3. The GGOV1 model assumes a constant steam pressure, and linear relationships between the governor signal, valve position, and mechanical

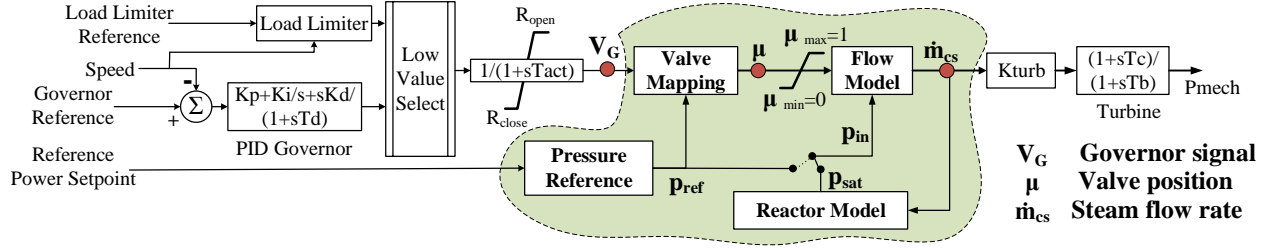


**Figure 4.3:** GGOV1 modified and integrated with the SMR model; shaded region shows the modifications with new modules.

output of the turbine. In the modified GGOV1, the governor signal is mapped to match the nonlinear valve model obtained from the International Atomic Energy Agency (IAEA)-based iPWR simulator [88]. The mapped signal represents the effective valve position at the SG outlet with the power change rate limits described by  $R_{open}$  and  $R_{close}$  settings. Fig. 4.4 shows the valve position corresponding to the governor signal for three different constant pressure setpoints.

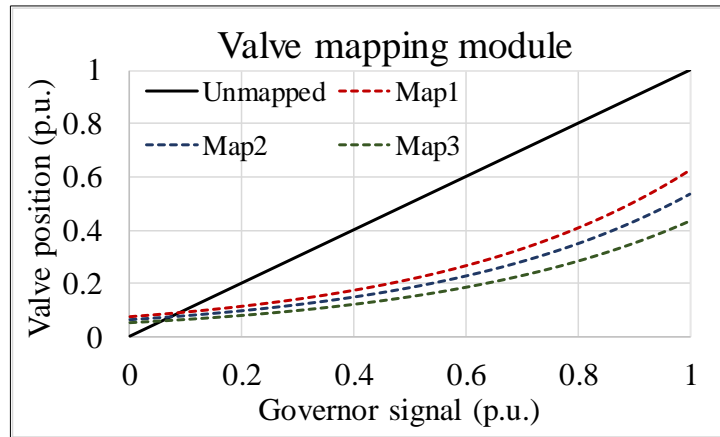


**Figure 4.4:** Valve mapping process with  $p_{ref}$  corresponding to: Map1-100%, Map2-90%, and Map3-50% REO of SMR

The flow model takes the pressure and valve position as the inputs to calculate the steam flow. The flow model is equipped with an option to switch the pressure input  $p_{in}$  to reference pressure  $p_{ref}$  or steam pressure  $p_{sat}$ . For the simulation without considering the reactor, the flow model takes the valve position along with  $p_{ref}$ , based on the current power setpoint, thus acting as an inverse function of valve mapping and bypassing the reactor. When considering the reactor,  $p_{in}$  is switched back to  $p_{sat}$ , obtained from the reactor model.

## 4.5 Reactor Model Performance and Validation

Table 4.1 lists the major values used for the modeling. The primary coolant remains at a constant pressure of 12.46 MPa with different temperatures across the coolant circuit. The temperature of preheated feedwater in the secondary coolant circuit is kept constant at 170 °C.

**Table 4.1:** Reactor core and SG parameters [56] [57]

Fuel:	
Mass	11252 kg
Specific heat capacity	0.467 kJ/(kg °C)
Fuel to coolant:	
Heat transfer area	583 m <sup>2</sup>
Heat transfer coefficient	1135 W/(m <sup>2</sup> °C)
Coolant volumes:	
Core region	1.879 m <sup>3</sup>
Hot leg	9.7 m <sup>3</sup>
Cold leg	26.8 m <sup>3</sup>
SG primary	3.564 m <sup>3</sup>
Primary coolant to SG:	
Heat transfer area	1123 m <sup>2</sup>
Heat transfer coefficient	20391 W/(m <sup>2</sup> °C)
SG to secondary coolant:	
Heat transfer area	1214 m <sup>2</sup>
Heat transfer coefficient	4950 W/(m <sup>2</sup> °C)
SG lump:	
Mass	7869 kg
specific heat capacity	0.450 kJ/(kg °C)

Although the pressure of the secondary circuit varies with the reactor power level, the changes in the specific heat ( $c_{pi}$ ) and internal energy of steam ( $U_v$ ) are very small. In fact,

the changes balance each other, and the term  $(U_v - c_{pi}T_{fi})$  in (4.11) is taken as a constant for the simulation. The mechanical power ( $P_{mech}$ ) is a function of the enthalpy difference between the turbine inlet and outlet ( $\Delta h$ ) and  $\dot{m}_{cs}$ , as shown in (4.12).

$$P_{mech} = \eta_T \Delta h \dot{m}_{cs} \quad (4.12)$$

During a power change, the variation in  $\Delta h$  is very small compared to the change in  $\dot{m}_{cs}$ . As a result,  $P_{mech}$  is taken as a function of  $\dot{m}_{cs}$ . The turbine efficiency  $\eta_T$ , on the other hand, varies with the steam flow rate. The relationship between  $\eta_T$  and  $\dot{m}_{cs}$  is obtained from the iPWR simulator.

Constant average coolant temperature control mode is chosen as the control mode for the reactor. Fig. 4.5 shows the temperatures and steam pressure variations with respect to the change in reactor power. The positive slope of the hot leg temperature and the negative slope of the cold leg temperature ensures a constant average temperature while maintaining the temperature difference necessary for various power outputs. The secondary side pressure and temperature show decreasing trends for the increase in reactor power.

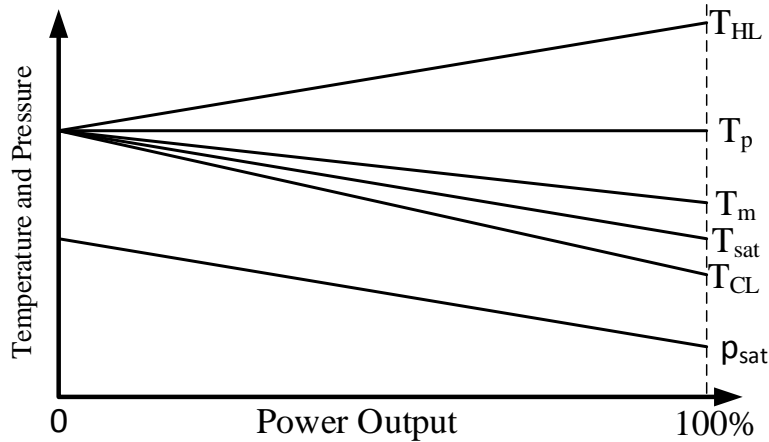


**Figure 4.5:** Constant average coolant temperature control mode

IAEA-based iPWR simulator software simulates the 45 MWe Nuscale iPWR module [88]. Steady-state setpoints of the modeled SMR are adjusted to obtain the steam pressure values equivalent to those obtained from the iPWR simulator. With these modeling principles, the model is developed as a user-defined model using the PSS®E software platform and

FORTRAN programming environment<sup>2</sup>. The overall reactor model is simulated in a steady state for various reactor power levels. The dynamic performance of an isolated reactor model is analyzed by simulating the reactor for step changes in valve opening and reactivity.

### 4.5.1 Steady-State Performance and Validation

The average primary coolant temperature setting of 252.5 °C is chosen for the proposed model as it provides a pressure range similar to those obtained from the iPWR simulator [88]. The steady-state evaluation of the SMR model generates a power balance equation, (4.13), that represents the solution model for the power transfer between the primary and secondary coolant.

$$\frac{P_0\phi}{2m_p K_m c_{pc}} = T_p - T_m = \frac{K_{ms}\dot{m}_{cs}(U_v - c_{pi}T_{fi})}{K_{mp}K_{sm}} \quad (4.13)$$

The expression on the left-hand side represents the temperature difference leading to thermal power being transferred from the reactor core to the primary coolant. The expression on the right-hand side represents the temperature difference causing thermal power transfer to the secondary coolant. The middle expression relates the power terms with the temperature difference created. As  $T_p$  is kept constant at 252.5 °C, the power balance equation generates the solution in terms of  $T_m$  and  $\phi$  for an electrical demand. All other variables of the reactor model are evaluated using the modeling equations in steady state. This steady-state evaluation provides the basis for setting up the initial conditions for the dynamic simulation.

Table 4.2 lists some representative steady-state results obtained from the SMR model at different power levels. As the electrical demand decreases, the pressure and temperature of the secondary coolant increase. The reactor, on the other hand, readjusts the hot leg and cold leg temperatures while keeping the average temperature constant. Consequently, the temperature difference between the primary and secondary decreases, thus reducing the thermal power transfer between the two sides and matching the new electrical demand.

---

<sup>2</sup>The FORTRAN code for SMR dynamic model in PSS®E is provided in Section B.1 of Appendix B.

**Table 4.2:** SMR steady-state results for various power levels

$P_{elec}$ (MWe)	$\dot{m}_{cs}$ (kg/s)	$p_{sat}$ (MPa)	$T_p$ (°C)	$T_{HL}$ (°C)	$T_{CL}$ (°C)	$P_{th}$ (MWt)	$T_f$ (°C)	$\dot{m}_{cp}$ (kg/s)
45	77.93	2.71	252.5	285.08	219.92	159.89	488.09	586.86
36	63.53	2.99	252.5	280.93	224.07	130.32	444.51	548.19
27	49.13	3.27	252.5	276.45	228.55	100.77	400.98	503.16
18	34.73	3.55	252.5	271.50	233.50	71.22	357.43	448.18
9	20.33	3.83	252.5	265.80	239.20	41.68	313.92	374.90
4.5	13.13	3.97	252.5	262.43	242.57	26.91	292.16	324.06

## 4.5.2 Dynamic Performance of the Isolated SMR model

The SMR model is equipped with the provision of two control inputs necessary for power variation: reactivity and valve opening. To evaluate the isolated response of SMR to these two inputs, a step change in each variable is applied, with the results plotted in Fig. 4.6.

### 4.5.2.1 Response to Step Change in Reactivity

With the help of the control rod, a  $3.5 \times 10^{-4}$  (i.e., 5¢) step increase in reactivity is applied at 20 s. The valve opening is left unchanged, and the core temperatures are allowed to drift in response to the change in thermal power. Following the step increase in reactivity, the reactor thermal power promptly increases due to the increased neutron flux. The fuel temperature and the primary coolant flow increases, followed by a rise in the temperature of the coolant lumps in the hot leg, steam generator, and cold leg regions. The average temperature of the primary coolant increases, leading to a larger temperature difference between the primary and secondary sides, increasing the heat transfer rate between the two sides. As the valve position remains constant, the evaporation rate increases and leads to the rise in pressure and temperature of the secondary coolant. On the reactor side, the reactivity feedback due to the rise in coolant temperature balances the reactivity due to the control rod movement. Finally, the reactor settles in a new steady-state condition with a 3.8 MW(th) increase in thermal power. The solid lines in Fig. 4.6 are the responses to a 5¢ step increase in reactivity.

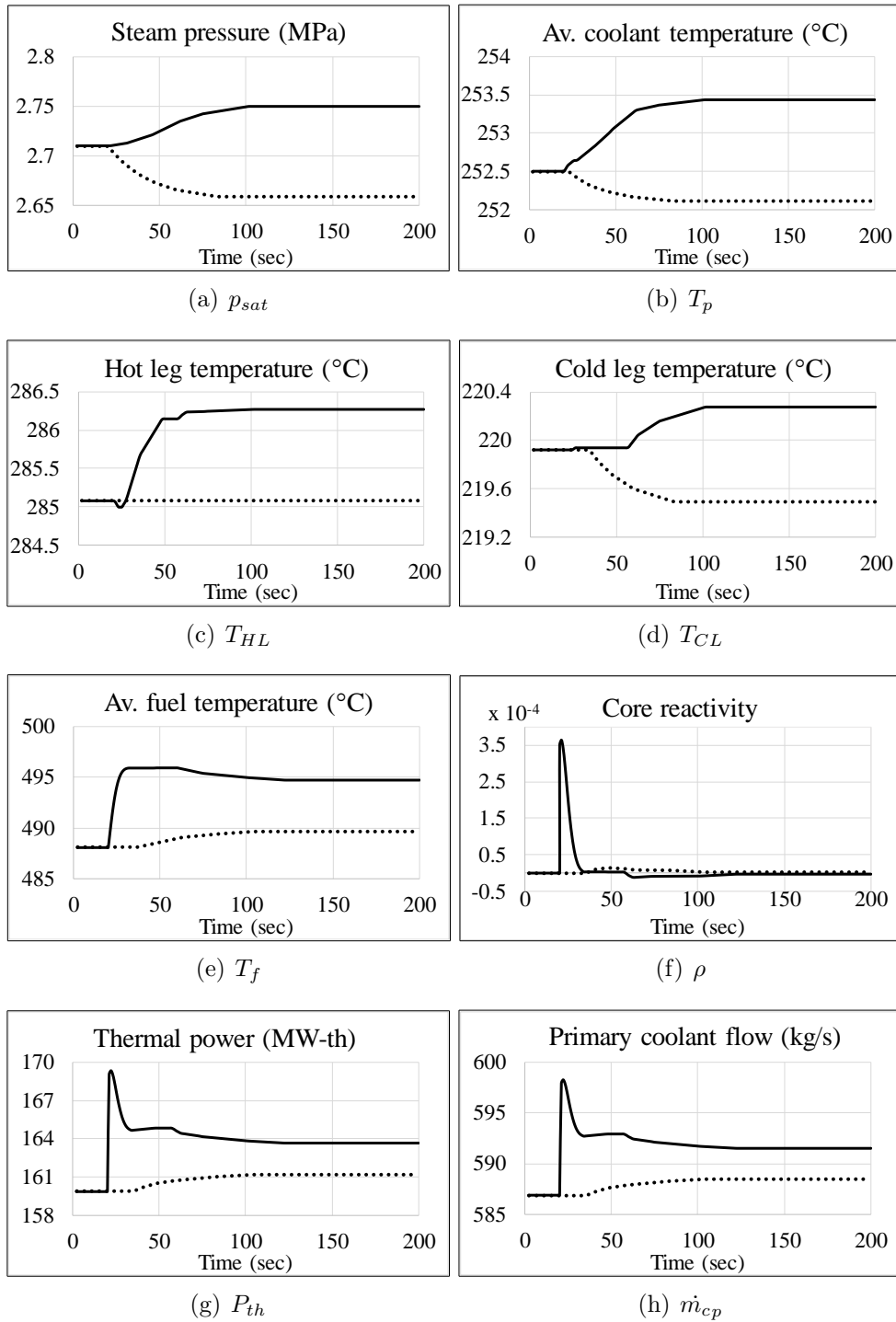


**Figure 4.6:** Dynamic responses for a step change in input variables. Solid lines represent the responses for 5% step increase in reactivity; dotted lines represent the responses for 10% step increase in valve opening.

### 4.5.2.2 Response to Step Change in Valve Opening

In the second case, a 10% step increase in valve opening is applied, while keeping the control rod inactive. The secondary coolant temperature and pressure decrease with the increase in valve opening. The decrease in temperature of secondary coolant leads to a larger temperature difference between the primary and secondary sides, thus increasing the heat transfer rate between the two sides. Because the control rod is disabled, the temperature of the primary coolant in the SG region drops, leading to a decrease in cold leg temperature. The temperature of the primary coolant at the core region also decreases, increasing the net core reactivity. The increase in reactivity is followed by a small rise in thermal power, fuel temperature, and primary coolant flow rate. The reactivity feedback, due to the rise in fuel temperature and decrease in coolant temperature, balances each other. Due to this balancing effect, the hot leg temperature remains almost constant. Finally, the reactor settles in a new steady-state condition with a 1.31 MW(th) increase in thermal power. The dotted lines in Fig. 4.6 are the plots for the responses to a 10% step increase in valve opening.

## 4.6 Power System Dynamic Studies with SMR

This investigation aims to incorporate the reactor dynamics into the power system dynamics and evaluate the flexibility of SMR to offer the primary frequency response. Fig. 4.7 depicts the power system model for the proposed dynamic study with the SMR model. The case system intends to mimic an isolated portion of the electrical grid in northern Canada. The system details are as follows: a 45 MWe, 13.8 kV SMR, stepped up to 33 kV to feed the load at the receiving end of a small 33 kV feeder. The line reactance is 0.03 pu, and transformer reactance is 0.08 pu, based on a 50 MVA system base.

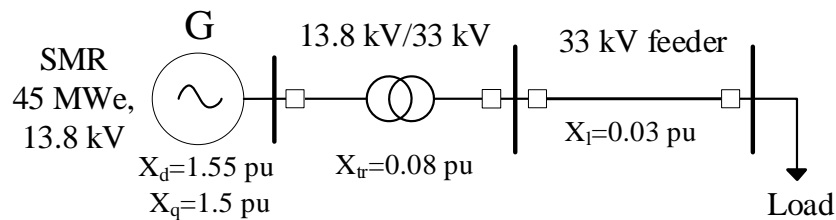


Figure 4.7: SMR connected to a power system

Before integrating the SMR model with the power system model, the controllers should be appropriately designed to meet the power system requirements while respecting the reactor’s design capability. The two control variables are the reactivity and the valve opening, automated with the rod control system and the governor system, respectively. The governor control and rod control actuators are designed to complete the power maneuvering process smoothly under an extreme case scenario, which is taken as a 50% step decrease in electrical load.

A simple proportional-integral (PI) controller is designed to steer the control rod based on the deviation of average primary coolant temperature from the reference setpoint, as shown in (4.14).

$$\rho_{ext} = \left[ K_P + \frac{K_I}{s} \right] (T_p - T_{p,ref}) \quad (4.14)$$

Four different control settings are considered and the valve control is set without any rate limits. Fig. 4.8(a) shows the reactor thermal power response corresponding to different control settings: *C1*:  $K_P=0.1$ ,  $K_I=0.01$ ; *C2*:  $K_P=0.05$ ,  $K_I=0.005$ ; *C3*:  $K_P=0.02$ ,  $K_I=0.002$ ; and *C4*:  $K_P=0.01$ ,  $K_I=0.001$ . The control setting *C4*:  $K_P=0.01$ ,  $K_I=0.001$  ensures a smooth transition.

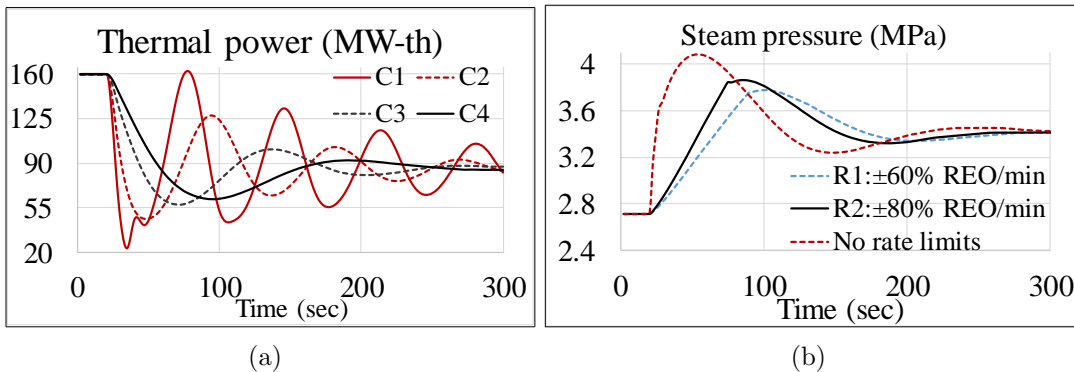


**Figure 4.8:** Responses: (a) Thermal power with rod control, (b) Steam pressure with different valve rate limits.

The governor control settings,  $R_{open}$  and  $R_{close}$ , limit the rate of valve operation. Three different rate limits are considered: (a)  $\pm 60\%$  REO/min, (b)  $\pm 80\%$  REO/min, and (c) no rate limits. The overshoot beyond 4 MPa in steam pressure is considered a violation. Fig. 4.8(b) shows the steam pressure response for the three cases. Both  $\pm 60\%$  and  $\pm 80\%$  REO/min

provide satisfactory responses. Therefore, the valve rate limit of  $\pm 80\%$  REO/min ( $\pm 1.33\%$  REO/s) is selected.

After designing the controllers for governor and rod control systems, the power system setup is simulated for electrical load demand changes. With the change in electrical load, the system frequency drifts from 60 Hz, and the governor will respond by operating the turbine valve to achieve the new demand. The governor system is controlled in isochronous mode, which will bring the system frequency back to the original 60 Hz. The turbine valve operation disrupts the power flow balance between the primary and secondary coolant. The control rod is steered to regulate the thermal power to reestablish the power balance. For the primary frequency control, the SMR may opt to operate without the control rod movement. Power adjustments without the control rod for up to 25% REO are seen occasionally, even for conventional NPPs [116].

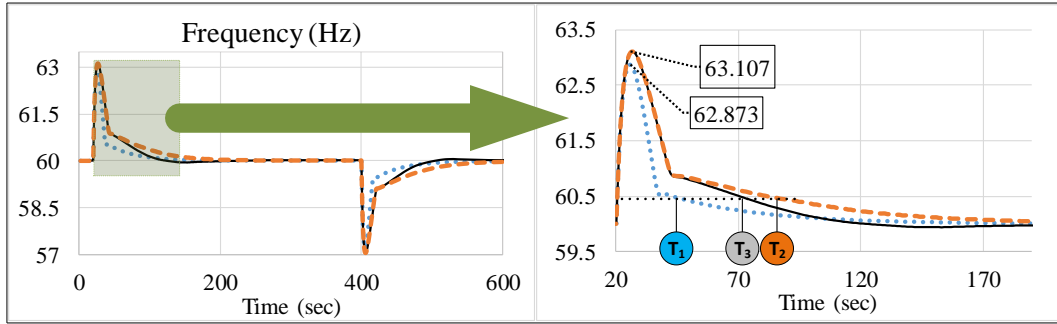
The total simulation time is 600 s. The electrical load changes from 100% to 80% REO of the SMR at 20 s. The system is allowed to settle until 400 s. At 400 s, a 20% step increase brings the load back to 100% REO of SMR. Load step changes of  $\pm 20\%$  REO are considered here to evaluate the reactor model for an extreme case scenario of primary frequency control. In actual practice, the frequency disturbances would be smaller and, SMR may also share the demand fluctuations with other flexible power sources. Power system dynamics in this investigation is assessed in terms of the maximum frequency deviation and frequency recovery time. The frequency recovery within  $\pm 0.5$  Hz is considered a recovered state or a no trip zone, which also mimics the NERC standard for frequency relays for generators [49, 76]. As the simulation assumes an isolated configuration with large step changes in electrical load, the frequency deviations are bound to be much larger than in actual practical scenarios.

Three cases are considered: Case I-without reactor, Case II-with uncontrolled reactor, and Case III-with controlled reactor. The power system responses are plotted in Fig. 4.9. The reactor side responses are plotted in Fig. 4.10.

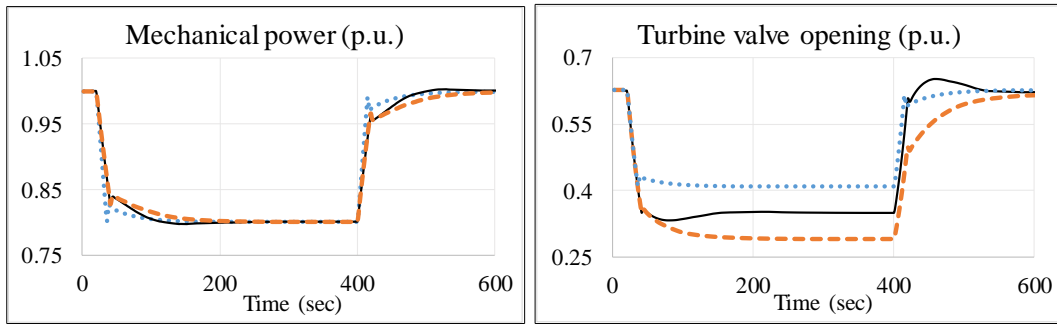
#### **4.6.1 Case I: Without Reactor**

Case I is activated by switching the pressure input  $p_{in}$  of the flow model in Fig. 4.3 to  $p_{ref}$ . The turbine-governor model with a valve rate limit of  $\pm 80\%$  REO/min replicates the design

limit of SMR to offer the power variation. The zoomed section of the frequency response in Fig. 4.9(a) shows the frequency response corresponding to the step decrease in load at 20 s. The frequency overshoot in Case I is 62.873 Hz, while the frequency recovers at  $T_1$ (=43 s) of the simulation. A similar trend is seen for the load step increase occurring at 400 s. As the reactor model is kept inactive for Case I, the reactor side responses are not available.



(a) Frequency: fullscale and zoomed section



(b)  $P_{mech}$

(c)  $\mu$

**Figure 4.9:** Power system dynamic responses for step changes in electrical demand. Legend: Case I(.....), Case II(- - -), Case III(—).

## 4.6.2 Case II: With Uncontrolled Reactor

The reactor model is activated by switching  $p_{in}$  of the flow model back to  $p_{sat}$ . The control rod system is disabled; thus, the average coolant temperature will not remain constant. The change in thermal power occurs due to the temperature feedback on core reactivity. Because the reactor model is activated, the flow model receives variable pressure from the reactor model. When the load demand decreases at 20 s, the valve closes and leads to an increase in steam pressure, which in turn necessitates the valve to close even more to match the

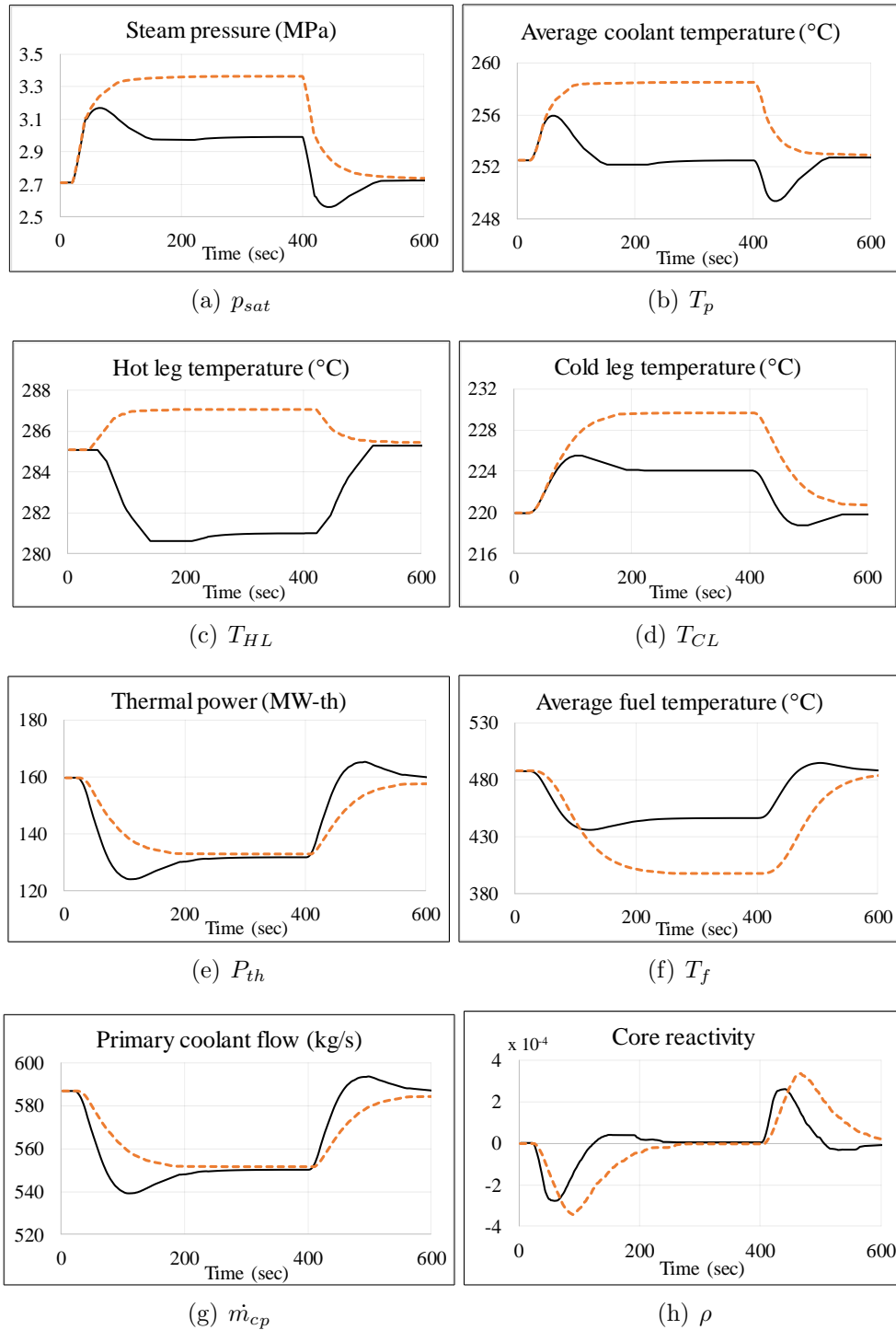


**Figure 4.10:** Reactor dynamic responses for step changes in electrical demand. Legend: Case II(- - -), Case III(—).

new load demand. The case is worsened when the reactor is not controlled to maintain the average coolant temperature, causing the steam pressure to rise even more. The temperature of the primary coolant increases, decreasing the net core reactivity. The reactor thermal power and fuel temperature decrease, and the reactor settle when the reactivity feedbacks due to the decrease in fuel temperature and an increase in coolant temperature balance each other. The steam pressure settles at 3.37 MPa, while the system thermal power settles with a net decrease of 26.98 MW(th), as shown in Fig. 4.10(e). With a bigger change in valve opening, shown in Fig. 4.9(c), the turbine takes more time to achieve the new mechanical power. Consequently, the frequency response will be slower with a frequency recovery time of  $T_2(=81\text{ s})$ , as shown in Fig. 4.9(a). The frequency overshoot is 63.107 Hz. A similar trend is seen for the load step increase occurring at 400 s.

### 4.6.3 Case III: With Controlled Reactor

The control rod system is activated, and the reactivity of the core is controlled to maintain the average primary coolant temperature constant. When the load decreases at 20 s, the valve closes and causes an increase in steam pressure. However, due to the control rod insertion, the core reactivity decreases, reducing the thermal power, average fuel temperature, and primary coolant flow rate. As a result, the hot leg temperature decreases, keeping the average coolant temperature constant. The steam pressure recovers and settles at 2.99 MPa, as shown in Fig. 4.10(a). The pressure recovery allows the turbine to achieve the new mechanical power at a higher valve position, thus reducing the change required in the valve position. Fig. 4.9(a) shows the frequency recovery time is  $T_3(=70\text{ s})$ , while the frequency overshoot is 63.107 Hz. The thermal power settles with a net decrease of 28.1 MW(th), as shown in Fig. 4.10(e).

### 4.6.4 Comparison

In Case I, the reactor dynamics was not considered, and, as a result, the electrical side responses had inaccuracies. The frequency overshoot was 0.234 Hz less than the other two cases, and the frequency recovery time was 38 and 27 s less than in Case II and Case III, respectively. In Case II, the frequency response was obtained without control rod operation.

Although the frequency overshoot was about the same, the frequency recovery time was 11 s slower compared to Case III for the same electrical disturbance. The change in steam pressure was 0.38 MPa more than in Case III. Similarly, the overshoot in core reactivity, variation of fuel temperature, and range of primary coolant temperature were significantly more for Case II. These results indicate the range of power variation possible with an uncontrolled reactor is considerably less than with a controlled reactor. Therefore, the controlled reactor-based frequency response is faster, more stable, and relatively safer than the uncontrolled case.

## 4.7 Conclusion

This paper proposed a dynamic model of an iPWR-type SMR to facilitate the inclusion of SMR dynamics in power system dynamic studies. The SMR model included the heat generation process based on point kinetics, RPV thermal hydraulics based on natural circulation, and a simplified three lump representation of SG. The generic GGOV1 turbine-governor model was modified with a valve mapping module to incorporate the steam pressure variation from the reactor. A power system dynamic study was conducted to evaluate the contribution of the reactor dynamics in power system frequency response. The results showed the power system and reactor responses for a 20% step change in electrical load for three different cases: without reactor, with uncontrolled reactor, and with controlled reactor. The comparisons showed the significance of an SMR model for power system dynamic studies and the necessity of reactor control for primary frequency control.

# 5 Small Modular Reactor Based Hybrid Energy System for Electricity & District Heating

## Preamble

This study aims to fulfill a part of the third objective of the thesis mentioned in Section 1.3. The contribution of this chapter to the overall research is to develop a simulation model of SMR-RES hybrid energy system for electricity and district heating.

In this study, the SMR dynamic model proposed in Chapter 4 will be further developed to incorporate steam bypass and steam extraction systems for cogeneration simulation. The models will then be integrated with the electrical and heating systems consisting of PV, wind, BESS, DH system and TES. A case study will demonstrate the simulation of proposed models with 24-hr load and generation profiles.

<sup>1</sup>This manuscript is being considered for publication (with revisions) in *IEEE Transactions on Energy Conversion*, September 2020. I developed the hybrid energy system model in PSS®E and PSS®Sincal under the guidance of Prof. Gokaraju. I also prepared the preliminary draft and carried out the revisions in the paper.

## 5.1 Abstract

Hybrid energy systems with small modular reactors (SMRs) and renewable energy sources (RESs) hold a significant promise for the development of clean energy systems. This paper

---

<sup>1</sup>B. Poudel and R. Gokaraju, "Small modular reactor (SMR) NPP based hybrid energy system for electricity & district heating," submitted to *IEEE Transactions on Energy Conversion*, June 2020(Under review).

proposes a model of SMR based hybrid energy system for electricity and district heating (DH) with a detailed dynamic model of the reactor and a quasi-static model of the DH system. A multi-timescale approach, decoupling load following (LF) and frequency control (FC) operations, is proposed to assess the flexible operation in the presence of highly intermittent RESs. A portion of IEEE 30-bus network is used as a test system for simulating the proposed hybrid energy system. The simulation results shown for a 24-hr period demonstrates the benefit of including the DH system, thermal energy storage, and electrical energy storage for SMR's flexible operation.

## 5.2 Nomenclature

$\dot{m}_{cs}$	Total steam flow output of SMR module, kg/s
$\dot{m}_{HX2}^{max}, \dot{m}_{HX2}^{max}$	Maximum flow limits of HX1 & HX2, kg/s
$\dot{m}_{bv}, \dot{m}_{ev}$	Steam flow to the bypass valve & extraction valve, kg/s
$\dot{m}_{DH}, \dot{m}_{waste}$	Steam flow to DH system, waste steam, kg/s
$\dot{m}_{ext}$	Steam extracted from an SMR module, kg/s
$\dot{m}_{HX1}, \dot{m}_{HX2}$	Steam flow to HX1 and HX2, kg/s
$\dot{m}_{HP}, \dot{m}_{LP}$	Steam flow to HP and LP turbines, kg/s
$\dot{m}_{pipe}$	DH pipeline water flow, kg/s
$\eta_T$	Turbine efficiency
$\mu_{b,max}, \mu_{b,min}$	Maximum and minimum bypass valve position
$\mu_{max}, \mu_{min}$	Maximum and minimum main steam valve position
$\rho_{str}$	Density of storage material, kg/m <sup>3</sup>
$c_p, c_{pstr}$	Specific heat capacity of DH pipeline water & TES storage material, kJ/(kg °C)
$f$	Power system frequency, Hz
$G_p$	PV irradiance, W/m <sup>2</sup>
$i, j$	Index numbers for load following (LF) interval and SMR modules
$K_P, K_I$	Proportional and integral gain
$P_{wind}^r$	Rated power output of a wind turbine, MW

$P_{BESS}$	Power output of BESS, MW
$p_{sat}, p_{ref}$	Steam pressure, reference pressure setpoint, MPa
$P_{SMR}$	SMR electrical power output, MW
$P_{wind}, P_{PV}$	Power output of wind and PV plants, MW
$q_{HX3}^{max}$	Maximum thermal power output of the TES, MWth
$q_{dem}$	Heating load demand, MWth
$q_{DH}, q_{HX1}$	Thermal power transferred to the DH system and HX1, MWth
$q_{HX2}, q_{HX3}$	Thermal power transferred to HX2 and HX3, MWth
$T_{str}^{max}, T_{str}^{min}$	TES maximum and minimum temperature limits, °C
$T_{DH,out}^r$	DH pipeline outlet rated temperature, °C
$T_p, T_{p,ref}$	Average primary coolant temperature, reference temperature setpoint, °C
$T_{DH,in}, T'_{DH}$	Temperatures: DH inlet, DH intermediate, °C
$T_{DH,out}, T_{str}$	Temperatures: DH outlet, and TES, °C
$T_{ext}$	Steam extraction temperature, °C
$V_G$	GGOV1 governor signal output, p.u.
$V_{str}$	TES volume, m <sup>3</sup>
$ws, ws_r$	Instantaneous wind speed and wind turbine rated speed, km/hr
$ws_{ci}, ws_{co}$	Wind turbine cut-in speed and cut-out speed, km/hr
$\Delta H_{ext}$	Useful enthalpy of extracted steam, kJ/kg
$\Delta H_{LP}, \Delta H_{LP}$	Enthalpy used at HP turbine, LP turbine, kJ/kg
$\Delta t_{LF}$	Resolution of long time frame simulation, s

### 5.3 Introduction

Small modular reactor (SMR) based nuclear power plants (NPPs), characterized by their smaller size, modular construction and faster response rates, are being advocated along with intermittent renewable energy sources (RESs) to form sustainable clean energy systems in remote communities and isolated electrical grids [25, 106].

Although the new SMRs are designed to offer flexible operation, they will still have technical challenges similar to the large NPPs. Frequent use of control rod for large power

variations aggravates various issues such as thermal fatigue and ageing of the reactor components, erosion and corrosion of active hydraulic components, core power redistribution, and fission product poisoning [17,18]. The increased turbine bypass use results in additional wear and tear of condenser shell and tubes, steam bypass lines, and associated valves [18]. Due to these challenges, the reactor control is restricted within the design limits defined in terms of rate of change, total variation and the total number of large power cycles over the reactor lifetime [17,18].

Cogeneration not only fast tracks the payback of the capital investment with NPPs but also offers a means to solve the reactor's techno-economical limitations to provide flexible operation [60,61]. Various cogeneration possibilities of the nuclear-renewable hybrid energy system (NRHES) are explored in Idaho National Laboratory-based research projects reported in [42–44,117,118]. Reference [42] investigates opportunities, issues, and cost-benefits scenarios of NRHES with different interaction modes. References [43,44,118] analyze the financial and dynamic aspects of hybrid energy systems proposed for industrial applications such as gasoline production, seawater desalination and hydrogen production.

In the context of isolated communities such as the ones located in northern part of Canada where the access to both the electrical grid and the natural gas is limited, a hybrid energy system based on SMR can provide a solution for both electricity and district heating requirements. The use of SMR for heat and electricity is investigated in some recent references, such as [22,58,68,69]. Reference [68] investigates the techno-economic aspects of NuScale and DHR-400 reactors in heating and cooling applications. Reference [58] proposes a model of NHR200-II reactor for electricity and district heating. Reference [22] models a cogeneration system with a GTHTR300C reactor to support the electrical load following. Reference [69] models a flexible heating load to compensate electrical side variation while keeping the SMR output effectively at baseload condition. While some of the references developed the thermodynamic model of the reactor for cogeneration, there have been no attempts to incorporate and simulate the operation of such models in electrical and heating systems.

Apart from the heat generation process and the extended safety-related precautions, the combined heat and electricity with SMR is similar to the combined heat and power (CHP) based on thermal plants. Thus, the modeling and simulation work based on CHP plants

available in the literature would be a good starting point to develop the model of SMR based hybrid energy system for electricity and district heating (DH). Reference [119] shows a methodology to investigate the coordinated operation of electrical and district heating systems. A market-driven approach to decentralize the interdependent power and heating networks is proposed in [120]. The flexibility of CHP plants to accommodate the intermittent RESs is analyzed in [121–123]. Reference [124] discusses the role of thermal energy storage (TES), heat pumps, and electric boilers to improve the flexibility of CHP plants to accommodate larger wind penetration in the system. Reference [125] discusses a dynamic model of the hot water storage tank and designs the controllers for charging and discharging processes. Reference [126] presents the accurate models of sensible heat and latent heat TES devices to utilize their full potential in CHP plants. Reference [127] proposes the pipeline energy storage models for the DH system, while [128] uses the models to optimize the unit-commitment coordinating the electrical and the DH systems.

The hybrid energy system with SMR and RES for electricity and DH has a significant potential to develop a sustainable clean energy system for isolated communities. There is a clear need for proper simulation models to investigate the operation of such energy systems.

In authors’ earlier paper [101], a dynamic model of NuScale integral pressurized water reactor (iPWR)-type SMR was developed and integrated with a standard turbine-governor model in PSS®E. A case study was also shown simulating the reactor model for electrical load variations. In this paper, the reactor model is further developed by including the turbine bypass and steam extraction systems for cogeneration simulation. The resulting SMR model is then integrated with the electrical and DH systems. The major contributions of this paper are summarized below:

1. A model of SMR-RES hybrid energy system for electricity and DH with a detailed dynamic model of SMR coupled with a quasi-static model of the district heating system,
2. A multi-timescale approach, decoupling the flexible operation in two separate time frames for frequency control (FC) and LF operations.

The rest of the paper is organized as follows. Section 5.4 provides a general description of the SMR based hybrid energy system cogenerating heat and electricity. Section 5.5 discusses

the detailed modeling of the hybrid energy system components. Section 5.6 implements the proposed models in a test system for the multi-timescale simulation. Section 5.7 gives the conclusions of the research work.

## 5.4 Proposed SMR Plant Coupled to DH System

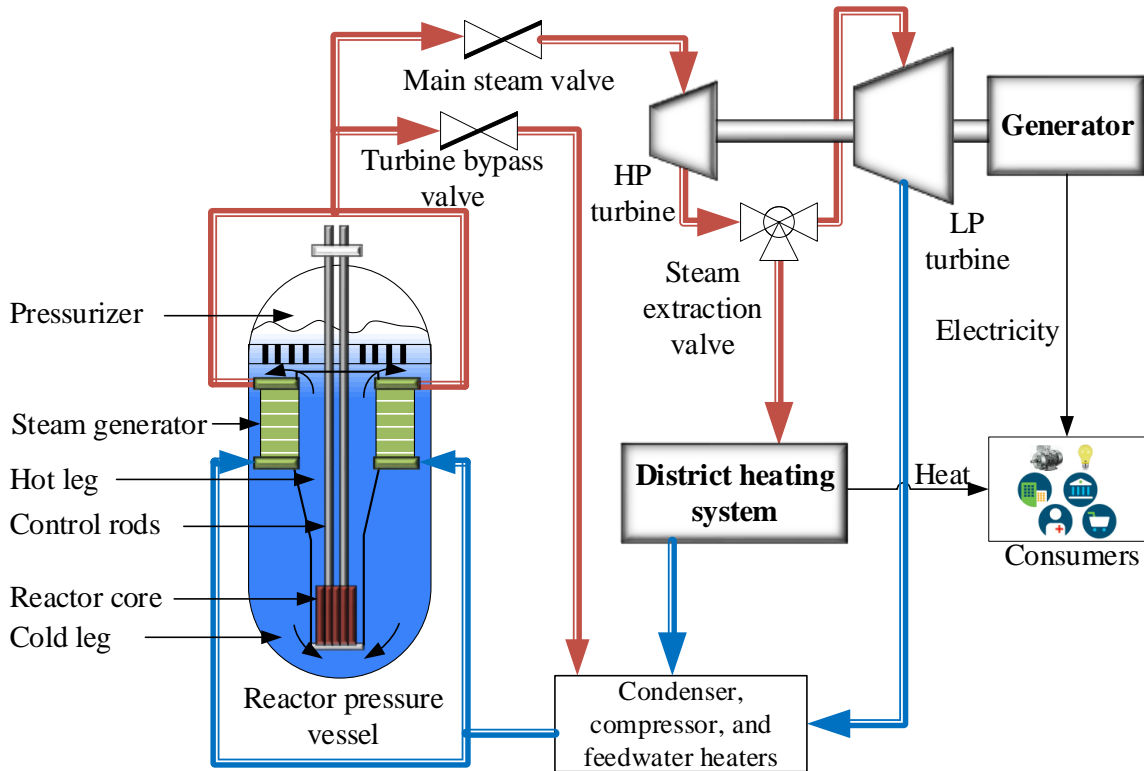


**Figure 5.1:** NuScale iPWR module cogenerating heat and electricity

Fig. 5.1 depicts the schematic diagram of a NuScale iPWR module cogenerating heat and electricity. The reactor core consists of 37 standard  $17 \times 17$  fuel assemblies, with the core height almost half the height of a nominal pressurized water reactor (PWR) [109]. The primary coolant flow is based on natural circulation. The reactor module consists of two vertical, once-through, helical coil steam generators (HCSG) located between the hot leg riser and the external diameter wall [110]. Preheated feedwater enters through the lower plenum of the steam generator, where it boils after receiving heat from the primary coolant. The upper plenum of the steam generator delivers steam to the turbine units. The main steam valve (MSV) regulates the steam flow to the turbines.

The turbine bypass system dumps the excess steam directly to the condenser. It is designed to bypass up to 100% of the rated steam flow. The turbine bypass system offers independent adjustability for the electrical load while avoiding the reactor control for short-term variations.

The flexibility offered by the cogenerating system depends upon the type of steam turbine used. In backpressure turbines, the turbine exhaust is adjusted at a temperature and pressure suitable for the process application. Though highly efficient, backpressure turbines operate with a fixed power-to-heat ratio, making them less flexible than extraction turbines where the extraction flow is regulated using valves. For the proposed system where SMRs' flexible operation is crucial, the extraction turbines are more suitable.

Steam is expanded in a number of turbine stages. Reference [115] shows the turbine configuration of the NuScale SMR module, where the steam expands over eight turbine stages. The steam at a temperature suitable for the DH application (120 to 130 °C) is extracted from one of those turbine stages. Fig. 5.1 groups the multiple turbine stages into two sets, high pressure (HP) and low pressure (LP) turbines. The steam extraction system is placed between HP and LP turbines. The LF signal regulates the steam extraction.

## **5.5 Dynamic Modeling**

The authors' earlier publication [101] discusses the dynamic models of the reactor pressure vessel (RPV) and steam generator (SG) in detail. They are not discussed in this paper to avoid repetition. This paper only discusses the dynamic models of new system components.

### **5.5.1 Secondary Coolant**

#### **5.5.1.1 Turbine Bypass System**

The variation of average primary coolant temperature is sensed by the PI controller, which generates a signal to operate the bypass valve. The control block diagram of the turbine bypass system is shown in Fig. 5.2.

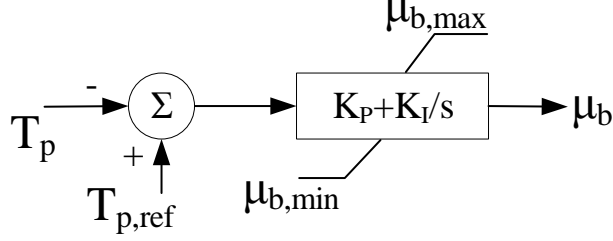


**Figure 5.2:** Control block for the turbine bypass system

### 5.5.1.2 Steam Extraction System

The steam extraction system operates in response to the LF signal. The extraction level is changed linearly irrespective of the short-term disturbances during the LF interval. The variation of steam extraction flow by (5.1).

$$\frac{d\dot{m}_{ev}}{dt} = \frac{\dot{m}_{ext}(i+1) - \dot{m}_{ext}(i)}{\Delta t_{LF}} \quad (5.1)$$

### 5.5.2 Turbine-Governor Model

The authors' SMR modeling paper [101] describes the integration of GGOV1 turbine-governor model with the reactor model. Fig. 5.3 shows the additional modifications in GGOV1 to include the turbine bypass and steam extraction systems.

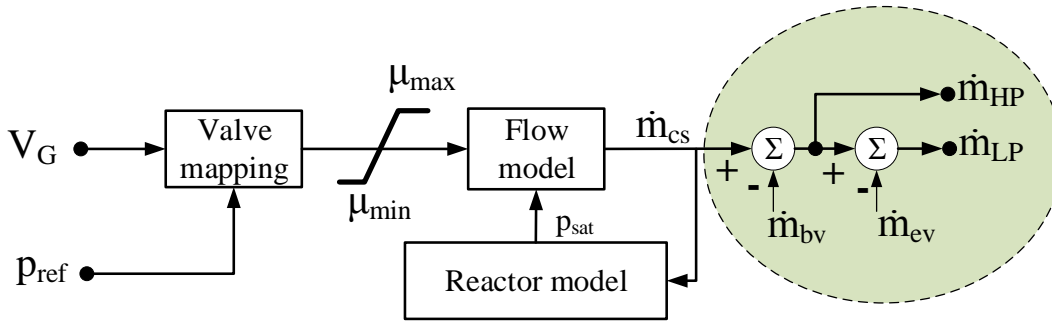


**Figure 5.3:** A section of modified GGOV1. Encircled portion shows the inclusion of turbine bypass and steam extraction systems.

The mechanical power ( $P_{mech}$ ) is a function of enthalpy differences and steam flowrates, as given by (5.2).

$$P_{mech} = \eta_T(\Delta H_{HP}\dot{m}_{HP} + \Delta H_{LP}\dot{m}_{LP}) \quad (5.2)$$

The variations in  $\Delta H_{HP}$  and  $\Delta H_{LP}$  are very small. Therefore,  $P_{mech}$  can be taken as a function of steam flowrates,  $\dot{m}_{HP}$  and  $\dot{m}_{LP}$ .

### 5.5.3 District Heating System Model

Fig. 5.4 shows the block diagram of the DH system. The steam extracted from the SMR modules is transferred to the steam distribution system, which distributes the steam flow to the heat exchange stations (HXs) using dedicated valves. A hot water storage tank is used as the TES device. The HXs used in the DH system are counter-flow heat exchangers.

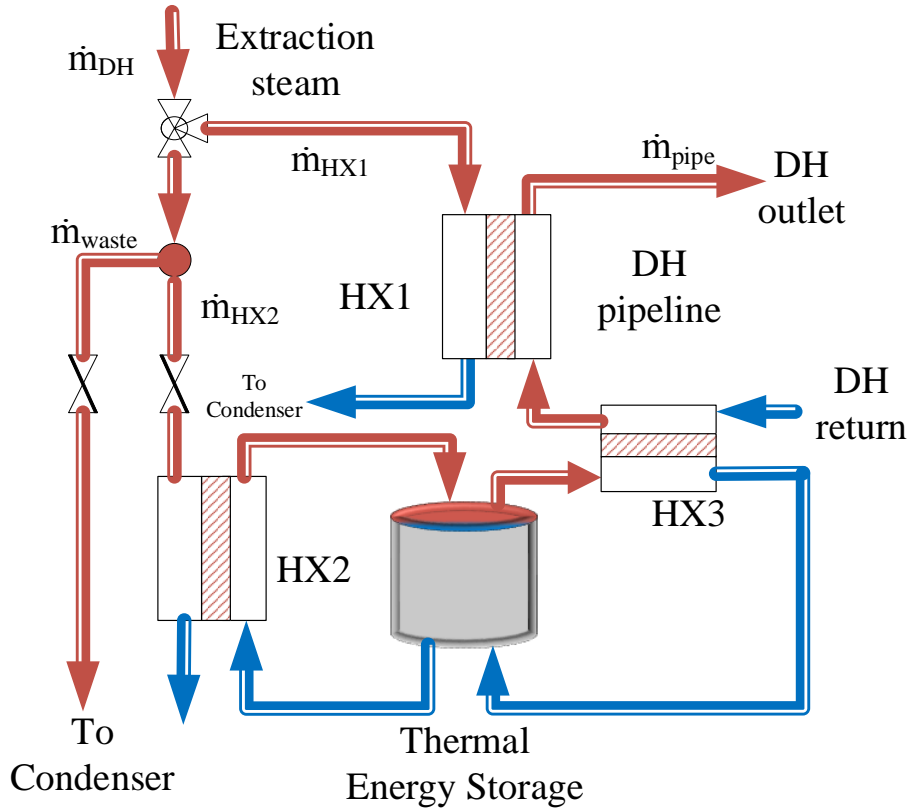


Figure 5.4: Block diagram of the DH system

The extracted steam from the SMR modules is collected and supplied to the DH system. The steam flow rate to the DH system is the sum of individual extracted flows, as given by (5.3).

$$\dot{m}_{DH}(i) = \sum_{j=0}^N \dot{m}_{ext}^j(i) \quad (5.3)$$

where  $N$  is the number of reactor modules in the SMR plant.

The DH system uses the latent heat present in the extracted steam. The thermal power utilized from the extracted steam is given by (5.4).

$$q_{DH}(i) = \dot{m}_{DH}(i)\Delta H_{ext}(i) \quad (5.4)$$

A portion of extracted steam is supplied to HX1 based on the heating demand. The rest of the steam is supplied towards HX2. The steam excess to HX1 and HX2 is diverted to the condenser as a waste steam.

$$\dot{m}_{waste}(i) = \dot{m}_{DH}(i) - \dot{m}_{HX1}(i) - \dot{m}_{HX2}(i) \quad (5.5)$$

$\dot{m}_{HX1}$  is regulated based on the heating demand.  $\dot{m}_{HX2}$  is limited by the design flow limit of HX2 and upper temperature limit of the TES.

$$\dot{m}_{HX1}(i) = \begin{cases} \dot{m}_{DH}(i), & \text{if } q_{DH}(i) \geq q_{dem}(i) \\ \frac{q_{dem}(i)}{q_{DH}(i)}\dot{m}_{DH}(i), & \text{otherwise} \end{cases} \quad (5.6)$$

$$\dot{m}_{HX2}(i) = \begin{cases} 0, & \text{if } T_{str}(i) \geq T_{str}^{max} \\ \dot{m}_{HX2}^{max}, & \text{if } \dot{m}_{DH}(i) - \dot{m}_{HX1}(i) \geq \dot{m}_{HX2}^{max} \\ \dot{m}_{DH}(i) - \dot{m}_{HX1}(i), & \text{otherwise} \end{cases} \quad (5.7)$$

### 5.5.3.1 Heat Exchange Stations

It is assumed that the latent heat of the extracted steam is completely utilized in the heat exchangers. The thermal power transferred to HX1 and HX2 is given by (5.8) and (5.9).

$$q_{HX1}(i) = \dot{m}_{HX1}(i)\Delta H_{ext}(i) \quad (5.8)$$

$$q_{HX2}(i) = \dot{m}_{HX2}(i)\Delta H_{ext}(i) \quad (5.9)$$

HX3, on the other hand, utilizes the heat stored in the TES to preheat the DH return at HX3. The heat transferred to HX3 is limited by the TES's thermal power transfer limit. Additionally, the TES can't provide heat to the DH water beyond its own temperature. The thermal power supplied by HX3 to the DH pipeline water is given by (5.10).

$$q_{HX3}(i) = \dot{m}_{pipe} c_p [T'_{DH}(i) - T_{DH,in}(i)] \quad (5.10)$$

where  $q_{HX3}(i) \leq q_{HX3}^{max}$ ;  $q_{HX3}(i) = 0$  if  $T_{str}(i) \leq T_{str}^{min}$ ;  $T'_{DH}(i) < T_{str}(i)$ .

### 5.5.3.2 Thermal Energy Storage

TES receives heat at HX2 and supplies to the DH pipeline water at HX3. The average temperature of the water inside the TES represents the energy stored. The tank is assumed to be well insulated, and the heat loss through the walls is neglected. TES temperature is given by (5.11).

$$T_{str}(i+1) = T_{str}(i) + \frac{q_{HX2}(i) - q_{HX3}(i)}{V_{str} \rho_{str} c_{pstr}} \Delta t_{LF} \quad (5.11)$$

where  $T_{str}^{min} \leq T_{str}(i) \leq T_{str}^{max}$ .

### 5.5.3.3 DH Pipeline

The DH supply temperature is maintained at  $T'_{DH,out}$ , while the pipeline flow is maintained constant at  $\dot{m}_{pipe}$ . The return temperature,  $T_{DH,in}$ , however, varies with the heating demand. If the heat from the extracted steam is not sufficient to fulfill the heating demand, the DH return is preheated to temperature  $T'_{DH}$  at HX3. If the heat supplied from both TES and HX1 is insufficient, the DH supply temperature  $T_{DH,out}$  decreases and consequently  $T_{DH,in}$  also decreases. With the DH system temperature lowered in both supply and return, the TES would be able to fulfill the heating demand at lower temperatures during that interval. The temperatures of DH water at different stages are given by (5.12)-(5.14).

$$T_{DH,in}(i) = T_{DH,out}(i) - \frac{q_{dem}(i)}{\dot{m}_{pipe} c_p} \quad (5.12)$$

$$T'_{DH}(i+1) = T_{DH,in}(i) + \frac{q_{HX3}(i)}{\dot{m}_{pipe}c_p} \quad (5.13)$$

$$T_{DH,out}(i+1) = T'_{DH}(i+1) + \frac{q_{HX1}(i)}{\dot{m}_{pipe}c_p} \quad (5.14)$$

### 5.5.4 Power Output Models of Wind and PV Plants

The instantaneous wind speed and wind turbine parameters are used to calculate the wind turbine output [129]. The cut-in and cut-out speed define the operating zone. The power output of a wind turbine is given by (5.15).

$$P_{wind} = \begin{cases} (A + Bws + Cws^2)P_{wind}^r, & \text{if } ws_{ci} \leq ws < ws_r \\ P_{wind}^r, & \text{if } ws_r \leq ws \leq ws_{co} \\ 0, & \text{otherwise} \end{cases} \quad (5.15)$$

where the wind turbine parameters  $A$ ,  $B$ , and  $C$  are the functions of  $ws_{ci}$  and  $ws_{co}$ .

Similarly, the power output of a PV plant is calculated from the irradiance data using (5.16) [130].

$$P_{PV} = \eta_p A_p G_p (1 - 0.005(T_a - 25)) \quad (5.16)$$

The panel array area  $A_p$  and efficiency  $\eta_p$  are the plant constants. The dependence on ambient temperature  $T_a$  could be excluded for a very variable irradiance scenario. Therefore, the power output of a PV plant can be considered a linear function of the irradiance.

### 5.5.5 Battery Energy Storage System (BESS) Dynamic Model

The Electrical Power Research Industry (EPRI) based CBEST model is used to represent the BESS [131]. BESS is controlled to provide the primary frequency response. The capability of BESS to provide inertial support and long term storage is not considered in this paper. A simple PI controller is designed to regulate BESS output in response to the frequency

deviation. The power output of the BESS model is given by (5.17).

$$P_{BESS} = (K_{P,B} + \frac{K_{I,B}}{s})(f - 60) \quad (5.17)$$

## 5.6 Case Study

The proposed models are used to investigate the operation of the SMR-RES hybrid energy system for heat and electricity. The models are integrated with the power system models in PSS®E and PSS®Sincal simulation software platforms<sup>2</sup>. The overall study is divided into two parts— long-time-frame (LTF) assessment and short-time-frame (STF) assessment.

The LTF assessment investigates the flexible operation of the hybrid energy system in the LF mode. The 24-hr demand variation profiles with 15-min resolution datasets are utilized to examine the feasibility of the LF operation. The STF assessment, on the other hand, investigates the flexible operation in the FC mode within each 15-min duration.

It should be noted here that the reactor model is updated with new design parameters obtained from [109, 110, 115]. The rated electrical output (REO) of the reactor module is now 50 MWe. The rated steam flow on the secondary side is 65.93 kg/s. The temperature of preheated feedwater in the secondary coolant circuit is kept constant at 148.1 °C. The reactor is controlled using the constant average primary coolant temperature control method. The average temperature setting of 260 °C is chosen to match the steam pressure at rated power close to the one provided in [115].

### 5.6.1 Test System Description

The 33 kV portion of the IEEE 30-bus network with a total installed load of 105 MW is selected as the case system. It could be isolated from the 230 kV portion by taking four 230/33 kV transformers out of service. A NuScale SMR plant with two reactor modules, 50 MWe each, is chosen for this case study.

Fig. 5.5 shows the case system with SMR and RESs hosted at different nodes. The 100 MWe SMR plant is hosted at node 10; a 40 MW wind plant is hosted at node 15;

---

<sup>2</sup>The MATLAB code for the quasi-static model of DH system is provided in Section B.2 of Appendix B.

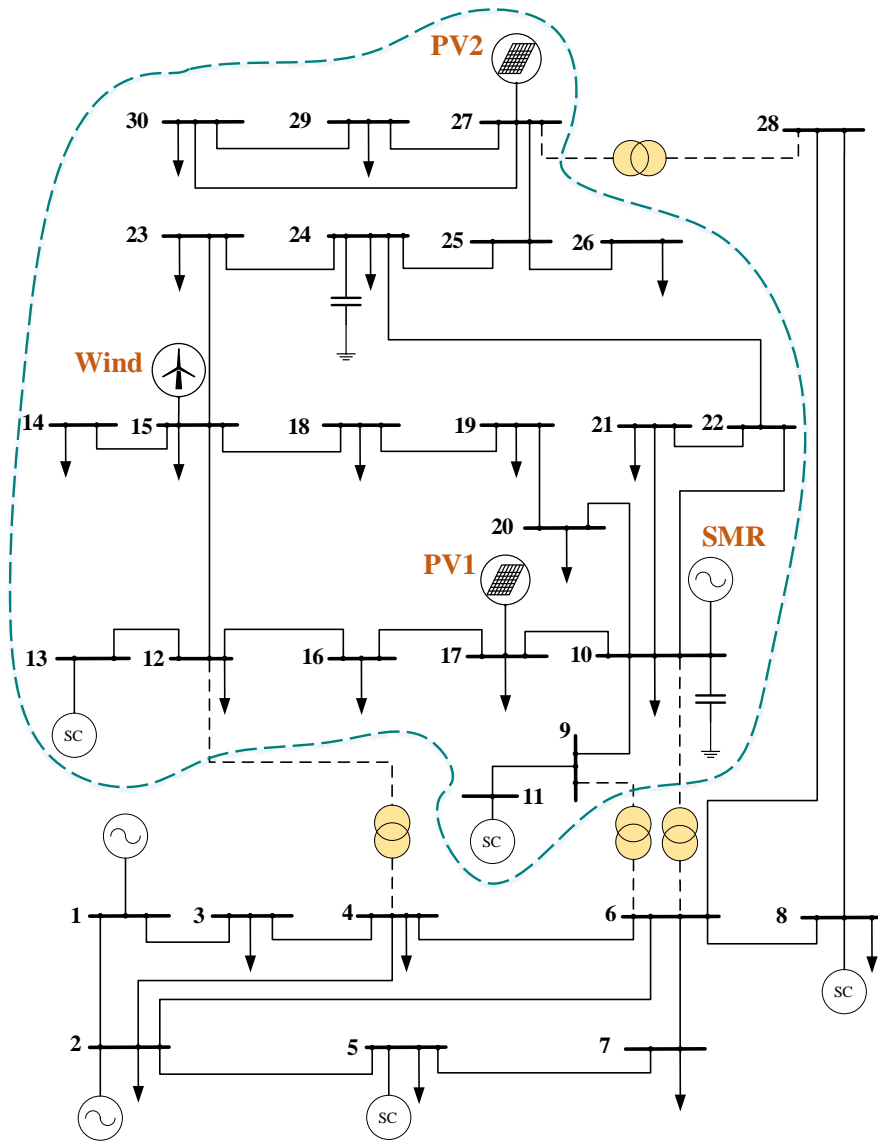


**Figure 5.5:** IEEE 30-bus network used for the case study. Encircled 33 kV portion is isolated by keeping four 230/33 kV transformers out of service.

two PV plants, 15 MW each, are hosted at nodes 17 and 27. The 15 load points of the modified IEEE-30 bus network are populated with a combination of industrial, commercial and residential load profiles of 15-min resolution. A high-resolution (sub-second) datasets of the PV irradiance profile for a very variable scenario is obtained from [103]. The wind speed profile of a 1-min resolution is obtained from [132]. With these RES profiles, the power output of wind and PV plants can vary as high as 47% and 61%, respectively, of their rated outputs within a minute duration. The heating demand is taken from [133] and scaled to match the size of the test system.

Fig. 5.6(a) provides the 24-hr electrical and heating load demand profiles. Fig. 5.6(b) provides the 24-hr wind speed and PV irradiance profiles. Table 5.2 lists the parameters for the wind and PV plants. Table 5.1 lists the DH system design parameters.

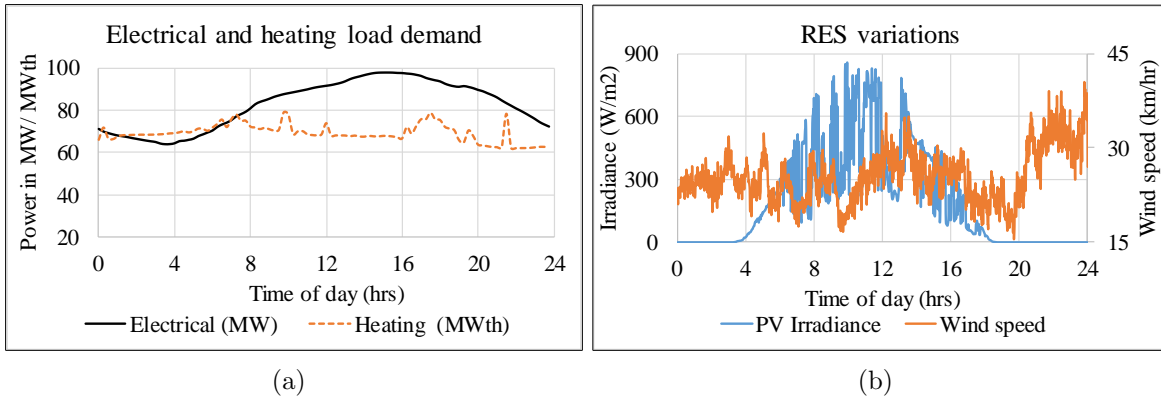


**Figure 5.6:** (a) Electrical and heating load demand profiles, (b) PV irradiance and wind speed profiles.

**Table 5.1:** DH system design parameters

DH components	Parameters
Steam extraction	$T_{ext} = 128 \text{ }^\circ\text{C}$
HX1	$\dot{m}_{HX1}^{max} = 50 \text{ kg/s}$
HX2	$\dot{m}_{HX2}^{max} = 50 \text{ kg/s}$
HX3	$q_{HX3}^{max} = 70 \text{ MWth}$
TES	$V_{str} = 10000 \text{ m}^3$ ; $T_{str}^{min} = 65 \text{ }^\circ\text{C}$ ; $T_{str}^{max} = 98 \text{ }^\circ\text{C}$ ; $c_{p,str} = 4.18 \text{ kJ}/(\text{kg } ^\circ\text{C})$
DH pipeline	$\dot{m}_{pipe} = 270 \text{ kg/s}$ ; $T_{DH,out}^r = 90 \text{ }^\circ\text{C}$ ; $c_p = 4.18 \text{ kJ}/(\text{kg } ^\circ\text{C})$

**Table 5.2:** Wind and PV parameters

Generation	Parameters
Wind Plant	No of turbines= 20; $P_{wind}^r = 2$ MW; $w_{s_{ci}} = 14.4$ km/hr; $w_{s_r} = 37$ km/hr; $w_{s_{co}} = 90$ km/h
PV plants (PV1 & PV2)	$\eta_p = 16\%$ ; $A_p = 109649.1$ m <sup>2</sup>

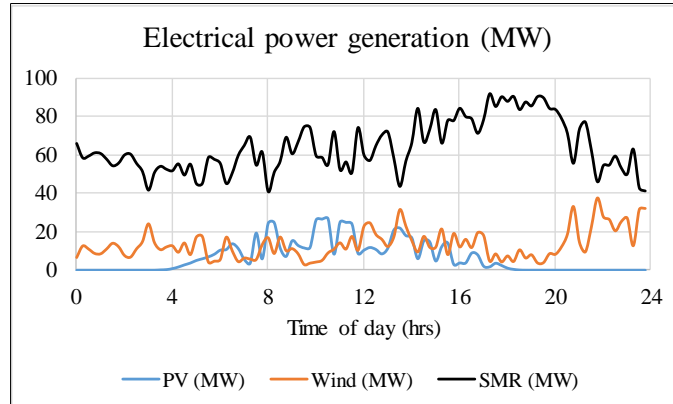
### 5.6.2 LTF Simulation Results

The time series power flow (TSPF) is conducted in the test system with 24-hr RES and load demand profiles with 15-min resolution. SMR plant is modeled as a slack bus.

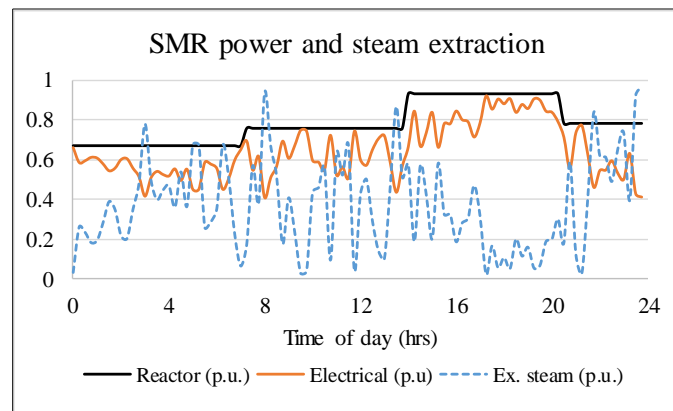
Fig. 5.7(a) plots the electrical outputs from PV, wind and SMR plants. The electrical output of SMR is varied with the help of DH extraction and control rod maneuvering. The DH system utilizes the excess steam while keeping the reactor variation at a feasible level. In the presence of the DH system, the SMR plant is maneuvered to four power levels in a 24-hr period with a 5-hour interval between the reactor power variations. The reactor modules could alternate the variations to limit the total variation per reactor twice per day. However, to simplify the results, it is assumed that both the reactor modules operate at four power levels and share demand equally during the 24-hr period. The reactor power level transition occurs within the ramp rate limits of  $\pm 2\%$  REO/min.

Fig. 5.7(b) provides the reactor power level (per unit of rated thermal power of the plant), electrical output (per unit of rated electrical power of the plant) and the steam extraction level (per unit of steam flow) of the SMR plant for the 24-hr period. Due to the large difference between electrical output and the reactor power level, the steam extraction reached a maximum of 0.938 p.u. at 8:00.

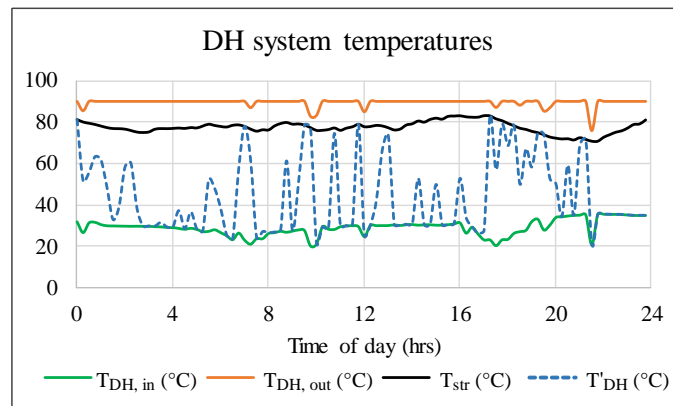
Fig. 5.7(c), on the other hand, plots the DH pipeline return, intermediate and outlet temperatures, and the TES temperature. Fig. 5.8(a) shows the distribution of extracted steam for the 24-hr period. For 52% of the time, the steam extracted was insufficient for the DH system and the heat energy stored in the TES was utilized. Since the TES couldn't provide heat beyond its temperature, the DH system was unable to maintain the supply temperature  $T_{DH,out}$  at 90 °C during ten separate intervals. With the decrease in  $T_{DH,out}$ ,



(a)

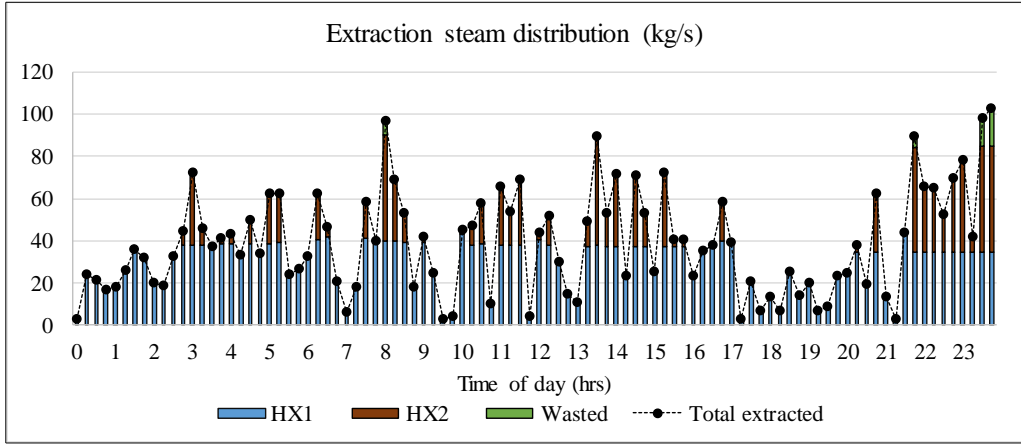


(b)

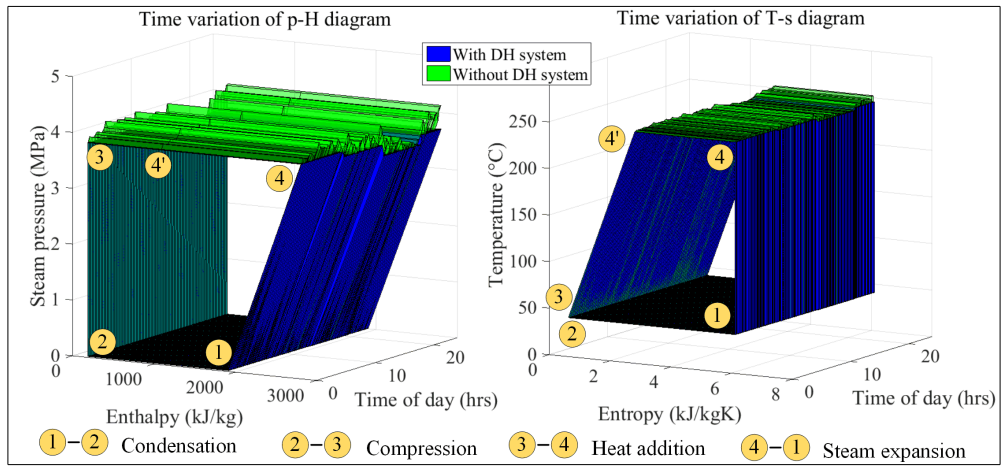


(c)

**Figure 5.7:** LTF system response considering the daily load and RES profiles. (Part-1)



(a)



(b)

**Figure 5.8:** LTF system response considering the daily load and RES profiles. (Part-2)

$T_{DH,in}$  also decreased. However, the temperature of TES remained well within limits during the 24-hr period and was always available for charging and discharging to support the DH system.  $T_{str}$  was 81 °C at the start of the day and 80.83 °C at the end of the day.

During the three separate intervals,  $\dot{m}_{HX2}$  exceeded the flow limit of HX2, and a portion of extracted steam was diverted directly to the condenser. A total of 20 MJ of extracted heat energy is wasted in the 24-hr period, which is 1.21% of the total heat extracted to the DH system.

Technically, the reactor is capable of load following with the reactivity control alone. For the sake of comparison, the secondary side p-H and T-s Rankine cycle diagrams are

shown in Fig. 5.8(b) to demonstrate the reactor secondary side thermodynamics with and without DH system. The four stages of the Rankine cycle—condensation, compression, heat addition, and expansion—are shown in the diagrams. Without the DH system, the reactor has to operate every 15 minutes, which is implied with the variations seen in the steam condition (temperature, pressure, enthalpy and entropy) in Fig. 5.8(b). The steam pressure and temperature vary respectively by 0.084 MPa and 1.27 °C on average per interval with maximum variations of 0.26 MPa and 4.077 °C occurring at 11:45. With the DH system, the steam condition varies just three times in a 24-hr period. The maximum variations in the steam pressure and temperature are 0.198 MPa and 3.16 °C occurring at 14:00 during the second change.

### 5.6.3 STF Dynamic Results

To simplify the STF assessment with the proposed dynamic models, a 3-bus equivalent of the test system is obtained with an SMR bus, a BESS bus and a load bus, as shown in Fig. 5.9. The per second equivalent demand at load bus represents the total variable demand, obtained by performing the TSPF in the test case network with the load profile, wind speed profile with 1-min resolution and PV irradiance profile of 1-sec resolution.

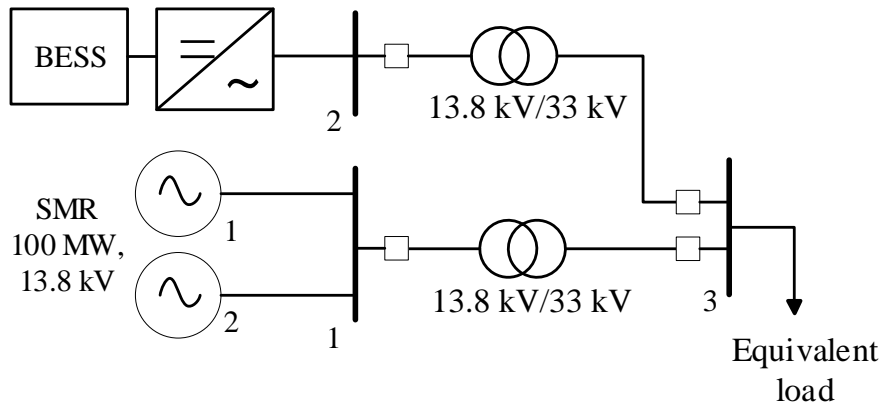
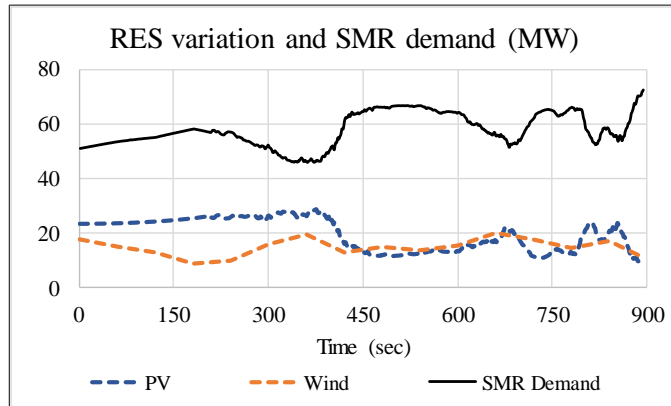
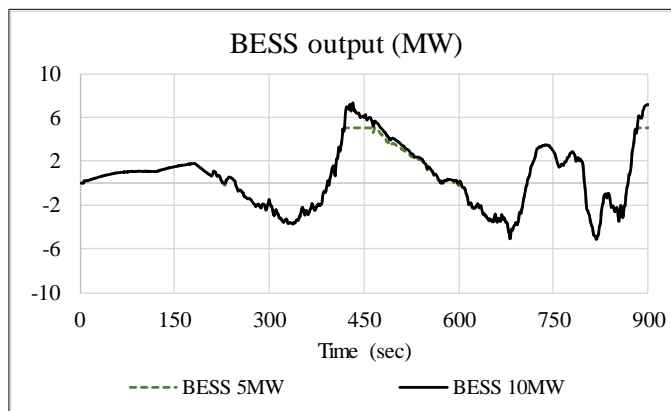


**Figure 5.9:** 3-bus equivalent network for STF assessment.

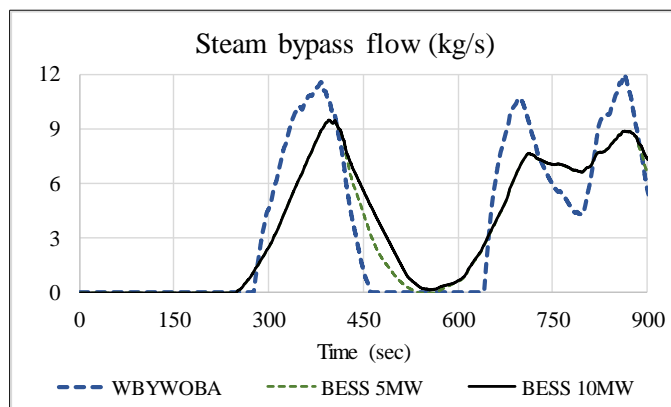
The 15 minutes period between 11:30 and 11:45 represents the worst-case scenario with the largest demand fluctuations. Fig. 5.10(a)-(c) and Fig. 5.11(a)-(b) provide the power system responses during the period of 900 s. The power output of PV and wind plants and



(a)

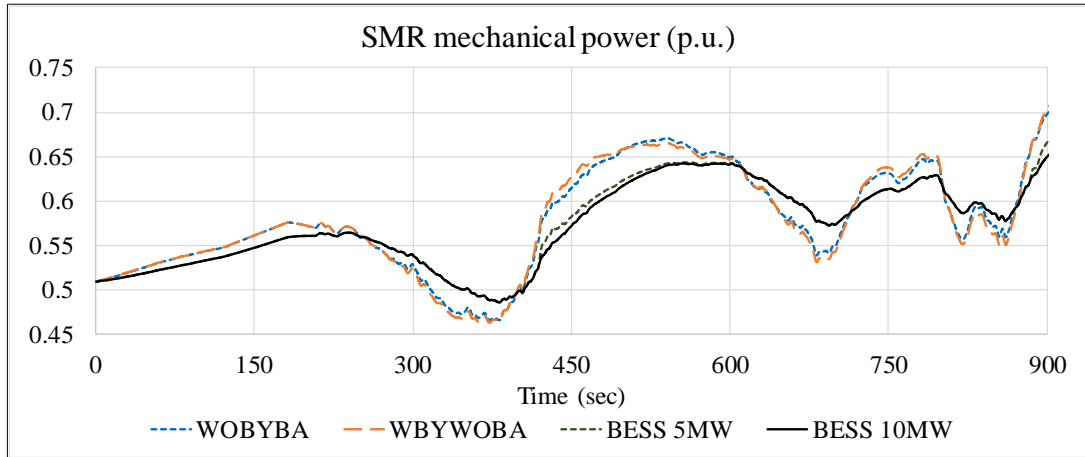


(b)

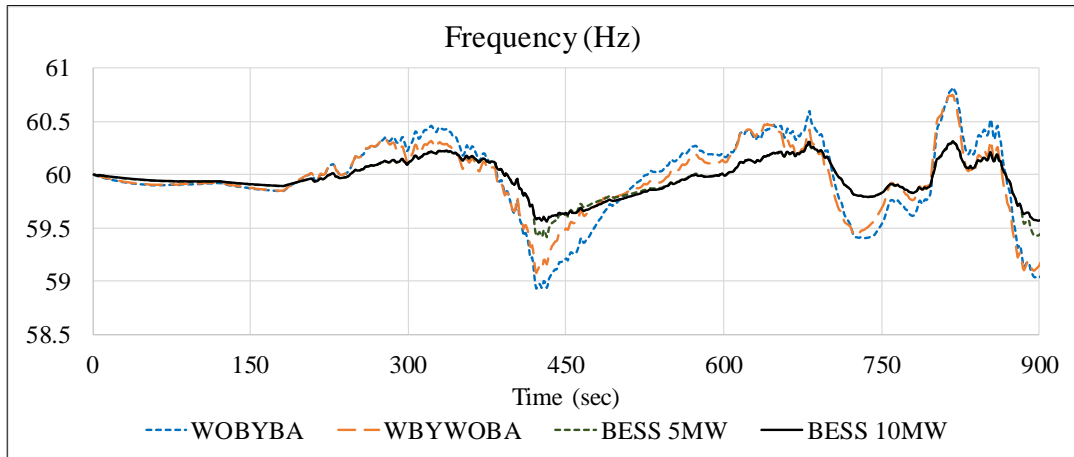


(c)

**Figure 5.10:** Power system responses during the worst 15 min of the day. Legend: WBYWOBA-with turbine bypass without BESS, BESS 5 MW-with turbine bypass and BESS of size 5 MW, BESS 10MW-with turbine bypass and BESS of 10 MW. (Part-1)

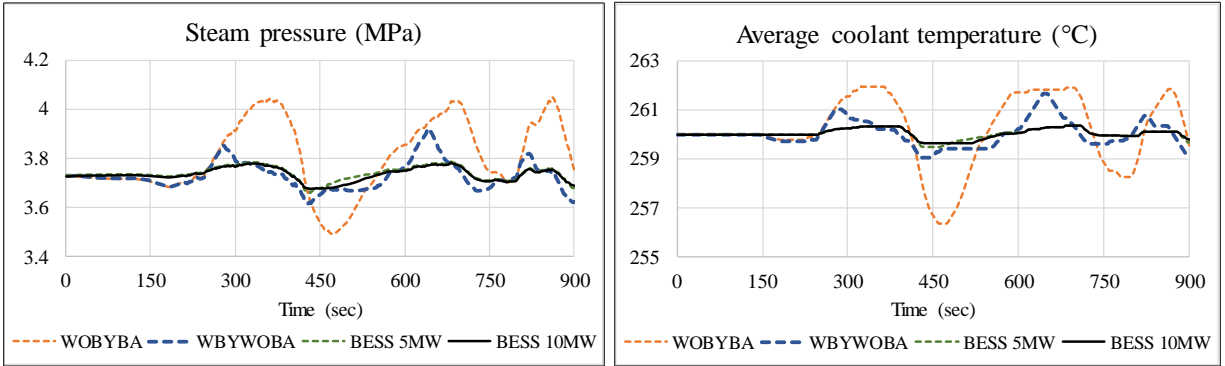


(a)



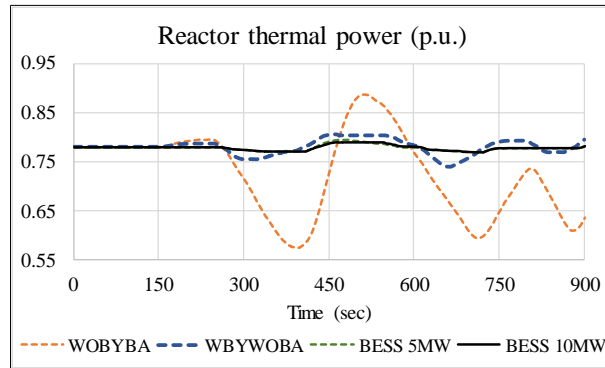
(b)

**Figure 5.11:** Power system responses during the worst 15 min of the day. Legend: WOBYBA-without turbine bypass and BESS, WBYWOBA-with turbine bypass without BESS, BESS 5 MW-with turbine bypass and BESS of size 5 MW, BESS 10MW-with turbine bypass and BESS of size 10 MW. (Part-2)



(a)

(b)



(c)

**Figure 5.12:** Reactor side responses during the worst 15 min of the day. Legend: WOBYBA-without turbine bypass and BESS, WBYWOBA-with turbine bypass without BESS, BESS 5 MW-with turbine bypass and BESS of size 5 MW, BESS 10MW-with turbine bypass and BESS of size 10 MW.

the equivalent demand variation at the load bus for 900 s duration are shown in Fig. 5.10(a). The SMR electrical output is varied by bypassing the steam directly to the condenser in response to the governor action. The actuation time of MSV and bypass valves result in transients in power system response. BESS is also included in this assessment to improve the power system dynamic response.

Four different cases are considered to illustrate the role of the turbine bypass system and BESS. In the first case, WOBYBA, the turbine bypass system and BESS are not included, and the power variation is achieved only with the reactivity control. The other three cases, WBYWOBA, BESS 5MW and BESS 10MW, include the turbine bypass system and BESS size of 0 MW, 5 MW and 10 MW, respectively. The power output of BESS is shown in Fig. 5.10(b). Fig. 5.10(c) provides the bypass flow, whereas Fig. 5.11(a) and (b) show the

SMR mechanical power and system frequency response during the period of 900 s. Since the results from the two reactor modules are identical, only one set of reactor response is provided.

The presence of BESS significantly improves the system frequency response as it can ramp quickly in response to the demand variations. With 10 MW BESS, the maximum frequency deviation is limited to  $\pm 0.5$  Hz. The turbine bypass system also operates slowly in the presence of BESS, and consequently, the mechanical power output of SMR ramps smoothly.

Fig. 5.12(a)-(c) provide the reactor side responses during the period of 900 s. In the absence of the turbine bypass system and BESS, the steam pressure overshoots beyond 4 MPa, as seen in Fig. 5.12(a). This results in a larger variation in average coolant temperature and the larger oscillation in the reactor thermal power, as shown in Fig. 5.12(b) and (c). For the latter 3 cases, the variation in temperature and pressure of the secondary coolant is very small resulting in minimal transient inside the reactor vessel. The small fluctuation seen in RPV variables in Fig. 5.12(a)-(c) is mainly due to the actuation of the bypass valve.

## 5.7 Conclusion

This paper proposed a model of SMR-RES hybrid energy system for electricity and district heating. The reactor model included the dynamic models of the reactor pressure vessel, turbine bypass system, and steam extraction system. The DH system was modeled to represent the steam distribution among heat exchangers and the quasi-static variation of DH system temperatures. A multi-timescale operational scheme was proposed to decouple the LF and FC operations. The reactor was controlled for coarse-level load shaping with a maximum of 3-4 variations per day. With the peak electrical demand predicted during the preceding five-hour duration, the reactor power level for the subsequent five hours was obtained in real-time. The steam extraction followed the same pattern but for every 15 minutes. On the other hand, the short-term variations were handled by the steam bypass system and BESS operating autonomously.

A case study with the modified IEEE 30-bus system showed that the proposed hybrid energy system is capable of providing flexible operation in the presence of highly variable

RESs. The LTF results showed that the steam surplus to the turbine demand could fulfill the heating demand. The DH system temperatures were maintained at an acceptable level, with only a small portion of steam wasted throughout the day. The STF results showed that the SMR, with the help of the turbine bypass system and BESS, is capable of providing satisfactory power system dynamic response while keeping the reactor side transients to a minimum.

# 6 Optimal Operation and RES hosting in SMR Based Hybrid Energy System for Electricity & District Heating

## Preamble

This study ensues the modeling work of Chapter 5 to fulfill the third objective of the thesis mentioned in Section 1.3. The contribution of this chapter to the overall research is to investigate the flexible operation and RES hosting capability of an SMR-RES hybrid energy system for electricity and district heating.

In this chapter, the models developed in Chapter 5 will be utilized to simulate the operation of the SMR-RES hybrid energy system in load following and frequency control modes with a month-long load and generation profiles. The sample results will be shown to demonstrate the optimal operation of the proposed hybrid energy system. An optimization problem will be formulated to evaluate the maximum size of PV and wind plants for the system.

<sup>1</sup>This manuscript has been submitted to *IEEE Transactions on Energy Conversion*, September 2020. I developed the operational framework for the hybrid energy system and formulated the optimization problem under the supervision of Prof. Gokaraju. I also performed the required simulations and wrote the paper.

---

<sup>1</sup>B. Poudel and R. Gokaraju, "Optimal operation of SMR-RES hybrid energy system for electricity & district heating," submitted to *IEEE Transactions on Energy Conversion*, September 2020 (Under review).

## 6.1 Abstract

Cogeneration coupling of the small modular reactor (SMR) based nuclear power plant (NPP) with district heating (DH) system enhances SMR's ability to provide flexible operation. The coordinated reactor control and DH steam extraction can fulfill the load following requirements, while the battery energy storage system (BESS) and the steam bypass system can absorb the short term disturbances, allowing the SMRs to host renewable energy sources (RESs) such as wind and photovoltaics (PV) in the system. This paper develops an optimal operational framework for the SMR-RES hybrid energy system for electricity and DH and utilizes the proposed scheme in a portion of the IEEE-30 bus system. The simulation results from a set of studies are provided to demonstrate the load following (LF) and frequency control (FC) operation for a month-long period. The optimization results are discussed to evaluate the optimum size of wind and PV plants for the proposed hybrid energy system.

## 6.2 Nomenclature

### 6.2.1 System Variables

$\Delta p_{max}$	Maximum limit of steam pressure deviation, MPa
$\dot{m}_{g,t}^{cs/bv/ev}$	Steam flow rate in reactor secondary/ to bypass valve/ to extraction valve, kg/s
$\dot{m}_{g,t}^{ext}$	Steam extracted from an SMR module, kg/s
$\dot{m}_{g,t}^{HP/LP}$	Steam flow rate to HP/LP turbine, kg/s
$\dot{m}_{max}^{HX1/HX2}$	Maximum steam flow to HX1/ HX2, kg/s
$\dot{m}_t^{DH/HX1/HX2/waste}$	Steam flow to DH system/ HX1/ HX2/ waste steam, kg/s
$\dot{m}_t^{waste}$	Waste steam flow to the condenser, kg/s
$\dot{m}_{pipe}$	DH pipeline water flow, kg/s
$\eta_B$	Battery efficiency
$\eta_T$	Turbine efficiency
$\mu_{max/min}$	Maximum/ minimum main steam valve position

$\mu_{max/min}^b$	Maximum/ minimum bypass valve position
$\rho_{str}$	Density of storage material, kg/m <sup>3</sup>
$c_{p/pstr}$	Specific heat capacity of DH pipeline water/ TES storage material, kJ/(kg °C)
$f_{max/min}$	Maximum/ minimum frequency limits, Hz
$K_P, K_I$	Proportional and integral gain
$P_t^B$	Power output of BESS, MW
$P_{max/min}^B$	Maximum/ minimum active power output of BESS, MW
$P_{i,t}^{G/D}$	Active power gen/ demand at $i^{\text{th}}$ bus, MW
$P_g^{max/min}$	Maximum/ minimum active power output of $g^{\text{th}}$ unit, MW
$P_{g,t}^m$	SMR mechanical power output, MW
$P_t^{PV/wind}$	Per unit power available from solar/wind, pu
$P_{g,t}^R$	SMR reactor power level, pu
$p_{g,t}^{sat/ref}$	Steam pressure/ reference pressure setpoint of an SMR unit, MPa
$P_{i,j,t}^{TL}$	Loss in transmission line connecting $i^{\text{th}}$ and $j^{\text{th}}$ bus, MW
$P_{g,t}$	Active power output of $g^{\text{th}}$ unit, MW
$q_t^{dem}$	Heating load demand, MWth
$q_t^{DH/HX1/HX2/HX3}$	Thermal power transferred to the DH system/ HX1/ HX2/ HX3, MWth
$Q_{i,t}^{G/D}$	Reactive power generation/ demand at $i^{\text{th}}$ bus, MVAR
$q_{max}^{HX3}$	Maximum thermal power output of the TES, MWth
$Q_g^{max/min}$	Maximum/ minimum reactive power of $g^{\text{th}}$ unit, MW
$Q_{g,t}$	Reactive power output of $g^{\text{th}}$ unit, MVAR
$R_g^{U/D}$	SMR ramping up/down rate limits, pu/hr
$S_{i,j}^{max}$	Maximum MVA flow limit for a transmission line between $i^{\text{th}}$ and $j^{\text{th}}$ bus, MVA
$S_{i,j,t}$	MVA flow in line between $i^{\text{th}}$ and $j^{\text{th}}$ bus, MVA
$SOC_{0/t}$	BESS SOC at start/at time $t$ , MWhr
$SOC_{max/min}$	Maximum/ minimum limits of BESS SOC, MWhr

$T_t^{DHin/DH'/DHout/str}$	Temperatures: DH inlet/ DH intermediate/ DH outlet/ TES storage material, °C
$T_{g,t}^{p/pref}$	Average primary coolant temperature/ reference temperature set-point of an SMR unit, °C
$t_{E/D/H}$	Time duration: SMR ramping time/ SMR maneuvering disabled time/ expected hold duration for individual unit, hr
$T_{ext}$	Steam extraction temperature, °C
$T_{max/min}^{str}$	TES Maximum/ minimum temperatures, °C
$T_{min}^{DHout}$	Minimum temperature limit for DH outlet, °C
$T_{rat}^{DHout}$	DH pipeline outlet rated temperature, °C
$u_{g,\tau}$	SMR ramping logic
$V_i^{max/min}$	Maximum/ minimum voltage limits of $i^{\text{th}}$ bus, pu
$V_{i,t}$	Voltage of $i^{\text{th}}$ bus in polar coordinates, pu
$v_{str}$	TES volume, m <sup>3</sup>
$Y_{i,j}$	Y-bus matrix element, $\mathcal{U}$
$\Delta H_t^{ext}$	Useful enthalpy of extracted steam, kJ/kg
$\Delta H_{g,t}^{LP/LP}$	Useful enthalpy at HP/LP turbine, kJ/kg
$\Delta t_{LF}$	Resolution of LF simulation, hr

## 6.2.2 Sets and Subscripts

$\mathcal{I}^{bus}$	Set of indices for power system nodes
$\mathcal{I}^{SMR/PV/wind}$	Set of indices for SMR/PV/wind units
$\mathcal{T}^c$	Continuous time domain
$\mathcal{T}^{LFI}$	Set of discrete time steps for LF simulation
$g, g1, g2$	Integers representing generation units
$i, j$	Integers representing power system bus
$t, \tau, k$	Positive real numbers for discrete or continuous simulation time

## 6.3 Introduction

The nuclear power plants (NPPs), predominantly used as baseload generation in the past, are widely considered for flexible operation due to the increasing presence of intermittent power from renewable energy sources (RESs) in electrical grids. Due to various reactor specific challenges, the flexible operation of NPPs, including small modular reactors (SMRs), is restricted in terms of the rate of power variation, total power change, and the number of reactor maneuvers in reactor lifetime [17, 18]. By utilizing the excess steam for heat application, cogeneration strengthens the load following capability of SMRs, facilitating RES hosting in isolated communities and electrical grids [60–66].

References [42–44, 117, 118] explored modeling, operation and financial aspects of nuclear-renewable hybrid energy systems with a variety of industrial coupling, including gasoline production, seawater desalination and hydrogen production. References [22, 58, 69] discussed the dynamic models of SMR for heat and electricity, whereas [68] investigated the techno-economic aspect of two different reactor technologies for heating and cooling applications.

The SMR-RES hybrid energy system for electricity and district heating (DH) holds a significant promise for comprehensive energy solutions to the communities with limited access to electrical and heating networks. However, there have been no attempts to investigate the planning and operation of such a system, understandably, due to the recentness of the technology.

In this context, the authors’ earlier works proposed the dynamic model of SMR in [101] and the hybrid energy system model for electricity and DH in Chapter 5, Section 5.5 (pp. 102–108). Chapter 5 also implemented the system models in a case system and simulated the operation for a 24-hr period.

This paper further extends the work in Chapter 5 by investigating the optimal operation and renewable hosting capability of the proposed hybrid energy system. As compared to our previous work in Chapter 5, the following are the additional contributions reported in this paper:

1. An optimization problem integrating reactor maneuvering, DH system and power system constraints for optimal operation and RES hosting in SMR-RES hybrid energy

system,

2. A multi-time scale operational scheme to schedule the system operation in load following (LF) and frequency control (FC) modes. The scheme allows the system to dynamically evaluate the optimum setpoints of DH extraction and reactor power level.

The proposed optimization framework is implemented in a test system to evaluate the RES hosting capability considering a month-long load and generation profiles.

The rest of the paper is organized as follows. Section 6.4 provides a brief overview of hybrid energy system model. Section 6.5 describes the multi-timescale operational scheme. Section 6.6 formulates the optimization problem for optimal operation and RES hosting. Section 6.7 provides a case study with sample simulation results and final optimization results. Section 6.8 gives conclusions of the research work.

## 6.4 System Modeling

The authors' recent publication [101] discusses the dynamic model of SMR and its integration to the turbine-governor model. Similarly, a manuscript based on Chapter 5 (pp. 96-118) presented a simulation model of SMR based hybrid energy system for electricity and district heating. This section provides a brief overview of the hybrid energy system model before proceeding to the optimization problem.

### 6.4.1 SMR Dynamic Model

Fig. 6.1 shows the block diagram of the reactor model interfaced with the governor output and the turbine input of the turbine-governor model. The heat produced from nuclear fission is transferred to the primary coolant in the core region represented by two coolant nodes. The coolant flows naturally from the hot leg to the cold leg through the steam generator (SG) that transfers the heat to the secondary side. The valve mapping module calculates the physical valve position using the governor signal  $GS$ . The flow model calculates the steam flow rate using the valve position and the steam pressure. Steam flows through the bypass

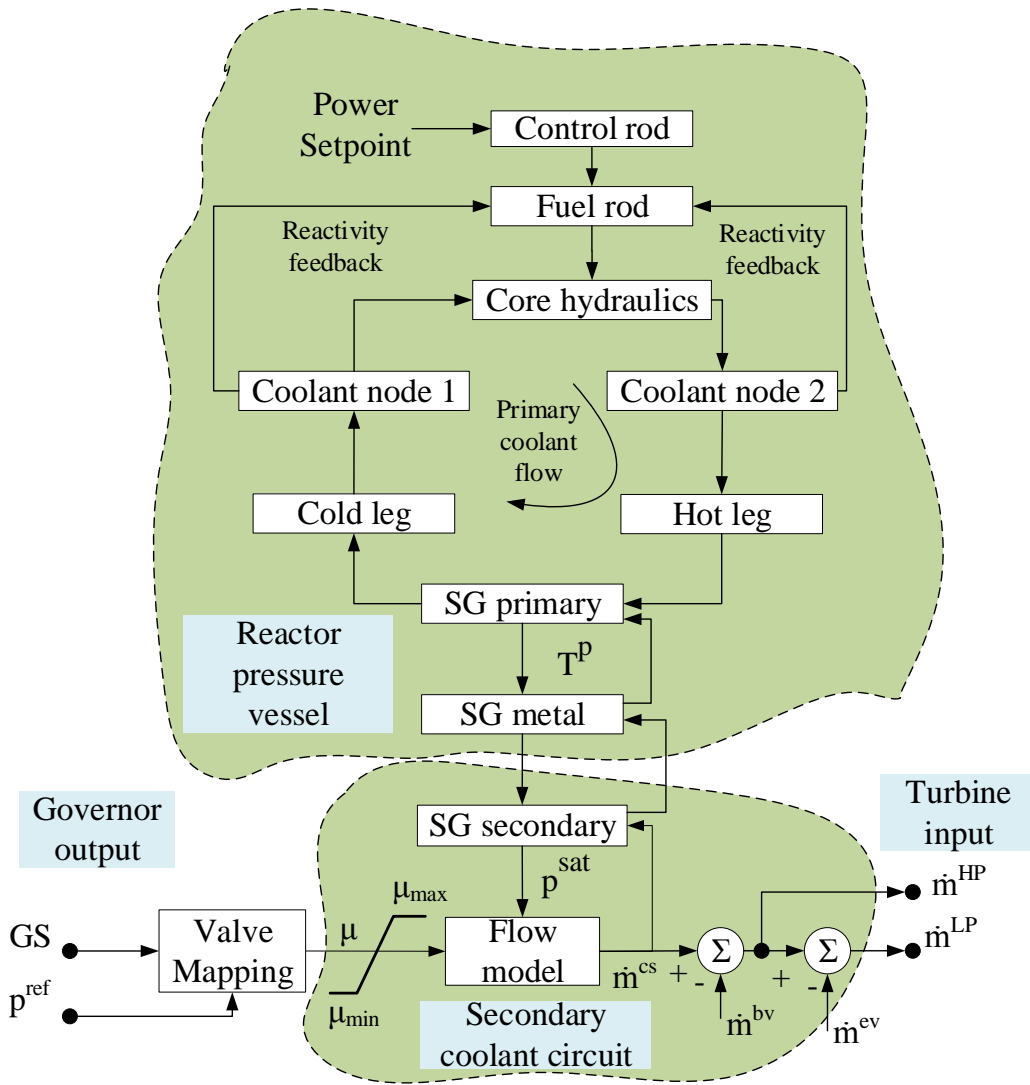


**Figure 6.1:** Block diagram of the SMR model interfaced between the governor output and turbine input of the turbine-governor model.

valve, high pressure turbine, extraction valve and low pressure turbine before returning back to the SG through the condenser.

The variation in average primary coolant temperature is sensed by the PI controller, which generates a signal to operate the bypass valve. The dynamic model of the turbine bypass system is represented by the block diagram shown in Fig. 6.2.

The steam extraction system operates in response to the LF signal. The extraction level is changed linearly to the new setpoint irrespective of the short-term disturbances. The

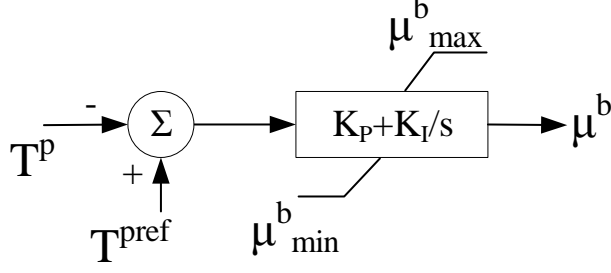


**Figure 6.2:** Control block for the turbine bypass system

dynamics of the steam extraction system is given by (6.1).

$$\frac{d\dot{m}_{g,\tau+t}^{ev}}{dt} = \frac{\dot{m}_{g,\tau+\Delta t_{LF}}^{ext} - \dot{m}_{g,\tau}^{ext}}{\Delta t_{LF}}, \forall \tau \in \mathcal{T}^{LFI}, t < \Delta t_{LF} \quad (6.1)$$

The mechanical power output is a function of enthalpy differences and steam flowrates, as given by (6.2).

$$P_{g,t}^m = \eta_T (\Delta H_{g,t}^{HP} \dot{m}_{g,t}^{HP} + \Delta H_{g,t}^{LP} \dot{m}_{g,t}^{LP}) \quad (6.2)$$

## 6.4.2 District Heating System Model

Fig. 6.3 shows the block diagram of the DH system model. The extraction steam from SMR modules is transferred to the steam distribution system, where the dedicated valves distribute steam to the heat exchange stations (HXs).

The steam flow rate to the DH system is the sum of extracted steam flows from SMR modules, as given by (6.3).

$$\dot{m}_t^{DH} = \sum_{g \in \mathcal{I}^{SMR}} \dot{m}_{g,t}^{ext} \quad (6.3)$$

The thermal power utilized from the extracted steam is given by (6.4).

$$q_t^{DH} = \dot{m}_t^{DH} \Delta H_t^{ext} \quad (6.4)$$

The steam flow rates to HX1 and HX2 are given by (6.5) and (6.6), respectively.

$$\dot{m}_t^{HX1} = \begin{cases} \dot{m}_t^{DH}, & \text{if } q_t^{DH} \geq q_t^{dem} \\ \frac{q_t^{dem}}{q_t^{DH}} \dot{m}_t^{DH}, & \text{otherwise} \end{cases} \quad (6.5)$$

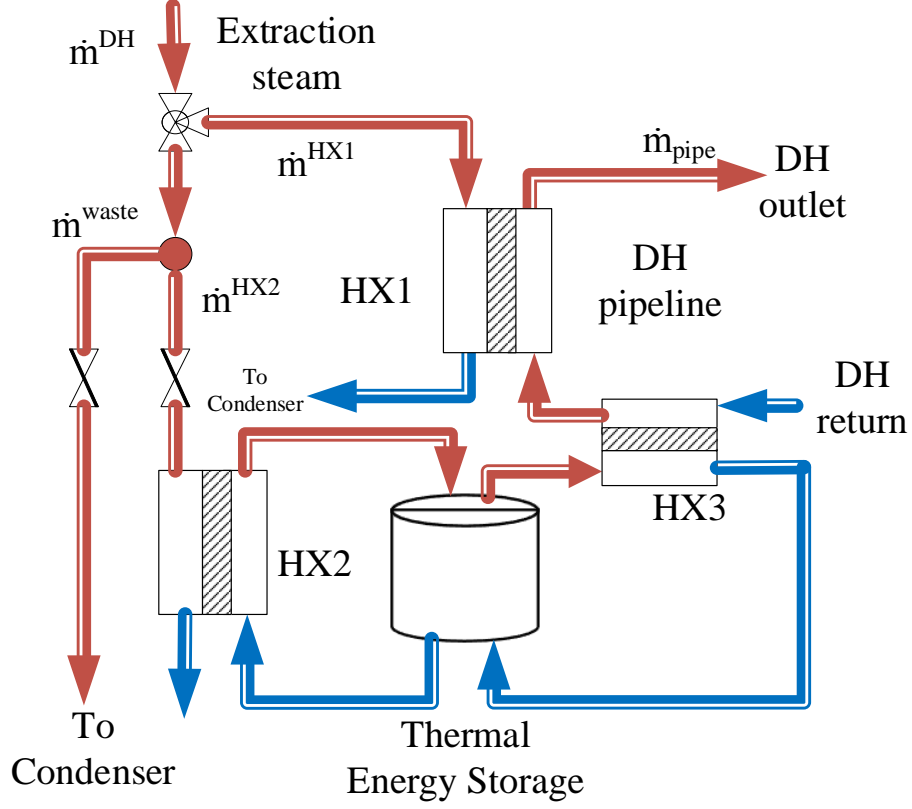


Figure 6.3: Block diagram of the DH system

$$\dot{m}_t^{HX2} = \begin{cases} 0, & \text{if } T_t^{str} \geq T_{max}^{str} \\ \dot{m}_{max}^{HX2}, & \text{if } \dot{m}_t^{DH} - \dot{m}_t^{HX1} \geq \dot{m}_{max}^{HX2} \\ \dot{m}_t^{DH} - \dot{m}_t^{HX1}, & \text{otherwise} \end{cases} \quad (6.6)$$

A portion of extracted steam is wasted, as given by (6.7).

$$\dot{m}_t^{waste} = \dot{m}_t^{DH} - \dot{m}_t^{HX1} - \dot{m}_t^{HX2} \quad (6.7)$$

The heat transferred to HX1 and HX2 is given by (6.8) and (6.9).

$$q_t^{HX1} = \dot{m}_t^{HX1} \Delta H_t^{ext} \quad (6.8)$$

$$q_t^{HX2} = \dot{m}_t^{HX2} \Delta H_t^{ext} \quad (6.9)$$

The heat transfer from HX3 to the DH pipeline is given by (6.10).

$$q_t^{HX3} = \dot{m}_{pipe} c_p [T_t^{DH'} - T_t^{DHin}] \quad (6.10)$$

The TES temperature is given by (6.11).

$$T_{t+\Delta t_{LF}}^{str} = T_t^{str} + \frac{q_t^{HX2} - q_t^{HX3}}{v_{str} \rho_{str} c_{pstr}} \Delta t_{LF} \quad (6.11)$$

The temperatures of DH pipeline water at different stages are given by (6.12)-(6.14).

$$T_t^{DHin} = T_t^{DHout} - \frac{q_t^{dem}}{\dot{m}_{pipe} c_p} \quad (6.12)$$

$$T_{t+\Delta t_{LF}}^{DH'} = T_t^{DHin} + \frac{q_t^{HX3}}{\dot{m}_{pipe} c_p} \quad (6.13)$$

$$T_{t+\Delta t_{LF}}^{DHout} = T_{t+\Delta t_{LF}}^{DH'} + \frac{q_t^{HX1}}{\dot{m}_{pipe} c_p} \quad (6.14)$$

### 6.4.3 BESS Dynamic Model

The power output of the BESS is controlled in response to the frequency disturbance, as given by (6.15).

$$P_t^B = K_{PB}(f_t - 60) + K_{IB} \int_0^t (f_t - 60) dt \quad (6.15)$$

The BESS state of charge (SOC) at time  $t$  is given by (6.16).

$$SOC_t = SOC_0 + \eta_B \int_0^t P_t^B dt \quad (6.16)$$

## 6.5 Multi-Timescale Operational Scheme

Fig. 6.4 depicts the proposed multi-timescale operational scheme. The SMR plant is maneuvered once in a  $t_E + t_D$  period, representing an operating frame of the hybrid energy system. The SMR plant ramps to a new reactor power level in  $t_E$  duration and remains unchanged

for the rest of the operating frame. During the dormant period  $t_D$ , the reactor power setpoint for the next operating frame is predicted. The steam extraction level is changed every LF interval during which the steam extraction setpoint for the next LF interval is also decided. Fig. 6.4 divides each operational frame into three zones: Op-z1 for steam extraction, Op-z2 for SMR ramping and Op-z3 representing a complete operational frame. Similarly, Pr-z1 and Pr-z2 represent the time to predict the steam extraction and the reactor power level setpoints. Any short-term disturbance within each LF interval is handled by the steam bypass system and battery energy storage system (BESS) operating autonomously in response to the frequency disturbance.

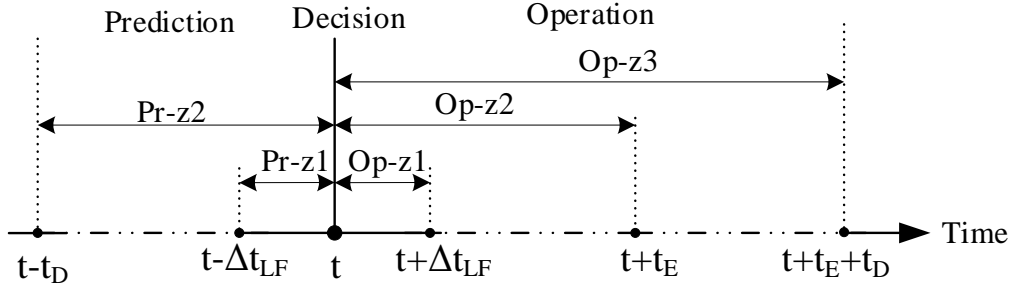


**Figure 6.4:** Proposed multi-timescale operational scheme

The steam extraction level is calculated based on electrical demand. The reactor power setpoint is evaluated based on various factors, including peak electrical demand for the next operating frame, BESS state of charge, and thermal energy storage temperature.

## 6.6 Problem Formulation

### 6.6.1 Objective Function

The optimization problem is formulated to maximize the total energy harvested from PV and wind plants. The objective function referred as hosting capacity (HC) is given by (6.17).

$$HC = \max \sum_{t \in \mathcal{T}^{LF}} \sum_{g \in \mathcal{I}^{PV} \cup \mathcal{I}^{wind}} P_{g,t} \Delta t_{LF} \quad (6.17)$$

The flexibility of the SMR-DH system in the short and long term is the major constraint of this optimization. Additionally, the constraints based on power network, power balance

equation, DH system design limits and system's dynamic performance are also included.

## 6.6.2 Constraints

### 6.6.2.1 Power Flow and Network Limits

The active and reactive power balance at each bus in the network is given by (6.18).

$$(P_{i,t}^G - P_{i,t}^D) - j(Q_{i,t}^G - Q_{i,t}^D) = V_{i,t}^* * \sum_{n \in \mathcal{I}^{bus}} Y_{i,n} V_{n,t}, \forall i \in \mathcal{I}^{bus} \quad (6.18)$$

where  $V_{i,t} = |V_{i,t}| \angle \delta_{i,t}$  and  $Y_{i,j} = |Y_{i,j}| \angle \theta_{i,j}$ . The voltage limits and the transmission line loading limits are given by (6.19) and (6.20) respectively.

$$V_i^{max} < |V_{i,t}| < V_i^{min}, \forall i \in \mathcal{I}^{bus} \quad (6.19)$$

$$S_{i,j}^{max} < S_{i,j,t} < S_{i,j}^{min}, \forall i \in \mathcal{I}^{bus}, j \in \mathcal{I}^{bus} \quad (6.20)$$

### 6.6.2.2 Power Balance and Generator Limits

The total electrical power generation and consumption are balanced, as given by (6.21).

$$\sum_{g \in \mathcal{I}^{SMR} \cup \mathcal{I}^{PV} \cup \mathcal{I}^{wind}} P_{g,t} = \sum_{i \in \mathcal{I}^{bus}} P_{i,t}^D + \sum_{i \in \mathcal{I}^{bus}, j \in \mathcal{I}^{bus}} P_{i,j,t}^{TL} \quad (6.21)$$

The active power output limits of the generation units are given by (6.22)-(6.24) for SMR, wind and PV plants, respectively. Fig. 6.5 shows the feasible operation region of a cogenerating SMR unit. Although SMR can operate at any point inside the irregular quadrilateral, it needs to follow the operating procedure while changing the operating point. The two values  $P_g^{max}$  and  $P_g^{min}$  are the upper and lower electrical power limits of the SMR unit. The maximum electrical output of PV and wind plants are obtained by scaling the per unit power available at a time with their size.

$$P_g^{min} < P_{g,t} < P_g^{max}, \forall g \in \mathcal{I}^{SMR} \quad (6.22)$$

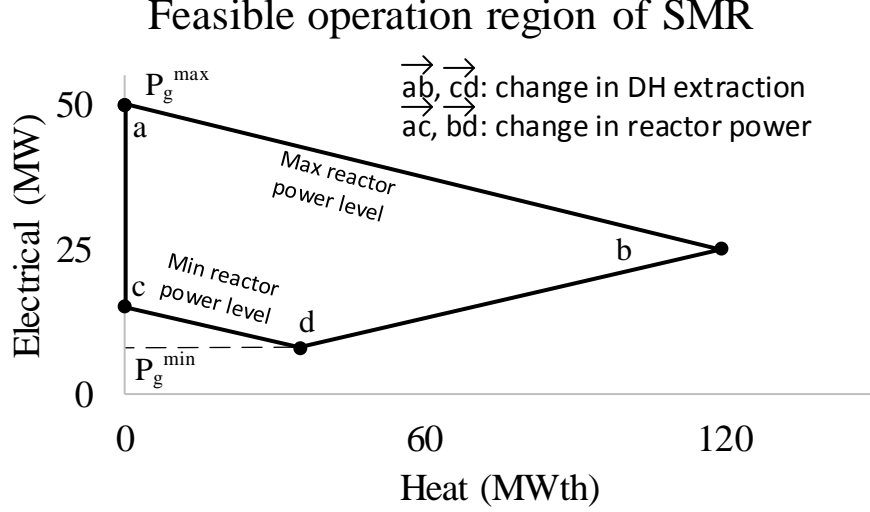


**Figure 6.5:** Feasible operation region of a cogenerating SMR unit.

$$0 < P_{g,t} < P_t^{PV} P_g^{max}, \forall g \in \mathcal{I}^{PV} \quad (6.23)$$

$$0 < P_{g,t} < P_t^{wind} P_g^{max}, \forall g \in \mathcal{I}^{wind} \quad (6.24)$$

The reactive power output of generation units should be within limits:

$$Q_g^{max} < Q_{g,t} < Q_g^{min}, \forall g \in \mathcal{I}^{SMR} \cup \mathcal{I}^{PV} \cup \mathcal{I}^{wind} \quad (6.25)$$

### 6.6.2.3 SMR Ramping Constraints

The power maneuvering of reactor units is coordinated to maintain  $t_H$  hold time between two consecutive power maneuvers for each unit. The ramping logic  $u_{g,t}$  is enabled provided that a reactor unit has held the same power for  $t_H$  duration. The ramping is achieved in  $t_E$  duration irrespective of the net power change required.

$$(u_{g,\tau})_{\tau=t}^{t+t_E} = \begin{cases} 1, & \text{if } \bigcap_{k=t-t_H}^t \neg u_{g,k} = 1 \\ 0, & \text{otherwise} \end{cases}, \forall t \in \mathcal{T}^{LFI}, g \in \mathcal{I}^{SMR} \quad (6.26)$$

The ramp rate of reactor control should be within the pre-specified limits, as given by

(6.27).

$$R_g^D u_{g,t} \geq \frac{P_{g,t}^R - P_{g,t-\Delta t_{LF}}^R}{\Delta t_{LF}} \geq R_g^U u_{g,t}, \forall t \in \mathcal{T}^{LFI}, g \in \mathcal{I}^{SMR} \quad (6.27)$$

#### 6.6.2.4 DH System Design Constraints

The DH extraction flow is less than or equal to the steam flow in the reactor secondary.

$$\dot{m}_{g,t}^{ext} \leq \dot{m}_{g,t}^{cs}, \forall t \in \mathcal{T}^{LFI}, g \in \mathcal{I}^{SMR} \quad (6.28)$$

The steam flow to HX1 and HX2 are limited by the design flow limits as given by (6.29) and (6.30).

$$\dot{m}_t^{HX1} \leq \dot{m}_{max}^{HX1}, \forall t \in \mathcal{T}^{LFI} \quad (6.29)$$

$$\dot{m}_t^{HX2} \leq \dot{m}_{max}^{HX2}, \forall t \in \mathcal{T}^{LFI} \quad (6.30)$$

The heat transferred to HX3 from the TES is limited by the TES's thermal power transfer limit.

$$q_t^{HX3} \leq q_{max}^{HX3}, \forall t \in \mathcal{T}^{LFI} \quad (6.31)$$

The TES can't provide heat to the DH water beyond its temperature:

$$T_t^{DH'} < T_t^{str}, \forall t \in \mathcal{T}^{LFI} \quad (6.32)$$

The TES temperature should remain within the predefined limits as given by (6.33).

$$T_{min}^{str} \leq T_t^{str} \leq T_{max}^{str}, \forall t \in \mathcal{T}^{LFI} \quad (6.33)$$

The temperature of the DH pipeline outlet shouldn't be lower than the minimum bound as given by (6.34).

$$T_t^{DHout} \geq T_{min}^{DHout}, \forall t \in \mathcal{T}^{LFI} \quad (6.34)$$

### 6.6.2.5 STF Dynamic Response Constraints

The dynamic constraints of the optimization problem involves the performance-based constraints and the device capacity limits. As the limitations are already imposed on the reactor maneuvering, the reactor vessel thermodynamic constraints are not included. The simulated values are observed and validated in continuous time.

The bypass flow is always less than the total flow in the reactor secondary, as given by (6.35).

$$0 \leq \dot{m}_{g,t}^{bv} \leq \dot{m}_{g,t}^{cs}, \forall t \in \mathcal{T}^c, g \in \mathcal{I}^{SMR} \quad (6.35)$$

The steam pressure variation should not exceed the predefined limits during the dynamic simulation (6.36).

$$\Delta p_{max} \geq |p_{g,t}^{sat} - p_{g,t}^{ref}|, \forall t \in \mathcal{T}^c, g \in \mathcal{I}^{SMR} \quad (6.36)$$

The frequency should be within limits defined for the network:

$$f_{min} \leq f_t \leq f_{max}, \forall t \in \mathcal{T}^c \quad (6.37)$$

The BESS power output should be within its upper and lower limits:

$$-P_{min}^B \leq P_t^B \leq P_{max}^B, \forall t \in \mathcal{T}^c \quad (6.38)$$

The state of charge of BESS is controlled within the predefined limits:

$$SOC_{min} \leq SOC_t \leq SOC_{max}, \forall t \in \mathcal{T}^c \quad (6.39)$$

## 6.6.3 RES Hosting and Optimal Operation Problem

The hosting capacity evaluation of a hybrid energy system is a multi-level problem which in the lower level, evaluates the optimal operational schedule and, in the upper level, identifies

the maximum hosting capacity.

$$\begin{aligned}
& \max_{\mathbf{P}_{\mathbf{g},t}, \mathbf{P}_{\mathbf{g}}^{PV}, \mathbf{P}_{\mathbf{g}}^{wind}} \sum_{t \in \mathcal{T}^{LFI}} \sum_{g \in \mathcal{I}^{PV} \cup \mathcal{I}^{wind}} P_{g,t} \Delta t_{LF} \\
\text{s.t.} \quad & (6.18) - (6.25), (6.35) - (6.39) \\
& P_{g_1,t} = P_t^{PV} P_{g_1}^{max}, \forall g_1 \in \mathcal{I}^{PV} \\
& P_{g_2,t} = P_t^{wind} P_{g_2}^{max}, \forall g_2 \in \mathcal{I}^{wind} \\
& \min_{\mathbf{P}_{\mathbf{g},t}^R, \mathbf{u}_{\mathbf{g},t}, \dot{m}_{\mathbf{g},t}^{ext}} \sum_{t \in \mathcal{T}^{LFI}} \dot{m}_t^{waste} \Delta t_{LF} \\
\text{s.t.} \quad & (6.26) - (6.34)
\end{aligned} \tag{6.40}$$

The upper level maximizes the energy harvested from RES and yields the decision in terms of the size of PV and wind plants, and the electrical outputs of the SMR plant over the simulation time horizon. The renewable curtailment is avoided, and the generation from wind and PVs were captured in full. The lower level optimization dictates the flexible operation in LF mode. The lower level objective evaluates the reactor power setpoints and steam extraction level for individual units over the simulation duration that minimize the heat waste while fulfilling the requirements of SMR maneuvering and the DH system. It should be noted here that the reactor hold time constraint (6.26) is allowed to be breached in unavoidable circumstances. However, the  $T_D$  duration of SMR's inactivity is always maintained after a ramping event.

## 6.7 Case Study

### 6.7.1 Test System Description

The simulation model of SMR coupled to the DH system is developed in PSS®E and PSS®Sincal simulation software platforms and integrated with the test system, the 33 kV portion of the IEEE-30 bus system. Fig. 6.6 shows the test system with SMR and RESs hosted at different nodes. The SMR plant is hosted at node 10; a wind plant is hosted at node 15; and two PV plants are hosted at nodes 17 and 27, respectively. The SMR plant

consisting of two NuScale SMR modules, 50 MW (160 MWth) each, is suitable for the test system.

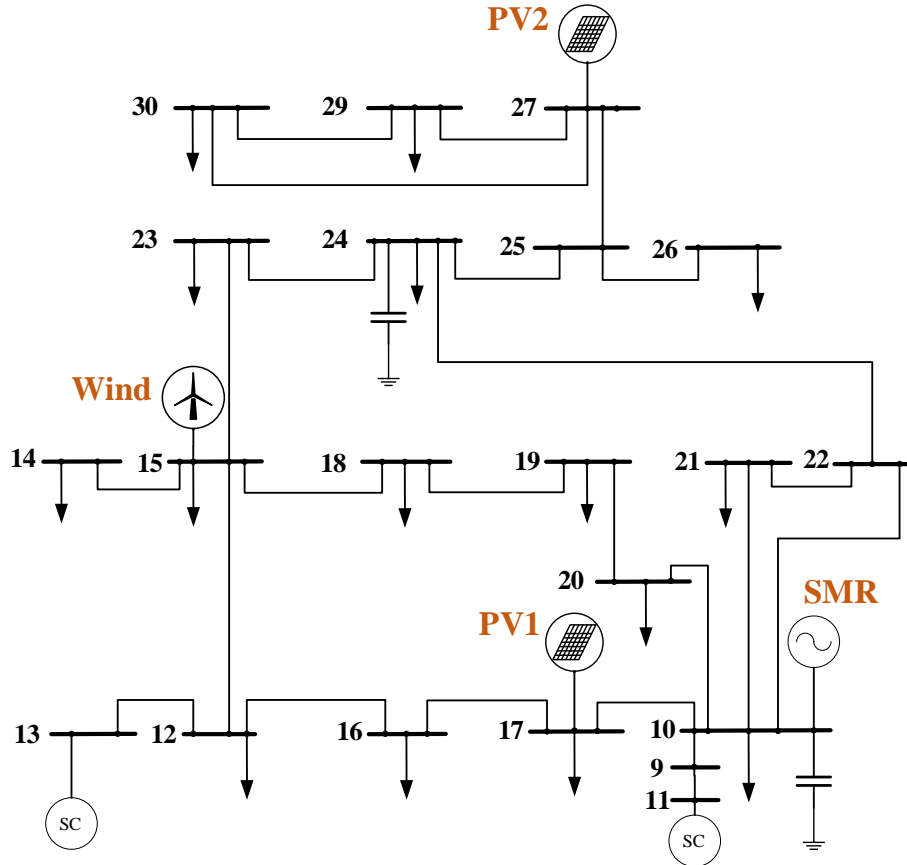


**Figure 6.6:** 33 kV portion of IEEE 30-bus network used for the case study. The respective node numbers are same as the original test system.

The 15 load points in the test network are populated with industrial, commercial and residential load profiles of 15-min resolution. The PV power output profile is obtained from [134]. The wind power output profile is obtained from [132]. The heating demand is taken from [133] and scaled to match the size of the test system. Fig. 6.7(a) provides a month-long electrical and heating load demand profiles. Fig. 6.7(b) provides a month-long per-unit wind and PV power output profiles. Table 6.1 lists the major system parameters used for the simulation.

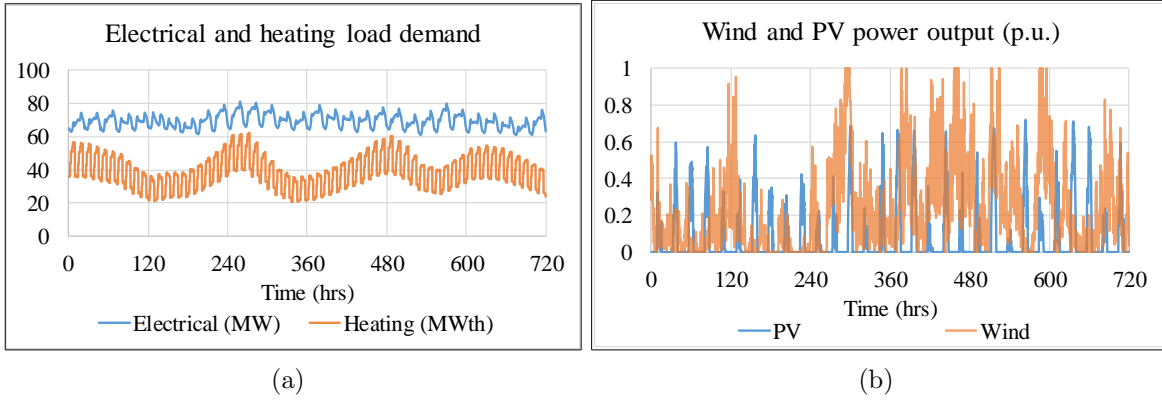


**Figure 6.7:** (a) Electricity and heat load demand profiles, (b) PV irradiance and wind speed profiles.

## 6.7.2 Sample Simulation Results

The sample simulation result for 50 MW RES penetration is discussed in this subsection. The size of the wind plant at node 15 is 30 MW, and the PV plants at node 17 and 27 are 10 MW each.

### 6.7.2.1 LF Simulation Results

The time series power flow (TSPF) analysis is conducted in the test system with a month-long RES and load demand profiles of 15-min resolution. SMR plant is modeled as the slack bus.

Fig. 6.8(a) plots the electrical outputs from PV, wind and SMR plants. Fig. 6.8(b) provides the reactor power level (pu of rated plant thermal output), electrical output (pu of rated plant electrical output) and the steam extraction level (pu of the steam flow) of the SMR plant. The reactor power setpoints are optimized dynamically by considering the peak electrical and heating demands for an operational frame and the TES temperature at the decision point, as discussed in Section 6.5. Since the reactor is only used for coarse-load shaping, the steam surplus from electrical power production is extracted and utilized in the DH system. Due to the large difference between electrical output and the reactor power level, the steam extraction reaches 1 pu on one occasion at 513.75 hr. During that interval, the steam bypass system or BESS should be utilized throughout the interval to achieve the

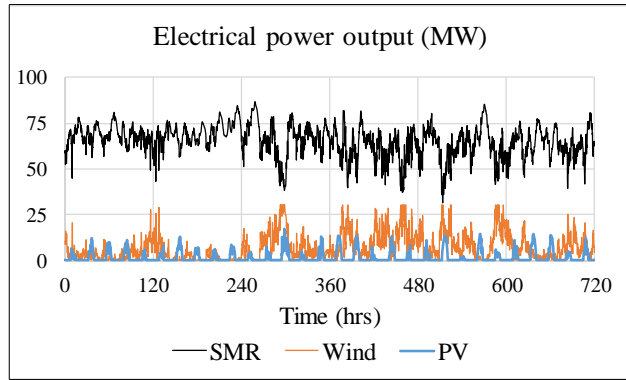
**Table 6.1:** System parameters

System components	Parameters
Power system	$V_i^{max} = 1.05$ pu; $V_i^{min} = 0.95$ pu; $f_{max} = 61$ Hz; $f_{min} = 59$ Hz; $\Delta t_{LF} = 0.25$ hr
BESS	$P_{max}^B = 10$ MW; $P_{min}^B = -10$ MW
SMR plant	$P_g^{max} = 50$ MW; $P_g^{min} = 7.82$ MW; $R_g^U = 0.25$ pu/hr; $R_g^D = -0.25$ pu/hr; $t_E = 2$ hr; $t_D = 4$ hr; $t_H = 10$ hr; $\Delta p_{max} = 0.5$ MPa
DH system	$T_{ext} = 128$ °C; $\dot{m}_{max}^{HX1} = 50$ kg/s; $\dot{m}_{max}^{HX2} = 50$ kg/s; $q_{max}^{HX3} = 70$ MWth; $v_{str} = 20000$ m <sup>3</sup> ; $T_{min}^{str} = 65$ °C; $T_{min}^{str} = 98$ °C; $c_{pstr} = 4.18$ kJ/(kg °C); $\dot{m}_{pipe} = 270$ kg/s; $T_{rat}^{DHout} = 90$ °C; $c_p = 4.18$ kJ/(kg °C); $T_{min}^{DHout} = 80$ °C

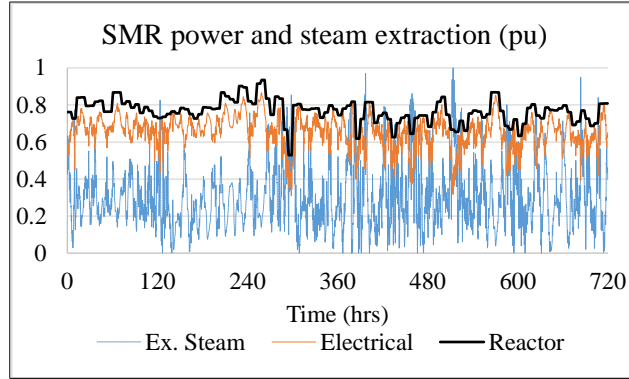
generation-demand balance on the electrical side.

Fig. 6.8(c) plots the reactor power level of the two SMR units. The SMR units alternate the reactor maneuvering to keep the minimum hold duration of each unit to 10 hours. However, due to large demand variation in three different instances, both reactor units are simultaneously maneuvered to meet the required variation. Similarly, in 17 separate instances, the unit with maneuvering responsibility isn't able to provide the necessary variation, and the unit that is supposed to stay dormant completes the power maneuvering. Fig. 6.9(a) shows the distribution of extraction steam over a month. The area "HX1" represents the extracted steam supplied directly to the HX1. The area "HX2" represents the steam supplied to the TES. The area "Waste" refers to the DH steam bypassed to the condenser. The total of 1048.38 MJ of extracted heat energy is wasted in a month duration, which represents 2.58% of the total heat extracted to the DH system.

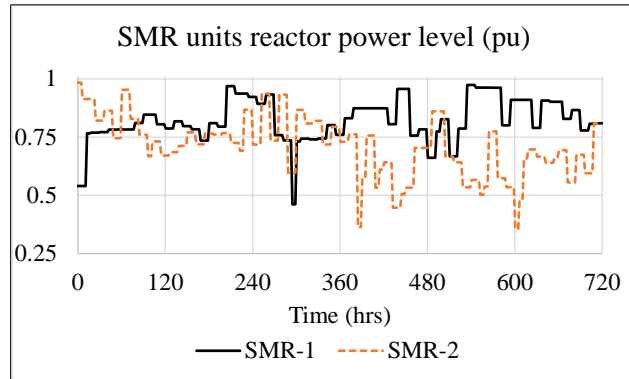
Fig. 6.9(b) shows the variation of return, intermediate, and outlet temperatures of the DH pipeline, and the TES temperature. For 53.8% of the time, the steam extracted is insufficient for the DH system and the heat energy stored in the TES is utilized. Since the TES can't provide heat beyond its temperature, the DH system is unable to maintain the supply temperature at 90 °C during 27 separate intervals. Nevertheless, the maximum decrease in DH outlet temperature of 4.47 °C is well within the allowed limits. For 2.39%



(a)

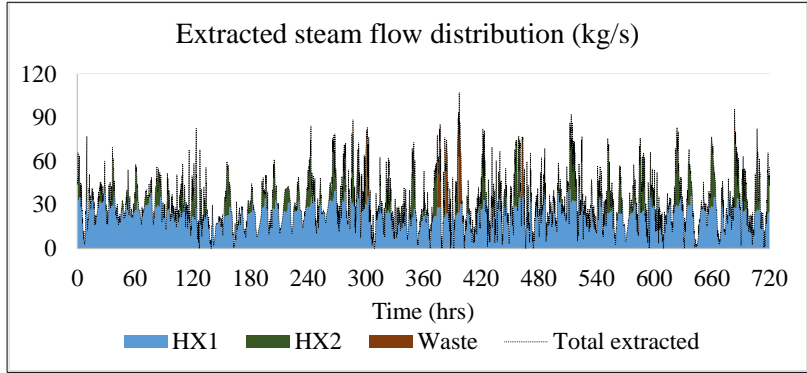


(b)

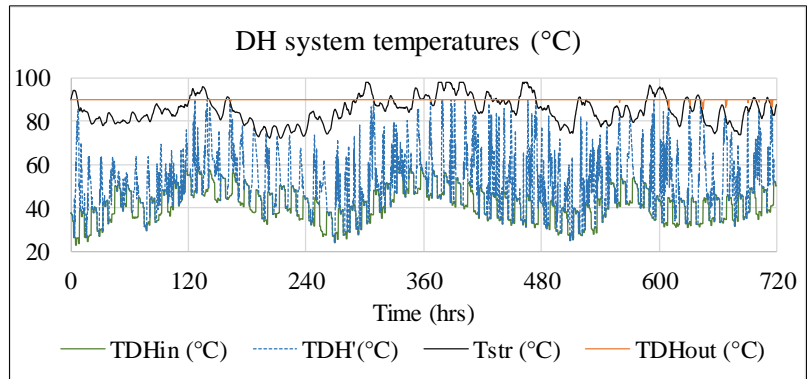


(c)

**Figure 6.8:** Results for optimal operation in LF mode for 1 month period with 50 MW RES penetration. (Part-1)



(a)



(b)

**Figure 6.9:** Results for optimal operation in LF mode for 1 month period with 50 MW RES penetration. (Part-2)

of the time, the TES temperature is at its upper limit, and HX2 diverts the steam flow to the condenser. The TES temperature, however, never reached its lower limit and was always available to support the DH system when the extracted flow was not sufficient for DH system.

### 6.7.2.2 Dynamic Simulation Results

A 3-bus equivalent of the test system is obtained with an SMR bus, a BESS bus, and a load bus, respectively, as shown in Fig. 6.10. The equivalent load at the load bus represents the total per second demand for SMR obtained by performing the TSPF in the test network in Fig. 6.6. The PV power profile of 5-sec resolution and wind power profile of 1-min resolution is used for the simulation. The electrical output of SMR is varied by bypassing the steam directly to the condenser in response to the AGC action. SMR units are also allowed to increase their output by up to 3% REO without control rod operation. The turbine valve

operation rate limits are set at  $\pm 60\%$  REO/min. The BESS covers the rest of the generation-demand mismatch.

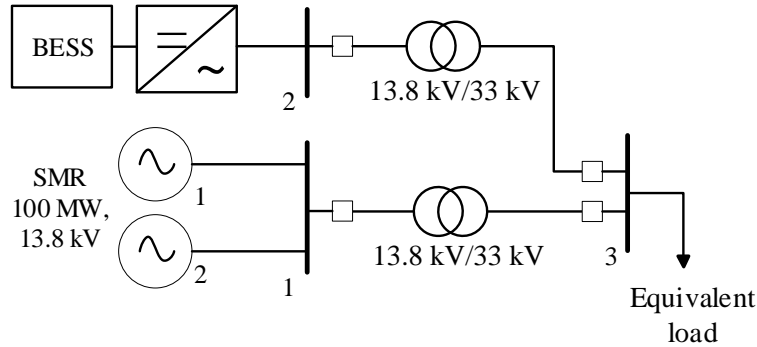


**Figure 6.10:** 3-bus equivalent network for dynamic simulation.

The worst 2.5 hours of the LF simulation, between 298.5 and 301 hrs, is used to analyze the dynamic operation of the proposed system. The selected period also includes a 2-hour SMR ramping occurring between 298.75 hr and 300.75 hr. Due to the large change in SMR demand, both units are ramped simultaneously during this period. Fig. 6.11(a)-(e) provide the power system responses for the 2.5 hr period. The electrical power output of PV and wind plants and the equivalent SMR demand are shown in Fig. 6.11(a). The electrical power output of the BESS and two SMR units are shown in Fig. 6.11(b), whereas Fig. 6.11(c) shows the system frequency response. The BESS output reaches a maximum of 10 MW at 299.104 hr, at which the frequency deviation is -0.8276 Hz.

Fig. 6.12(a)-(c) provide the reactor side responses for the 2.5 hr period. Fig. 6.12(a) provides the steam pressure, whereas Fig. 6.12(b) and (c) provide the steam bypass flow and the reactor power output of the two units. Since both units are maneuvered simultaneously, the steam pressure and reactor power of both units ramp linearly to the new setpoints. The smaller fluctuations seen in pressure and reactor power plots are due to the actuation of the turbine valve and bypass valve.

### 6.7.3 Optimization Results

Based on the transmission capacity of the network and the minimum power level of the reactor units, the maximum size of RES plants at proposed hosting nodes were evaluated as

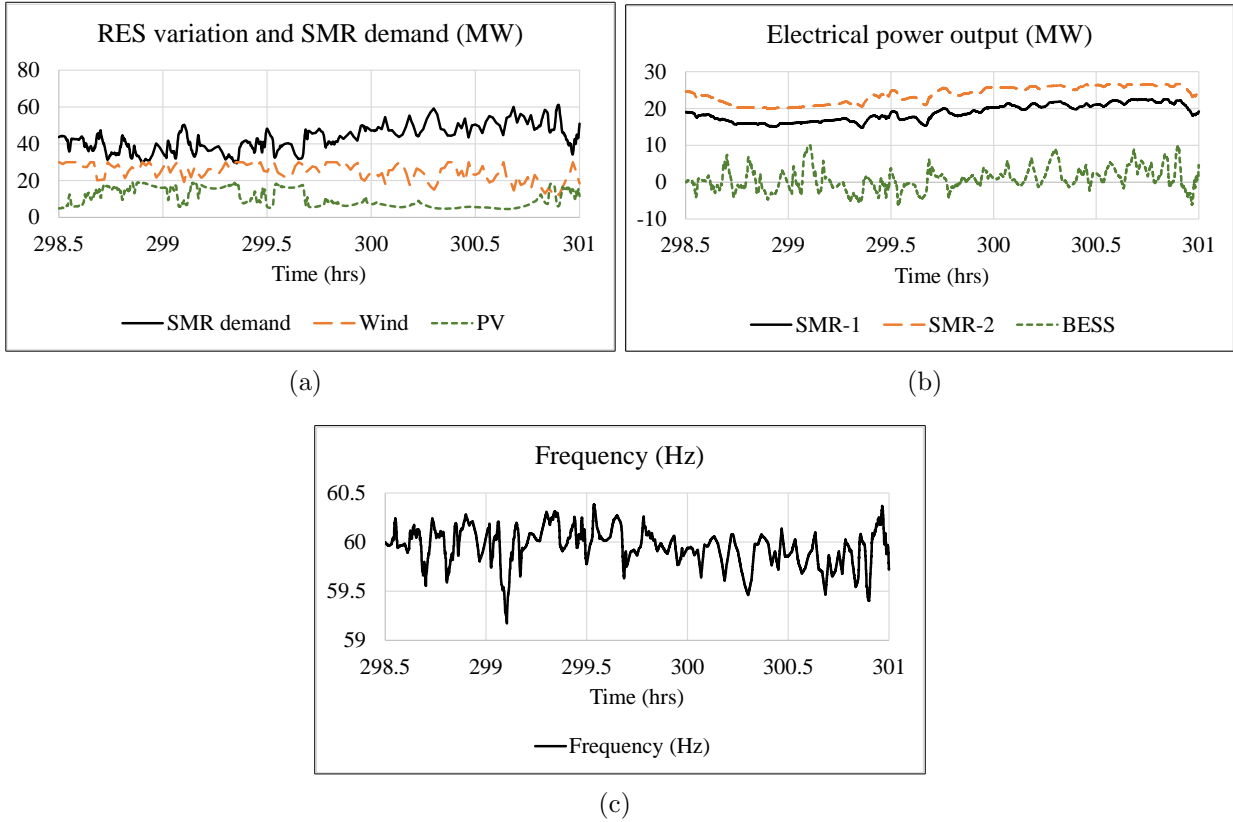


**Figure 6.11:** Power system responses during the worst 2.5 hour period of the month.

50 MW for wind and 15 MW for each of the two PV plants. The size of RES plants are varied up to the ratings mentioned above, and the operational simulation is conducted.

Fig. 6.13(a)-(d) plot the key decision quantities against the total RES energy hosted in the proposed system in a month duration. The horizontal axis represents the total sum of energy harvested from PV and wind plants. It should be noted here that the fluctuations seen in the plots of decision quantities are due to the diverse combination of PV and wind plant sizes taken for the corresponding RES energy hosting levels.

The increase in RES penetration increases heat energy waste as shown in Fig. 6.13(a). With the increase in demand variation due to increased RES penetration levels, the number of large reactor maneuvers also increases. Fig. 6.13(b) shows the SMR maneuvering stats in terms of the total number of maneuvers with power change exceeding 20% and 30% of rated thermal power, and the number of maneuvers for which both units are simultaneously maneuvered. The stats are based on the simulation in a month, during which the two SMR

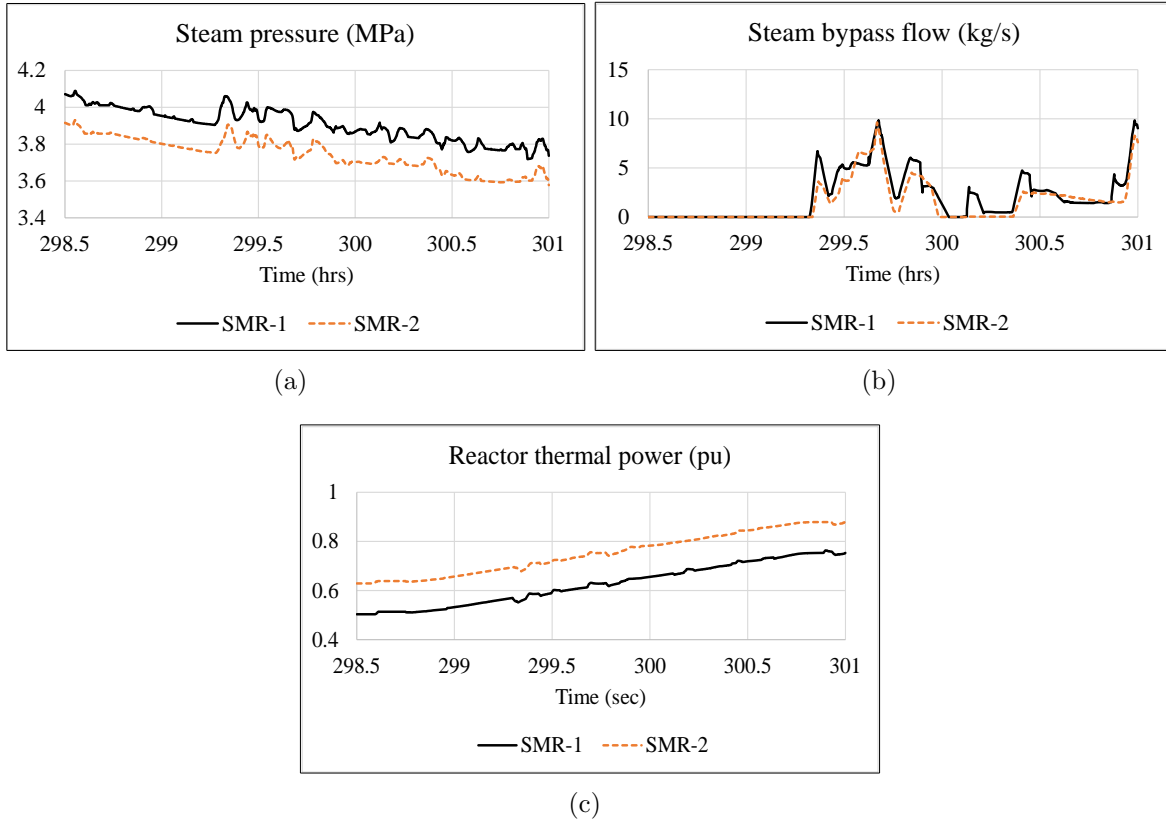


**Figure 6.12:** Reactor side responses during the worst 2.5 hour period of the month.

units were maneuvered close to 115 times in total.

Fig. 6.13(c) and (d) show the variations of maximum frequency deviation and maximum SOC utilization in a single operational frame. The plots in Fig. 6.13(c) and (d) is based on the dynamic simulation of the worst 2.5 hours between 298.5 and 301 hrs. The maximum frequency deviation and the SOC utilization appear to recover at a higher RES penetration level. However, a large portion of the steam is wasted due to the overcommitment of reactor power. The maximum BESS SOC utilization gives an idea of the energy rating of BESS required for the system. For example, assuming the SOC level is allowed to fluctuate by up to  $\pm 25\%$  in one operational frame, the BESS with an energy rating of 2 MWhr is sufficient for the RES hosting levels that have SOC utilization below 0.5 MWhr, while the energy rating of 4 MWhr is necessary for safe operation if the SOC utilization is beyond 0.5 MWhr.

The power system frequency deviations shall not exceed the predefined limits set for the system. Considering the isolated configuration of the test system, frequency deviation limit

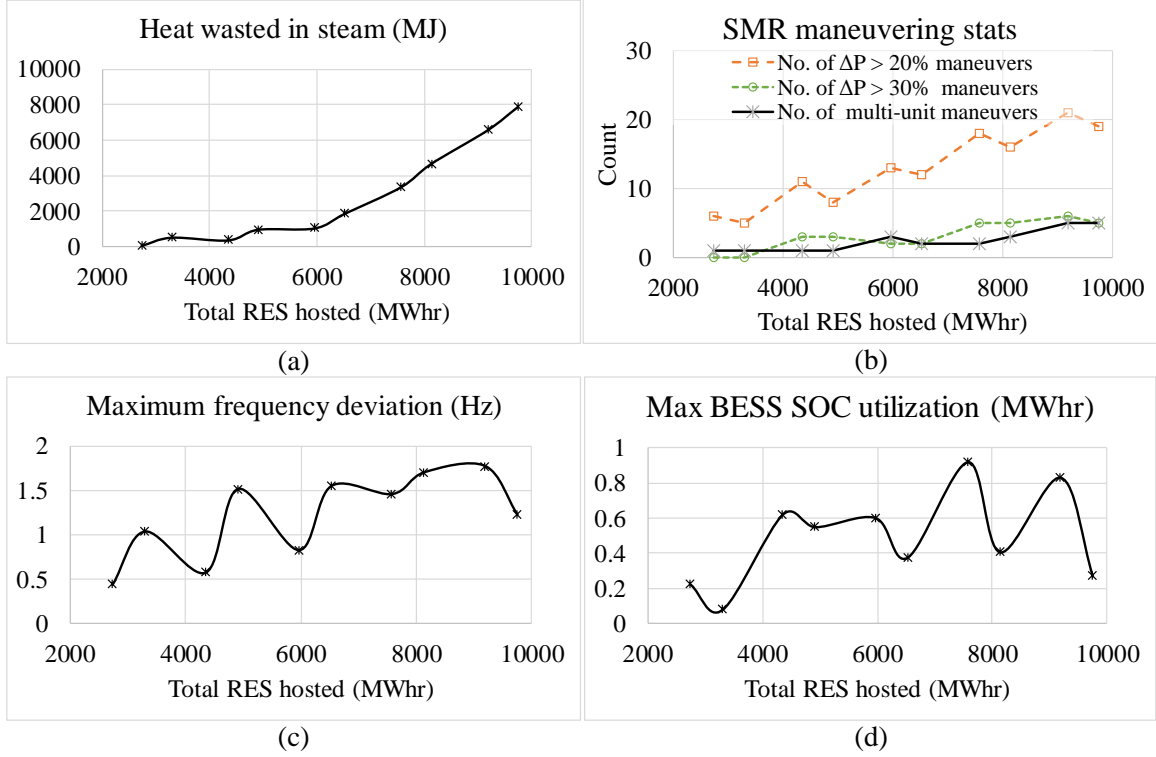


**Figure 6.13:** Optimization results for different RES penetration for  $V_{str} = 20000 \text{ m}^3$  and BESS size of 10 MW.

of  $\pm 1 \text{ Hz}$  is chosen for this assessment, which is also close to the limits defined for various NERC interconnections [76]. With the increase in RES penetration levels, the maximum frequency deviation exceeds the defined limits as the BESS could only offer up to  $\pm 10 \text{ MW}$  of flexible power. In order to keep the frequency limits within limits, BESS of higher MW rating will be needed.

Based on the optimization results in Fig. 6.13, the optimum solution for the RES hosting problem is the penetration level selected for the sample simulation, i.e. 30 MW of wind plant at node 15 and PV plants of 10 MW each at node 17 and 27 respectively. This combination results a total of 5961.16 MWhr of RES energy in a month duration.

## 6.8 Conclusion

A multi-level optimization problem was formulated in this paper to optimally operate and evaluate the renewable hosting capability of the SMR-RES hybrid energy system for electric-

ity and DH. The optimization problem was constrained by various limits based on the power system, reactor and DH system. With the operational algorithms for reactor maneuvering, steam extraction, steam bypass, and the BESS, a multi-time scale method was proposed to operate the hybrid energy system in real-time. Different RES penetration levels were simulated, and the optimum hosting solution was evaluated based on heat wasted in the DH system, BESS SOC utilization, maximum frequency deviation, and SMR maneuvering stats.

From a practical viewpoint, the problem of RES hosting is driven by the investment decision. The DH side challenges, such as increased heat waste could be mitigated by oversizing the TES, while the dynamic performance of the system could be improved by increasing the size of the BESS.

# 7 Analysis for Siting and Sizing of a Small Modular Reactor – A Case Study in Canada

## Preamble

This study aims to fulfill a part of the fourth objective of the thesis mentioned in Section 1.3. The contribution of this chapter to the overall research is to investigate the steady-state aspects of siting and sizing SMR in weak electrical grids.

In this study, various sites in Northern SEG will be analyzed in terms of their capability to host an SMR based on steady-state aspects. The steady-state optimal power flow (OPF) assessment will consider the load reduction as the primary objective constrained by various power system limits under probable contingencies. The maximum size of SMR at each hosting site will be evaluated, followed by the recommendation for the best site for SMR in Northern SEG. The role of PHES in improving the size of SMR at each location will also be discussed.

The transmission line information for the Northern SEG is obtained from the facility map of the SaskPower utility. The load and generation data are obtained from various publicly available documents on the SaskPower website.

<sup>1</sup>A paper based on this work was presented in *20th National Power Systems Conference (NPSC-2018)*, Trichy, India, in December 2018. I developed the approach, performed the case study and documented the results under the supervision of Prof. Gokaraju. As a co-author of this paper, Dr. Joshi provided feedback on the work and helped me with the paper write-up.

---

<sup>1</sup>B. Poudel, K. A. Joshi, and R. Gokaraju, “Analysis for siting and sizing of a small modular reactor—a case study in Canada,” in *20th National Power System Conference*, Tiruchirappalli, India, Dec 2018, pp. 1–6.

## 7.1 Abstract

This paper analyzes the problem of siting and sizing of small modular reactors (SMRs) in a weakly connected section of an existing electrical grid in the north-central part of Canada. Although various sizes are available, the limited capacity of SMR to respond to sudden changes in operating conditions – a concern specific to SMR and other nuclear plants – confines the prospect of having plant size suitable for the economic operation. A study is carried out to determine the size of SMR suitable for the system at various hosting locations and the relative impact of the size on the economic operation. The prospect of having pumped hydroelectric energy storage (PHES) along with an SMR is also investigated, and the optimum size of SMR with and without PHES is obtained.

## 7.2 Introduction

The environmental concerns over greenhouse gas emissions have resulted in an increased emphasis on electricity generation technologies with a low carbon footprint. With sophistication and innovation in design over the past decade, small modular reactors (SMRs) offer several advantages over traditional nuclear power technologies, notably – the reduced size, modular construction, reduced up-front capital costs, simpler plant configuration, and reduced staff complement [15, 20]. Under the Paris Agreement, Canada has committed to reducing GHG emissions by 30% below 2005 levels by 2030. While the availability of renewable energy sources such as wind and solar is limited in the northern section of Canada [135, 136], SMRs are recognized as a clean energy alternative. They are available in sizes from 3MW to 300 MW, suitable for remote grids. Many Canadian utilities are weighing the possibility of having SMRs in the system [19, 59]. The utility grids with a strong transmission network and interconnections can easily host SMR in the system. However, many issues could arise while hosting SMRs on weak grids. Although the SMR technology is being developed to offer flexibility in dispatch, it is strictly limited to avoid the thermal transients in the reactors for safety reasons [16, 17, 137, 138]. Thus, SMR is still a source of a generation with limited capacity to respond to the load following and contingencies. It can be considered a base

power plant of smaller size with the output variation limited to long-term variations and sudden tripping under abnormal circumstances.

Power utilities widely use pumped hydroelectric energy storage (PHES) for load balancing in the system. It can be operated in both pumping and generating modes and can be constructed in sizes from several MW to more than 1000 MW [139, 140]. It stores the electrical power as gravitational potential energy by pumping the water to an upper reservoir during the off-peak load. The stored energy can then be used during peak hours to fulfill the demand economically. It can quickly ramp up to maximum capacity in both generating and pumping mode. The prospect of having PHES with SMR could be very beneficial as it can complement the SMR's flexibility limitations and ensure the economic operation with significant improvement in safety and reliability.

This paper analyze the problem of siting and sizing of an SMR in a weakly connected section of an electrical grid in northern Canada along with an extended analysis including PHES. The problem formulation first finds the maximum possible size of SMR at various sites based on loss minimization with all operational constraints, including voltage limits, transmission line limits and power balance. It then extends the analysis for post-contingency abnormal operating conditions. The problem of the evacuation of SMR power under abnormal operating conditions is of critical significance. Finally, the complementary role of PHES is explored, and the optimum SMR size with and without PHES is obtained for different siting scenarios.

The paper is organized into four sections. Section 7.3 introduces the case system for the problem of SMR sitting and sizing. The methodology adopted is explained in Section 7.4, with a flowchart depicting the overall approach and the problem formulations based on optimal power flow. Results for various scenarios are discussed in Section 7.5, followed by the conclusion in Section 7.6.

### **7.3 The Case System**

The case system, a 115 kV feeder close to 800 km in length, fed by hydro stations at both ends and having an interconnection with System 2, is shown in Fig. 7.1. Table 7.1 sum-

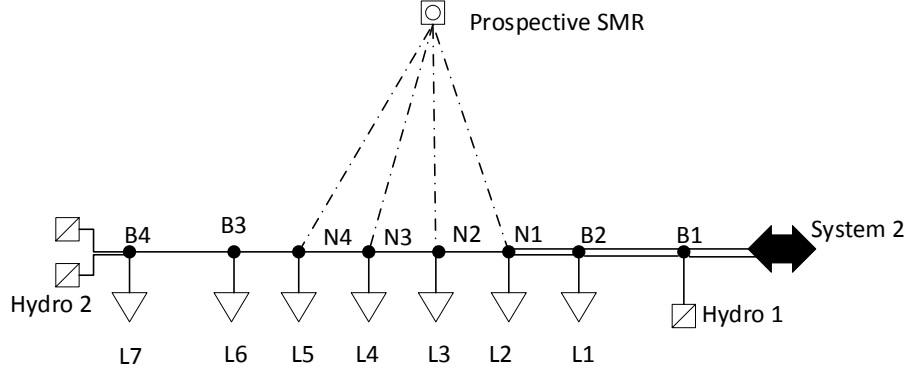


**Figure 7.1:** The case system

marizes the demand-generation scenario of the case system. It is clear that the generation capacity available is not enough to fulfill the projected load demands, and thus the new power alternative is necessary for continuity of power supply. One option might be to import more power from System 2. However, it is found that the bulk power transfer along this long feeder can result in very high transmission losses with the given capacity of the lines. A large-scale transmission reinforcement and reactive compensation throughout the network will be necessary with this option. Another option is to have a new generation plant in the system in the form of SMR. Four sites are identified to be capable of hosting a nuclear plant based on various non-electrical criteria. N1, N2, N3, and N4 in Fig. 7.1 represent the four connection points in the feeder for the proposed SMR plant. B1, B2, B3, and B4 are other nodes where various load centers and generation facilities are connected. The case system is modeled in Siemens PSS<sup>®</sup>E software.

**Table 7.1:** Demand-generation scenario

Load or Generation	$P_{max}$ (MW)	$P_{min}$ (MW)
Hydro 1	111	0
Hydro 2	23	0
System 2	25	-25
Projected system load	161	-

## 7.4 Methodology

### 7.4.1 Overall Approach

The optimum size and site for SMR are determined based on two-stage exercise using optimal power flow (OPF) and contingency analysis. Given that a set of hydropower plants primarily feeds the case system, economical operation in this assessment is assumed to be based on the loss reduction with levelled fuel cost for all the generation plants. The system with SMR is then assessed for the probable contingencies that could lead to the power evacuation problem. The hydro units can vary their output between 0 to  $P_{max}$  under all possible scenarios.

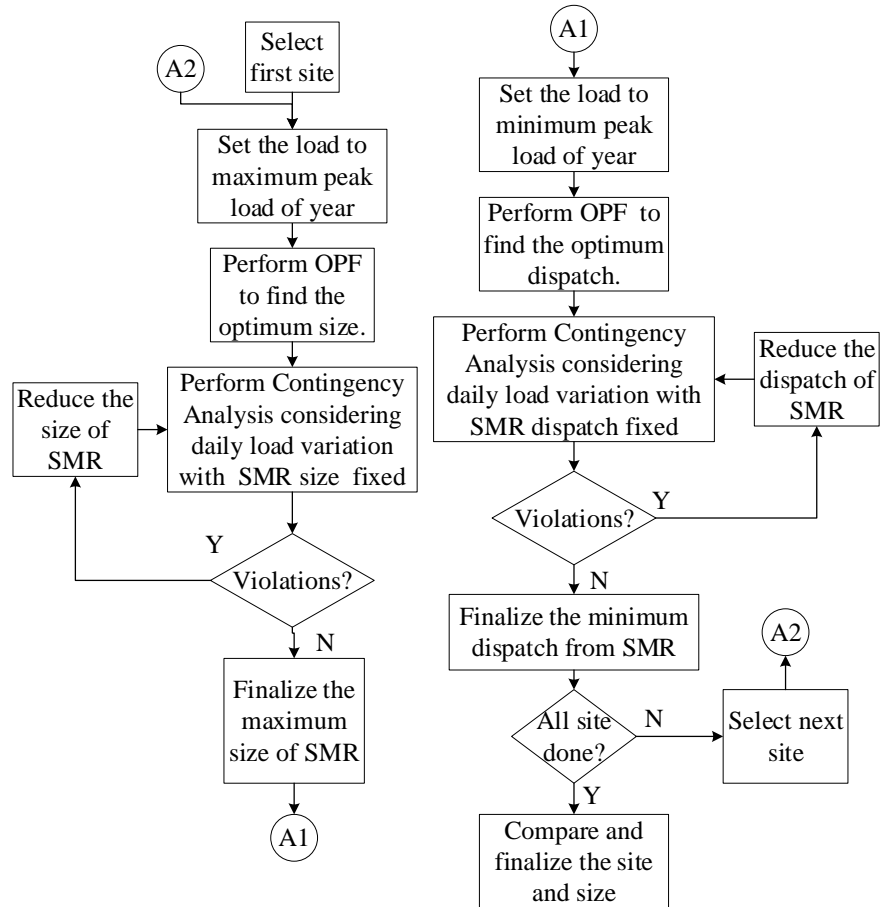


**Figure 7.2:** Overall approach for the siting and sizing problem of SMR

The general flow diagram for the assessment is shown in Fig. 7.2. It starts with a site, sets the load to system peak load, and performs the loss reduction based OPF to determine

the optimum size of SMR. N-1 contingency assessment is then performed for the peak load and the baseload scenarios. This step verifies and cross-checks the size of SMR and signals the size reduction to avoid the problem of power evacuation and other limit violations, if any. The SMR is characterized by its maximum limit of generation and the minimum power that can be safely dispatched under various contingencies. Thus, the minimum dispatch necessary from SMR is evaluated as a second step. The load in the system varies throughout the day. However, the dispatch from SMR is kept constant for a day based on the peak load for that day.

For this study, we need four different operating points: the system maximum daily peak load and the minimum load of that day to determine the maximum size of SMR, and the system minimum daily peak load and the minimum load of that day to determine the maximum limit of minimum dispatch necessary from SMR. The daily and annual variation of the load is given by the annual peak load variation curve and daily load variation curve, as shown in Fig. 7.3 (a) and Fig. 7.3 (b) respectively. The four extremes needed for assessment are represented by the point-sets, A1D1, A1D2, A2D1 and A2D2.

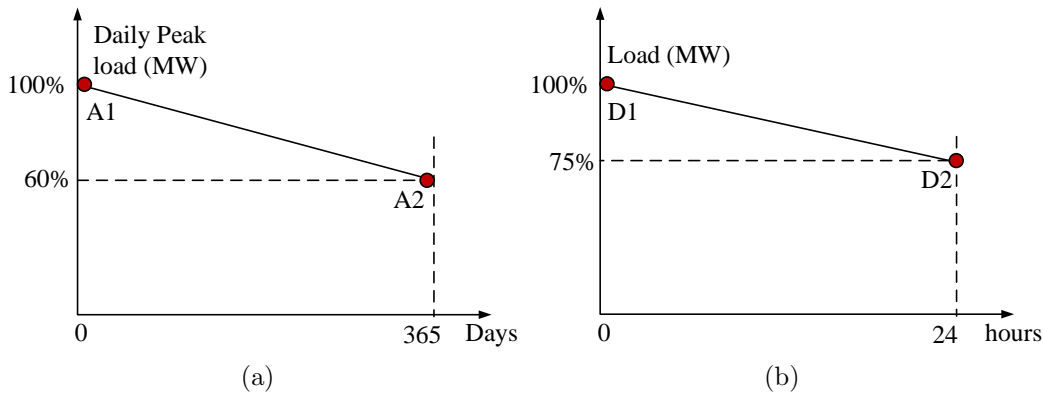


**Figure 7.3:** (a) Daily peak load variation curve (b) Load duration curve

## 7.4.2 OPF Formulation

As a first step, an OPF based loss minimization problem is formulated to obtain the preliminary size for SMR at each potential site, as shown in (7.1). The operational constraints are

given by (7.2).

$$\phi = \text{Minimize} \left\{ \sum_k P_k^{loss}(P^{h1}, P^{h2}, P^{SMR}) \right\} \quad (7.1)$$

Subject to:

$$\begin{aligned} P_i - jQ_i &= V_i^* * \sum_{n=1}^N Y_{in} V_n \\ P^{h1} + P^{h2} + P^{SMR} + \sum_o P_{l,o} - \sum_k P_k^{loss} &= 0 \\ V_{i,max} < V_i < V_{i,min}, \quad S_{k,max} < S_k < S_{k,min} \\ P_{max}^h < P^h < P_{min}^h, \quad Q_{max}^h < Q^h < Q_{min}^h \end{aligned} \quad (7.2)$$

for all nodes represented by  $i$ , transmission lines represented by  $k$ , and load centers represented by  $o$ .

$P^{h1}$  and  $P^{h2}$  represent the power output from the two hydro plants;  $P^{SMR}$  represents the power output from SMR;  $P_k^{loss}$  is the power loss at various transmission segments which is the function of generations from each plant;  $P_{l,o}$  represents the load connected at the seven equivalent load centers.  $P_i$  and  $Q_i$  represent the active and reactive power in the  $i^{\text{th}}$  node.  $V_i$  and  $V_n$  represent the voltage of  $i^{\text{th}}$  and  $n^{\text{th}}$  node respectively.  $Y_{in}$  is the admittance between  $i^{\text{th}}$  and  $n^{\text{th}}$  node.  $S_k$  represents the thermal limit of  $k^{\text{th}}$  line. The first constraint of the optimization problem represents the power flow problem. The second constraint represents the active power balance for OPF. The third constraint represents the voltage and transmission line violation criteria. The fourth constraint represents the active and reactive power limits of individual hydro units.

### 7.4.3 Modified OPF Including Contingency Assessment

The optimal size of SMR obtained from (7.1) is assessed in terms of the system capacity to host the power at nodes under probable contingencies. Three major problems that could arise under contingencies are voltage limit violation, transmission line overloading, and power evacuation problem. Voltage limit violation and transmission line overloading could be solved with proper corrective actions such as generation re-dispatch (from generating plants other than SMR), transformer tap adjustments, switch shunt adjustments, and load curtailments.

However, it is not the same in the case of the power evacuation problem.

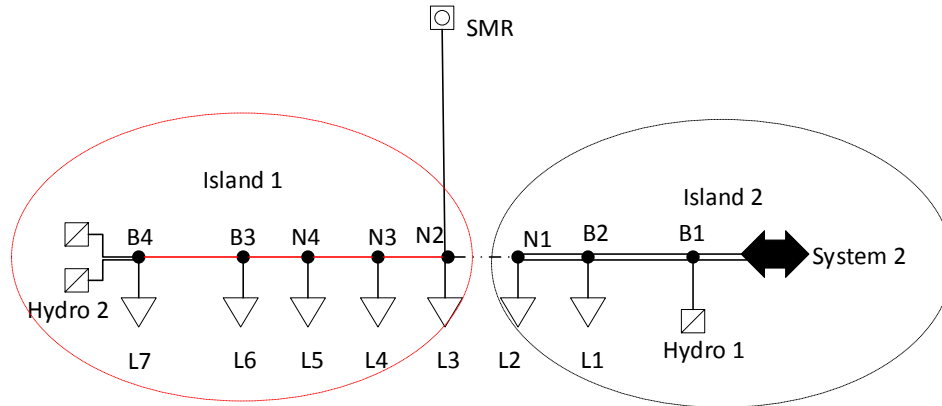


**Figure 7.4:** Island formation under contingency

The power evacuation problem arises due to the inability of SMR to immediately reduce its power output in response to a sudden contingency. For example, let us consider an SMR is placed at node N2, as shown in Fig. 7.4, dispatching the power defined by the OPF for a day. If there is a loss of transmission line between N1 and N2, the whole system will break down into two islands. In that case, if the power generation is deficient in any island after contingency, the connected generating plants (other than SMR) will increase the power up to their limits till the generation in the island becomes equal to the load connected to that island. If the generating plants are unable to supply enough power, the system will opt for the load curtailment options. Whereas, if there is excess power in an island compared to the load demand, the generating plants should decrease the power up to their minimum limit until the generation is equal to the load demand. However, SMR, as it is considered a baseload plant with limited flexibility in this assessment, can not alter its power immediately. Therefore, other generating units on that island need to complement this incapability of SMR. If the generation-demand mismatch persists when all the connected plants reach their lower limits, the system faces the power evacuation problem. There is no practical solution to the power evacuation problem except tripping the SMR.

The power evacuation problem faced during the minimum load of a day is worst as there will be additional excess power on the island with fewer load consumers. Thus, the dispatch from SMR for a day is constrained with unsolved voltage violations, transmission line overloading, and power evacuation problem under various contingencies with the consideration

of the daily load variation. N-1 contingency analysis is performed to assess these problems with a maximum of one major component loss at a time. The loss of transmission lines and generating units are considered for the contingencies, and all other failures are neglected from the assessment. The failure rates and repair times are taken, respectively, as 0.1 f/mile/yr and 10 hours for all transmission lines, and 1 f/yr and 50 hours for all generating units. As the power evacuation problem is considered a critical issue, it is assumed that there will be no support from the interconnected system 2 to consume excess power. In sum, the OPF optimization problem formulated in (7.1) is constrained by the three additional contingency based problems given by (7.3).

$$\begin{aligned}
V_{i,max} < V_i < V_{i,min}, \quad S_{k,max} < S_k < S_{k,min} \\
\sum_{Is1} P_{gen,min} + P^{SMR} &\leq \sum_{Is1} P_{l,max} + \sum_{Is1} P_{loss} (\{P_{gen,min}\}_{Is1}, P^{SMR}, \{P_{l,max}\}_{Is1}) \\
\sum_{Is1} P_{gen,min} + P^{SMR} &\leq \sum_{Is1} P_{l,min} + \sum_{Is1} P_{loss} (\{P_{gen,min}\}_{Is1}, P^{SMR}, \{P_{l,min}\}_{Is1})
\end{aligned} \tag{7.3}$$

where Is1 represents the island with SMR,  $P_{gen,min}$  represents the minimum possible output from all the generation source, except SMR, connected to Is1.  $P_{l,max}$  and  $P_{l,min}$  are the load arrays with maximum and minimum loads of a day for various load centers connected to the Is1. The first constraint represents the voltage and transmission line violation criteria under contingency. Second and third constraints represent the power evacuation problem criteria on an island with SMR for a maximum and minimum load of the day.

The modified OPF with additional constraints is solved using the combination of PSS®E OPF and Contingency Analysis tools. The power output from SMR with the maximum peak load day of the year (A1D1 and A1D2 points from Fig. 7.3 (a) and (b)) provides the maximum size of SMR,  $P^{SMR,max}$ , and power output from SMR with minimum peak load day of the year (A2D1 and A2D2 points from Fig. 7.3 (a) and (b)) gives the maximum limit of minimum dispatch necessary for SMR,  $P^{SMR,min}$ .

#### 7.4.4 SMR with PHES

The power evacuation problem can severely limit the size of SMR at a site. PHES, if installed along with SMR, can capture the excess power to avoid the power evacuation problem. The presence of PHES will allow the system to have a larger size of SMR and more dispatch from SMR at any given time. In addition, PHES, in its generating mode, can provide the additional flexible power in the system to ensure the most economical operation. Having a PHES at the SMR site can also improve the reliability of offsite power.

For this assessment, it is assumed that PHES is placed at the same node where SMR is placed. The sizing of PHES should consider all previously defined considerations that during normal operation, it should be able to provide the most economical power output from a site—since both are placed at same node—and, also should be able to evacuate the excess power from the island, in case there is a contingency in the system at any time of the day. The new optimization problem for the sizing of SMR along with PHES can be stated as:

$$\phi = \text{Minimize} \left\{ \sum_k P_k^{\text{loss}}(P^{h1}, P^{h2}, P^{\text{Tot}}) \right\} \quad (7.4)$$

Subject to:

$$\begin{aligned} P^{\text{Tot}} &= P^{\text{SMR}} + P^{\text{PHG,max}} \\ P_i - jQ_i &= V_i^* * \sum_{n=1}^N Y_{in} V_n \\ P^{h1} + P^{h2} + P^{\text{Tot}} + \sum_o P_{l,o} - \sum_k P_k^{\text{loss}} &= 0 \\ V_{i,\text{max}} < V_i < V_{i,\text{min}}, \quad S_{k,\text{max}} < S_k < S_{k,\text{min}} \\ P_{\text{max}}^h < P^h < P_{\text{min}}^h, \quad Q_{\text{max}}^h < Q^h < Q_{\text{min}}^h \end{aligned} \quad (7.5)$$

The first set of constraints, (7.5), includes the maximum size of PHES in generating mode,  $P^{\text{PHG,max}}$ , for the most economical operation. The second set of constraints, (7.6), includes the maximum size of PHES in motoring mode  $P^{\text{PHP,max}}$ , to protect the SMR under all N-1 contingencies leading to the power evacuation problem. It could have many combinations of sizes of PHES and SMR but, for simplicity, we assume  $P^{\text{PHG,max}} = P^{\text{PHP,max}}$  and the limiting (minimum) size of PHES needed for the prospective site of SMR is determined along

with the maximum power from SMR. All other symbols have the usual meanings as previously defined in (7.1)-(7.3).

$$\begin{aligned}
&V_{i,max} < V_i < V_{i,min}, \quad S_{k,max} < S_k < S_{k,min} \\
&\sum_{Is1} P_{gen,min} + P^{SMR} - P^{PHP,max} \leq \sum_{Is1} P_{l,max} + \\
&\sum_{Is1} P_{loss} (\{P_{gen,min}\}_{Is1}, P^{SMR}, P^{PHP,max}, \{P_{l,max}\}_{Is1}) \\
&\sum_{Is1} P_{gen,min} + P^{SMR} \leq \sum_{Is1} P_{l,min} + \\
&\sum_{Is1} P_{loss} (\{P_{gen,min}\}_{Is1}, P^{SMR}, P^{PHP,max}, \{P_{l,min}\}_{Is1})
\end{aligned} \tag{7.6}$$

The maximum size of SMR,  $P^{SMR,max}$ , and the complete size of PHES,  $[P^{PHG,max}, P^{PHP,max}]$ , is determined by considering the maximum peak load day of the year (A1D1 and A1D2 points from Fig. 7.3 (a) and (b)) and the maximum limit of minimum dispatch necessary for SMR,  $P^{SMR,min}$ , is determined by considering the minimum peak load day of the year (A2D1 and A2D2 points from Fig. 7.3 (a) and (b)).

## 7.5 Case Study and Results

Different cases are analyzed to identify the optimum site and size of SMR in the case system. The transmission loss and expected energy not supplied (EENS) are calculated and compared.

### 7.5.1 Case 1: Without SMR

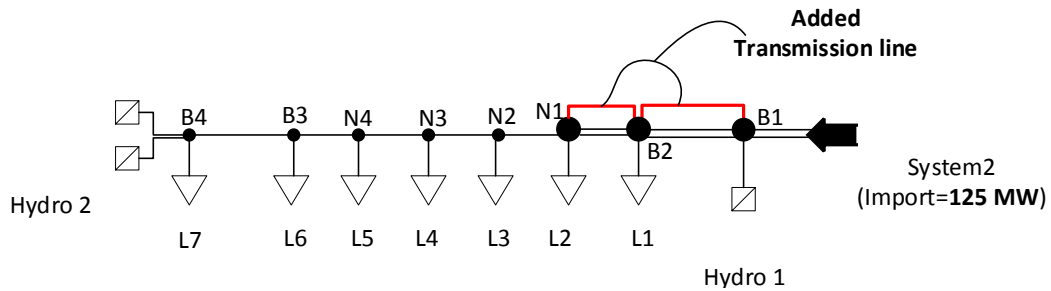


**Figure 7.5:** Future scenario without new generation

If there is no SMR in the system, the deficient power must be imported from the System 2 interconnection. The transmission line upgrades and reactive compensation are needed to ensure the continuous power supply to the distant consumer of the feeder. The two major changes in the systems for this case are: the transmission line B1B2 and B2N1 should be upgraded, and the power import from system 2 should be increased to 125 MW.

### 7.5.2 Case 2: With 100 MW SMR at Each Site

In this case, a 100 MW SMR is considered at each potential site. The transmission loss is calculated using PSS®E OPF for system peak load. The results are shown in Table 7.2. Having an SMR in the system reduces the transmission loss, and the loss is minimum when SMR is placed at N4.

**Table 7.2:** Transmission loss with 100 MW SMR at each site

Case	Loss (MW)
No SMR	43.6698
100 MW SMR at N1	24.361
100 MW SMR at N2	14.6631
100 MW SMR at N3	11.5123
100 MW SMR at N4	9.542

### 7.5.3 Case 3: Optimum SMR Size with Loss Minimization

The OPF problem defined in (7.1) is used to obtain an optimum size of SMR at various sites. However, placing that size of SMR leads to the power evacuation problem for contingencies shown in Table 7.3. The contingencies stated are for the worst scenario. The power evacuation problem leads to the island's shutdown and curtailment of SMR's island loads. The power evacuation problem is, thus, reflected in the EENS of the system. The EENS has worsened in the presence of SMR.

Similarly, the assessment is repeated to determine the dispatch for the lowest peak load day of the year. The dispatch for the lowest peak load day and the corresponding losses are

**Table 7.3:** SMR for highest daily peak load day of the year

SMR at	Opt.size of SMR (MW)	Loss (MW)	Contingencies	EENS (MWhr/yr)
N1	120.17	23.43	Tr line: N1N2, N2N3, N3N4, N4B3, B3B4	25577.88
N2	107.85	14.76	Tr line: N1N2, N2N3, N3N4, N4B3	17788.15
N3	102.26	11.71	Tr line: N1N2, N2N3, N3N4, N4B3	15473.09
N4	96.84	9.40	Tr line: N1N2, N2N3, N3N4, N4B3	13287.24
NO SMR	-	43.66	-	14661.63

**Table 7.4:** SMR dispatch for lowest daily peak load day of the year

SMR at	SMR output (MW)	Loss (MW)	Contingencies
N1	56.06	4.52	Tr line loss: N1N2, N2N3, N3N4, N4B3
N2	51.84	2.72	Tr line loss: N1N2, N2N3, N3N4, N4B3
N3	49.62	2.11	Tr line loss: N1N2, N2N3, N3N4, N4B3
N4	47.23	1.72	Tr line loss: N2N3, N3N4, N4B3

shown in Table 7.4. However, that dispatch will lead to the power evacuation problem in the system for various contingencies on that day, as shown in Table 7.4.

Based on the above assessment, the size of SMR for the most economical operation is shown in Table 7.5. It is clear from the assessment that having given dispatch of SMR in a day will constitute a considerable risk as many single contingencies will lead to the power evacuation problem. Thus, the size of the SMR placed in the system should be limited.

**Table 7.5:** Sizing of SMR for maximum loss reduction

SMR at	Max. size of SMR $P^{SMR,max}$ , MW	Min. dispatch of SMR $P^{SMR,min}$ , MW
N1	120.172	56.0627
N2	107.8538	51.8498
N3	102.263	49.628
N4	96.8497	47.2332

#### 7.5.4 Case 4: N-1 Contingency Constrained OPF

The sizing and dispatch of SMR for economical operation alone led to the power evacuation problem on the island where SMR was connected. An additional set of constraints defined in (7.3) is used to limit the size of SMR to be placed at specific sites. The new maximum sizes of SMR are listed in Table 7.6 along with the corresponding losses for the system peak load. The size of SMR is critically limited, and for the SMR siting N1 and N2, the power is not sufficient to meet the future demand, and at least the 25 MW import from system 2 has to be continued. For the SMR added at N3 and N4, the system can survive without the 25 MW import. The new size of SMR is the new optimum dispatch for the highest peak load day, and there will be no power evacuation problem for all N-1 contingencies.

**Table 7.6:** SMR for highest peak load day of the year

SMR at	Cont. constrained opt. size (MW)	Import from Syst. 2 (MW)	Loss with OPF (MW)	EENS (MWhr/yr)
N1	44	25	33.2552	14493.69
N2	51	25	22.6182	9952.62
N3	58	0	17.1171	9039.91
N4	67	0	12.243	6840.72

The elimination of power evacuation problem is also reflected in EENS, which is sharply reduced for the new size of SMR. The EENS is evaluated using the constant load profile equal to system peak load throughout the year. Similarly, the maximum constrained dispatch for

**Table 7.7:** SMR dispatch for lowest daily peak load day of the year

SMR at	Dispatch from SMR constrained by contingencies (MW)	Loss based on OPF(MW)
N1	25	5.897
N2	30	3.7814
N3	34	2.7344
N4	38	1.965

the lowest peak load day of the year is evaluated using (7.1) with additional constraints defined in (7.3). The dispatch and the transmission loss for the peak load of that day are shown in Table 7.7. This power dispatch on the lowest peak load day will not cause any problem for all N-1 contingencies. Based on this assessment, the complete sizing of SMR that could be placed at various nodes is shown in Table 7.8.

**Table 7.8:** Contingency constrained final sizing of SMR

SMR at	Max. size of SMR $P^{SMR,max}$ , MW	Min. dispatch of SMR $P^{SMR,min}$ , MW
N1	44	25
N2	51	30
N3	58	34
N4	67	38

### 7.5.5 Case 5: With PHES

With PHES, a larger size of SMR can be chosen to fulfill the requirement of economical operation while avoiding the power evacuation problem. The optimum size combination of SMR and PHES for various sites is evaluated using the optimization problem stated in (7.4). The results at various sites are shown in Table 7.9. The respective sizing of SMR and PHES at each site will reduce transmission loss and EENS. The transmission loss based on OPF for minimum and the maximum daily peak of the system with the new size of SMR is shown in

Table 7.10. Table 7.10 also shows the improvement in the EENS.

**Table 7.9:** Sizing of SMR with PHES

SMR & PHES at	SMR		PHES	
	$P^{SMR,max}$ (MW)	$P^{SMR,min}$ (MW)	$P^{PHG,max}$ (MW)	$P^{PHP,max}$ (MW)
N1	81	56.0627	39	39
N2	79	51.8498	29	29
N3	80	49.628	22	22
N4	81	47.2332	16	16

**Table 7.10:** With SMR and PHES

SMR and PHES at	Loss for max. daily peak load (MW)	Loss for min. daily peak load (MW)	EENS (MWhr/yr)
N1	23.432	4.523	12290
N2	14.7671	2.7284	7391.67
N3	11.7177	2.111	5909.13
N4	9.4082	1.7245	4640.51

### 7.5.6 Comparison of Various Cases

The transmission loss for different cases with system peak load are compared in Fig. 7.6 (a). Similarly, EENS for various cases are in Fig. 7.6 (b). Transmission loss is significantly reduced with SMR in the system, and the optimum sizing of SMR achieves the best overall loss reduction. Based on the results, N4 is the best site to place an SMR as it provides the minimum loss for all cases and can host a bigger size of SMR even without PHES. SMR's placement at N4 will also not require the power import from system 2 in the absence of PHES. The EENS for site N4 is lowest among the sites. Similarly, the size of PHES needed at N4 is also smaller.

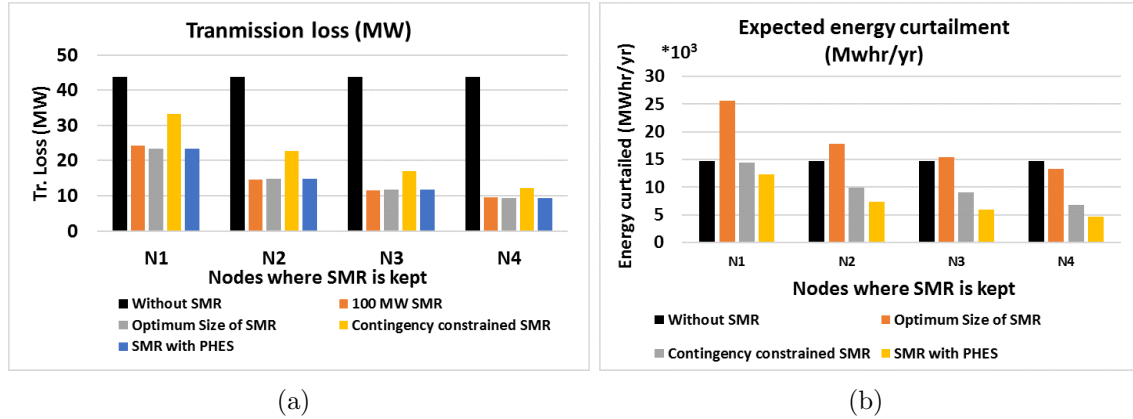


Figure 7.6: Comparison of various cases(a) Tr. loss (b) EENS

## 7.6 Conclusion

This paper discusses the optimum placement and sizing of an SMR in a weak electrical grid. The paper demonstrates that the preferred size of an SMR plant at a hosting location could be higher, but the planner might have to limit the size to avoid various issues such as voltage limit violations, transmission line overloading, and power evacuation problem under normal and abnormal operating conditions. The weak case system considered in this study faced the power evacuation problem for several contingencies, imposing limitations on SMR's sizing. For two out of four potential sites, the constrained size of the SMR plant was not sufficient to meet future load demand, and the deficient power had to be imported from the interconnected system. The other two sites (N3 and N4) were capable of meeting the load demand with the added SMR generation.

Finally, this study showed that the inclusion of PHES could address the power evacuation problem to realize the objective of transmission loss reduction. The optimum site of SMR was N4, with the optimum size of 67 MW without PHES and 81 MW with PHES.

# 8 An Approach to Assess Reliability of Offsite Power as Site Selection Criteria for a Nuclear Power Plant

## Preamble

This study aims to fulfill a part of the fourth objective of the thesis mentioned in Section 1.3. The contribution of this chapter to the overall research is to investigate the safety aspects of siting and sizing SMR in electrical grids.

In this study, various sites in Southern and Northern SEG will be analyzed in terms of their capability to provide reliable offsite power. The failure rate and restoration time of the offsite power at each hosting site will be calculated to evaluate the SBO probability of a hypothetical SMR plant placed in each of those sites.

The network data for the Northern and Southern SEG are obtained from the facility map of the SaskPower utility. The load and generation data are obtained from various publicly available documents on the SaskPower website.

<sup>1</sup>A part of this work has been published in the proceedings of *42nd Annual CNS/CNA Student Conference*, Saskatoon, in June 2018. I came up with this approach and the methodology to incorporate the offsite power reliability as a site selection criteria under the supervision of Prof. Gokaraju. I performed the case study, documented the results and wrote the paper. As a second author, Dr. Joshi provided me with the feedback comments and helped me with the paper write-up.

---

<sup>1</sup>B. Poudel, K. Joshi, and R. Gokaraju, “An approach to assess reliability of offsite power as site selection criteria for a nuclear power plant,” in *42nd Annual CNS/CNA Student Conference*, Saskatoon, Canada, June 2018, pp. 1–6.

## 8.1 Abstract

Various initiating events (IE) trigger the operation of emergency core cooling systems (ECCS) in a nuclear power plant (NPP). The offsite power - one of the major power sources for the ECCS - if reliable, can significantly reduce the chances of station blackout (SBO) and, thus, the nuclear core meltdowns. Hence, it is important to include the reliability of offsite power as a criterion for site selection of NPP during the planning phase. This paper proposes an approach based on the reliability block diagram (RBD) technique to assess various sites for their suitability to host an small modular reactor (SMR) based NPP in terms of reliability of the offsite power. The proposed approach is discussed as a part of the site selection problem for SMR in the Saskatchewan electrical grid<sup>2</sup>.

## 8.2 Introduction

Site selection for a nuclear power plant (NPP) is a herculean task in itself and associates many factors that contribute to the suitability of sites; for example, (a) NPP's safety, (b) hosting capacity of the grid infrastructure, (c) load demand of a site, (d) dynamic and steady-state performance of grid with the new plant; among plenty many other factors. According to the Saskatchewan nuclear attitude study conducted by the University of Saskatchewan, 43% of the general public regard NPP as dangerous [141]. The public fear is stronger than ever due to some recent nuclear accidents. With nuclear generation, the safety assessment is of fundamental importance.

The probabilistic safety assessment (PSA) is widely used to analyze and explore probable accidents in an NPP. In PSA, all possible NPP scenarios are explored from the safety point of view, and the severe initiating events (IEs) are identified along with overall core damage frequency. International Nuclear Safety Advisory Group (INSAG) has set an objective of Core Damage Frequency (CDF) of  $10^{-5}$  per reactor-year for all future nuclear reactors [78]. Loss-of-coolant-accident (LOCA) has been identified as a major IE, leading to most of the core damage accidents. A hypothetical sequence of events in which the loss of offsite power

---

<sup>2</sup>This study is applicable for all NPPs, including SMRs.

(LOOP) occurs during LOCA followed by failure of the emergency onsite power supply is identified as the major contributor for the risk of core meltdown accident [142,143].

Every NPP has emergency core cooling system (ECCS) to deal with such an unforeseen scenario. ECCS consists of emergency cooling pumps, depressurizer, and the water spray system to cool down the reactors following the major incident. The power supply to the ECCS is, therefore, non-negotiable. In accordance, three major sources, namely onsite main generator, offsite power, and the onsite emergency power generators, ensure the uninterrupted supply to the ECCS. During most nuclear accidents, the onsite main generator goes for an emergency shutdown. In such a scenario, the offsite power has to power the ECCS as a first back-up to remove the decay heat and cool down the reactor to a safe state. Even after the emergency shutdown of main generator, the offsite power should be able to supply the ECCS with standard voltage and frequency as per the requirements of critical cooling equipment [144]. If the voltage and frequency go out of the standard limits, the system immediately shuts the offsite supply and looks for onsite emergency power [145]. This paper proposes an approach to evaluate the relative impact of LOOP on the reliability of power supply to ECCS. The objective is to formulate a simple way to make comparisons among various sites in terms of their capability to keep NPP safe. The reliability block diagram (RBD) technique is used to formulate the expressions relating to the reliability of offsite power to the probability of failure of power supply to the ECCS.

## **8.3 System Model**

The case system for this assessment is divided into two different sub-systems: (1) the emergency power supply system (EPSS) in an NPP and (2) the offsite power system. It should be noted that the offsite power's reliability is taken as a variable quantity for site selection as it is not consistent at different sites throughout the electrical grid.

### **8.3.1 The Electrical Grid**

The Saskatchewan Electrical Grid (SEG) is considered as a case network to host the proposed small modular reactor (SMR) based NPP. The SEG, as shown in Fig. 8.1(b), consists of two



### 8.3.2 Emergency Power Supply System

The emergency power supply system (EPSS) is an electrical system feeding power to ECCS. The two train distribution network configuration of an EPSS of a single unit SMR based NPP is shown in Fig. 8.1(a). The two distribution trains are physically isolated and electrically independent from each other. EPSS receives the power from on-site main generator (MG, Fig. 8.1(a)), and offsite power grid (230 kV switchyard, Fig. 8.1(a)) and emergency power generators (DG, Fig. 8.1(a)) as stand-by back-ups. The EPSS consists of two redundant safety buses - 3AS and 3BS - that provide the electrical power to reactor protection system (RPS) and engineering safety features (ESF) - including ECCS - to ensure the safe shut down of the plant during an emergency. Both safety buses are equipped with enough resources to maintain reactor safety under normal and abnormal circumstances.

## 8.4 The Overall Approach

The objective is to formulate a simple way to make a comparison among various sites in terms of their capability to keep SMR safe. The offsite power failure rate and the restoration time are considered, while the plant-centred events are kept as simple as possible. The overall assessment is broken down into two segments. The first segment evaluates the failure rate and average restoration time of the offsite power supply at the different potential sites. In the second segment, the reliability block diagram is constructed for the EPSS, considering it a mission-oriented system. The potential SMR sites with identical onsite system are compared in terms of the station blackout(SBO) probability.

### 8.4.1 Reliability Evaluation of Offsite Power

A model of entire SEG is developed in Siemens PSS®E software. The data needed for the modelling of the generation plants, transmission system and the load demands are taken from the publicly available documents from the Saskpower website [93,146].

Both Southern and Northern SEG are combined in this assessment with 16 HV nodes (230 kV and 138 kV) representing the hosting sites of Southern SEG, while 7 HV nodes(115 kV)

representing the hosting sites of Northern SEG. The reliability assessment is performed in the modelled networks by considering the unavailability of up to three major components (N-3 contingencies) simultaneously. The contingencies resulting in failure/loss of offsite power are identified for each node. Voltage violations unsolved with corrective actions, bus isolation, and generation deficiency are considered major criteria, leading to offsite power failure. Immediate corrective action such as load curtailments, generation re-dispatch, switched shunt control and transformer tap control are also considered to alleviate any network problems. The loss of generating unit and transmission lines are considered as the major contingencies for the assessment, and the failure rates and repair time are taken respectively as 0.1 f/mile/yr and 10 hours for all transmission lines and 1 f/yr and 50 hours for all generating units. The probability and frequency of offsite power failure are evaluated from the probabilistic assessment of the contingencies. These values are used to calculate the meantime to failure (MTTF). The average failure rate of offsite power is the reciprocal of MTTF. The switchyard-centred and plant-centred LOOP events are neglected as SMRs located at different potential sites have identical configurations. The weather-related LOOP events, not considered for this study, will have a bigger impact on average failure rate and restoration time considering Saskatchewan's climate and geography.

The average failure rates of offsite power at different nodes throughout the network are plotted, as shown in Fig. 8.2. It is clear from the results that the Northern SEG sites have higher failure rates as compared to the Southern SEG sites. The offsite power failure is mostly due to the bus isolation and generation deficiency. Only three locations in the network were found with voltage problems and only one contingency set for each case led to the loss of offsite power.

The restoration time (repair time) of offsite power is another factor to consider while evaluating the impact of the offsite power on station blackout (SBO) probability.<sup>4</sup> The site with less offsite power failure rate, while larger repair time could be unsafe for the SMR placement. Once the offsite power is lost, the station-based backups have to maintain the power supply until the offsite power comes back to the service. Thus, the whole process

---

<sup>4</sup>The paper originally didn't consider the restoration time. However, quick restoration of the offsite power supply would be crucial for an NPP. The subsequent assessments and the results, thus, incorporates the restoration time in this Chapter.

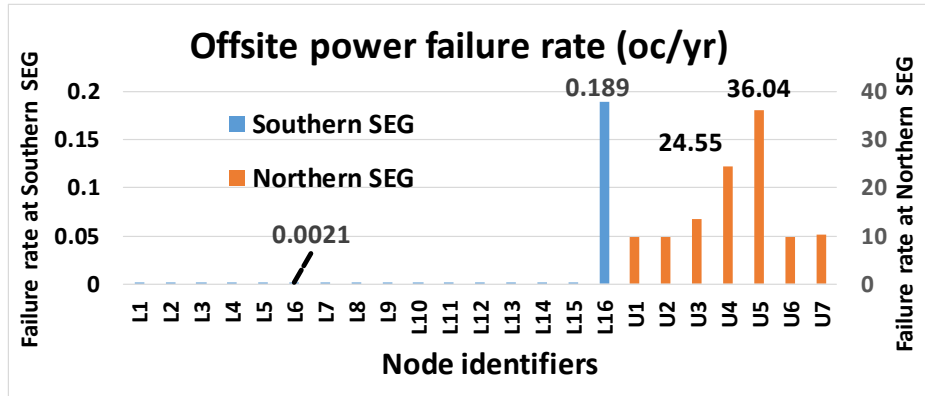


Figure 8.2: Offsite power failure rates

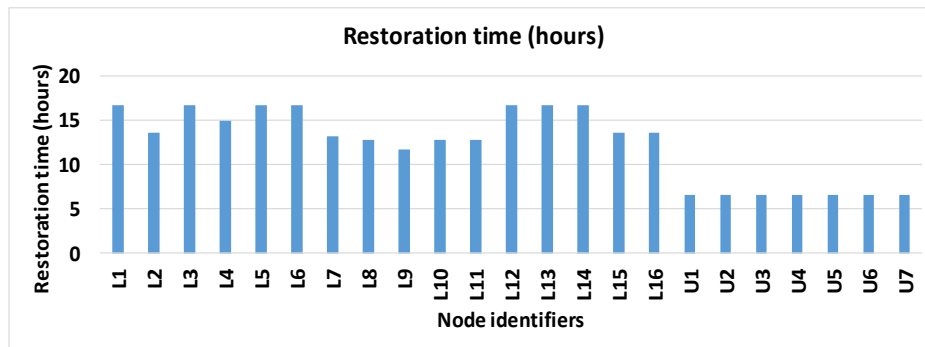


Figure 8.3: Offsite power restoration times

could be considered a mission-oriented system with mission time equal to the offsite power restoration time. Fig. 8.3 shows the offsite power restoration time for failures at different nodes at SEG, which will be taken as a mission time for onsite SBO evaluation.

### 8.4.2 Reliability Assessment of Onsite EPSS

The reliability of EPSS is the reliability of power supply to either of the two safety buses 3AS or 3BS, as the two safety buses are redundant to each other. The reliability assessment for the safety bus 3BS will be identical to the assessment for bus 3AS. The reliability block diagram (RBD) representing the power supply to safety bus 3AS is deduced from the distribution network, as shown in Fig. 8.4. It shows the three branches feeding power to the safety bus 3AS. The first branch is the supply from MG, which has the components normally operating (NO) and characterized by failure rates ( $\lambda$ ). The second branch represents the supply from the offsite power, which has the equipment that can fail during the start (with failure probability

Q per demand) as well as during operation (with failure rate  $\lambda$ ). The third branch is DG, and it also has components that can fail during the start and operation.

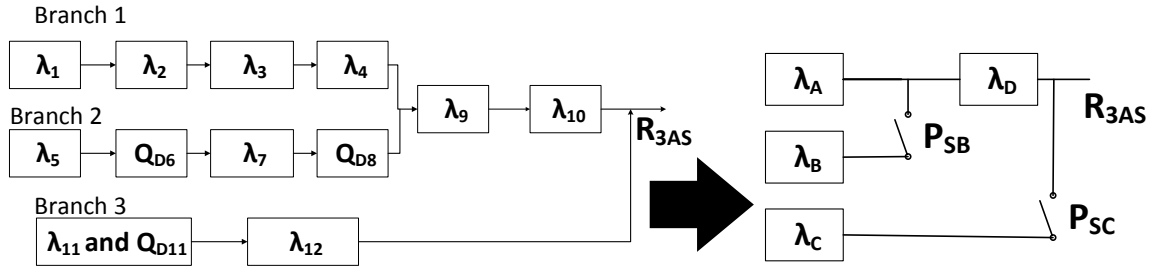


**Figure 8.4:** RBD for power supply to bus 3AS

**Table 8.1:** Component failure data

Component Id	Sym.	Mode of failure	Median
Main Generator	$\lambda_1$	Trip Out	$1.159 \cdot 10^{-3}/\text{hr}$
Disconnect 285A	$\lambda_2$	Fail Open	$1 \cdot 10^{-6}/\text{hr}$
Transformer UAT-A	$\lambda_3$	Short Circuit	$1 \cdot 10^{-6}/\text{hr}$
Feeder Breaker 1-2A	$\lambda_4$	Trip Open	$1 \cdot 10^{-6}/\text{hr}$
Offsite power	$\lambda_5$	Power Failure	-
EDS-A	$Q_{D6}$	Fail to Operate	$3 \cdot 10^{-4}/\text{d}$
Transformer ST-A	$\lambda_1$	Short Circuit	$1 \cdot 10^{-6}/\text{hr}$
Feeder Breaker 4-2A	$Q_{D8}$	Fail to Close	$1 \cdot 10^{-3}/\text{d}$
Feeder Breaker 8-2A	$\lambda_9$	Trip Open	$1 \cdot 10^{-6}/\text{hr}$
Tie Breaker 11-3AS	$\lambda_{10}$	Trip Open	$1 \cdot 10^{-3}/\text{hr}$
DG	$Q_{D11}$	Fail to Start	$1.5 \cdot 10^{-2}/\text{d}$
DG	$\lambda_{11}$	Fail to Run	$2.6 \cdot 10^{-2}/\text{hr}$
Ckt. Brk 14-3AS	$\lambda_{12}$	Trip Open	$1 \cdot 10^{-6}/\text{hr}$

For the reduction of the block diagram, the failure rates ( $\lambda_x$ ) in each branch are combined to represent the operating failures, whereas the starting failure probabilities ( $Q_{DX}$ ) in each branch are combined and represented by the imperfect switches as shown in Fig. 8.4. The blocks A, B, and C represent the combined failure rates of various components connected to transmit power to the bus 3AS from MG, offsite power, and DG. Block D represents

the power distribution system connecting bus 2A to bus 3AS. The sample value of failure rates for different components representing their usual mode of failure is listed in Table 8.1. For simplicity, all other failure scenarios are neglected. The possibility of component repair during the mission is also not considered.

### 8.4.3 Result and Discussion

The block diagram in Fig. 8.4 can be solved using the reliability concepts of standby systems [147].  $R_{3AS}$  is the reliability of power supply to bus 3AS for a mission. The failure of the power supply system of both 3AS and identical system 3BS is a station blackout(SBO) scenario. The offsite power failure rate represents the number of times the mission occurs in a year, whereas the average restoration time provides the time for each mission. Fig. 8.5 shows the SBO probability per reactor year of the SMR station with the placement of SMR at different potential sites <sup>5</sup>.

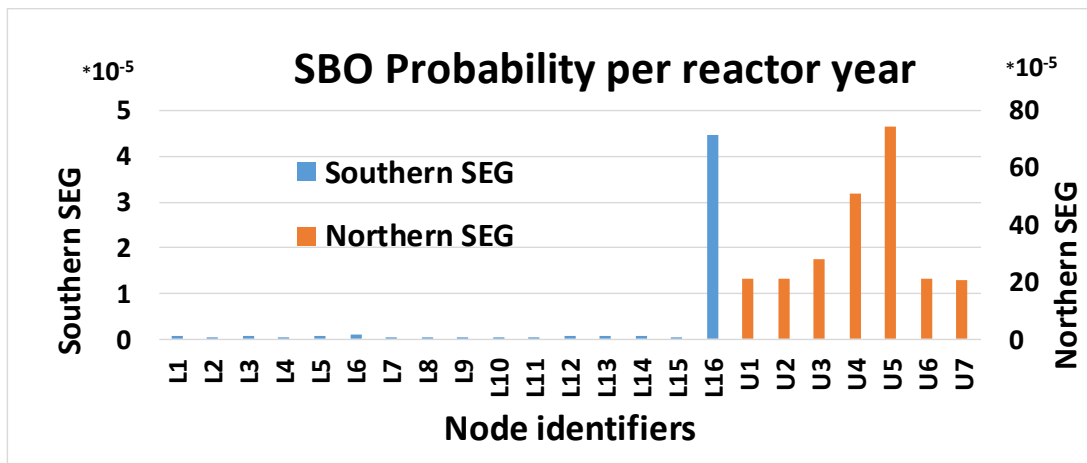


Figure 8.5: SBO probability at different nodes in SEG

<sup>5</sup>The paper originally compared the various sites in terms of the unreliability of power supply to bus 3AS. However, it was realized that it makes more sense to analyze the sites in terms of the SBO probability. It includes all possible scenarios related to the failure of the power supply that may lead to nuclear accidents. Besides, SBO probability also includes the restoration time in the assessment.

## 8.5 Conclusion

An approach assessing the reliability of offsite power as a site selection criterion for SMR based NPP is discussed in this paper. Offsite power is one of the major power sources for ECCS, and thus its reliability directly impacts the safety of the nuclear plant. In the proposed method, the failure rates and restoration times of the offsite power at different nodes are calculated and used to evaluate the SBO probability. The probability of SBO event, one of the major IE leading to core-meltdown, represents the suitability of a site to host SMR. Thus, the results show the comparison among different sites based on their impact on the safety of SMR.

# 9 Conclusions and Future Works

## 9.1 Conclusions

The advantages of small modular reactors (SMRs) in terms of their smaller size, improved response rates, diverse energy application, and the potential synergy with renewable energy sources (RESs) present an excellent avenue to establish sustainable clean energy systems in electrical grids and remote communities. This thesis proposed the models of a comprehensive energy system comprising SMRs and RESs for power system operation and planning studies.

Part-I of the thesis consisted of Chapters 2 and 3. The first task carried out in this thesis in Chapter 2 was to investigate the potential synergy scenarios of SMR and renewables in remote and isolated communities. While the SMRs are a clean and reliable source of energy, they have limitations in flexible operation due to various technical and economic constraints. On the other hand, the non-dispatchable and intermittent nature of PV generation demands flexibility in proportion to their penetration levels. This bottleneck limiting the PV hosting in the SMR-PV system could be solved using electrical energy storage (EES). The case study in an existing feeder in northern Saskatchewan analyzed EES's role as an energy buffer to absorb demand variation and facilitate the synergy between SMR and PV generation. The plant load factor of SMR significantly improved in the presence of the battery energy storage system (BESS) while hosting PV generation in remote communities.

The flexible operation is crucial for the prospect of SMR hybridization with RESs in isolated systems. Chapter 3 investigated the operating limits of SMR for the net change in power and ramp rate in both load following and frequency control modes to analyze SMR's capability to host PV generation in a remote microcommunity. Three different operating limits were proposed and validated using a standard SMR simulator. The flexibility requirements of a microcommunity with different PV penetration levels were evaluated using multi-timescale

simulation— from quarter-hourly to per-second resolution—and analyzed against the operating limits of SMR. The GGOV1 turbine-governor model is adapted to represent the SMR for dynamic simulation to verify the maximum PV penetration level that keeps system frequency deviation within the system limits.

Part-II of the thesis consisted of Chapter 4. Conventional NPPs in North America are mostly operated in baseload mode and rarely used for the flexible operation—the power system studies seldom used the dynamic models of NPPs. However, with the SMR’s proposed application with highly intermittent RES and fluctuating load demands of smaller grids, it is essential to have reactor models to obtain accurate power system dynamics and investigate internal reactor dynamics for power system disturbances. Chapter 4 proposed a detailed dynamic model of an iPWR-type SMR. The proposed model included the dynamics of all four reactor sections: reactor core, primary coolant circuit, steam generator and the secondary coolant circuit before the turbine valve. The reactor model is integrated with the GGOV1 turbine-governor model. A case study was conducted to demonstrate the use of the reactor model for power system dynamic simulation. The results showed the power system and reactor responses for different cases with and without reactor control. It was found that the frequency response would be inaccurate if the reactor model is not included for the power system dynamic simulations with large disturbances.

Part-III of the thesis consisted of Chapters 5 and 6. The remote and isolated communities with limited access to the electrical grid and natural gas pipeline could significantly benefit by having an SMR plant cogenerating for electricity and district heating (DH). The integration of the DH system supported by thermal energy storage provides flexibility to both DH and power systems by coordinating steam distribution for heat and power applications. Chapter 5 proposed a model of SMR-RES hybrid energy system for electricity and district heating, which included a cogenerating SMR plant, wind and PV plants, district heating system, BESS and thermal energy storage. The reactor model introduced in Chapter 4 was further developed to include the turbine bypass and steam extraction systems. The DH system was modeled to represent the steam distribution among heat exchange stations and the quasi-static variation of DH system temperatures. A case study was conducted to demonstrate the flexible operation of the proposed hybrid energy system for a 24 hr period. A multi-timescale

scheme was proposed to decouple and separately analyze the load following and frequency regulation operations. The reactor maneuvering was used for coarse load shaping with 3-4 variations per day. The steam extraction setpoint for the DH system was rescheduled on a quarter-hourly basis. The steam bypass system and the BESS provided the frequency regulation. In the presence of high penetration of the RES, the hybrid energy system was capable of offering both load following and frequency control while keeping the reactor, DH and power system variables within an acceptable level.

The hybrid energy system model developed in Chapter 5 was implemented in Chapter 6 to investigate the optimal operation and renewable hosting capability. An optimization problem was formulated for RES hosting and optimal operation considering the constraints based on power system network, power balance equations, DH system design limits, reactor limits and dynamic performance. An operational scheme was also introduced to operate the hybrid energy system. The reactor was maneuvered for coarse load-shaping, steam extraction was controlled for load following, and steam bypass system and BESS were used for continuous frequency control. A case study was conducted on the modified IEEE 30-bus system with 30-days generation and demand profiles to demonstrate the optimal operation of the hybrid energy system and evaluate its renewable hosting capability. Based on four key decision quantities, namely heat wasted in the DH system, BESS SOC utilization, maximum frequency deviation and SMR maneuvering stats, the optimum size of PV and wind were evaluated. The total number of reactor maneuvers was less than 120 times in a month's duration with the DH system. Without the DH system, the SMR plant would have to be maneuvered every 15 minutes to fulfill the electrical load following. The multi-module feature of the SMR plant also allowed the reduction of the total number of maneuvers and maintaining a reasonable hold duration between two successive maneuvers for each reactor unit.

Part-IV of the thesis consisted of Chapters 7 and 8, and Appendix A. While Chapters 2-6 focused on the SMRs use in remote and isolated communities, Chapters 7 and 8, and Appendix A investigated SMR's siting and sizing issues in typical electrical grids. This thesis includes the electrical grid considerations part of a multidisciplinary project investigating the aspects of siting SMRs. Saskatchewan Electrical Grid (SEG) consists of two isolated electrical networks. Southern SEG representing a strong electrical grid and the Northern SEG

representing a weak electrical grid, were considered the case systems. The overall problem of SMR's siting and sizing was studied in three different aspects: steady-state, dynamic, and safety. A case study investigating the steady-state aspect of siting and sizing of SMR in a weak electrical grid (Northern SEG) was discussed in Chapter 7. Even though the expected sizing of SMR was higher, the sizing had to be curtailed due to various constraints such as voltage limits, transmission line limits and the power evacuation problem under probable contingencies. The case study also analyzed the role of pumped hydro energy storage (PHES) to improve the size of SMR at various hosting locations.

Chapter 8 analyzed the safety aspect by assessing the reliability of the offsite power as a site selection criteria of NPPs (including SMRs). The station blackout (SBO) probabilities of identical SMR substations placed at different hosting locations throughout Southern and Northern SEG were calculated using the offsite power failure rate and restoration time for each hosting location. The problem was analyzed as a mission-oriented system with offsite power failure as a loss of offsite power (LOOP) event and the restoration time as the onsite system mission time. The onsite system, if failed, resulted in the SBO scenario. The hosting locations were thus compared exclusively in terms of their capability to keep SMR safe.

The steady-state and dynamic aspects of SMR sizing and placement in Southern SEG were discussed in Appendix A. The steady-state aspect evaluated the hosting capacity of different potential sites throughout Southern SEG for SMRs. The dynamic aspect analyzed the system's dynamic response in terms of frequency nadir, voltage nadir, rate of change of frequency, and the NERC based frequency response measure. Major generation contingencies were imposed in the system, and the dynamic response metrics were evaluated for different cases with a baseload SMR at various locations. The dynamic assessments were repeated with different sizes of SMR and considering the flexible operation from SMR.

In a nutshell, this research work investigated the opportunities and issues with SMR, including the SMR-RES synergy, SMR-RES hybrid energy system for electricity and district heating and the siting and sizing of SMR in strong and weak electrical grids. With the flexible operation of SMRs supported by BESS in micro-communities, SMR can support the RES hosting. The cogeneration for electricity and DH provides a multi-energy solution and supports the flexible operation of SMRs, improving the RES hosting capability.

## 9.2 Future Works

Based on the research work in this thesis, the following possible extensions are suggested as future works:

1. Implementation of the proposed SMR dynamic model in RTDS for EMT studies: The SMR dynamic model presented in this research could be implemented in RTDS to simulate the reactor response against transient disturbances. The dynamic model presented in this thesis was simulated in PSS<sup>®</sup>E in the phasor domain, mainly against the 3-phase load disturbances and demand fluctuations. It would be interesting to analyze the reactor response in the time domain against transients such as switching events, unbalanced faults and lightning.
2. Investigating the economic performance of SMR-RES hybrid energy systems: This research primarily focused on the modeling and operational feasibility of the hybrid energy system with SMR and RES such as wind and PV in an isolated configuration. Although the proposed hybrid energy system was feasible, it must be financially beneficial amid uncertainty in market structure. The hybrid energy system proposed in Chapter 2, 3, 5 and 6 could be further explored in terms of their potential to integrate with different local industrial heat applications to boost the financial payback.

## References

- [1] IPCC, “Special Report on 1.5 degrees: Summary for Policymakers,” in *Global Warming of 1.5°C. An IPCC Special Report on the impacts of global warming of 1.5°C above pre-industrial levels and related global greenhouse gas emission pathways, in the context of strengthening the global response to the threat of climate change, sustainable development, and efforts to eradicate poverty*, Geneva, Switzerland, 2018.
- [2] S. Tselepis and J. Nikolettatos, “Renewable Energy Integration in Power Grids,” *IEA-ETSAP IRENA Technology Brief*, April 2015.
- [3] A. Von Meier, S. Ghadiri, F. Pina, and R. P. Oglesby, “Challenges to the Integration of Renewable Resources at High System Penetration,” California Institute for Energy and Environment, California, Tech. Rep., 2014. [Online]. Available: <http://uc-ciee.org/>
- [4] C. Underwood, J. Ramachandran, R. Giddings, and Z. Alwan, “Renewable-energy clusters for remote communities,” *Applied Energy*, vol. 84, no. 6, pp. 579 – 598, 2007. [Online]. Available: <http://www.sciencedirect.com/science/article/pii/S0306261907000219>
- [5] J. Royer, “Status of Remote/Off-grid Communities in Canada,” Aboriginal Affairs and Northern Development Canada and Natural Resources Canada, Ottawa, Tech. Rep. 2013-118, August 2011. [Online]. Available: [https://www.nrcan.gc.ca/sites/www.nrcan.gc.ca/files/canmetenergy/files/pubs/2013-118\\_en.pdf](https://www.nrcan.gc.ca/sites/www.nrcan.gc.ca/files/canmetenergy/files/pubs/2013-118_en.pdf)
- [6] C. A. MacKinlay, “Reducing Diesel Reliance in Canada’s Rural and Remote Communities,” in *Generate 2017: First Nation’s Workshop*. Natural Resources Canada, November 2017.

- [7] M. Arriaga, C. A. Caizares, and M. Kazerani, “Long-term renewable energy planning model for remote communities,” *IEEE Transactions on Sustainable Energy*, vol. 7, no. 1, pp. 221–231, 2016.
- [8] K. Joshi and R. R. Gokaraju, “An iterative approach to improve PV hosting capacity for a remote community,” in *2018 IEEE Power Energy Society General Meeting (PESGM)*, Portland, OR, 2018, pp. 1–5.
- [9] M. Arriaga, C. A. Cañizares, and M. Kazerani, “Renewable energy alternatives for remote communities in northern ontario, canada,” *IEEE Transactions on Sustainable Energy*, vol. 4, no. 3, pp. 661–670, 2013.
- [10] CNSC Fukushima Task Force, “Nuclear Power Plant Safety Review Criteria,” Canadian Nuclear Safety Commission, Tech. Rep. E-doc:3743877, July 2011.
- [11] P. Doig and L. Durante, “Nuclear’s comeback greater demand, more plants, new hope,” *IEEE Power and Energy Magazine*, vol. 4, no. 6, pp. 4–6, 2006.
- [12] J. Disosway, “Generations - the nuclear family comes of age,” *IEEE Power and Energy Magazine*, vol. 4, no. 6, pp. 18–24, Nov 2006.
- [13] J. P. Carter, “The transformation of the nuclear power industry,” *IEEE Power and Energy Magazine*, vol. 4, no. 6, pp. 25–33, Nov 2006.
- [14] S. W. Semmes, “A nuclear renaissance,” *IEEE Power and Energy Magazine*, vol. 4, no. 6, pp. 34–42, Nov 2006.
- [15] Nuclear Power Technology Development Section, *Advances in Small Modular Reactor Technology Developments: A Supplement to IAEA Advanced Reactors Information System (ARIS)*, 2018th ed. Vienna, Austria: International Atomic Energy Agency, 2018.
- [16] A. Lokhov, “Load-following with nuclear power plants,” *NEA News*, vol. 29, no. 2, pp. 18–20, 2011.

- [17] Nuclear Development Division, “Technical and economic aspects of load following with nuclear power plants,” Nuclear Energy Agency, Tech. Rep., June 2011. [Online]. Available: <https://www.oecd-nea.org/ndd/reports/2011/load-following-npp.pdf>
- [18] International Atomic Energy Agency, *Non-baseload Operation in Nuclear Power Plants: Load Following and Frequency Control Modes of Flexible Operation*, ser. Nuclear Energy Series. Vienna: IAEA, 2018, no. NP-T-3.23.
- [19] M. R. Islam and H. A. Gabbar, “Study of small modular reactors in modern micro-grids,” *International Transactions on Electrical Energy Systems*, vol. 25, no. 9, pp. 1943–1951, 2015.
- [20] M. Hadid Subki, “Small modular reactors update on international technology development activities,” in *13th INPRO Dialogue Forum on Legal and Institutional Issues in the Global Deployment of SMRs*, 2016, pp. 1–24.
- [21] K. Rogers and M. Ragheb, “Symbiotic coupling of wind power and nuclear power generation,” in *2010 1st International Nuclear Renewable Energy Conference (INREC)*, March 2010, pp. 1–9.
- [22] H. Sato, X. L. Yan, Y. Tachibana, and Y. Kato, “Load-following operations of VHTR gas-turbine cogeneration system for developing countries,” *International Journal of Gas Turbine, Propulsion and Power Systems*, vol. 4, no. 3, pp. 17–24, 2012.
- [23] D. T. Ingersoll, “1 - energy, nuclear power, and small modular reactors,” in *Small Modular Reactors*, D. T. Ingersoll, Ed. Boston: Woodhead Publishing, 2016, pp. 3 – 19. [Online]. Available: <http://www.sciencedirect.com/science/article/pii/B978008100252000001X>
- [24] B.Redekop, “Pinawa eyes nuclear-powered future: Town in talks with small modular reactor industry to become demonstration site,” pp. 1–6, 2017. [Online]. Available: <https://www.winnipegfreepress.com/business/pinawa-eyes-nuclear-powered-future-465364263.html>

- [25] D. T. Ingersoll, C. Colbert, Z. Houghton, R. Snuggerud, J. W. Gaston, and M. Empey, “Can nuclear power and renewables be friends?” in *Proceedings of ICAPP*, Nice, France, May 2015, pp. 1–9.
- [26] V. Tulkki, E. Pursiheimo, and T. Lindroos, *District heat with Small Modular Reactors (SMR)*. Finland: VTT Technical Research Centre of Finland, 2017, project code: 115523.
- [27] V. Tulkki, E. Pursiheimo, T. J. Lindroos, and V. Sahlberg, “Small modular reactors as a part of a district heating system,” *Transactions of the American Nuclear Society*, vol. 118, no. 1, pp. 685–687, 2018.
- [28] Advanced Reactor Information System, “NuScale Power Modular and Scalable Reactor,” International Atomic Energy Agency, Vienna, Austria, Tech. Rep., July 2013. [Online]. Available: <https://aris.iaea.org/PDF/NuScale.pdf>
- [29] M. Tayal, M. Floyd, D. Rattan, Z. Xu, A. Manzer, J. Lau, and E. Kohn, “Load-following performance and assessment of CANDU fuel,” Atomic Energy of Canada Limited, Tech. Rep. AECL–12035, September 1999.
- [30] International Atomic Energy Agency, “Power ramping, cycling and load following behaviour of water reactor fuel,” IAEA, Vienna, Austria, Tech. Rep. IWGFTP/28, May 1988.
- [31] M. Tayal, A. Manzer, R. Sejnoha, Y. Kinoshita, and A. Hains, “The integrity of CANDU fuel during load following,” Atomic Energy of Canada Limited, Tech. Rep. AECL–9797, August 1989.
- [32] N. P. Mueller, “Response of pressurized water reactors to network power generation demands,” *IEEE Transactions on Power Apparatus and Systems*, vol. PAS-101, no. 10, pp. 3943–3950, Oct 1982.
- [33] Q. B. Chou, “Characteristics and maneuverability of CANDU nuclear power stations operated for base-load and load-following generation,” *IEEE Transactions on Power Apparatus and Systems*, vol. 94, no. 3, pp. 792–801, May 1975.

- [34] Q. B. Chou, P. Kundur, P. N. Acchione, and B. Lautsch, “Improving nuclear generating station response for electrical grid islanding,” *IEEE Transactions on Energy Conversion*, vol. 4, no. 3, pp. 406–413, Sep. 1989.
- [35] T. D. Younkins, J. R. Winkelman, J. J. Sanchez-Gasca, and J. A. McGrady, “Output feedback multivariable control for an advanced boiling water reactor,” *IEEE Transactions on Energy Conversion*, vol. 2, no. 3, pp. 349–354, Sep. 1987.
- [36] S. Feutry, “Load following and frequency control transients - EDF experience and practice,” in *IAEA Technical Meeting on Flexible Operation Approaches of Nuclear Power Plants*. Paris, France: International Atomic Energy Agency, September 2013.
- [37] D. Bose, S. Banerjee, M. Kumar, P. P. Marathe, S. Mukhopadhyay, and A. Gupta, “An interval approach to nonlinear controller design for load-following operation of a small modular pressurized water reactor,” *IEEE Transactions on Nuclear Science*, vol. 64, no. 9, pp. 2474–2488, 2017.
- [38] EirGrid and SONI, “DS3: Rate of Change of Frequency (RoCoF) Workstream,” CIGRE, Tech. Rep., 2011.
- [39] N. A. Masood, “Security Assessment due to Increased Wind Generation in a Complex Power Grid,” Ph.D. Dissertation, The University of Queensland, 2017.
- [40] N.-A. Masood, R. Yan, and T. K. Saha, “Cascading contingencies in low inertia power systems: Frequency response challenges and a potential solution,” in *2016 Australasian Universities Power Engineering Conference (AUPEC)*, 2016, pp. 3–7.
- [41] M. Ruth, M. Antkowiak, and S. Gossett, “Nuclear and renewable energy synergies workshop: Report of proceedings,” National Renewable Energy Laboratory, Golden, CO, USA, Tech. Rep. NREL/TP-6A30-52256, 2011.
- [42] M. F. Ruth, O. R. Zinaman, M. Antkowiak, R. D. Boardman, R. S. Cherry, and M. D. Bazilian, “Nuclear-renewable hybrid energy systems: Opportunities, interconnections, and needs,” *Energy Conversion and Management*, vol. 78, pp. 684–694, 2014.

- [43] H. E. Garcia, J. Chen, J. S. Kim, R. B. Vilim, W. R. Binder, S. M. B. Sitton, R. D. Boardman, M. G. McKellar, and C. J. Paredis, “Dynamic performance analysis of two regional nuclear hybrid energy systems,” *Energy*, vol. 107, pp. 234–258, 2016.
- [44] M. Ruth, D. Cutler, F. Flores-Espino, G. Stark, T. Jenkin, T. Simpkins, and J. Macknick, “The economic potential of two nuclear-renewable hybrid energy systems,” National Renewable Energy Lab.(NREL), Golden, CO (United States), Tech. Rep. NREL/TP-6A50-66073, 2016.
- [45] M. Ruth, D. Cutler, F. Flores-Espino, G. Stark, and T. Jenkin, “The economic potential of three nuclear-renewable hybrid energy systems providing thermal energy to industry,” National Renewable Energy Lab.(NREL), Golden, CO (United States), Tech. Rep. NREL/TP-6A50-66745, 2016.
- [46] J. Suk Kim, M. McKellar, S. M. Bragg-Sitton, and R. D. Boardman, “Status on the component models developed in the modelica framework: High-temperature steam electrolysis plant & gas turbine power plant,” Idaho National Lab.(INL), Idaho Falls, ID (United States), Tech. Rep. INL/EXT-16-40305, 2016.
- [47] N. W. Miller, K. Clark, and M. Shao, “Frequency responsive wind plant controls: Impacts on grid performance,” in *2011 IEEE Power and Energy Society General Meeting*, Detroit, MI, USA, 2011, pp. 1–8.
- [48] K. Fehrenbacher, “Nuclear Can Be Friends With Renewables — If It’s Modular.” 2017. [Online]. Available: <https://www.greentechmedia.com/articles/read/nuclear-can-be-friends-with-renewables>
- [49] Task Force on Turbine-Governor Modeling, “Dynamic models for turbine-governors in power system studies,” IEEE Power and Energy Society, Tech. Rep. PES-TR1, 2013.
- [50] T. Ichikawa and T. Inoue, “Light water reactor plant modeling for power system dynamics simulation,” *IEEE Transactions on Power Systems*, vol. 3, no. 2, pp. 463–471, May 1988.

- [51] T. Inoue, T. Ichikawa, P. Kundur, and P. Hirsch, “Nuclear plant models for medium-to long-term power system stability studies,” *IEEE Transactions on Power Systems*, vol. 10, no. 1, pp. 141–148, Feb 1995.
- [52] S. E. Arda and K. E. Holbert, “Implementing a pressurized water reactor nuclear power plant model into grid simulations,” in *2014 IEEE PES General Meeting — Conference Exposition*, July 2014, pp. 1–5.
- [53] L. Xiong, D. Liu, B. Wang, P. Wu, J. Zhao, and X. Shi, “Dynamic characteristics analyse of pressurized water reactor nuclear power plant based on PSASP,” *2009 4th IEEE Conference on Industrial Electronics and Applications, ICIEA 2009*, pp. 3629–3634, 2009.
- [54] H. Gao, C. Wang, and W. Pan, “A detailed nuclear power plant model for power system analysis based on PSS/E,” *2006 IEEE PES Power Systems Conference and Exposition, PSCE 2006 - Proceedings*, pp. 1582–1586, 2006.
- [55] S. E. Arda, K. E. Holbert, and J. Undrill, “Development of a linearized model of a pressurized water reactor generating station for power system dynamic simulations,” in *2013 North American Power Symposium (NAPS)*, Sep. 2013, pp. 1–6.
- [56] S. E. Arda and K. E. Holbert, “A dynamic model of a passively cooled small modular reactor for controller design purposes,” *Nuclear Engineering and Design*, vol. 289, pp. 218–230, 2015.
- [57] —, “Nonlinear dynamic modeling and simulation of a passively cooled small modular reactor,” *Progress in Nuclear Energy*, vol. 91, pp. 116–131, 2016.
- [58] Z. Dong and Y. Pan, “A lumped-parameter dynamical model of a nuclear heating reactor cogeneration plant,” *Energy*, vol. 145, pp. 638 – 656, 2018.
- [59] H. Sam-Aggrey, “Opportunities and challenges related to the deployment of small modular reactors in mines in the Northern Territories of Canada,” *CNL Nuclear Review*, vol. 5, no. 1, pp. 143–153, 2016. [Online]. Available: <http://dx.doi.org/10.12943/CNR.2015.00058>

- [60] International Atomic Energy Agency, *Opportunities for Cogeneration with Nuclear Energy*, ser. Nuclear Energy Series. Vienna: IAEA, 2017, no. NP-T-4.1.
- [61] G. Locatelli, S. Boarin, A. Fiordaliso, and M. E. Ricotti, “Load following of small modular reactors (SMR) by cogeneration of hydrogen: A techno-economic analysis,” *Energy*, vol. 148, pp. 494 – 505, 2018.
- [62] G. Locatelli, S. Boarin, F. Pellegrino, and M. E. Ricotti, “Load following with small modular reactors (SMR): A real options analysis,” *Energy*, vol. 80, pp. 41 – 54, 2015.
- [63] D. Ingersoll, Z. Houghton, R. Bromm, and C. Desportes, “Integration of NuScale SMR with desalination technologies,” in *ASME 2014 Small Modular Reactors Symposium*. American Society of Mechanical Engineers Digital Collection, 2014.
- [64] —, “NuScale small modular reactor for co-generation of electricity and water,” *Desalination*, vol. 340, pp. 84 – 93, 2014. [Online]. Available: <http://www.sciencedirect.com/science/article/pii/S0011916414000885>
- [65] D. Ingersoll, C. Colbert, R. Bromm, and Z. Houghton, “NuScale energy supply for oil recovery and refining applications,” in *Proc. ICAPP*, 2014, pp. 1–8.
- [66] D. Ingersoll, Z. Houghton, R. Bromm, C. Desportes, M. McKellar, and R. Boardman, “Extending nuclear energy to non-electrical applications,” in *19th Pacific Basin Nuclear Conference (PBNC 2014)*, 2014, p. 3.
- [67] Alexander Glaser, M. Ramana, A. Ahmad, R. Socolow, and Balkcom, “Small modular reactors: A window on nuclear energy- an energy technology distillate,” Andlinger Center for Energy and the Environment at Princeton University, Princeton, NJ, Tech. Rep., 2015. [Online]. Available: <http://acee.princeton.edu/distillates>.
- [68] T. J. Lindroos, E. Pursiheimo, V. Sahlberg, and V. Tulkki, “A techno-economic assessment of NuScale and DHR-400 reactors in a district heating and cooling grid,” *Energy Sources, Part B: Economics, Planning, and Policy*, vol. 14, no. 1, pp. 13–24, 2019.
- [69] Q. Ma, X. Wei, J. Qing, W. Jiao, and R. Xu, “Load following of SMR based on a flexible load,” *Energy*, vol. 183, pp. 733 – 746, 2019.

- [70] E. Hussein, R. Gokaraju, I. Al-Anabagi, S. Bend, K. Bethune, J. Dale, G. Ferguson, G. Huang, D. McMartin, B. Mehran, D. Newman, J. Piwowar, S. Sharma, and D. Wagner, “A case study on introducing small modular reactors into a new non-nuclear jurisdiction,” in *38th Annual Conference of the Canadian Nuclear Society and 42nd Annual CNS/CNA Student Conferenc*, Saskatoon, Canada, 2018. [Online]. Available: <http://link.springer.com/10.1007/BF01118672>
- [71] R. Belles, G. Mays, O. Omitaomu, and W. Poore, “Updated application of spatial data modeling and geographical information systems (GIS) for identification of potential siting options for small modular reactors,” Oak Ridge National Laboratory, Oak Ridge, TN, USA, Tech. Rep. ORNL/TM-2012/403, September 2012.
- [72] K. Söderholm, “Challenges of SMR licensing practices,” *AECL Nuclear Review*, vol. 1, no. 2, pp. 19–31, 2012.
- [73] R. Belles, G. Mays, B. Blevins, S. Hadley, T. J. Harrison, W. Jochem, B. Neish, O. Omitaomu, and A. Rose, “Application of spatial data modeling and geographical information systems (GIS) for identification of potential siting options for various electrical generation sources,” Oak Ridge National Laboratory(ORNL), Oak Ridge, TN, USA, Tech. Rep. ORNL/TM-2011/157/R1, May 2012.
- [74] B. Lulik, D. DeMontigny, and E. Hussein, “Is an exclusion zone needed for a small modular reactor?” in *38th Annual Conference of the Canadian Nuclear Society and 42nd Annual CNS/CNA Student Conference*, Saskatoon, Canada, June 2018.
- [75] B. Poudel, K. A. Joshi, and R. Gokaraju, “Analysis for siting and sizing of a small modular reactor – a case study in canada,” in *20th National Power System Conference*, Tiruchirappalli, India, Dec 2018, pp. 1–6.
- [76] North American Electric Reliability Council (NERC), “NERC Reliability Standard PRC-024-2: Generator Frequency and Voltage Protective Relay Settings,” pp. 1–12.
- [77] —, “NERC Reliability Standard BAL-003-1: Frequency Response and Frequency Bias Setting,” pp. 1–12.

- [78] International Nuclear Safety Advisory Group, “Basic safety principles for nuclear power plants,” IAEA, Tech. Rep. 75-INSAG-3 Rev.1, 1999.
- [79] International Atomic Energy Agency, *Use of a Graded Approach in the Application of the Safety Requirements for Research Reactors*, ser. Specific Safety Guides. Vienna, Austria: IAEA, 2012, no. SSG-22.
- [80] US Nuclear Regulatory Commission, “Station Blackout Mitigation Strategies: Proposed Rules,” USNRC, Tech. Rep. RIN number: 3150-AJ08, NRC Docket ID: NRC-2011-0299, July 2013.
- [81] —, “Reevaluation of Station Blackout Risk at Nuclear Power Plants: Analysis of Station Blackout Risk,” USNRC, Tech. Rep. NUREG/CR-6890, 2004.
- [82] G. Brundtland, “Report of the World Commission on Environment and Development: Our Common Future,” *Oxford paperbacks*, 1987.
- [83] National Energy Board, “Canada’s Renewable Power Landscape: Energy Market Analysis 2017,” NEB, Government of Canada, Ottawa, ON, Canada, Tech. Rep., 2017.
- [84] S. Suman, “Hybrid nuclear-renewable energy systems: A review,” *Journal of Cleaner Production*, vol. 181, pp. 166–177, 2018.
- [85] Canadian Nuclear Safety Commission, “Small Modular Reactors: Regulatory Strategy, Approaches and Challenges,” CNSC, Ottawa, ON, Canada, Tech. Rep. DIS-16-04, May 2016.
- [86] C. Cany, C. Mansilla, G. Mathonnière, and P. Da Costa, “Nuclear contribution to the penetration of variable renewable energy sources in a french decarbonised power mix,” *Energy*, vol. 150, pp. 544–555, 2018.
- [87] S. Hong, C. J. Bradshaw, and B. W. Brook, “Global zero-carbon energy pathways using viable mixes of nuclear and renewables,” *Applied Energy*, vol. 143, pp. 451–459, 2015.
- [88] C. Batra, *Integral Pressurized Water Reactor Simulator Manual*. Vienna, Austria: International Atomic Energy Agency, 2018, vol. 1.

- [89] National Renewable Energy Laboratory, “National Solar Radiation Database,” 2017. [Online]. Available: [http://rredc.nrel.gov/solar/old\\_data/nsrdb/](http://rredc.nrel.gov/solar/old_data/nsrdb/)
- [90] M. G. Villalva, J. R. Gazoli, and E. Ruppert Filho, “Comprehensive approach to modeling and simulation of photovoltaic arrays,” *IEEE Transactions on Power Electronics*, vol. 24, no. 5, pp. 1198–1208, 2009.
- [91] National Renewable Energy Laboratory, “PVWatts Calculator,” 2015. [Online]. Available: <https://pvwatts.nrel.gov/>
- [92] A. A. Akhil, G. Huff, A. B. Currier, B. C. Kaun, D. M. Rastler, S. B. Chen, A. L. Cotter, D. T. Bradshaw, and W. D. Gauntlett, *DOE/EPRI 2013 electricity storage handbook in collaboration with NRECA*. Albuquerque, NM, USA: Sandia National Laboratories, 2013.
- [93] SaskPower, “Connection Availability- T & D system,” 2016. [Online]. Available: <https://www.saskpower.com/-/media/saskpower/our-power-future/renewables-roadmap/presentation-renewables-connectionavailability-tdsystem.ashx>
- [94] Market Surveillance Administrator, “Residential Load Profiles,” Calgary, Canada, April 2004. [Online]. Available: <https://www.albertamsa.ca/>
- [95] G. Freudenthaler, “Comparison between electricity storage and existing alberta site dispatch profiles,” Alberta Electric System Operator, Calgary, AB, Canada, Tech. Rep., 2016. [Online]. Available: <https://www.aeso.ca/assets/Uploads/Appendix-P-Comparison-between-Storage-and-Existing-Alberta-Site-Dispatch-Proiles.pdf>
- [96] Canada Standards Association, “CAN3-C235-83 (R2015)-Preferred Voltage Levels for AC Systems, 0 to 50000 V,” 2015. [Online]. Available: <https://webstore.ansi.org/standards/csa/csacan3c2351983r2015>
- [97] C. Underwood, J. Ramachandran, R. Giddings, and Z. Alwan, “Renewable-energy clusters for remote communities,” *Applied Energy*, vol. 84, no. 6, pp. 579–598, 2007.

- [98] J. Jenkins, Z. Zhou, R. Ponciroli, R. Vilim, F. Ganda, F. de Sisternes, and A. Botterud, “The benefits of nuclear flexibility in power system operations with renewable energy,” *Applied Energy*, vol. 222, pp. 872–884, Jul 2018.
- [99] Q. B. Chou, P. Kundur, P. N. Acchione, and B. Lautsch, “Improving nuclear generating station response for electrical grid islanding,” *IEEE Power Engineering Review*, vol. 9, no. 9, pp. 42–42, Sep. 1989.
- [100] B. Poudel, K. Joshi, and R. Gokaraju, “An approach to assess reliability of offsite power as site selection criteria for a nuclear power plant,” in *38th Annual Conference of the Canadian Nuclear Society and 42nd Annual CNS/CNA Student Conference*, Saskatoon, Canada, June 2018, pp. 1–6.
- [101] B. Poudel, K. Joshi, and R. Gokaraju, “A dynamic model of small modular reactor based nuclear plant for power system studies,” *IEEE Transactions on Energy Conversion*, vol. 35, no. 2, pp. 977–985, 2020.
- [102] K. Joshi, B. Poudel, and R. Gokaraju, “Exploring synergy among new generation technologies—small modular reactor, energy storage, and distributed generation: A strong case for remote communities,” *Journal of Nuclear Engineering and Radiation Science*, vol. 6, no. 2, 2020.
- [103] CanmetENERGY Laboratory, “High-Resolution Solar Radiation Datasets — Natural Resources Canada,” 2019. [Online]. Available: <https://www.nrcan.gc.ca/energy/renewable-electricity/solar-photovoltaic/18409>
- [104] J. Buongiorno, M. Corradini, J. Parsons, and D. Petti, “Nuclear energy in a carbon-constrained world: Big challenges and big opportunities,” *IEEE Power and Energy Magazine*, vol. 17, no. 2, pp. 69–77, Mar 2019.
- [105] International Energy Agency, “World Energy Outlook 2014, Executive Summary,” International Energy Agency, Paris, France, Tech. Rep., 2014. [Online]. Available: [www.iea.org](http://www.iea.org)

- [106] C. Marcinkiewicz, “NuScale small modular reactors: Advanced, scalable, flexible, economic,” in *PNWER Energy Working Group Presentation*, July 2017. [Online]. Available: [http://www.pnwer.org/uploads/2/3/2/9/23295822/charles\\_mercinkiewicz-energy\\_session.pdf](http://www.pnwer.org/uploads/2/3/2/9/23295822/charles_mercinkiewicz-energy_session.pdf)
- [107] G. Li, X. Wang, B. Liang, X. Li, B. Zhang, and Y. Zou, “Modeling and control of nuclear reactor cores for electricity generation: A review of advanced technologies,” *Renewable and Sustainable Energy Reviews*, vol. 60, pp. 116–128, Jul 2016.
- [108] L. Pereira, J. Undrill, D. Kosterev, D. Davies, and S. Patterson, “A new thermal governor modeling approach in the WECC,” *IEEE Transactions on Power Systems*, vol. 18, no. 2, pp. 819–829, May 2003.
- [109] NuScale Power, “Final Safety Analysis Report (Rev. 2) - Part 02 - Chapter 04 - Reactor,” NuScale Power LLC, Corvallis, Oregon, Tech. Rep. October, 2018.
- [110] —, “Final Safety Analysis Report (Rev. 2) - Part 02 - Chapter 05 - Reactor Coolant System and Connecting Systems,” NuScale Power LLC, Corvallis, Oregon, Tech. Rep. October, 2018.
- [111] S. E. Arda, “Nonlinear dynamic modeling and simulation of a passively cooled small modular reactor,” Doctoral Dissertation, Arizona State University, 2016. [Online]. Available: <https://repository.asu.edu/items/40760>
- [112] G. Wu, P. Ju, X. Song, C. Xie, and W. Zhong, “Interaction and coordination among nuclear power plants, power grids and their protection systems,” *Energies*, vol. 9, no. 4, p. 306, 2016.
- [113] T. W. Kerlin, E. Katz, J. G. Thakkar, and J. E. Strange, “Theoretical and experimental dynamic analysis of the H. B. Robinson nuclear plant,” *Nuclear Technology*, vol. 30, no. 3, pp. 299–316, 1976.
- [114] M. R. A. Ali, “Lumped parameter, state variable dynamic models for U-tube recirculation type nuclear steam generators,” PhD Dissertation, University of Tennessee, Knoxville, 1976.

- [115] NuScale Power, “Final Safety Analysis Report (Rev. 2) - Part 02 - Chapter 10 - Steam and Power Conversion System,” NuScale Power LLC, Corvallis, Oregon, Tech. Rep. October, 2018.
- [116] L. E. Weaver, “Reactor control,” in *Nuclear Power Safety*, J. H. Rust and L. E. Weaver, Eds. Oxford: Pergamon, 1976, pp. 169 – 208.
- [117] S. Bragg-Sitton, R. Boardman, M. Ruth, O. Zinaman, C. Forsberg, and J. Collins, “Integrated nuclear-renewable energy systems: Foundational workshop report,” Idaho National Lab.(INL), Idaho Falls, ID (United States), Tech. Rep. INL/EXT-14-32857, 2014.
- [118] M. Ruth, D. Cutler, F. Flores-Espino, and G. Stark, “The economic potential of nuclear-renewable hybrid energy systems producing hydrogen,” National Renewable Energy Lab.(NREL), Golden, CO (United States), Tech. Rep. NREL/TP-6A50-66764, 2017.
- [119] R. Yuan, J. Ye, J. Lei, and T. Li, “Integrated combined heat and power system dispatch considering electrical and thermal energy storage,” *Energies*, vol. 9, no. 6, 2016.
- [120] Y. Cao, W. Wei, L. Wu, S. Mei, M. Shahidehpour, and Z. Li, “Decentralized operation of interdependent power distribution network and district heating network: A market-driven approach,” *IEEE Transactions on Smart Grid*, vol. 10, no. 5, pp. 5374–5385, Sep. 2019.
- [121] X. Chen, C. Kang, M. O’Malley, Q. Xia, J. Bai, C. Liu, R. Sun, W. Wang, and H. Li, “Increasing the flexibility of combined heat and power for wind power integration in china: Modeling and implications,” *IEEE Transactions on Power Systems*, vol. 30, no. 4, pp. 1848–1857, July 2015.
- [122] J. Li, J. Fang, Q. Zeng, and Z. Chen, “Optimal operation of the integrated electrical and heating systems to accommodate the intermittent renewable sources,” *Applied Energy*, vol. 167, pp. 244 – 254, 2016.

- [123] Q. Cui, X. Bai, and W. Dong, “Collaborative planning of distributed wind power generation and distribution network with large-scale heat pumps,” *CSEE Journal of Power and Energy Systems*, vol. 5, no. 3, pp. 335–347, Sep. 2019.
- [124] I. Dimoukias, M. Amelin, and F. Leivhn, “District heating system operation in power systems with high share of wind power,” *Journal of Modern Power Systems and Clean Energy*, vol. 5, no. 6, pp. 850–862, November 2017.
- [125] H. Bastida, C. E. Ugalde-Loo, M. Abeysekera, M. Qadrdan, J. Wu, and N. Jenkins, “Dynamic modelling and control of thermal energy storage,” *Energy Procedia*, vol. 158, pp. 2890 – 2895, 2019, innovative Solutions for Energy Transitions.
- [126] Y. Dai, L. Chen, Y. Min, P. Mancarella, Q. Chen, J. Hao, K. Hu, and F. Xu, “A general model for thermal energy storage in combined heat and power dispatch considering heat transfer constraints,” *IEEE Transactions on Sustainable Energy*, vol. 9, no. 4, pp. 1518–1528, Oct 2018.
- [127] Z. Li, W. Wu, M. Shahidehpour, J. Wang, and B. Zhang, “Combined heat and power dispatch considering pipeline energy storage of district heating network,” *IEEE Transactions on Sustainable Energy*, vol. 7, no. 1, pp. 12–22, Jan 2016.
- [128] Z. Li, W. Wu, J. Wang, B. Zhang, and T. Zheng, “Transmission-constrained unit commitment considering combined electricity and district heating networks,” *IEEE Transactions on Sustainable Energy*, vol. 7, no. 2, pp. 480–492, April 2016.
- [129] P. Wang, Z. Gao, and L. Bertling, “Operational adequacy studies of power systems with wind farms and energy storages,” *IEEE Transactions on Power Systems*, vol. 27, no. 4, pp. 2377–2384, Nov 2012.
- [130] D. T. Nguyen and L. B. Le, “Optimal bidding strategy for microgrids considering renewable energy and building thermal dynamics,” *IEEE Transactions on Smart Grid*, vol. 5, no. 4, pp. 1608–1620, July 2014.
- [131] Siemens Power Technologies International, *PSS®E 33.5 Program Operation Manual*. NY, USA: Siemens PTI, 2013, no. October.

- [132] Sotavento Galicia, “Real Time Data of Sotavento Experimental Wind Farm,” 2019. [Online]. Available: <http://www.sotaventogalicia.com/en/technical-area/real-time-data/real-time-data-instantaneous-wild-farm/>
- [133] A. Baumanis, D. Lee, N. Marinos, and F. Ross, “Heat Demand Profile Analysis of Gigha,” 2012. [Online]. Available: [http://www.esru.strath.ac.uk/EandE/Web\\_sites/17-18/gigha/heat-demand-profile.html](http://www.esru.strath.ac.uk/EandE/Web_sites/17-18/gigha/heat-demand-profile.html)
- [134] National Renewable Energy Laboratory (NREL), “Solar Power Data for Integration Studies,” 2019. [Online]. Available: <https://www.nrel.gov/grid/solar-power-data.html>
- [135] Energyhub, “Solar Energy Maps Canada,” 2018. [Online]. Available: <https://www.energyhub.org/solar-energy-maps-canada/>
- [136] Natural Resources Canada, “Wind Energy — Canada’s Wind TRM,” 2009. [Online]. Available: <http://www.nrcan.gc.ca/energy/renewable-electricity/wind/7323>
- [137] International Atomic Energy Agency, *Electric Grid Reliability and Interface with Nuclear Power Plants*, ser. Nuclear Energy Series. Vienna: IAEA, 2012, no. NG-T-3.8. [Online]. Available: <https://www.iaea.org/publications/8754/electric-grid-reliability-and-interface-with-nuclear-power-plants>
- [138] —, “Interfacing Nuclear Power Plants with the Electric Grid: The Need for Reliability amid Complexity,” in *Nuclear Technology Review*. Vienna, Austria: IAEA, 2009, ch. Annex V, pp. 100–115.
- [139] E. Barbour, I. A. Wilson, J. Radcliffe, Y. Ding, and Y. Li, “A review of pumped hydro energy storage development in significant international electricity markets,” *Renewable and Sustainable Energy Reviews*, vol. 61, pp. 421–432, 2016.
- [140] M. Manwaring, “Understanding Pumped Storage Hydropower,” in *NHA Pumped Storage Development Council*, November 2012.
- [141] GlobalNews, “Survey reveals Saskatchewan attitudes toward nuclear power — Globalnews.ca,” pp. 14–15, 2014. [Online]. Available: <http://globalnews.ca/news/1329114/survey-reveals-saskatchewan-attitudes-towards-nuclear-power/>

- [142] V. Manno, “Station blackout: An opportunity for formulating less prescriptive nuclear safety regulation,” Cambridge, Massachusetts: Massachusetts Institute of Technology, Dept. of Nuclear Engineering, Tech. Rep. MTNE-261, 1984.
- [143] S.-M. Wong, “Reliability analysis for the emergency power system of a pressurized water reactor facility during a loss of offsite power transient,” Ph.D. dissertation, IOWA State University, 1984. [Online]. Available: <http://lib.dr.iastate.edu/rtd>
- [144] R. Michal, “The challenge of offsite power reliability,” *Nuclear News*, vol. 43, no. 6, pp. 24–29, May 2000.
- [145] Office of Nuclear Regulatory Research, “Application and testing of safety-related diesel generators in nuclear power plants,” US Nuclear Regulatory Commission, Tech. Rep. DG-1172, March 2007.
- [146] SaskPower, “SaskPower system map,” 2018. [Online]. Available: <https://www.saskpower.com/Our-Power-Future/Our-Electricity/Electrical-System/System-Map>
- [147] R. Billinton and R. N. Allan, *Reliability Evaluation of Engineering Systems*. New York: Plenum Press and Pitman Publishing Limited, 1992.
- [148] CBC News, “Researchers looking into use of small nuclear power plants in Sask.” pp. 1–2, 2018. [Online]. Available: <https://www.cbc.ca/news/canada/saskatchewan/university-regina-saskatchewan-nuclear-power-plants-research-1.4031429>
- [149] Fedoruk Centre, “Backgrounder: Saskatchewan university researchers to examine technical, regulatory aspects of small nuclear power plants,” 2018. [Online]. Available: <http://www.fedorukcentre.ca/news/news-releases/bgr-20170315-technical-capacity-project.php>
- [150] SaskPower, “Plans for a Sustainable Power Future,” in *Saskatchewan Renewable IPP and Supplier Information Session*, Regina, Saskatchewan, November 2016.
- [151] Natural Resources Canada, “Maps of the National Topographic System of Canada: Prairie Provinces (Index4).” [Online]. Available: <https://open.canada.ca/data/en/dataset/055919c2-101e-4329-bfd7-1d0c333c0e62>

# Appendix A

## Project Specific Studies: SMR Siting and Sizing in Saskatchewan Electrical Grid

<sup>1</sup> The Fedoruk project aims to investigate various electrical and non-electrical aspects of siting an SMR in the Province of Saskatchewan, a non-nuclear jurisdiction. It is an interdisciplinary project funded by the Sylvia Fedoruk Canadian Centre for Nuclear Innovation, which involves 14 researchers from five different faculties and their graduate students, post-doctoral fellows and research associates from the University of Saskatchewan and the University of Regina [148, 149].

The electrical grid considerations of SMR siting and sizing are categorized into three different aspects: steady-state aspects, dynamic aspects, and safety aspects. In general, the research requires the case systems to be simulated for various studies such as load flow, optimal power flow, contingency analysis, dynamic simulation, and hosting capacity analysis. Siemens PSS<sup>®</sup>E is used for dynamic simulations, while PSS<sup>®</sup>E and PSS<sup>®</sup>Sincal are used for steady-state simulations.

### A.1 The Case Systems

Two power system cases of Saskatchewan Electrical Grid (SEG) are identified as the case systems for the siting and sizing optimization. Southern SEG represents the strong electrical grid, and Northern SEG represents the weak electrical grid. The present and future scenarios for the power system cases are developed using publicly available information [93, 146, 150]. The total load and generation for the present case, short-term(2020) case and medium-term(2025) case of Southern and Northern SEG based on system forecast are listed in Table A.1. Fig. A.1 shows the topographical map with the transmission network inside Saskatchewan province and medium-term(2025) cases for Southern and Northern SEG.

---

<sup>1</sup>The contents of this Appendix are submitted as a report to the Sylvia Fedoruk Canadian Centre for Nuclear Innovation and will be presented in a future conference.

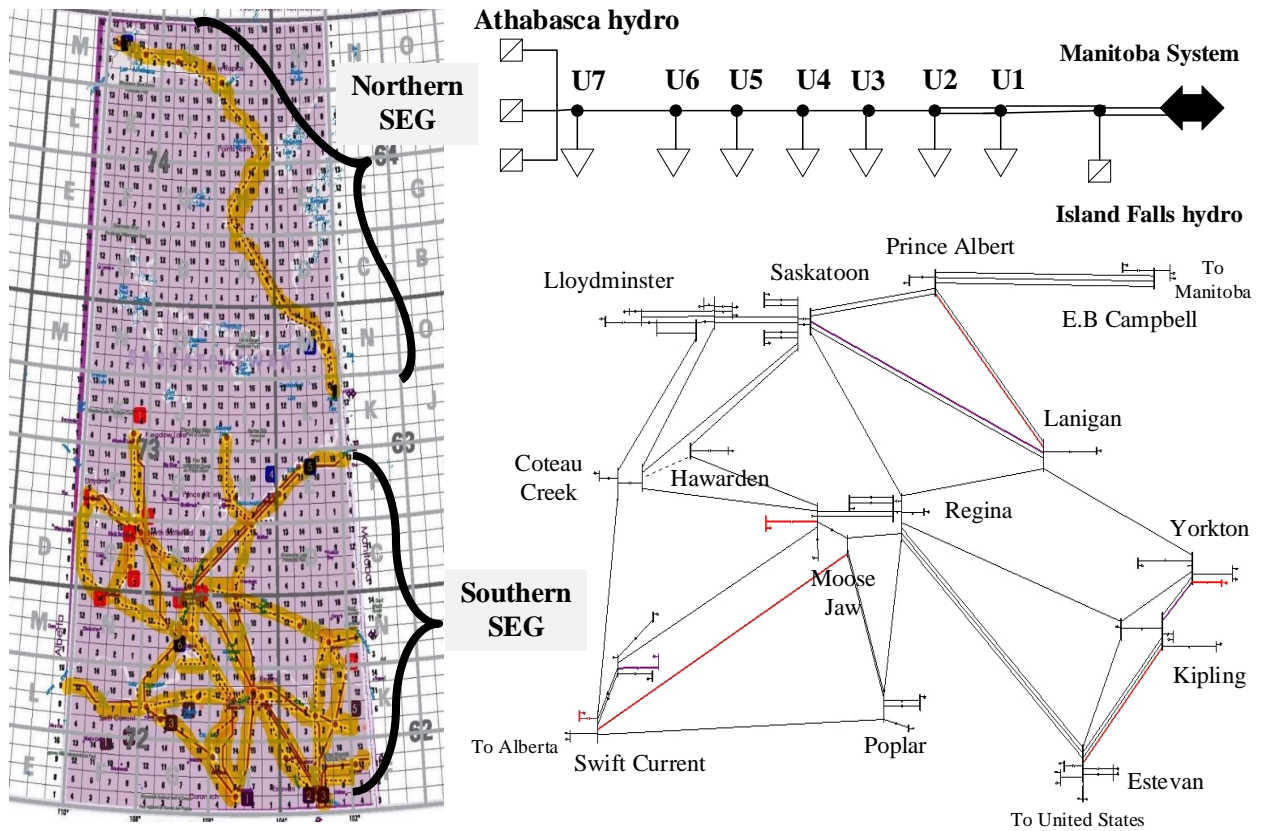


**Figure A.1:** Topographical map and medium term cases of Southern and Northern SEG developed in PSS®E

Southern SEG has strong interconnection with Alberta, the United States, and Manitoba. In contrast, the Northern SEG is a 115 kV long radial transmission feeder—close to 800 km in length—starting from the Manitoba border and reaching up to Athabasca hydro in Uranium city. The medium-term equivalent network for Southern SEG is developed in PSS®E and PSS®Sincal with 55 total nodes, while the Northern SEG is developed with eight nodes.

A significant portion of electrical power in Southern SEG comes from the coal-based generation plants, Boundary Dam(672 MW) and Shand(276 MW) power stations near Estevan and the Poplar River Power Station(582 MW) located near Coronach. With most of the coal-based units set to be decommissioned by 2030, SaskPower is looking for clean energy replacements. The issues Southern SEG will be facing in the future are like-for-like replacements for decommissioned coal-based plants, dispersing the generation congestion that is prevalent in the system at present, and maintaining/improving the power system reliability with the changes in generation configuration.

The Northern SEG, on the other hand, is a weak network which, at present, faces issues such as very high transmission loss, low power system reliability and insufficient generation. The Island Falls hydro(111 MW) and three hydro stations of Athabasca hydro (collectively 23 MW) supply electrical power to Northern SEG. The Northern SEG has a power exchange agreement of  $\pm 25$  MW with Manitoba hydro. The generation deficiency forces the load consumers in Northern SEG to rely on diesel-based electricity as the contingency back-ups. The Northern SEG is set to keep facing these issues with no new generation coming up in the immediate future. The generation capacity available is not enough to fulfill the projected load demand, and thus, the new power alternative is necessary for continuity of power supply to the system. One option might be to import more power from Manitoba hydro. However, the bulk power transfer along this long feeder will result in very high transmission loss. Large-scale transmission system reinforcement and reactive compensation throughout the network will be necessary.

**Table A.1:** Load and generation for present and future cases

	Present Case	Short-term(2020)	Medium Term(2025)
Southern SEG:			
Total Load(MW)	3430	3888	4180
Generation(MW)	4250	4650	5400
Northern SEG:			
Total Load(MW)	101	-	163
Generation(MW)	134	134	134

## A.2 Steady-State Aspects

The steady-state aspect focuses on investigating various SEG sites regarding accessibility to the electrical grid, load demand, transmission capacity to host SMR and evacuate power under contingency scenarios.

## A.2.1 Southern Saskatchewan Electrical Grid

Southern SEG, with a strong network, has the potential to host a larger size of SMR. Fig. A.2 shows the generation-load scenario of Southern SEG for medium-term(2025) case. The South West region of Southern SEG is forecasted to have the largest generation-load imbalance, with more generation than load.

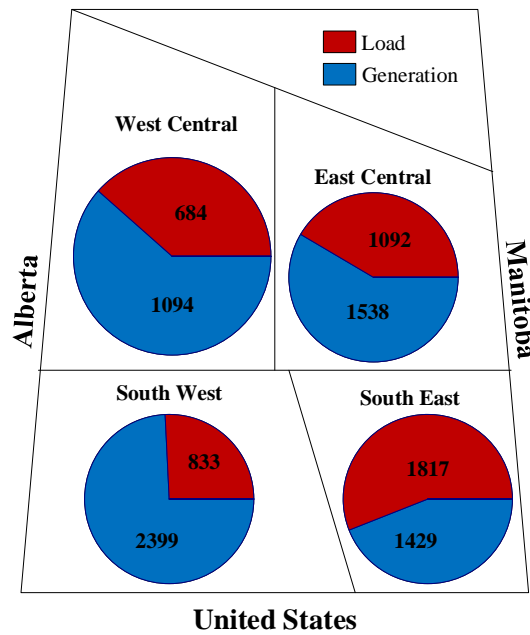


**Figure A.2:** Generation-load scenario of Southern SEG regions for medium-term

The maximum size of SMR that could be integrated into various transmission nodes is evaluated with the hosting capacity analysis. In hosting capacity analysis, the active power injection at a node is increased incrementally until the system faces the violation of voltage limits or transmission line loading limits. The optimization problem for the hosting capacity analysis is shown in equation (A.1), while the constraints are listed in equation (A.2).

$$\text{Maximize } (P_m^{SMR}) \tag{A.1}$$

Subject to:

$$P_i - jQ_i = V_i * \sum_{n=1}^N Y_{in} V_n \quad (A.2)$$

$$V_{i,max} < V_i < V_{i,min}, \quad S_{k,max} < S_k < S_{k,min}$$

$$P_{i,max}^G < P_i^G < P_{i,min}^G, \quad Q_{i,max}^G < Q_i^G < Q_{i,min}^G$$

For all nodes represented by 'i' and transmission lines represented by 'k.'

Where  $P_m^{SMR} = P_m - P_m^G$ .  $P_m^{SMR}$  is the size of SMR hosted in  $m^{th}$  node.  $P_m^G$  is the existing generation in the  $m^{th}$  node.  $P_i$  and  $Q_i$  represent the active and reactive power in the  $i^{th}$  node.  $V_i$  and  $V_n$  represent the voltage of  $i^{th}$  and  $n^{th}$  node, respectively.  $Y_{in}$  is the admittance between  $i^{th}$  and  $n^{th}$  node.  $S_k$  represents the thermal limit of  $k^{th}$  line. The first constraint of the optimization problem represents the power flow problem. The second constraint represents the voltage and transmission line violation criteria. The third constraint represents the active and reactive power limits of the individual generation unit.

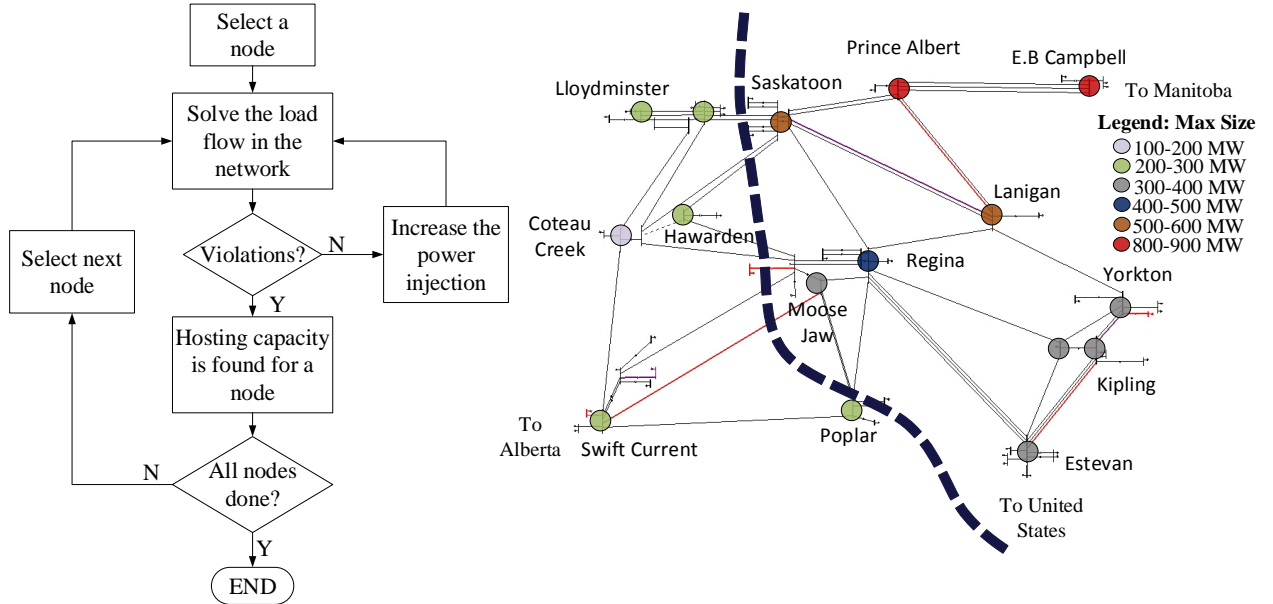


**Figure A.3:** Hosting capacity analysis: flowchart and the results obtained

The problem is solved using PSS®Sincal. Fig. A.3 shows the flowchart for the hosting capacity analysis and the results evaluated for 16 representative HV nodes (230 kV and 138 kV) of Southern SEG. The results of hosting capacity analysis show that the South East and East Central region of Southern SEG can host a larger size of SMR compared to other

regions.

## A.2.2 Northern Saskatchewan Electrical Grid

Discussed in Chapter 7 (pp. 146-162)

## A.3 Dynamic Aspects in Southern SEG

The dynamic aspect focuses on investigating the impact of SMR placed in different locations on the system voltage and frequency dynamics during large disturbances. Fifteen 230 kV nodes in Southern SEG are selected as the potential sites to host an SMR. Six major generation unit losses are identified as the major contingencies for the dynamic simulation. The system voltage and frequency response following the contingencies are simulated with SMR placed at each node. Voltage and frequency nadirs and the initial rate of change of frequency (ROCOF) measures are determined from the dynamic responses. Fig. A.4 shows a typical frequency response after a contingency along with the measurements of interest.

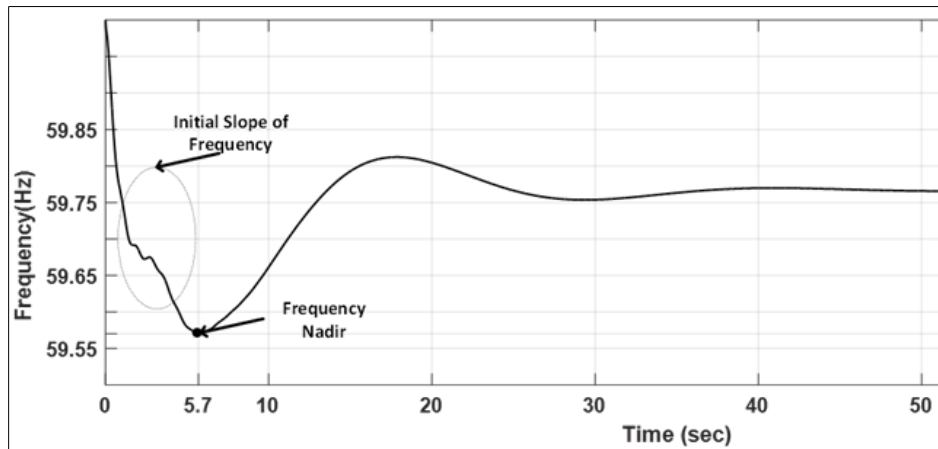


**Figure A.4:** A frequency response showing the measurements of interest

The total power loss in each contingency is 350 MW. The size of the machine and the inertia loss for each contingency is different. The Southern SEG network in the PSS®E slider diagram in Fig. A.5 shows the potential SMR sites and the location of contingencies applied for dynamic simulation.

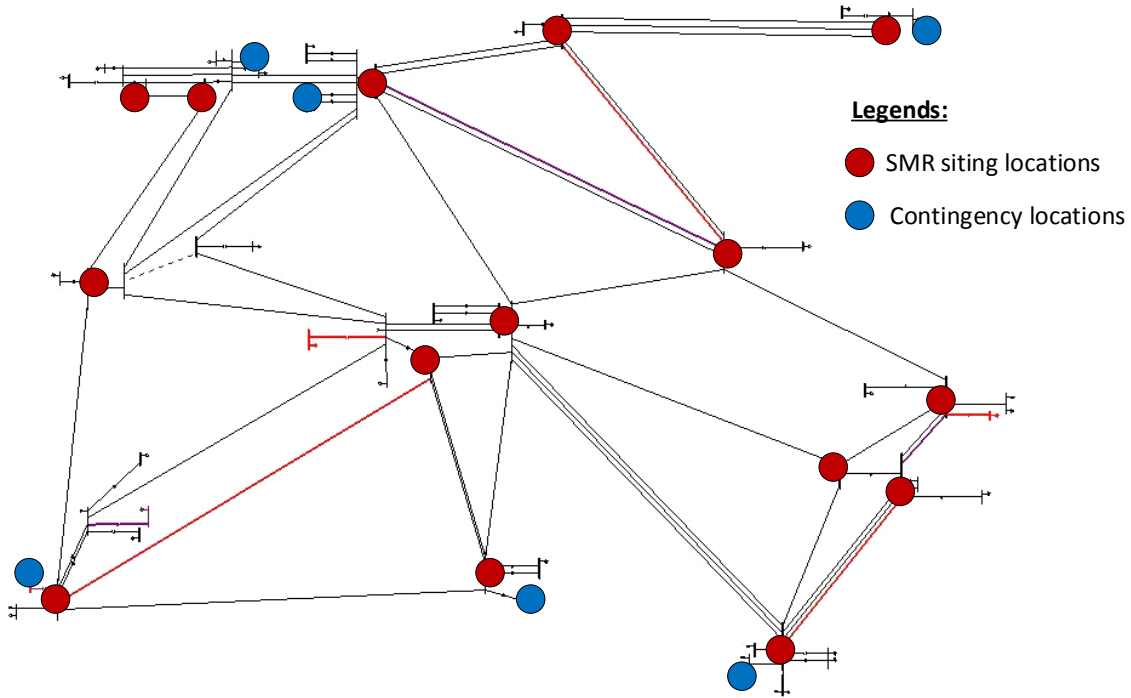


**Figure A.5:** Southern SEG with SMR hosting locations and contingency location for dynamic simulation

The system is simulated for 90 dynamic simulation scenarios with six major contingencies applied for a 300 MW SMR placed in each of the 15 different siting locations<sup>2</sup>. The inter-connection ties with Alberta, Manitoba and United States are removed to investigate the dynamic improvements of the isolated system with SMR in place. The dynamic responses are obtained by assuming SMR as a baseload plant and without considering its frequency response capability. The load is considered to be 100% constant current for active load and 100% constant impedance for the reactive load. The frequency nadir, voltage nadir, and ROCOF measurements at contingency point are presented in boxplots in Figures A.6, A.7, and A.8 respectively. The dotted line in the figures represents the average of respective measurements without SMR in place. The boxplot for each SMR placement provides information about the variation of respective measurement with six different contingencies. The asterisk(\*) in each boxplot represents the average of respective measurements obtained with SMR in place.

<sup>2</sup>The Python code programmed to automate the dynamic simulation is provided in Section B.3 of Appendix B.

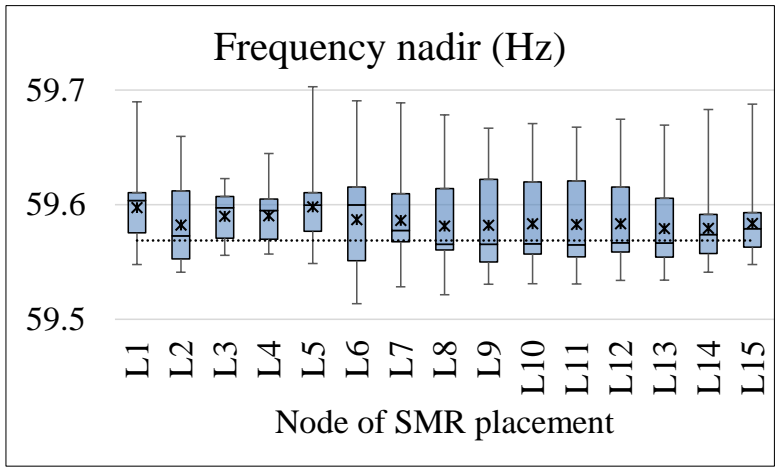


**Figure A.6:** Frequency nadir boxplots for major contingencies with SMR at different nodes

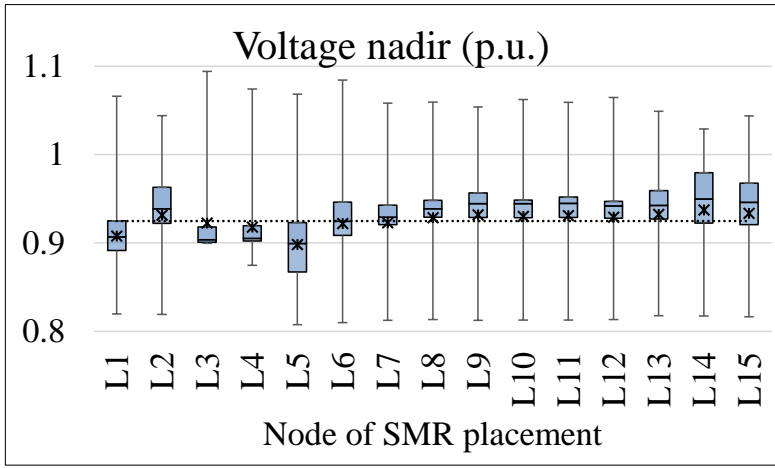


**Figure A.7:** Voltage nadir boxplots for major contingencies with SMR at different nodes

Fig. A.6 shows that the average of the frequency nadirs improves in the presence of SMR. This improvement is due to the additional inertia offered by SMR, even though it doesn't participate in frequency regulation. Analysis of individual results showed that the frequency nadir improves when SMR is far from the contingency location. If SMR is placed near the contingency location, it will improve the system voltage at the contingency site. As the active load is assumed to be 100% constant current, the net power imbalance will increase with the placement of SMR near contingency location, thus, worsening the frequency nadir.

The voltage nadir plots in Fig. A.7, on the other hand, show an overall improvement in average voltage nadir with some of the placement cases, while the rest of them worsen the

voltage response. Analysis of individual results showed that the voltage nadir improves when SMR is near the contingency location as it can offer reactive power. When SMR is placed far from the contingency location, the voltage response gets worsened as the transmission system has to reroute the power flow to adapt to the contingency scenario with SMR not adjusting its active power output.

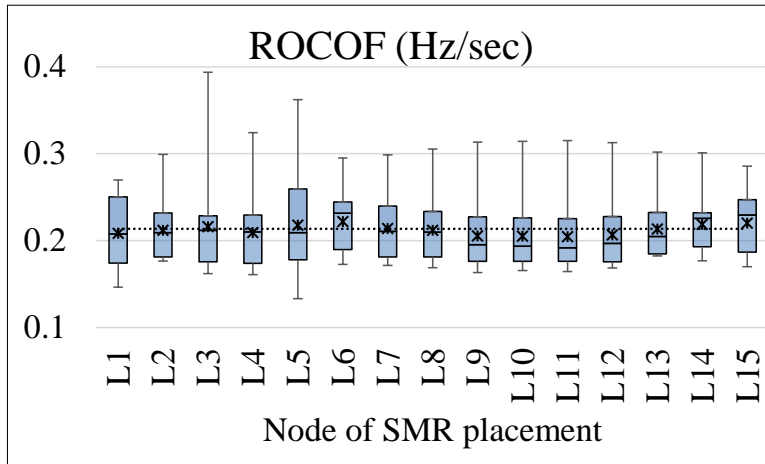


**Figure A.8:** ROCOF boxplots for major contingencies with SMR at different nodes

The ROCOF plots in Fig. A.8 show that the average ROCOF worsens with the placement of SMR in the system. The individual responses indicated that the ROCOF is worse when SMR is placed far from the contingency location. If SMR is far from the contingency location, the bulk generation from SMR exists at the expense of the generation reduction from the plants near the contingency location. Following the contingency, due to the lack of reroutable power nearby, there will be a larger initial power imbalance near the contingent location, thus, worsening the initial ROCOF. When SMR is placed near the contingent location, it can support the initial power imbalance immediately after contingency.

In NERC interconnection, every Balancing Authority(BA) should provide a frequency response for internal disturbance within BA and external disturbances outside BA. One widely used frequency response standard is the nadir based frequency response measure(FRM), which is defined as the size of the contingency in MW required to cause the frequency excursion of 0.1 Hz. The nadir based FRM of the system is compared against the minimum frequency response obligation(FRO) set by NERC for Saskatchewan Power Corporation(SPC), one of the BAs under Eastern interconnection of the NERC. The FRO of each BA can be

calculated from equation(A.3) as a part of the interconnection frequency response obligation(IFRO) set by NERC for each interconnection [77].

$$FRO_{BA} = IFRO \times \frac{Annual\ Gen_{BA} + Annual\ Load_{BA}}{Annual\ Gen_{Int} + Annual\ Load_{Int}} \quad (A.3)$$

IFRO for eastern interconnection is 1002 MW/0.1Hz. This will result in the FRO of SPC to be less than 10 MW/0.1Hz. However, this measure is the requirement for external and internal disturbances while interconnected within the eastern interconnection.

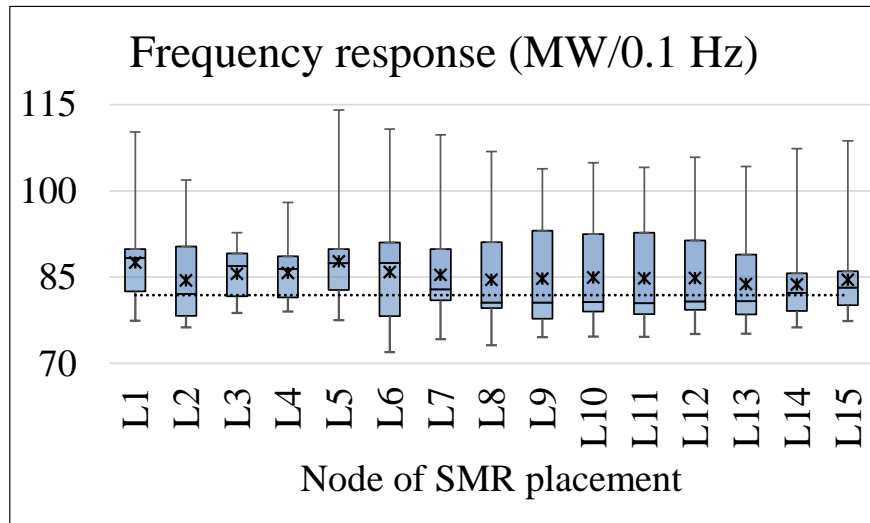


**Figure A.9:** Nadir based FRM boxplots with SMR at different nodes

As seen in the boxplots in Fig. A.9, the nadir based FRM of the isolated Southern SEG is always higher than the FRO of SPC irrespective of the SMR placements. However, the variation of nadir based FRM with SMR sites shows the impact SMR placement has on the relative strength of the system against contingency.

In sum, the dynamic responses were dependent on various factors such as the MVA size of the machine lost, the location of contingency, the SMR siting location, and the electrical separation between the contingency and the SMR sites. The frequency nadir and initial ROCOF are based on the net power imbalance in their respective time frame. The load near contingency also has an impact on the dynamic response. Similarly, the assumptions made for the equivalent load models for dynamic simulation also plays a role in deciding the system dynamics. Choosing a site for an SMR based on a dynamic aspect is a complex problem due

to its dependency on a network. The boxplot based assessment, accumulating the individual response measures for all major contingencies, offers a way to compare and grade different potential sites.

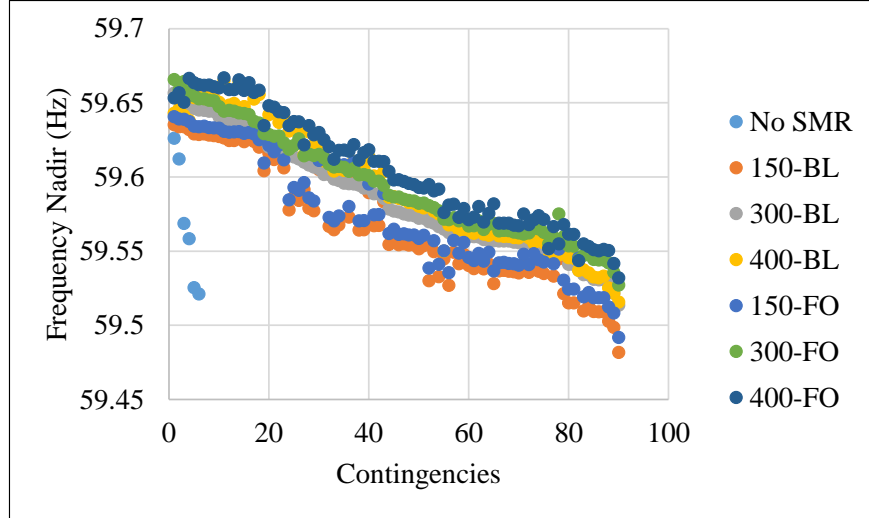


**Figure A.10:** Frequency nadir for different cases

Until now, this assessment considered SMR as a baseload generation. However, SMRs can offer flexible operation to improve the system response for large disturbances. The range of operating limits of SMRs for frequency control was discussed in Chapter 3 where three operating limits were proposed: Conventional ( $\pm 10\% \text{REO} @ 60\% \text{REO}/\text{min}$ ), Advanced ( $\pm 20\% \text{REO} @ 80\% \text{REO}/\text{min}$ ) and Extreme ( $\pm 10\% \text{REO} @ 60\% \text{REO}/\text{min}$ ). Since the SMR is placed in a relatively strong electrical grid, the conventional operating limit is selected. Seven different cases considered are No SMR, 150 MW SMR as a baseload plant, 300 MW SMR as a baseload plant, 400 MW SMR as a baseload plant, 150 MW SMR with flexible operation, 300 MW SMR with flexible operation and 400 MW SMR with flexible operation. Fig. A.10 plots the frequency nadir for different cases identically simulated under six specified contingencies with the placement of SMR in 15 prospective nodes. The frequency nadir data are plotted in descending order irrespective of the siting configuration. It clearly shows the improvement in frequency nadir with the increase in SMR size. Considering the frequency response further improves the frequency response.

Fig. A.11 plots the FRM boxplots with different sizes of SMR with and without frequency control. While the improvement in FRM with frequency control is apparent, the 300 MW

SMR plant, considered in the earlier part of the assessment, appears to provide the best response.

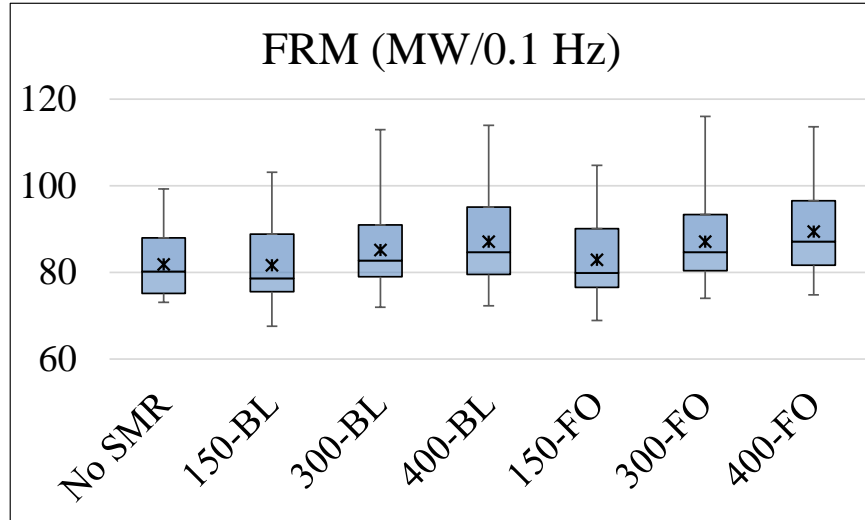


Figure A.11: FRM boxplots for different cases

## A.4 Safety Aspects

Discussed in Chapter 8 (pp. 163-172)

## A.5 Results and Discussion

Based on the results of the steady-state and safety aspects, several sites are excluded. Table A.2 lists the results for steady-state and safety aspects of the 16 sites in Southern SEGs. CP represents the connection point for SMR defined using the National Topographic Mapping System(NTS) of Canada [151]. The site L16 is rejected as it poses a significant risk in SMR safety compared to other Southern SEG sites. Besides, there are numerous sites in the vicinity of L16 that offer better SBO probability. Five other sites, L1, L3, L4, L5 and L6, have limited hosting capacity (HC) and are only suitable for SMR size below 300 MW. Regardless, the 15 sites, except L16, are further assessed to analyze the dynamic performance in the presence of SMR. Although the dynamic performance was analyzed in this thesis, it is not utilized to rank the sites. All of the sites examined in the dynamic simulation are

considered suitable to host SMR.

**Table A.2:** Final results for siting and sizing in Southern SEG

Node	CP#	Non-electric		Steady state	Safety
		Feasibility	Potential Site	HC (MW)	SBO Prob (per yr.)
L1	72-O-7	NA	Coteau Creek	155.78	6.19E-07
L2	73-B-2	NA	Saskatoon	508.98	3.31E-07
L3	73-F-4	NA	Lloydminster	221.64	7.07E-07
L4	73-C-16	NA	Battleford	220.92	4.36E-07
L5	72-J-5	NA	Swift Current	237.99	6.19E-07
L6	72-H-6	NA	Poplar	257.73	9.28E-07
L7	72-I-11	NA	Moose Jaw	340.25	5.16E-07
L8	72-I-9	NA	Regina	443.3	4.02E-07
L9	62-E-6	NA	Estevan	374.95	3.09E-07
L10	62-L-1	NA	Kipling	374.65	2.68E-07
L11	62-L-7	NA	Kipling-2	376.77	2.68E-07
L12	62-M-7	NA	Yorkton	392.79	6.19E-07
L13	72-P-14	NA	Lanigan	588.59	6.19E-07
L14	73-A-15	NA	Prince Albert	874.08	6.19E-07
L15	63-E-11	NA	E.B Campbell	882.35	3.31E-07
L16	72-O-9	NA	Hawarden	212.81	4.47E-05

Table A.3 shows sites representing the Northern SEGs in this siting and sizing assessment. Out of the seven sites considered, three sites U1, U6 and U7, are not feasible based on the non-electrical aspects. The rest of the site's hosting capacities are listed based on the results obtained in Chapter 7. The sites with larger hosting capacity appear to pose more risk in terms of SMR safety. As the Northern SEG is a radial network with no possibility of normal operation under major contingencies, the dynamic performance under contingency was not examined further.

**Table A.3:** Final results for siting and sizing in Northern SEG

Node	CP#	Non-electric		Steady state	Safety
		Feasibility	Potential Site	HC (MW)	SBO Prob (per yr.)
U1	63-M-13	0	Sandy Bay	NA	2.13E-04
U2	74-H-4	1	Key Lake	44	2.13E-04
U3	74-H-6	1	McArthur River	51	2.80E-04
U4	74-H-15	1	Cigar Lake	58	5.11E-04
U5	74-I-8	1	McClellan Lake	67	7.45E-04
U6	74-O-8	0	Stony Rapids	NA	2.13E-04
U7	74-N-11	0	Uranium City	NA	2.08E-04

## A.6 Conclusion

This study used the SEGs to investigate the siting and sizing of SMR based on steady-state, dynamic and safety aspects. Southern SEG represented a strong network while the Northern SEG represented a weak network. Firstly, the case systems were developed in PSS®E and PSS®Sincal software. The steady-state assessment analyzed various potential sites considering the accessibility of the electrical grid, load demand and transmission limits. Northern SEG being more susceptible to contingencies, is further analyzed, exploring issues such as the power evacuation problem under contingencies. The dynamic aspect analyzed the dynamic performance with SMR at suitable sites in terms of the frequency response and voltage response under major generation contingencies. Since the SMR placed in Northern SEG cannot operate normally under dynamic contingencies, only the Southern SEG's dynamic performance was analyzed. The dynamic performance measures such as voltage nadir, frequency nadir, ROCOF and nadir based frequency response were evaluated and compared for the potential sites with 300 MW SMR operating as a baseload plant. The role of flexible operation with different sizes of SMR is also examined in a separate site-independent assessment.

On the other hand, the safety aspect analyzed the suitability of various potential sites

in terms of the SBO probability. The failure frequency and restoration times of the offsite power were used to evaluate the SBO probability with an identical onsite system for the SMR plant at each potential site. Based on the results of these three aspects, the possible locations could be graded and ranked. The results from the electrical grid considerations will be merged with the non-electrical aspects to obtain the final site and size of the SMR plant in the Saskatchewan province.

# Appendix B

## Program Codes for Modeling and Simulation

### B.1 FORTRAN Code for SMR Model in PSS®E

```
SUBROUTINE Ureactor(IARG,ISLOT)
$INSERT COMON4.INS
INTEGER IARG, ISLOT
EXTERNAL BADMID
INTEGER I, J, K, L, JJ, KK, IERR, IB, IBUS, IBPTR
LOGICAL NEW
CHARACTER CB1*6, CB2*6
CHARACTER IM*2, VLTl*4
REAL VINP,VOUT,flow, flow1, VINP2, VOUT2,flowx
IF (MODE.EQ.8) GO TO 1500           ! GET DATA DESCRIPTIONS
I=IARG                             ! MACHINE ARRAY INDEX
J=STRIN(1,ISLOT)                   ! STARTING 'CON'
K=STRIN(2,ISLOT)                   ! STARTING 'STATE'
L=STRIN(3,ISLOT)                   ! STARTING 'VAR'
IF (MODE.GT.4) GO TO 1000
IB=NUMTRM(I)                       ! RETURN IF OFF-LINE
IF (IB.LE.0) RETURN                ! OR SVS OR INDUCTION MACHINE
! MODEL NOT IMPLEMENTED FOR MSTR/MRUN
IF (MIDTRM)
.  CALL BADMID(I,IB,'Ureactor')
.  RETURN
...FIN

! MODE 2 - CALCULATE DERIVATIVES
IF (MODE.EQ.2)                     ! CALCULATE DERIVATIVES
```

```

. VO=ETERM(I)
. FO=BSFREQ(I)+1
. STATE(K+14)=EXP((((STATE(K-6)*144/100+0.0824)/1.0695)*65.93
+114-53.02*LOG(VAR(L)))/33.62)/100
. IF (STATE(K+14)<0.03) STATE(K+14)=0.03
. IF (STATE(K+14)>1) STATE(K+14)=1
. IF (STATE(K+15)<0) STATE(K+15)=0
. IF (STATE(K+15)>1) STATE(K+15)=1
. flow=33.62*LOG((STATE(K+14)+STATE(K+15))*100)+53.02*LOG(STATE(K))-114
. DSTATE(K)=(CON(J)*STATE(K+1)/16.06-CON(J+1)*flow/16.06
-CON(J)*STATE(K)-CON(J)*184.6/16.06)/CON(J+2)
. DSTATE(K+1)=(CON(J+3)*STATE(K+2)+16.06*CON(J+4)*STATE(K)
+184.6*CON(J+4)-STATE(K+1))/CON(J+5)
. STATE(K+6)=CON(J+13)*(STATE(K+11)**0.3333334)
. DSTATE(K+2)=((CON(J+6)*STATE(K+6)/CON(J+13))*(STATE(K+4)-STATE(K+2))
+CON(J+7)*(STATE(K+1)-STATE(K+2)))/CON(J+8)
. DSTATE(K+3)=(2*STATE(K+2)-STATE(K+4)-STATE(K+3))/(CON(J+9)*
CON(J+13)/STATE(K+6))
. DSTATE(K+4)=(STATE(K+8)-STATE(K+4))/(CON(J+10)*CON(J+13)/STATE(K+6))
. DSTATE(K+5)=0
. Chk1=((1-CON(J+17))*CON(J+20)*STATE(K+11)+CON(J+18)*CON(J+19)*(STATE(K+9)
-STATE(K+7)))/CON(J+15)*CON(J+16))
. DSTATE(K+7)=chk1+2.0*STATE(K+6)*(STATE(K+3)-STATE(K+7))/CON(J+15)
. Chk2=((1-CON(J+17))*CON(J+20)*STATE(K+11)+CON(J+18)*CON(J+19)*(STATE(K+9)
-STATE(K+7)))/CON(J+15)*CON(J+16))
. DSTATE(K+8)=chk2+2.0*STATE(K+6)*(STATE(K+7)-STATE(K+8))/CON(J+15)
. Chk3=CON(J+17)*CON(J+20)*STATE(K+11)+CON(J+18)*CON(J+19)
*(STATE(K+7)-STATE(K+9))
. DSTATE(K+9)=chk3/(CON(J+21)*CON(J+22))
. U=-(STATE(K+11)-VAR(L+11))-(STATE(K+2)-VAR(L+2))/5
. VINP=U
. VOUT=PI_MODE2(CON(J+28),CON(J+29),VINP,K+5)

```

```

. U2=(STATE(K+2)-VAR(L+2))
. IF (U2.LT.CON(J+32).AND.U2.GT.-CON(J+32)) U2=0
. IF (U2.GT.CON(J+32)) U2=U2-CON(J+32)
. IF (U2.LT.-CON(J+32)) U2=U2+CON(J+32)
. VINP2=U2
. VOUT2=NWPI_MODE2(CON(J+33),CON(J+34),1.0,0.0,VINP2,K+16)
. STATE(K+10)=CON(J+23)*(STATE(K+13)+8.425)+CON(J+24)*STATE(K+9)
+CON(J+25)*(STATE(K+7)+STATE(K+8))/2
. DSTATE(K+11)=STATE(K+10)/CON(J+26)-(CON(J+23)*STATE(K+11)/CON(J+26))
+CON(J+27)*STATE(K+12)
. DSTATE(K+12)=CON(J+23)*STATE(K+11)/CON(J+26)-CON(J+27)*STATE(K+12)
. VAR(L+1)=STATE(K+1)
. VAR(L+3)=STATE(K+3)
. VAR(L+4)=STATE(K+4)
. VAR(L+7)=STATE(K+7)
. VAR(L+8)=STATE(K+8)
. VAR(L+9)=STATE(K+9)
. VAR(L+10)=STATE(K+10)
. VAR(L+13)=STATE(K+13)
. RETURN
...FIN

```

! MODE 3 - SET EFD

```

IF (MODE.EQ.3)
. STATE(K+14)=EXP((((STATE(K-6)*144/100+0.0824)/1.0695)*65.93+114
-53.02*LOG(VAR(L)))/33.62)/100
. IF (STATE(K+14)<0.03) STATE(K+14)=0.03
. IF (STATE(K+14)>1) STATE(K+14)=1
. PMECH(I)=((33.62*LOG(STATE(K+14)*100)
+53.02*LOG(STATE(K))-114)*1.0695/65.93-0.0824)*(1-CON(J+31))
. U=-((STATE(K+11)-VAR(L+11))-(STATE(K+2)-VAR(L+2)))/5
. VINP=U

```

```

. VOUT=PI_MODE3(CON(J+28),CON(J+29),VINP,K+5)
. STATE(K+13)=VOUT
. U2=(STATE(K+2)-VAR(L+2))
. IF (U2.LT.CON(J+32).AND.U2.GT.-CON(J+32)) U2=0
. IF (U2.GT.CON(J+32)) U2=U2-CON(J+32)
. IF (U2.LT.-CON(J+32)) U2=U2+CON(J+32)
. VINP2=U2
. VOUT2=NWPI_MODE3(CON(J+33),CON(J+34),1.0,0.0,VINP2,K+16)
. STATE(K+15)=VOUT2
. WHEN (MIDTRM) ! RESET STORES FOR CHANGE
. ...FIN
. ELSE VAR(L+13)=VAR(L+13) ! STATE SPACE
. RETURN
...FIN

! MODE 1 - INITIALIZATION
IF (MODE.EQ.1) ! INITIALIZE
. WHEN (MIDTRM)
. ...FIN
. ELSE
. . STATE(K+2)=CON(J+30)
. . STATE(K+1)=(CON(J+3)*STATE(K+2)-CON(J+4)*(65.93*(PMECH(I)/(1-CON(J+31))
+0.0824))/1.0695*CON(J+1)/CON(J))/(1-CON(J+4))
. . STATE(K)=(STATE(K+1)-(65.93*(PMECH(I)/(1-CON(J+31))+0.0824))/1.0695
*CON(J+1)/CON(J)-184.6)/16.06
. . STATE(K+11)=2*CON(J+16)*CON(J+13)*(STATE(K+2)-STATE(K+1))*CON(J+7)
/(CON(J+6)*CON(J+20))
. . STATE(K+14)=EXP((((PMECH(I)/(1-CON(J+31))+0.0824)/1.0695)*65.93
+114-53.02*LOG(STATE(K)))/33.62)/100
. . flow1=33.62*LOG(STATE(K+14)*100)+53.02*LOG(STATE(K))-114
. . STATE(K+6)=CON(J+13)*(STATE(K+11)**0.3333334)
. . STATE(K+4)=((CON(J+6)*STATE(K+6)/CON(J+13)+CON(J+7))*STATE(K+2)

```

```

-CON(J+7)*STATE(K+1))/(CON(J+6)*STATE(K+6)/CON(J+13))
. . STATE(K+3)=2*STATE(K+2)-STATE(K+4)
. . STATE(K+5)=1
. . STATE(K+8)=STATE(K+4)
. . STATE(K+7)=(STATE(K+3)+STATE(K+8))/2
. . STATE(K+9)=CON(J+17)*CON(J+20)*STATE(K+11)/(CON(J+18)*CON(J+19))
+STATE(K+7)
. . STATE(K+10)=0
. . STATE(K+13)=- (CON(J+24)*STATE(K+9)+CON(J+25)*(STATE(K+7)
+STATE(K+8))/2)/CON(J+23)-8.425
. . STATE(K+12)=STATE(K+11)*CON(J+23)/(CON(J+26)*CON(J+27))
. . STATE(K-8)=PMECH(I)/1.44/(1-CON(J+31))
. . STATE(K-7)=STATE(K-8)
. . STATE(K-6)=STATE(K-8)
. . STATE(K-5)=STATE(K-8)
. . STATE(K-4)=STATE(K-8)
. . VAR(L)=STATE(K)
. . VAR(L+6)=STATE(K+6)
. . VAR(L+5)=STATE(K+8)-STATE(K+7)
. . VAR(L+2)=STATE(K+2)
. . VAR(L+11)=STATE(K+11)
. . Y=STATE(K+13)
. . VOUT=Y
. . VINP=-PI_MODE1(CON(J+28),CON(J+29),VOUT,K+5,IERR)
. . STATE(K+15)=0
. . Y2=STATE(K+15)
. . VOUT2=Y2
. . VINP2=NWPI_MODE1(CON(J+33),CON(J+34),1.0,0.0,VOUT2,K+16,IERR)
. . . .FIN
. RETURN
. . . .FIN

```

```

!   MODE 4 -SET NINTEG
    IF (K+16.GT.NINTEG) NINTEG=K+16
    RETURN
    IF (MODE.EQ.6) GO TO 2000
    IF (MODE.EQ.5)
    .   CALL DOCUHD(*1900)
    .   GO TO 1100
    ...FIN

1000 IF (K+14.GT.NINTEG) NINTEG=K+14
    RETURN
    IM=MACHID(I)
    IB=ABS(NUMTRM(I))
    IBUS=NUMBUS(IB)

1500 CON_DSCRPT(1) ='K5'
    CON_DSCRPT(2) ='K6'
    CON_DSCRPT(3) ='Tau_ps'
    CON_DSCRPT(4) ='K3'
    CON_DSCRPT(5) ='K4'
    CON_DSCRPT(6) ='TAu_ms'
    CON_DSCRPT(7) ='K1'
    CON_DSCRPT(8) ='K2'
    CON_DSCRPT(9) ='Tau_p'
    CON_DSCRPT(10) ='Tau_cl'
    CON_DSCRPT(11) ='Tau_hl'
    CON_DSCRPT(12) ='Ke1'
    CON_DSCRPT(13) ='Ke2'
    CON_DSCRPT(14) ='MCN_dot'
    CON_DSCRPT(15) ='Wpn'
    CON_DSCRPT(16) ='Mc'
    CON_DSCRPT(17) ='Cpc'

```

```

CON_DSCRPT(18) ='Fuel power fraction'
CON_DSCRPT(19) ='hfc'
CON_DSCRPT(20) ='Afc'
CON_DSCRPT(21) ='Prat'
CON_DSCRPT(22) ='Mf'
CON_DSCRPT(23) ='Cpf'
CON_DSCRPT(24) ='Beta'
CON_DSCRPT(25) ='Sigmaf'
CON_DSCRPT(26) ='Sigmac'
CON_DSCRPT(27) ='Prompt neutron lifetime'
CON_DSCRPT(28) ='Decay constant(Lambda)'
CON_DSCRPT(29) ='Controller Propotional(Kp)'
CON_DSCRPT(30) ='Controller Integral(Ki)'
CON_DSCRPT(31) ='Tpset, Average Temperature Setpoint'
CON_DSCRPT(32) ='DH enthalpy percent bypass'
CON_DSCRPT(33) ='Temperature NOZ for Bypass'
CON_DSCRPT(34) ='Controller Propotional bypass(Kpb)'
CON_DSCRPT(35) ='Controller Integral bypass(Kib)'

```

```

RETURN

```

```

1100 JJ=J+31

```

```

    KK=K+14

```

```

    CALL VLTFOR(VLTI,BASVLT(IB))

```

```

    IBPTR = 0

```

```

    CALL ADINTN (JJ,CB1,IBPTR)

```

```

    IBPTR = 0

```

```

    CALL ADINTN (KK,CB2,IBPTR)

```

```

    WRITE(IPRT,17) IBUS,BUSNAM(IB),VLTI,IM,J,CB1,K,CB2

```

```

    WRITE(IPRT,27) (CON(K),K=J,JJ)

```

```

    RETURN

```

```

1900 RETURN

```

```

17  FORMAT(//6X,'** UEXC', ' ** BUS NAME  BSKV MACH',
*      '   C O N S   S T A T E S'/,
*      I23,1X,A8,1X,A4,2X,A2,1X,2(I7,'-',A6))
27  FORMAT(/5X,'TR   KA   TA   VRMAX   VRMIN   KE   TE',
*      '   KF   TF'/
*      3X,F5.3,F8.2,2F7.3,2F8.3,3F7.3)

2000 WRITE(IPRT,507) IBUS,IM,(CON(K),K=J,J+31)
      RETURN
507  FORMAT(I6,'  'USRMDL''',2X,A2,'  'Ureactor''',1X,4G13.5,/7X,5G13.5,')')
      .  UNLESS (NEW)
      .  .  NEW=.TRUE.
      .  .  CALL DOCUHD(*1900)
      .  .  WRITE(IPRT,97) IBUS,IM
      .  ...FIN
      ...FIN
97   FORMAT(//'  BUS',I7,'  MACHINE ',A,':')
      END

```

## B.2 Matlab Code for Quasi-Static DH System Model

```

clear
clc
% Electrical power and Heat Demand
[P_elec]=ElecSMR();
P_Hdem=Hdemand();
P_Hdem1=P_Hdem(:,1);

%The slack variable represent the additional power the reactor should be generate
such that the excess heat available is able to power the district heating
system. If the power is insufficient, the slack for certain timeframe has to

```

be increased. At the same time the slack shouldn't be very high to generate large steam waste. This problem considers the TES temperature limits for the optimization.

```

slackmax=0.08;
slack1=0.06*ones(length(P_elec),1);
for iter=1:1:20
    Pr=max(P_elec(1:5*4+4))+slack1(1);
    P_Hdem(:,1)=P_Hdem1;
    %Extraction steam for heating and demand-generation balance
    for i=1:1:length(P_elec)
        % Deciding the value of slack is an optimization problem
        if(rem(i,6*4)==0 && i<length(P_elec))
            if(i+6*4+4<length(P_elec))
                Pr=max(P_elec(i-3:i+6*4+3))+slack1(i);
            else
                Pr=max(P_elec(i-3:i+6*4))+slack1(i);
            end
        end
        if (Pr>0.99)
            Pr=0.99;
        end
        P_react(i)=Pr;
    end
    for i=1:1:length(P_elec)
        if(1<i-8 & i<length(P_elec)-8)
            if(4>rem(i,6*4) | rem(i,6*4)>6*4-4)
                P_react(i)=P_react(i-1)+(P_react(i+8)-P_react(i-8))/8;
            end
        end
        [H]=Rankine(P_react(i));
        Hsets(i,:)=H;
        y(i)=(P_react(i)-P_elec(i))/P_react(i)*(H(4)-H(5))/(H(6)-H(5));
    end
end

```

```

if(y(i)>1)
    Excess_Extr(i)= (y(i)-1)*65.93*(P_react(i)+0.0824)/1.0695;
    P_elec_Extr(i)=(y(i)-1)*P_react(i)*(H(6)-H(5))/((H(4)-H(5)));
    y(i)=1;
    disp('Need more extraction to meet new electrical power.');
```

```

else
    Excess_Extr(i)= 0;
    P_elec_Extr(i)=0;
end

mth(i)=y(i)*65.93*(P_react(i)+0.0824)/1.0695;
P_DH(i)=(H(6)-H(8))*mth(i)/1000;
end

Mpipe=270; % Pipe water flowrate constant, Kg/s
TDHout=90*ones(length(P_Hdem),2); % output temperature constant
cpwater=4.18; %KJ/KgC
TDHin=TDHout-P_Hdem*1000/(Mpipe*cpwater);
TDHin1=TDHin(:,1);
V_str=20000; %m3
rho_str=1000;
Mstr_in_max=50;
Tstr(1)=90;
T_interval=0.25; %hours
for i=1:1:length(P_elec)
    if(P_Hdem(i,1)<2*P_DH(i))
        Mhs(i)=P_Hdem(i,1)/(P_DH(i))*mth(i);
        Ths_inreq(i)=TDHin(i,1);
        Mstr_in(i)=2*mth(i)-Mhs(i);
        if (Mstr_in(i)>Mstr_in_max)
            Mwastesize(i)=Mstr_in(i)-Mstr_in_max;
            Mstr_in(i)=Mstr_in_max;
        else
            Mwastesize(i)=0;
        end
    end
end

```

```

end
if(Tstr(i)<98)
    Tstr(i+1)=Tstr(i)+Mstr_in(i)*P_DH(i)/mth(i)*3600*1000
    *T_interval/(V_str*rho_str*cpwater);
    Mwaste(i)=0;
    if(Tstr(i+1)>98)
        Tstr(i+1)=98;
        Mstr_in(i)=(Tstr(i+1)-Tstr(i))/(P_DH(i)mth(i)*3600*1000
        *T_interval/(V_str*rho_str*cpwater));
        %If Mstr_in(i)>Mstr_in_max logic needed
        Mwaste(i)=2*mth(i)-Mhs(i)-Mstr_in(i);
        Mwastesize(i)=0;
    end
else
    Tstr(i+1)=Tstr(i);
    Mwaste(i)=Mstr_in(i);
    Mstr_in(i)=0;
end
else
    Mhs(i)=2*mth(i);
    Ths_inreq(i)=90-2*P_DH(i)*1000/(Mpipe*cpwater);
    Mstr_in(i)=0;
    Mwaste(i)=0;
    % The temporal effect
    if(i<length(P_elec))
        if(Tstr(i)>65)
            if(Tstr(i)<Ths_inreq(i)+0.5)
                % If heat storage cannot fully support, the heat is supplied at
                lower temperature.
                disp('Heat Insufficient');
                TDHout(i+1,1)=Tstr(i)-0.5+2*P_DH(i)*1000/(Mpipe*cpwater);
                TDHin(i+1,1)=TDHout(i+1,1)-P_Hdem(i+1,1)*1000/(Mpipe*cpwater);

```

```

        P_Hdem(i+1,1)=(90-TDHin(i+1,1))*Mpipe*cpwater/1000;
        Tstr(i+1)=Tstr(i)-(Tstr(i)-0.5-TDHin(i, 1))*Mpipe
            *cpwater*3600*T_interval/(V_str*rho_str*cpwater);
    else
        Tstr(i+1)=Tstr(i)-(P_Hdem(i,1)-2*P_DH(i))*3600*1000
            *T_interval/(V_str*rho_str*cpwater);
    end
else
    Tstr(i+1)=Tstr(i);
    disp('Heat Storage Depleted');
    % If heat storage cannot support, the district heating system
        receives the power from the heat station only.
    TDHout(i+1,1)=TDHin(i,1)+2*P_DH(i)*1000/(Mpipe*cpwater);
    TDHin(i+1,1)=TDHout(i+1,1)-P_Hdem(i+1,1)*1000/(Mpipe*cpwater);
    P_Hdem(i+1,1)=(90-TDHin(i+1,1))*Mpipe*cpwater/1000;
end
end
end
end
%Heat storage stored energy
Pstr(i)=V_str*rho_str*cpwater*(Tstr(i+1)-Tstr(i))/(3600*1000*T_interval);
end

for i=1:1:length(P_elec)

    if (Tstr(i)>90)
        slack1(i)=slack1(i)-0.001*(Tstr(i)-90);
    elseif(Tstr(i)<75 && Mwastesize(i)==0)
        slack1(i)=slack1(i)+0.001*(75-Tstr(i));
    end
    if (slack1(i)<0)
        slack1(i)=0.00000001;
    elseif (slack1(i)>slackmax)

```

```

        slack1(i)=slackmax;
    end
end
end
time2D=0.25*[0:length(P_elec)-1];
figure(1)
plot(time2D,Ths_inreq,time2D,TDHout(:,1),time2D,TDHin(:,1),[time2D,720],Tstr);
xlim([0 720])
figure(2)
plot(time2D,Mwaste,time2D,Mstr_in,time2D,Mhs,time2D,2*mth);
xlim([0 720])
figure(3)
plot(time2D,P_elec,time2D,P_react);
xlim([0 720])

%Error in balance
Storedinaday=(Tstr(length(P_elec)+1)-Tstr(1))*(V_str*rho_str*cpwater)/1000/3600;
Wasted=sum((Mwaste+Mwastesize).*P_DH./mth)*T_interval;
Error=sum(2*P_DH'-P_Hdem1(:,1))*T_interval-Storedinaday-Wasted;
if(abs(Error)>10^-4)
    disp('Mismatch');
else
    disp('No mismatch');
end

for i=1:length(P_elec)
    [H_col2(i,:), P_col2(i,:), T_col2(i,:), S_col2(i,:)] = Rankine(P_elec(i));
end
Tab_all=table(time2D',P_elec,P_react',y',Excess_Extr',P_elec_Extr',2*mth',
,2*P_DH',Mhs',Mstr_in',Pstr',Mwaste',Mwastesize',P_Hdem1,Hsets,
TDHin1,Ths_inreq',TDHout(:,1),Tstr(1:2880)');

```

```

function [H,P,T,S] = Rankine(Pr)
% Finding Rankine cycle envelope from the reactor operating point
Tp=260;% Average temperature setting
Tm=(0.8735*Tp-0.1265*(65.93*(Pr+0.0824)/1.0695)*1/3.83)/(1-0.1265);
Press=(Tm-(65.93*(Pr+0.0824)/1.0695)*1/3.83-184.6)/16.06;
P(1)=0.0786002268314971;% Condenser pressure, MPa
P(2)=Press*10;% In bar
P(3)=P(2);
P(4)=P(2);
P(5)=P(1);
S(1)=XSteam('sL_p',P(1));
H(1)=XSteam('hL_p',P(1));
S(2)=S(1);
H(2)=XSteam('h_ps',P(2),S(2));
for i=1:1:5
    if (i == 2)
        T(i)= XSteam('T_ps',P(i),S(i));
    else
        T(i)=XSteam('Tsat_P',P(i));
    end
end
S(3)=XSteam('sL_p',P(3));
H(3)=XSteam('hL_p',P(3));
S(4)=XSteam('sV_p',P(4));
H(4)=XSteam('hV_p',P(4));
S(5)=S(4);
H(5)=XSteam('h_ps',P(5),S(5));
S(6)=S(1);
T(6)=T(1); %Extraction steam temperature
P(6)=P(1);
H(6)=H(1);
end

```

## B.3 Python Code for the Dynamic Simulation in PSS®E

```
import numpy as np
import xlswriter
import matplotlib.pyplot as plt
import sys
import os
PSSE_LOCATION = r'C:\Program Files (x86)\PTI\PSSE33\PSSBIN'
sys.path.append(PSSE_LOCATION)
os.environ['PATH'] += ';' + PSSE_LOCATION
import psspy
import redirect
redirect.psse2py()
import dyntools
from psspy import _i, _f, _s, _o
psspy.psseinit(80000)
branch_sequence=[100,202,211,212,300,301,342,402,403,500,501,503,505,600,601]
machine_sequence=[208,209,302,309,404,602]
it=0
FN=[0,0,0,0,0,0,0,0,0,0,0,0,0,0,0]
VN=[0,0,0,0,0,0,0,0,0,0,0,0,0,0,0]
workbook = xlswriter.Workbook('Database.xlsx')
psspy.opendiagfile(r""D:\Case\loaction\Mediumterm.sld""")
outfiles=r"D:\Case\loaction\outf.out"
mac=1;
Ma_seq=1;
worksheet = workbook.add_worksheet()
for iterat1 in machine_sequence:
    it=0
    FN=[0,0,0,0,0,0,0,0,0,0,0,0,0,0,0]
    VN=[0,0,0,0,0,0,0,0,0,0,0,0,0,0,0]
```

```

ROCOF=[0,0,0,0,0,0,0,0,0,0,0,0,0,0,0,0]
Br_seq=0;
for iterat in branch_sequence:
    psspy.case(r""D:\Caseloaction\Mediumterm.sav"")
    psspy.rstr(r""D:\Caseloaction\Mediumterm.snp"")
    psspy.purgbrn(104,342,r""1"")
    psspy.fdns([0,0,0,1,1,0,0,0])
    psspy.fdns([0,0,0,1,1,0,0,0])
    psspy.bsys(0,0,[ 11.0,
        230.],0,[],7,[201,208,209,302,309,404,602],0,[],0,[])
    psspy.chsb(0,0,[-1,-1,-1,1,12,0])
    psspy.chsb(0,0,[-1,-1,-1,1,13,0])
    psspy.cong(0)
    psspy.conl(0,1,1,[0,0],[ 100,0.0,0.0, 100.0])
    psspy.conl(0,1,2,[0,0],[ 100,0.0,0.0, 100.0])
    psspy.conl(0,1,3,[0,0],[ 100,0.0,0.0, 100.0])
    psspy.strt(0,r""D:\Caseloaction\outf.out"")
    psspy.run(0, 0.5,0,1,0)
    psspy.machine_chng_2(iterat1,r""1"",[0,_i,_i,_i,_i],
        [_f,_f,_f,_f,_f,_f,_f,_f,_f,_f,_f,_f,_f,_f,_f])
    psspy.run(0, 5.0,0,1,0)
    psspy.run(0, 70.0,0,1,0)
    abc=dyntools.CHNF(r""D:\Caseloaction\outf2.out"")
    a=abc.get_range()
    FN[it]=a[mac+1]['min']
    VN[it]=a[mac+8]['min']
    an,bn,cn=abc.get_data()
    time=cn['time']
    freq=cn[mac+1]
    volt=cn[mac+8]
    fig = plt.figure(1)
    plt.plot(time,freq,linestyle='-', linewidth=1,

```

```

        color='green',label="Frequency")
plt.savefig(r"D:\Outputlocation\machine"+str(iterat1)+r"\Jpeg"
+str(iterat)+r"frequency.png",dpi=200,facecolor='0.8')
fig = plt.figure(2)
plt.plot(time,volt,linestyle='-', linewidth=1,
        color='red',label="Voltage")
plt.savefig(r"D:\Outputlocation\machine"+str(iterat1)+r"\Jpeg"
+str(iterat)+r"voltage.png",dpi=200,facecolor='0.8')
freq=np.array(cn[mac+1])
freq=freq*60+60;
rocof=np.zeros(len(freq))
for i in xrange(12,len(freq)):
    rocof[i-11]=(freq[i]-freq[i-12])/0.1
    i=i+1
fig = plt.figure(3)
plt.plot(time,rocof,linestyle='-',
        linewidth=1,color='black',label="ROCOF")
plt.savefig(r"D:\Outputlocation\machine"+str(iterat1)+r"\Jpeg"
+str(iterat)+r"rocof.png",dpi=200,facecolor='0.8')
ROCOF[it]=max(abs(rocof));
worksheet.write(Br_seq,0, iterat)
worksheet.write(Br_seq,Ma_seq, FN[it])
worksheet.write(len(branch_sequence)+Br_seq+5,0, iterat)
worksheet.write(len(branch_sequence)+Br_seq+5,Ma_seq, VN[it])
worksheet.write(2*len(branch_sequence)+Br_seq+10,0, iterat)
worksheet.write(2*len(branch_sequence)+Br_seq+10,Ma_seq, ROCOF[it])
it=it+1
plt.close('all')
Br_seq=Br_seq+1;

mac=mac+1
Ma_seq=Ma_seq+1;
workbook.close()

```